Full Envelope Wind Turbine Controller Design for Power Regulation and Tower Load Reduction

Aristeidis – Panagiotis Chatzopoulos

Industrial Control Centre,
Department of Electronic and Electrical Engineering,
University of Strathclyde,
204 George Street,
Glasgow G1 1XW

Thesis submitted to the
University of Strathclyde
for the degree of
Doctor of Philosophy

August 2011

Acknowledgement

First of all I would like to thank my supervisor Professor Bill Leithead who has been an excellent mentor to me throughout the whole period of my PhD studies. His availability to answer all my questions and give me advice through long meetings is greatly appreciated. The conversations we had provided me with an analytical way of thinking, which is a key element for solving problems.

I would like to thank the engineers of MLS UK, especially Carlos Gonzales for all the time they spent for answering my questions and having useful conversations on how to approach problems concerning my research.

I am grateful for the support of EPSRC/SUPERGEN Wind Energy Technologies Consortium Grant Numbers: EP/D034566/1, EP/H018662/1 & EP/H018956/1 for supporting this work. Many thanks to everyone involved in the SUPERGEN Wind project, as well as for organising all the useful research and training events. I had the excellent experience of meeting and working with so many researchers, all working in the field of wind energy.

There aren't enough words to thank my parents, to whom I owe a lifetime of gratitude, for the continuous encouragement and support throughout my studies.

Last but not least, I owe a big thanks to Yiota. Her support has been invaluable and her patience to wait for me and encourage me all this time is greatly valued and appreciated.

Abstract

The main objective of this thesis is to design controllers for a 2MW wind turbine for power regulation and tower load reduction. Due to the highly stochastic nature of the wind, a wind turbine is exposed to strongly varying loads. More specifically tower loads are a major concern and there is little literature proposing solutions towards their mitigation. One of the objectives of the operation of a wind turbine is to maximize its energy capture in below rated wind speeds through the controller. A thorough assessment of what is possible in a modern MW scale wind turbine is undertaken in this thesis. A full envelope single input single output controller is designed to be used as a benchmark for comparison of the newly proposed coordinating controller which successfully mitigates tower fatigue loads. The design of the newly proposed coordinated controller is thoroughly explored and tested.

Table of Contents

Nomenclature

C	Central controller (above or below rated unless defined)
C_{ar}	Above rated controller (pitch control)
C_{br}	Below rated controller (torque control)
C_o, C_i	Outer and inner components of controller used in switching
$Gtfl$	Tower feedback controller
$Gactuator$	Dynamics of the pitch actuator
Q	In-plane aerodynamic torque
Q_2	Out-of-plane aerodynamic torque
P	Electrical Power
ρ	Air density
A	Area of Rotor
Ω	Rotor speed
Ω_0	Angular velocity
C_p	Power coefficient
C_T	Aerodynamic thrust coefficient
R	Radius of the rotor
β	Pitch angle
v	Wind speed
K_{opt}	Optimum controller gain for the tracking of the maximum power coefficient curve
ω, ω_g	Generator speed
ω_{ref}	Nominal Generator speed
L	Effective length of the blade
k	Weibull shape factor
c	Weibull scale factor
λ	Tip speed ratio
θ_R	In-plane rotational displacement of the centre of mass of the blade

$\boldsymbol{\theta_G}$	Rotational displacement of generator
$\boldsymbol{\Phi_R}$	Out-of-plane rotational displacement of the centre of mass of the blade
$\boldsymbol{\Phi_T}$	In-plane rotational displacement of the tower
$\boldsymbol{\theta_H}$	Angular position of the hub
$\boldsymbol{T_H}$	Hub torque
$\boldsymbol{T_{gen}}$	Generator torque
$\boldsymbol{a}$	Inflow factor (axial flow)
$\boldsymbol{J}$	Rotor inertia
$\boldsymbol{K_E}$	Edgewise blade stiffness
$\boldsymbol{K_F}$	Flapwise blade stiffness
$\boldsymbol{K_T}$	Fore-aft tower stiffness
$\boldsymbol{h}$	Hub height
$\boldsymbol{J_T}$	Fore aft tower inertia
$\boldsymbol{J_C}$	Tower-rotor cross coupling inertia
$\boldsymbol{B_T}$	Fore-aft aerodynamic damping of tower
$\boldsymbol{K_T}$	Tower stiffness
$\boldsymbol{F_1}$	In-plane aerodynamic torque
$\boldsymbol{F_2}$	Out-of-plane aerodynamic torque
$\boldsymbol{\omega_E}$	Frequency of blade edgewise moment
$\boldsymbol{\omega_F}$	Frequency of blade flapwise moment
$\boldsymbol{\gamma_1^*}$ & $\boldsymbol{\gamma_2^*}$	Material damping due to the twisting of the two shafts
$\boldsymbol{\gamma_{Hs}}$	Mechanical losses in the high-speed shaft of the drive-train
$\boldsymbol{\gamma_{Ls}}$	Mechanical losses in the low-speed shaft of the drive-train
$\boldsymbol{n}$	Gearbox ratio
$\boldsymbol{I_{Ls}}$	Inertia of the low speed shaft
$\boldsymbol{I_{Hs}}$	Inertia of the Gearbox relative to the high speed shaft
$\boldsymbol{J_{TS}}$	Inertia for the side-to-side movement of the tower
$\boldsymbol{B_{TS}}$	Damping for the side-to-side movement of the tower
$\boldsymbol{K_{TS}}$	Stiffness for the side-to-side movement of the tower
$\boldsymbol{X}, \boldsymbol{\tilde{X}}$	Co-ordinated controller transfer function

$Y, \tilde{Y}$	Tower frequency filter (High pass or Notch filter)
β_d	Pitch angle demand
T_d	Torque demand
T_u, K_u	Constants in wind speed model affected by the turbulence of wind
σ_u	Wins turbulence intensity
$\tilde{V}$	Short term mean wind speed
γ	Turbulent decay factor of spatial filter

Abbreviations List

WT	Wind turbine dynamics
SISO	Single Input Single Output
MIMO	Multi Input Multi Output
CCD	Coordinated Controller Design
PCC	Power Coordinated Controller
RHPZ	Right Half Plane Zeros
TFL	Tower Feedback Loop
HAWT	Horizontal Axis Wind Turbine
nP	n*Rotational speed
PID	Proportional Integral Derivative
CFD	Computational Fluid Dynamics
LTI	Linear Time Invariant
BEM	Blade Element Momentum Theory
DFIG	Doubly Fed Induction Generator
SCADA	Supervisory Control and Data Acquisition

1 Introduction

The exploitation of the energy found in the wind dates back thousands of years. Nowadays wind energy is exploited through large scale wind turbines used to produce electrical power. Undoubtedly, the rapid development of renewable energy sources is the most popular tool available internationally for the tackling of climate change. Wind turbines are machines which convert the kinetic energy of the wind into electrical power. This conversion is done in two stages; the first through the rotor converting the kinetic energy of the wind to mechanical energy and the second stage through the generator converting the mechanical rotational energy into electric energy.

In recent years, it has become common knowledge that wind farms are playing a very important role towards the development of green, natural energy. They completely eradicate carbon and gas emissions; to the extent that for a 50MW wind farm, approximately 2,300 tonnes of sulphuric acid, 128,000 tonnes of carbon dioxide and 180 tonnes of nitrogen dioxide are avoided from being emitted to the atmosphere, by using conventional power plants.

Around 40 GW of new wind energy capacity has been added this year alone (globally). The global installed wind energy capacity was close to 200 GW by the end of 2010. The European wind market on its own is expected to grow at a rate of over 9 GW annually, which takes the figure of annual investments to more than 11 billion Euros [45]. The Global Wind Energy Council (GWEC) predicts the global market for wind turbines will grow to more than 330 GW of total installed capacity by 2013. It is also anticipated that wind power could cover up to 13% of global electricity demand by 2020, according to GWEC, and up to roughly 25% in 2030 [45].

The figures discussed above are huge and show the rapid development of the wind energy market. Research is being done into every aspect of the wind turbine operation, and, as the wind turbines get continuously larger in size, see Figure 1.1, issues like their design, control, economics and location become more complex and demanding. Much research is being done on the materials used to build a wind turbine [60]. The trend is towards lighter, stronger, less expensive materials, especially for the tower and blades. In some case the cost of the tower and its foundations account for more than the 50% of the total cost of the wind turbine, the reason being that less costly material with high endurance have not yet been fully justified. In order for new materials to be used i.e. aluminium, concrete etc, the fatigue loads and the strength requirements must be fully met.

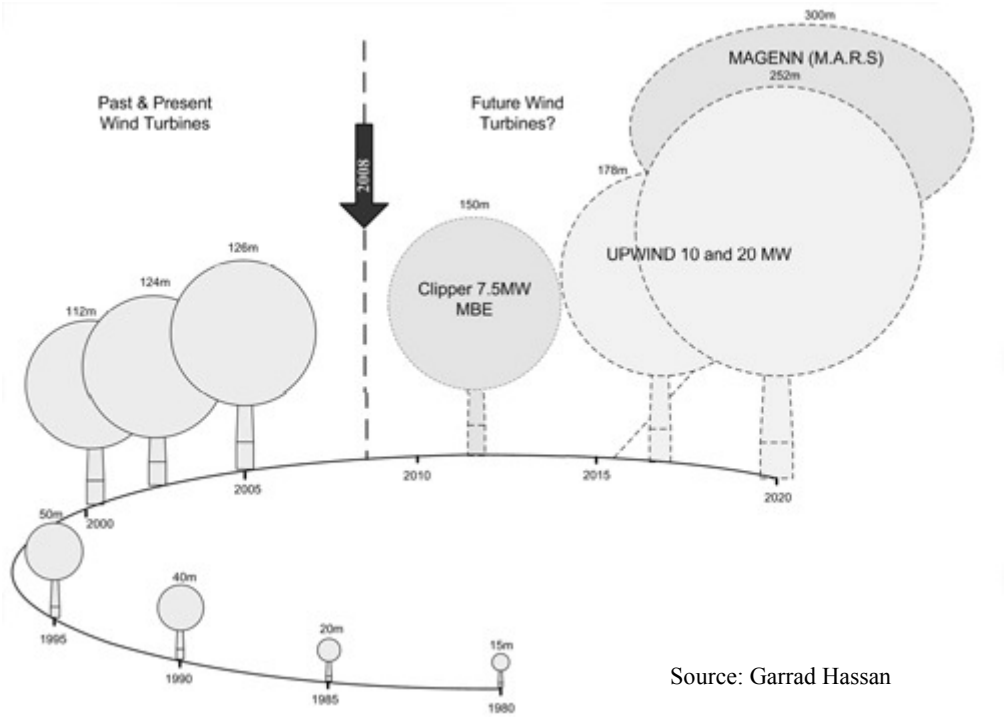

Figure 1.1: Size development of wind turbines [45]

The heart of the operation of a wind turbine is its controller. As the size of the wind turbine increases the controller becomes more complex and more tasks are assigned to it. Wind turbine structural elements have become structurally flexible and fatigue loads have become of major concern. If they are not taken into account the operating life of the wind turbine can be reduced and the costs for maintenance, down time and part replacement will be significantly increased.

The purpose of this thesis is to pronounce the significance of the controller and its contribution to energy capture, present the full envelope controller design of a modern large MW scale wind turbine, and introduce advance control algorithms towards the alleviation of tower fatigue loads.

1.1 Brief History of Wind Power

Historically wind power has followed a general evolution from the use of simple, light devices using aerodynamic drag force, to heavier material. Human efforts to exploit wind for energy date back thousands of years, when sails were used to propel ships and boats. Aerodynamic lift (the force making planes fly) is not a modern concept at all. The earliest use of wind power is the sailing boat, which is the predecessor of sail-type windmills. Ancient sailors didn't have the physics background knowledge to explain how aerodynamic lift and drag worked, however they used it in everyday life.

The earliest design of a wind mill documented, dates back to 200 B.C [63]. The Persians used them for grinding corn during this period. These were vertical axis machines and the grinding stone was attached to the vertical shaft.

Windmills were also widely used by the Chinese, and some people argue that China was their place of origin.

The first windmills in the western European region were horizontal-axis machines. The reason for the change from the Persian vertical-axis design is yet to be answered. This is probably due to their higher structural efficiency. The first illustrations (approximately 1270 A.D.) depict a four- bladed mill mounted on a central mast. These mills used wooden gears to transmit the motion of the shaft to rotate a grindstone.

The era of electricity generators using wind as their fuel began around 1890’s when the first wind turbine was designed in Denmark, specifically for electricity generation. Then in 1920 the Darrieus machine was developed, having narrow curved blades designed to rotate around the vertical axis. Wind electrical generators then evolved rapidly with new axis, rotor and blade design concepts. Constant speed wind turbines with rated power 100kW were developed later in the 70’s in Germany

having a diameter of about 15m. Thereafter the technology dramatically evolved, to the point where 5MW machines are proposed to exploit the offshore resource.

1.2 Thesis organisation

The thesis is organised as follows:

Here in Chapter 1, an introduction, the motivation and organisation of this thesis is presented, as well as a brief historical background of wind energy.

Chapter 2, provides the background to control of wind turbines. Details about the wind resource as well as the fatigue loads that wind turbines encounter are also included in this Chapter.

Chapter 3, describes the modelling and aerodynamic background of a modern horizontal axis wind turbine. Apart from the modelling details, a brief assessment is also made of commercial aeroelastic codes widely used by the wind energy community. The results and simulations included in this thesis are outputs from the aeroelastic software package GH Bladed.

Chapter 4, assesses fully the energy capture capability of a modern MW scale wind turbine. As explained in Chapter 2, one of the main and most important objectives of the controller during below rated operation is to ensure that the wind turbine maximises the amount of energy captured from the wind. It is investigated whether energy capture is dependent on the control strategy adopted and to what extent the wind turbine is exploiting the energy available in the wind.

Chapter 5, provides a description of a detailed full envelope controller design for the 2MW Supergen exemplar wind turbine. This wind turbine and its controller serve as a benchmark for comparison of the novel controller algorithms for tower load reduction, presented in Chapter 6.

Chapter 6, presents novel algorithms based on a parallel path modification to the existing controller, using a coordinated multi-input multi-output concept which significantly reduces the lifetime tower fatigue loads. This concept is extended to a power coordinated controller design, which manages to reduce the loads with no compromise in the performance of the wind turbine.

Finally, Chapter 7 summarises the results presented in this thesis, draws some conclusions and discusses the proposed further work to be done in this area of research.

1.3 Publications

The outcomes of this thesis resulted in the following publications:

1. A. Chatzopoulos, W.E. Leithead, *"Ensuring maximum energy capture by wind turbines during below rated operation"*, 5th PhD Wind Energy Conference in Europe, p.97-100, 30 September – 1 October 2009, Durham, UK

2. A. Chatzopoulos, W.E. Leithead, *"Assessing the Energy Capture Capability of a MW Scale Wind Turbine During Below Rated Operation"*, European Wind Energy Conference 2010, Scientific Proceedings, p.251-254, 20-23 April 2010, Warsaw, Poland

3. A. Chatzopoulos, W.E. Leithead, "*Reducing tower fatigue loads by a co-ordinated control of the Supergen 2MW exemplar wind turbine"*, Torque 2010: The Science of Making Torque From Wind, Proceedings of 3rd EWEA Conference, p.667-674, 28-30 June, Heraklion, Greece

To be presented in September 2011:

4. A. Chatzopoulos, W.E. Leithead, *"The Use of a Novel Power Co-ordinated Controller for the Effective Reduction of Wind Turbine Tower Fatigue Loads"*, eRA2011 – Conference for International Synergy in Energy, Environment, Tourism and contribution of Information Technology in Science, Economy, Society and Education, 19-24 September 2011, Greece

2 Overview of the Wind turbine and the Controller

2.1 General Background

Control plays a very important role in the efficient operation of the wind turbine. It allows for better exploitation of the wind energy capacity as well as the mitigation of fatigue loads that reduce the lifetime expectancy of the installation. Hence, active control has crucial impact on the cost of wind energy [69].

Wind turbines have to account for the stochastic nature of the wind and therefore, they include mechanisms that limit the captured power in high wind speeds to avoid damage of the machine. For low wind speeds the controller needs to adjust its mode of operation according to an ideal strategy of the wind turbine. The most common practice for power limitation is to reduce the blades lift by pitching the blades and discarding excess power. Alternatively, passive control methods are sometimes used for this job.

2.2 Preliminaries of the wind turbine controller

The control task of a modern wind turbine is to enable the wind turbine to maintain the appropriate operational state as conditions change and to improve its dynamic properties. It is divided into two main categories: Supervisory control and Operational control.

2.2.1 Supervisory Control

Supervisory control is responsible for assigning “supervisors” that restrict the behaviour of a plant such that the given manufacturers specifications are fulfilled. States of the wind turbine that supervisory control is responsible for, include the following [62], [65], [69]:

- System check: this includes a check of the most important parameters of the wind turbine that may indicate a start up fault. Examples of such parameters are the status of the brakes, pressure levels, temperatures etc.
- Stand by: referring to the low power mode in which the machines systems are checked and ready to start
- Start up: includes the pitching of the blades at the optimum angle of attack for below rated operation, and the rotor starts to rotate.
- Shut down: this is the case when the mean wind speed over a specific period of time remains outside of the wind speed operational limits of the wind turbine. The wind turbine goes back to its stand by state.
- Power production: this state refers to the connection of the generator to the grid. There is a distinction in load operation according to the wind speed. When the wind speed is below the rated value the wind turbine operates at partial load. When the wind speed is above the rated value then there is maximum power production and the wind turbine is operating at full load.

More states [65] can also be considered to be affected by supervisory control which, amongst others, includes the engagement and disengagement of the brakes of the shaft, the power up of the actuators and the employment of the closed loop pitch controller for power limitation. The supervisory controller must make sure that specific tasks are completed before moving to the next ones. If a test does not pass because of a fault or conflict then the turbine is shut down.

2.2.2 Operational Control

Focus on the operational controller and its design is the main goal of this thesis. The main goals of operational controller may be divided in two categories depending on whether the wind turbine is operating in the below or above rated region:

Below rated

The task of the controller in this region is to extract as much power from the wind as possible. The objective in this low wind speed region is to vary the reaction torque from the generator according to a measurement of either rotor speed or output power. In this region, pitch regulated, variable speed wind turbines which are the main type discussed in this thesis; operate with minimum pitch angle in order to produce as

much power as is theoretically possible. The full assessment of the energy capture capability of a modern large scale wind turbine is undertaken in Chapter 4 of this thesis. The results suggest that when the theoretical maximum Cp_{max} curve is tracked through careful choice of the controller gain, almost no energy losses are observed. However, on fixed speed wind turbines which are not discussed here, the optimum angle of attack may vary slightly and the blades may have to be pitched slightly in order to achieve maximum power output. Another important task of the controller in below rated operation is the smooth switching between the 1st constant speed region, Cp_{max} tracking region and 2nd constant speed region. A typical operating strategy of pitch regulated, variable speed wind turbine and the aforementioned regions are depicted in Figure 2.4.

Above rated

In above rated operation the power is limited at some pre-determined nominal value (reached at rated wind speed). The task of the controller in this region is amongst others to [2], [38], [65], [69]:

- Maintain power at its rated value
- Compensate for the aerodynamic nonlinearities
- Keep the required stability margins that will ensure stability
- Take action to alleviate increased tower and rotor loads
- Maintain generator speed and torque within the required band of operation, protecting from over speed
- Maintain pitch activity within the specified limits

Inevitably there are trade-offs that have to be considered and analysed when designing the controller. Effort to improve the performance of one aspect might have negative influence on another. The task of the control engineer is to balance the advantages and disadvantages and make the best decision for overall improved performance.

Many different control methods have been discussed in the literature. To name a few, the Linear Quadratic Gaussian control approach is discussed in [50], [51], [52] minimising an LQG cost function, aiming at maintaining the power output at its rated

value. A Model Predictive Controller is design and tested in [55], [56]. Fuzzy Logic approaches are discussed in [8], [53], [54] mainly in below rated wind speeds in order to maximize energy capture. The minimization of the H2/H∞ norm using a Linear Parameter Varying controller is proposed in [57], balancing the tradeoffs between loads and power output. All of the methods give good results, some better in load reduction and some better in power output performance. The classical design approach, mainly used here, involves the use of PI or PID controllers for the design of the controller and is nowadays the industrial standard. Once rated torque is reached, pitch control has to regulate the rotor speed while keeping the load of the torque constant and thereby maintain power at the rated level.

As discussed in [20], [33], [59], the bandwidth of a system is a very important indication of the benefits and drawbacks of applying classical feedback control. As far as performance is concerned, the speed of response of the system under study relates directly to the bandwidth frequency. In general a large bandwidth corresponds to a faster response since high frequency components are not attenuated. However, high bandwidth indicates a sensitivity to noise and to parameter variations. On the other hand a low bandwidth frequency indicates a slower but more robust system. It is easily understood that depending on the nature of the system, a balance of tradeoffs has to be made. Roughly speaking bandwidth is the frequency range over which the controller is effective. In the case of a wind turbine the highly stochastic nature of the turbulent wind requires a responsive controller.

2.3 Pitch versus Stall Control strategies

Passive stall controlled wind turbines do not pitch the blades, whereas, active stall controlled machines are similar to the pitch controlled ones. The existing types of control strategies are described below.

Constant speed Stall Control

The constant speed, stall regulated strategy, see Figure 2.1, involves no active aerodynamic control action during normal operation. There is a direct connection of the generator to the constant frequency grid.

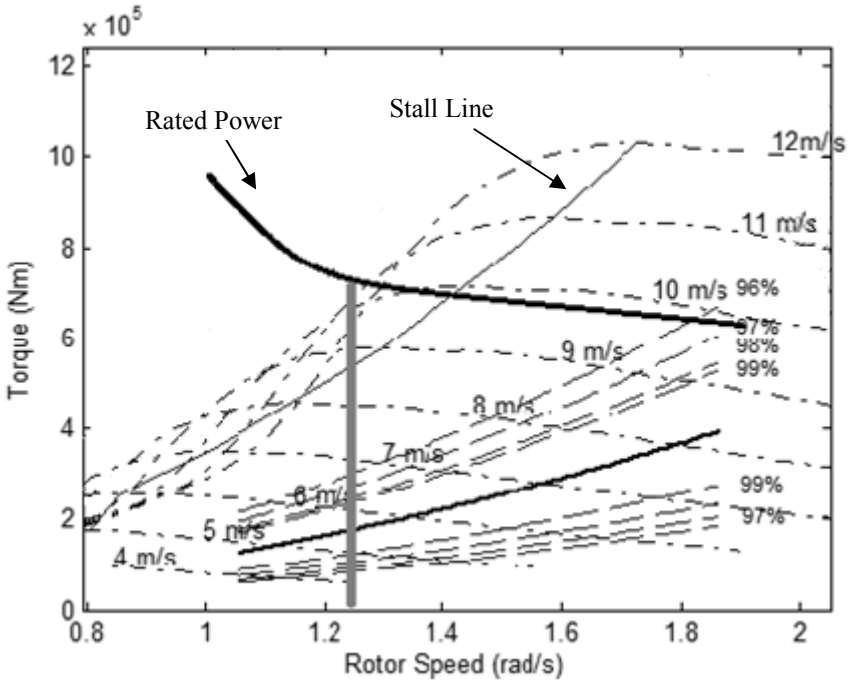

Figure 2.1: Stall regulated, Constant speed strategy

Variable speed Stall Regulated

The concept of active stall regulation is to reduce the aerodynamic power by pitching the blades in the negative angle opposite to that done in active pitch control, see Figure 2.5. This is done in order to increase the angle of attack of the wind on the blades [68]. The generator is decoupled from the grid and the rotor speed is controlled through varying the reaction torque from the generator. In variable speed stall control, the rotor speed is varied to vary the aerodynamic torque and so to limit the output power. The torque versus speed curve of this strategy is shown in Figure 2.2.

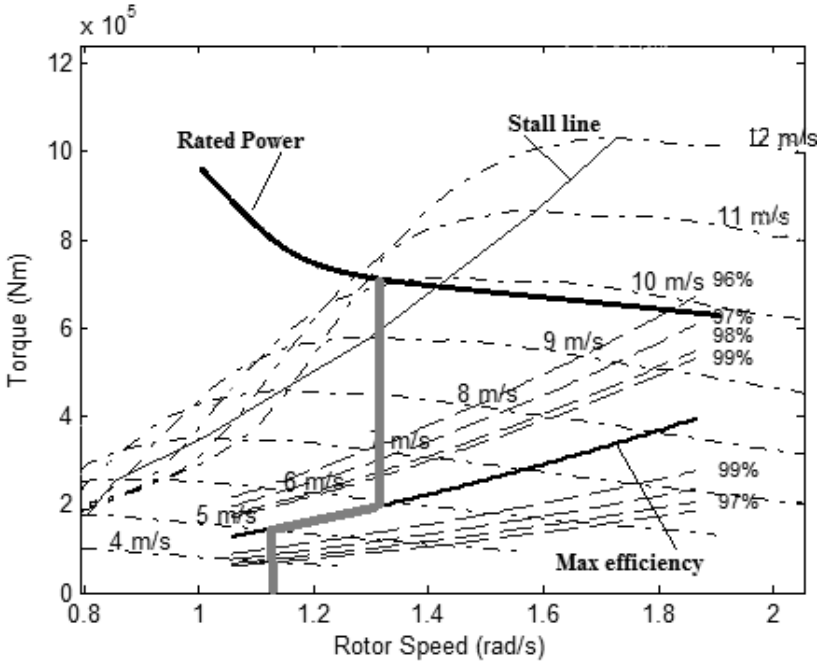

Figure 2.2: Variable speed Stall regulated strategy

Constant speed Pitch Regulated

This is another case where the generator is directly connected to a constant speed grid. This strategy is depicted in Figure 2.3, and the blades are pitched to limit the power in above rated wind speeds [31].

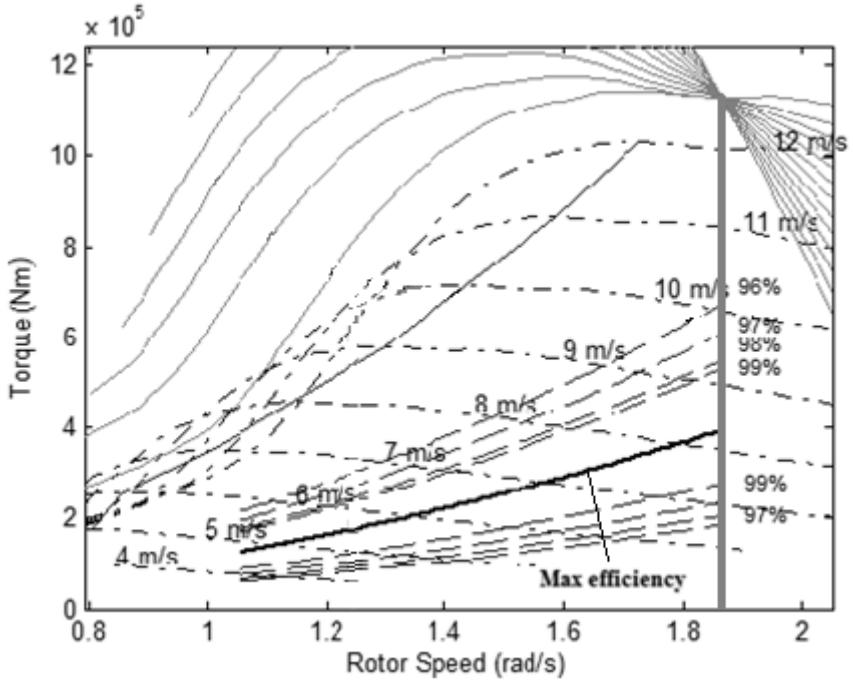

Figure 2.3: Constant speed Pitch regulated strategy

Variable speed Pitch Control

This control strategy is used to pitch the blades in such a way as to discard excess wind and limit the power output at its rated value. The 2MW wind turbine analysed in the present thesis adopts the active pitch control strategy and is therefore the main control strategy discussed. Its torque versus speed curve is presented in Figure 2.4.

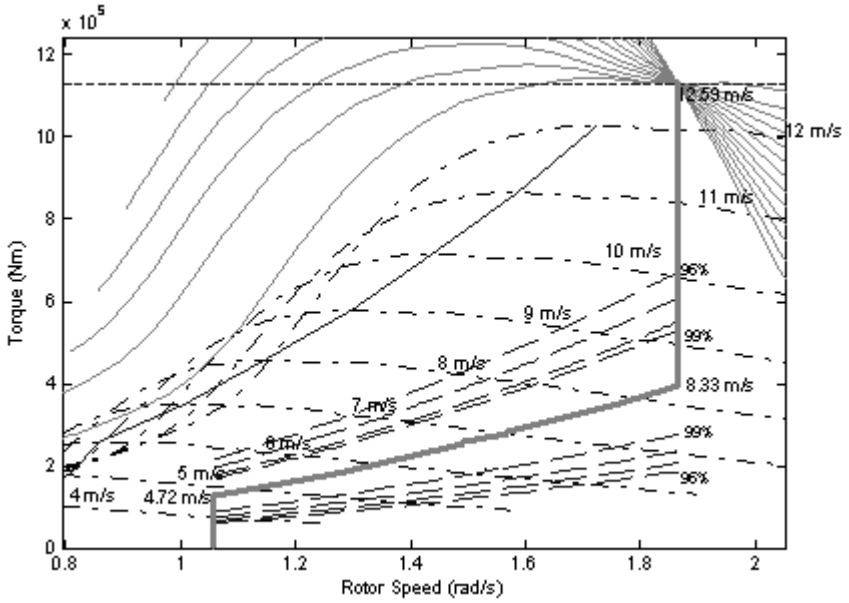

Figure 2.4: Ideal operating strategy for Variable speed, Pitch controlled wind turbines (Aerodynamic Torque – Rotor Speed)

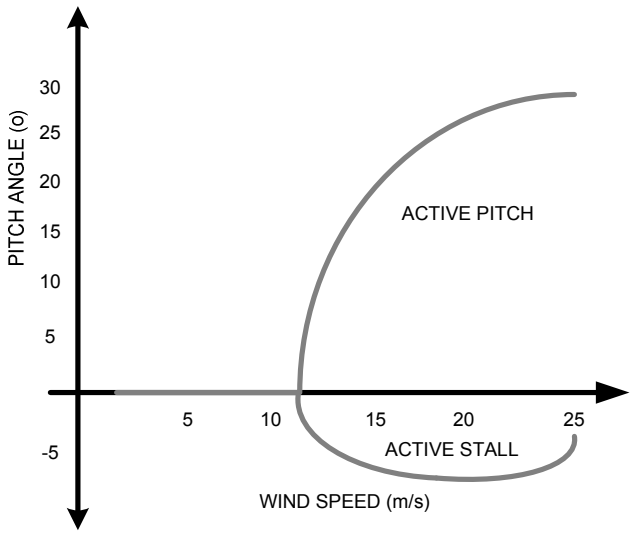

Figure 2.5: Active Pitch vs. Active Stall Control

2.4 Wind Resource

It is common knowledge that accurate prediction of the wind turbine performance depends on the knowledge of the behaviour of the wind. The most obvious characteristic of the wind resource is its variability. The wind speed at any location varies continuously in a stochastic manner and there are yearly, seasonal, daily and even turbulent second to second variations. All these variations make it difficult to accurately predict the exact energy capture performance and other aspects of the wind turbine behaviour. Typical wind speed time series plots are available in Appendix B.

The typical Van der Hoven spectrum see Figure 2.6, depicts the variance in wind speeds related with the time scales mentioned above. By observing this frequency plot we see slow variations occurring in a range of between 10 minutes and 2 hours. This explains the reason why wind statistics depend on mainly this timescale range.

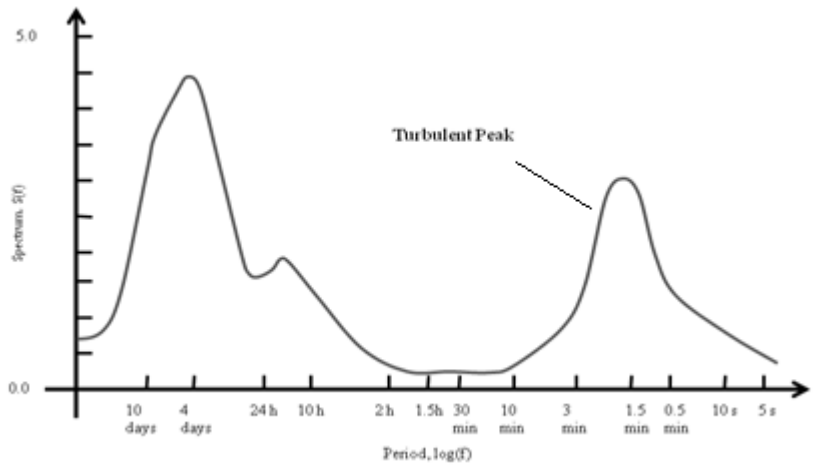

Figure 2.6: Typical Van der Hoven spectrum

2.5 Fatigue Loads

Due to the nature of the wind turbine it is subjected to various kinds of loads and stresses which are highly variable and affect almost all of its components. This is even more important as the size of the wind turbine increases and their components become more and more flexible. Even at the initial design process of the wind turbine it is crucial to assess its components and analyse the loads that the machine will experience during its lifetime. Moreover, very importantly as their size

increases, the controller must cater for and actively alleviate much of the fatigue loads where possible.

It is known that the wind field in which the wind turbine operates is non-uniform and stochastically time-varying. There is strong interaction between the stochastic wind field and the rotor which causes loads on the whole structure. The main categories of loadings that are usually taken into account are Aerodynamic, Inertial and Gravitational loads. These cause increased bending moments such as in the flapwise and edgewise modes of the blades, fore-aft modes of the tower, the drive train etc.

On the spectrum plot of Figure 2.7, it is easy to observe the loads, caused by the in-plane and out-of-plane moments of the blades, as large peaks placed at frequencies which are multiples of the frequency of the rotor. These are referred to as "nP" loads and may often cause damage to different components of the wind turbine. Another example is depicted in Figure 2.8, depicting the spectra of the fore-aft bending moment of the base of the tower. The large peak centred at the tower dominant frequency is causing excessive loads on the structure and must be alleviated through the controller. The reduction of the tower loads is one of the main objectives of this thesis and is thoroughly analysed in Chapters 5 and 6.

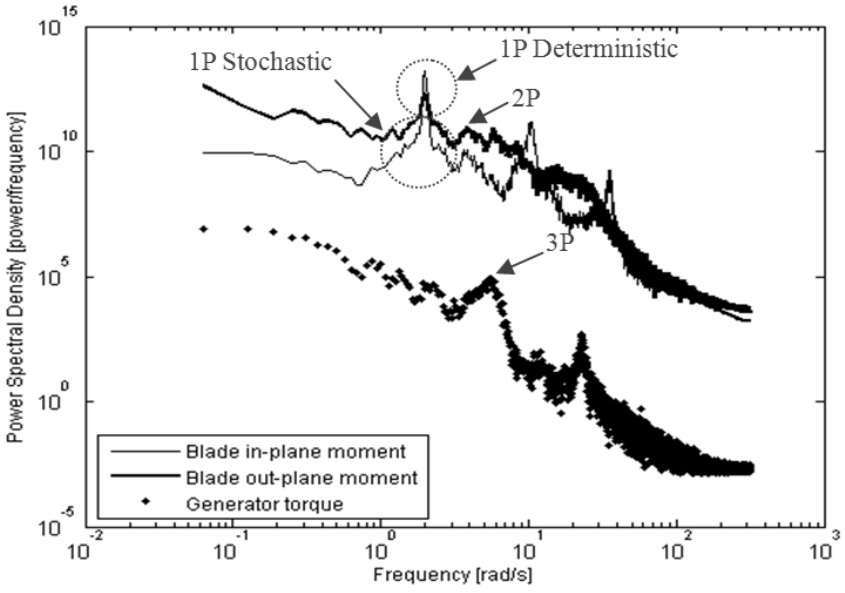

Figure 2.7: Unbalanced "nP" loads

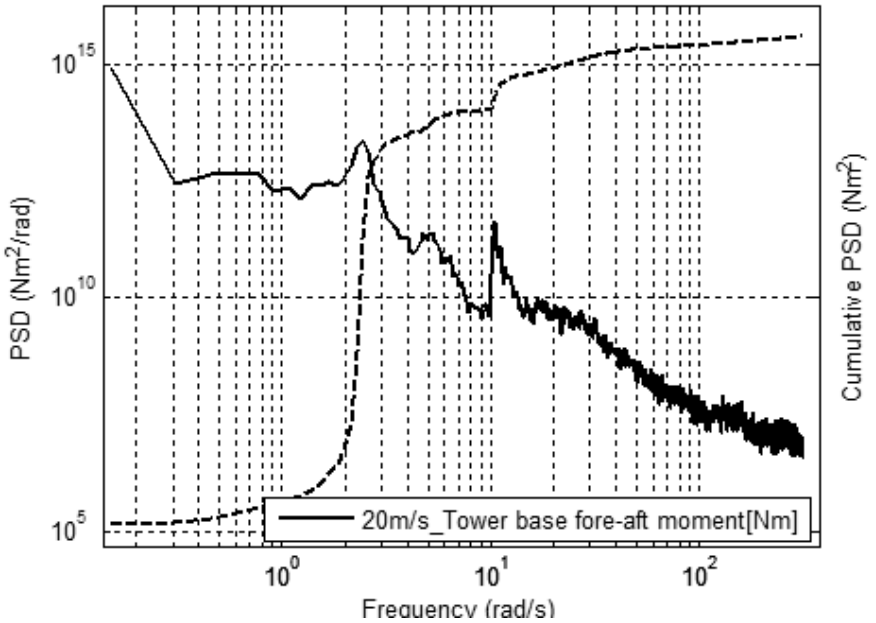

Figure 2.8: Spectrum of the fore-aft moment of the tower

3 Modelling and Aerodynamics of Variable Speed Wind Turbines

3.1 Main Wind Turbine Components

The most important components of a modern MW scale wind turbine are listed below and depicted in Figure 3.1.

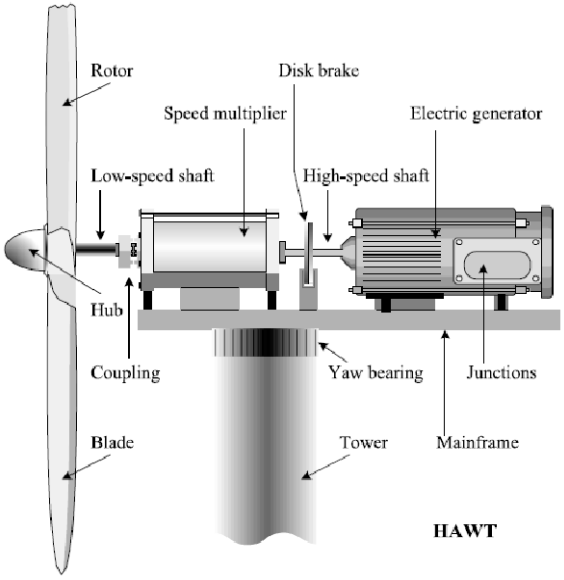

Figure 3.1: Main components of a HAWT [68]

- **Rotor:** The rotor of a wind turbine consists of the blades, the hub, the bearings and the shaft. It is the part of the wind turbine responsible for capturing the energy of the wind and transforming it into mechanical power. Modern wind turbines, such as the one discussed in this thesis, follow the Danish concept (i.e. three blades, upwind) which is nowadays the industrial standard. The size of a rotor depends on the turbines rated power, the higher the power output, the bigger the size of the rotor. Very early wind turbines of 25kW had a rotor diameter of 10m whereas a modern 2.5MW wind turbine rotor has a diameter of approximately 80m. To design a rotor, different methods are used by researchers and engineers,

such as the Blade Element Momentum theory, the Reynolds Navier stokes method (Fluid Dynamics approach) and the Vortex Lattice method.

- **Tower:** The tower serves the important role of supporting the rotor and the nacelle. Different concepts exist (Tubular, Lattice etc.) depending on the scale and the purpose of the turbine. Due to the fact that wind turbines are becoming larger in size, today towers may be in excess of 90m tall for a 5MW machine. It is inevitable that as towers become taller, the loads they experience become an important issue. This is one of the main topics of the present thesis.
- **Gearbox:** It is situated between the main shaft and the generator. Its use is to increase the rotational speed of the rotor to the generator rotation speed of 1000 or 1500 revolutions per minute (rpm). The gearbox has always a constant ratio (as opposed to car gearboxes), however they are prone to wear and high maintenance needs.
- **Generator:** The role of the generator is very demanding as they have to work under fluctuating power levels because of the nature of the stochastic wind. Depending on the operation and the type of the wind turbine, different types of generators are used. Most MW-scale wind generation plants are integrated with the grid, therefore three phase AC generators are commonly used. The most commonly commercial wind turbine configurations are the Doubly-fed induction generator (DFIG) wind turbines, see Figure 3.2, and the Wide-range variable-speed wind turbine based on a synchronous generator, see Figure 3.3.

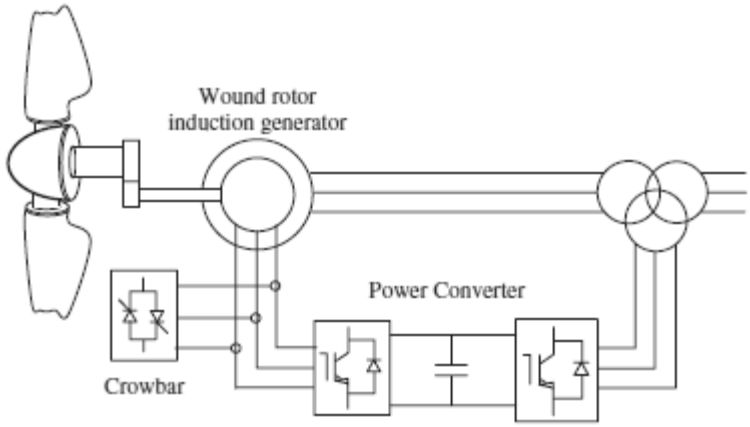

Figure 3.2: Typical DFIG Configuration [73]

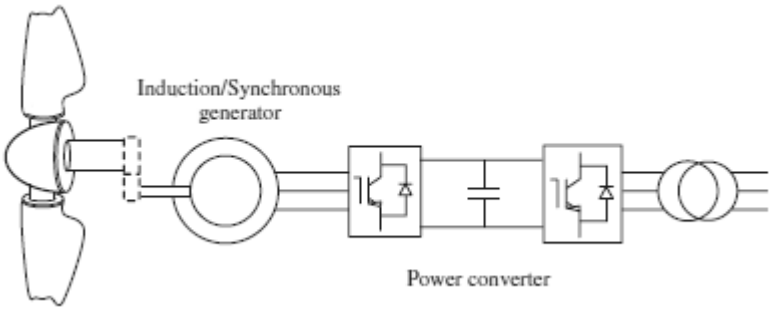

Figure 3.3: Wide range variable speed wind turbine configuration [73]

The first configuration uses an asynchronous generator combined with power electronics, and as its name implies, is able to decouple from the grid and operate in a specific speed range. Moreover, they are efficient with relatively little maintenance needs. The second configuration uses a synchronous generator in which the rotor and the generator rotor are completely decoupled from the grid, allowing operation in a wide range of speeds.

- **Sensors:** sensors are the electronic devices that measure various quantities from the different components and convert these measures to signals. Some of these are used by the controller in order to take corrective action while the rest allow the global monitoring of the system via the SCADA. One example is the measurement of output power several times per second. This allows orders the pitch control mechanism, to pitch the blades and discard the excess power.
- **Safety systems:** The wind turbine must have the capability of stopping in case of an emergency. Examples of emergency include an over-speed, highly turbulent wind speeds, disconnection of the generator from the grid, failure of one of the subsystems etc. For such an event the turbine is designed to use aerodynamic and mechanical breaks. In the case of aerodynamic braking, the wind turbine pitches the blades in order to cancel the aerodynamic lift and therefore stop the rotor. Mechanical brakes, usually discs braking are used as backup devices and are also used for parking the blades.

3.2 Basic Aerodynamics

The operating principal of a wind turbine is to extract kinetic energy from the wind. The aerodynamics of the rotor refers to the mutual interaction between the wind and the rotor. This interaction is most commonly described by Blade Element Momentum Theory (BEM), which considers the rotor as a disk, see Figure 3.4.

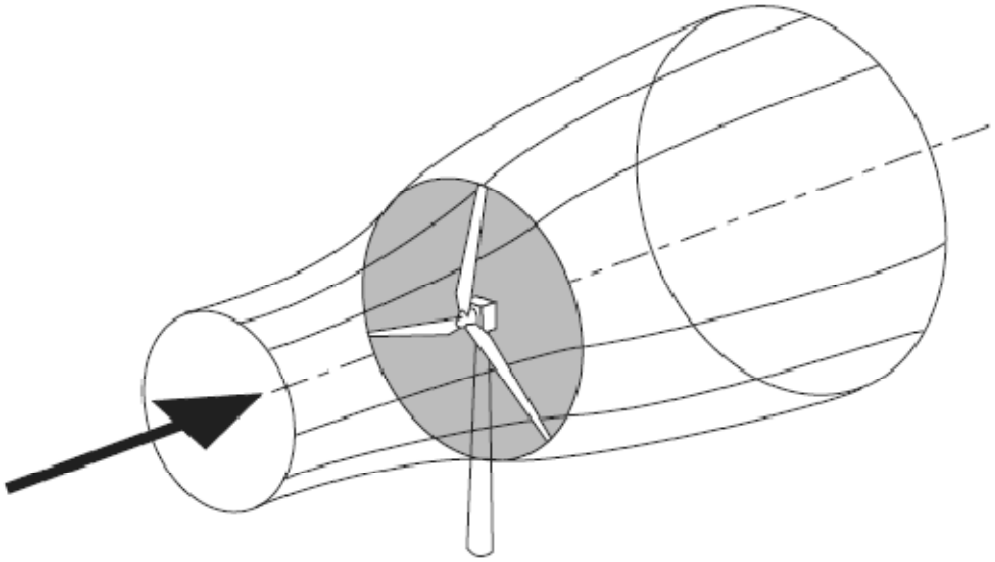

Figure 3.4: Disc representation of the turbine and the wind flow [65]

According to the BEM theory, the turbine extracts the energy by inducing a change in pressure across the swept disk. This causes part of the wind to slow down and this part is transformed from kinetic to mechanical energy by the turbine.

The ratio of the power extracted from wind over the energy going through the swept rotor area is called Power coefficient and is given by:

$$Cp = \frac{P}{\frac{1}{2}\rho A v^3} \tag{1}$$

In the above expression Cp is the power coefficient, P is the electrical power, A is the rotor area swept, v is the wind speed and ρ the air density ($1.225 kgr/m^3$).

The denominator of eq. (1) stands for the power available in the air if the rotor disk did not exist (theoretical power), hence the power coefficient is equal to [65], [68]:

$$Cp = 4\alpha(1-\alpha)^2 \tag{2}$$

where, α represents the axial inflow factor.

To find the maximum value we set the derivative of (2) equal to zero:

$$\frac{dCp}{d\alpha} = 0 \Rightarrow \alpha = 0.33 \tag{3}$$

Therefore the maximum possible value of the power coefficient is, $Cp_{max} = 0.59$, which is also known as the Betz limit or Betz coefficient.

3.3 Aeroelastic Design Codes

Detailed dynamic models are essential in any application where simulation is used to evaluate the design of a system. Especially for wind turbines, aeroelastic codes are an absolute must at all steps throughout the design and test process. For the task of designing and testing a controller such design codes provide the linear and nonlinear models. There are several commercial packages available, all with different levels of complexity and detail. The requirements that such a code must have are amongst others [70]:

- The ability to adapt to different wind turbine configurations. Standalone simulation software has to face the challenge of accounting for different number of blades, different types of generators, drive train configurations, masses changes, rotor imbalances etc.
- Exporting of linear models is an essential characteristic of such a piece of software. These are extremely useful when designing and tuning a controller, as well as when assessing the wind turbines dynamic behaviour.
- Accounting for couplings between different modes of the turbine that interact together.
- Ideally it must have a user friendly interface that allows for straightforward parameter adjustments for simulation and post-processing of data.
- Experience shows that easy exporting of data files, which can be read by other programs for manipulation and analysis (e.g. Matlab), is also very helpful.

A substantial presentation and comparison of most of the existing aeroelastic codes is also made in [70]. A brief description of a few of these codes follows:

- GH Bladed: It is "an integrated software package for wind turbine performance and loading calculations" [31]. It has a friendly user interface and is able to carry out sophisticated tasks having to do with:
    1. Manipulation of all the parameters of a wind turbine
    2. Specification of environmental inputs and load cases
    3. Rapid calculation of steady-state performance characteristics
    4. Dynamic simulation covering all turbine states and allowing the use of a user-defined controller
    5. Post-processing of results

GH Bladed has been certified by Germanischer Lloyd, and it is developed by Garrad Hassan & Partners in Bristol, England. This software package was used for the validation and simulation results presented in this thesis.

- FAST: Stands for Fatigue, Aerodynamics, Structures and Turbulence and was developed in the Oregon State University in collaboration with NREL. It is relatively fast because of the limited degrees of freedom and can model any wind turbine configuration [28]. It uses modal representation for the flexible parts of the wind turbine and also uses AeroDyn for the representation of the dynamics of the rotor. It is a public domain piece of software available to anyone.
- FLEX5: This software package was developed in the Technical University of Denmark. It can simulate wind turbines with different number of blades whether they are pitch controlled or stall controlled and fixed or variable speed. The user interface is not as friendly as in the previous codes mentioned, yet the simulations are very fast.
- GAST: It is a General Aerodynamic and Structural Prediction Tool, and was developed by the National Technical University of Athens in Greece. It is able to perform full simulations of wind turbines over a wide range of operational conditions [29], as well as post-processing of data and load analysis.

Other Design Codes, such as DUWECS, FOCUS, GAROS, PHATAS, GAROS, YawDyn, AeroDyn, etc., exist having similar possibilities with the ones described and a more complete discussion of these may be found in [70].

3.4 Wind Turbine Modelling and Dynamics

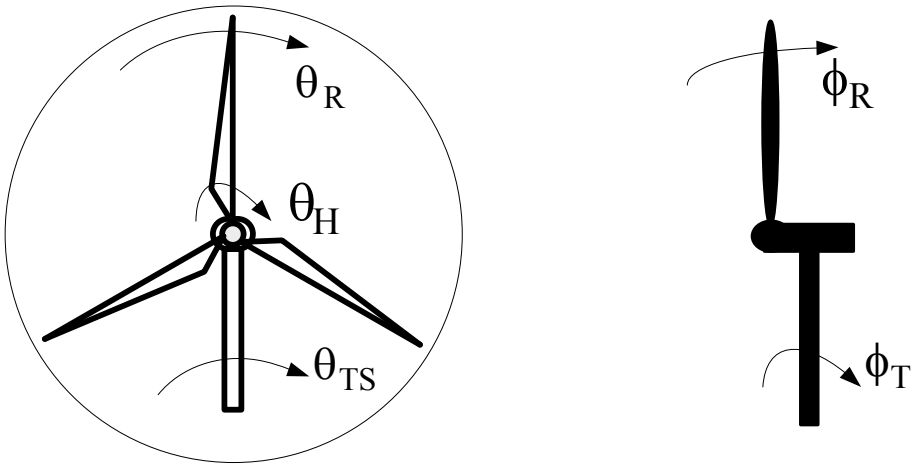

Figure 3.5: Modelling parameter representation of the Wind Turbine

The derivation of the dynamic wind turbine models used here in the Simulink simulation for the controller design is described in detail in [12], [13]. It includes all necessary components for a full wind turbine operation and includes, wind speed, aerodynamics, rotor dynamics, tower dynamics, drive-train dynamics, actuator dynamics, converter dynamics and of course the control dynamics.

As far as rotor dynamics are concerned, the structural (low frequency) modes that interact directly with the drive train are included. Each blade has two dominant modes, the flapwise and the edgewise. Both modes contribute to the dynamics of the drive train. There are three modes of the rotor with, one blade stationary and two oscillating at the same frequency but out of phase. Adding these motions together the result is zero and therefore they constitute only two independent modes of the rotor. The third mode is that with all three blades oscillating at the same frequency in phase. The frequency of the edgewise motion of the rotor is the same as the edgewise frequency of one individual blade. This third mode is the most important contribution to the rotor dynamics as it is the only low frequency mode to directly transmit low frequency loads to the drive train. Similarly, the only flapwise rotor mode essentially affecting the dynamics of the drive train is the one with all three blades oscillating in

phase (and having the same frequency). Therefore, the rotor can be modelled as a single blade.

The fore and aft movement of the tower, as well as the out of plane mode of the rotor couple with the rotor and drive train. As mentioned earlier all the dynamics affecting the design of the controller are included in the model. Therefore, dynamics, such as the in-plane and out-of-plane rotor modes and the first dominant mode of the tower, are modelled, as they may cause Right Half Plane Zeros (RHPZ's) and limit the controller design. These RHPZ's are apparent in the dynamics linking pitch angle to generator speed, and are thoroughly discussed in Chapter 6.

$$Q = \frac{1}{2}\frac{\rho\pi C_p(\lambda,\beta)R^2v^2}{\lambda} \tag{4}$$

where β is the pitch angle, R is the radius of the rotor and λ the tip-speed ratio.

The in-plane aerodynamic torque Q, is given by (4) and the out-of-plane aerodynamic torque $Q2$, is given by (5) and (6).

$$Q2 = \frac{1}{cos\beta}(Qf - Qsin\beta) \tag{5}$$

$$Qf = \frac{1}{2}\frac{L}{R}\rho\pi R^3 C_T(\lambda,\beta)v^2 \tag{6}$$

where, L is the effective length of the blade and C_T is the thrust coefficient.

The dynamics of the drive train comprise the hub, low speed shaft, gearbox, high speed shaft, generator, and the tower side-to-side movement, caused by the generator reaction torque. Different distributions of the inertias within the drive train may be made, however the dominant frequency of the drive train will remain the same. In order to keep the model simple the drive train is modelled as a two mass lumped parameter model (hub and generator rotor). The inertia of the hub is incorporated into the gearbox through the low speed shaft. The inertias of the two shafts are distributed to both their ends i.e. the hub and the generator rotor. The equations for the aerodynamics, rotor dynamics and tower dynamics are given in equations (7) to (9). The parameters are explained in the nomenclature and some of the parameters

regarding the movement of the blades and tower are depicted in Figure 3.5, in which θ_R is the in-plane rotational displacement of the centre of mass of the blade, is the angular position of the hub, Φ_R is the out-of-plane rotational displacement of the centre of mass of the blade, Φ_T is the in-plane rotational displacement of the tower and θ_{TS} is the side to side position of the tower.

Aerodynamics:

$$J\ddot{\theta}_R = -\left(K_E + J\dot{\theta}_R^2\right)[(\theta_R -)cos\beta - (\Phi_R - \Phi_T)sin\beta]cos\beta - \left(K_F + J\dot{\theta}_R^2\right)[(\theta_R - \theta_H)sin\beta + (\Phi_R - \Phi_T)cos\beta]sin\beta + F_1 \quad (7)$$

Rotor dynamics:

$$\frac{1 - \frac{J_C^2}{JJ_T}}{1 + \frac{J_C}{J_T}} J\ddot{\Phi}_R = +\left(K_E + J\dot{\theta}_R^2\right)[(\theta_R - \theta_H)cos\beta - (\Phi_R - \Phi_T)sin\beta]sin\beta - \left(K_F + J\dot{\theta}_R^2\right)[(\theta_R - \theta_H)sin\beta + (\Phi_R - \Phi_T)cos\beta]cos\beta + \left[F_2 + \frac{J_C}{J_T} B_T\dot{\Phi}_T + \frac{J_C}{J_T} K_T\Phi_T\right]/(1 + \frac{J_C}{J_T}) \quad (8)$$

Tower dynamics:

$$\frac{1 - J_C^2/JJ_T}{1 + J_C/J_T} J\ddot{\Phi}_T = -\left(K_E + J\dot{\theta}_R^2\right)[(\theta_R - \theta_H)cos\beta - (\Phi_R - \Phi_T)sin\beta]sin\beta + \left(+J\dot{\theta}_R^2\right)[(\theta_R - \theta_H)sin\beta + (\Phi_R - \Phi_T)cos\beta]cos\beta - \left[B_T\dot{\Phi}_T + K_T\Phi_T + \frac{J_C}{J} F_2\right]/(1 + \frac{J_C}{J}) \quad (9)$$

3.5 Full State Space Model

In order to take full advantage of the benefits that classical control provides it is convenient to convert the wind turbine model to a form that may be easily manipulated. The modern engineering trends are towards more complex models so that they may accommodate more degrees of freedom. The state space representation of a complex system gives access to all the input, output and state variables. Although the state space representation of a system is not unique and depends on the needs of the designer, the number of states remains always the same. The significance of state space equations is that the input, output and state variables are related to each other through first order differential equations. As this representation helps in the analysis and modelling of the wind turbine system, it is convenient to start by presenting the linearised dynamics of the entire system (aerodynamics, rotor dynamics, drive train dynamics and tower dynamics) in the state space format. These equations are the results of the research presented in [12], [13] and [41]. For ease of manipulation of the system it is presented in two state space models for two separate subsystems. The first one consists of the rotor dynamics and the other one contains the rest of the drive-train dynamics.

3.5.1 Rotor State Space Model

The state space model is represented by two subsystems. One consists of the rotor dynamics and the second one of the drive train dynamics.

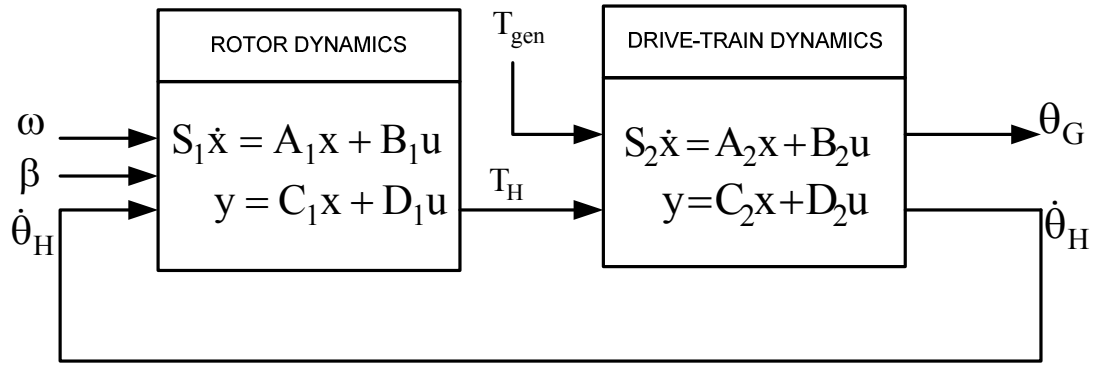

Figure 3.6: Wind Turbine State Space Representation

The states of the rotor dynamics are as follows:

$$x_1 = \theta_R - \theta_H,\ x_2 = \Phi_R, x_3 = \Phi_T, x_4 = \dot{\theta}_R, x_5 = \dot{\Phi}_R, x_6 = \dot{\Phi}_T, u_1 = \omega,$$

$$u_2 = \beta, y = T_H$$

The state space model is presented below:

$$\dot{x}_1 = x_4 - \dot{\theta}_{\mathrm{H}}$$

$$\dot{x}_2 = x_5$$

$$\dot{x}_3 = x_6$$

$$\dot{x}_4 = -(\omega_E^2 \cdot cos^2\beta_0 + \omega_F^2 \cdot sin^2\beta_0) \cdot x_1 + (\omega_E^2 - \omega_F^2) \cdot sin\beta_0 \cdot cos\beta_0 \cdot x_2 -$$

$$-(\omega_E^2 - \omega_F^2) \cdot sin\beta_0 \cdot cos\beta_0 \cdot x_3 + \frac{1}{J}\frac{\partial F_1}{\partial \dot{\theta}_R} \cdot x_4 - \frac{L}{J}\frac{\partial F_1}{\partial \omega} \cdot x_5 - \frac{h}{J}\frac{\partial F_1}{\partial \omega} \cdot x_6 +$$

$$+\frac{1}{J}\frac{\partial F_1}{\partial \omega} \cdot u_1 + \frac{1}{J}F_{1\beta} \cdot u_2$$

$$\frac{1 - \frac{J_C^2}{J_T J}}{1 + \frac{J_C}{J_T}} \cdot \dot{x}_5 = (\omega_E^2 - \omega_F^2) \cdot x_1 - (\omega_E^2 \cdot sin^2\beta_0 + \omega_F^2 \cdot cos^2\beta_0) \cdot x_2 +$$

$$+\left(\omega_{\mathrm{E}}^2 \cdot \sin^2\beta_0 + \omega_{\mathrm{F}}^2 \cdot \cos^2\beta_0 + \frac{\mathrm{J_C K_T}}{\mathrm{J(J_T + J_C)}}\right) \cdot \mathrm{x_3} + \frac{\mathrm{J_T}}{\mathrm{J(J_T + J_C)}}\frac{\partial \mathrm{F_2}}{\partial \dot{\theta}_{\mathrm{R}}} \cdot \mathrm{x_4} -$$

$$-\mathrm{L}\frac{\mathrm{J_T}}{\mathrm{J(J_T + J_C)}}\frac{\partial \mathrm{F_2}}{\partial \omega} \cdot \mathrm{x_5}\ \frac{\mathrm{J_T}}{\mathrm{J(J_T + J_C)}}\left(\mathrm{h}\frac{\partial \mathrm{F_2}}{\partial \omega} - \frac{\mathrm{J_C}}{\mathrm{J_T}}\mathrm{B_T}\right) \cdot \mathrm{x_6} +$$

$$+\frac{J_T}{J(J_T+J_C)}\frac{\partial F_2}{\partial \omega} \cdot u_1 + \frac{J_T}{J(J_T+J_C)}F_{2\beta} \cdot u_2$$

$$\frac{1-\frac{J_C^2}{J_T J}}{\mathrm{J}+J_C} J_T \cdot \dot{x}_6 = -(\omega_E^2 - \omega_F^2) \cdot sin\beta_0 \cdot cos\beta_0 \cdot x_1$$
$$- (\omega_E^2 \cdot sin^2\beta_0 + \omega_F^2 \cdot cos^2\beta_0) \cdot x_2$$
$$- \left(\omega_E^2 \cdot sin^2\beta_0 + \omega_F^2 \cdot cos^2\beta_0 + \frac{K_T}{J+J_C}\right) \cdot x_3 - \frac{J_C}{J(J+J_C)} \frac{\partial F_2}{\partial \dot{\theta}_R} \cdot x_4$$
$$+ \mathrm{L} \frac{J_C}{J(J+J_C)} \frac{\partial F_2}{\partial \omega} \cdot x_5 + \frac{1}{J+J_C} \left[\mathrm{h} \frac{J_C}{J} \frac{\partial F_2}{\partial \omega} - B_T\right] \cdot x_6 - \frac{J_C}{J(J+J_C)} \frac{\partial F_2}{\partial \omega}$$
$$\cdot u_1 - \frac{J_C}{J(J_T+J_C)} F_{2\beta} \cdot u_2$$

$$y = J(\omega_E^2 \cdot cos^2\beta_0 + \omega_F^2 \cdot sin^2\beta_0) \cdot x_1 - J(\omega_E^2 - \omega_F^2) \cdot \mathrm{sin}\beta_0 \cdot \mathrm{cos}\beta_0 \cdot x_2 +$$
$$+ J(\omega_E^2 - \omega_F^2) \cdot \mathrm{sin}\beta_0 \cdot \mathrm{cos}\beta_0 \cdot x_3 + \left(\frac{\partial F_1}{\partial \beta} - F_{1\beta}\right) \cdot u_1$$

3.5.2 Drive-Train State Space Model

The states and state space model for the drive-train model are presented below:

$$y_1 = x_1$$

$$y_2 = x_6$$

$$u_1 = T_H$$

$$u_2 = T_{gen}$$

$$\dot{x}_1 = \frac{1}{I_{Ls}} (u_1 - \gamma_{Ls} \cdot x_1 - \bar{x})$$

$$\dot{x}_2 = \bar{K}_{Ls} \left(x_1 - \frac{n-1}{n} \cdot x_3 + \frac{1}{n\gamma_2^*} \cdot x_5 - \frac{1}{n} \cdot x_6 - \frac{1}{n^2\gamma_2^*} \cdot \bar{x}\right)$$

$$\dot{x}_3 = \frac{1}{J_{TS}} \left(\frac{n-1}{n} \cdot \bar{x} - \mathrm{B_{TS}} \cdot x_3 - x_4\right)$$

$$\dot{x}_4 = \mathrm{K_{TS}} \cdot x_3$$

$$\dot{x}_5 = \frac{K_{Hs}}{\gamma_2^*}\left(\frac{\bar{x}}{n} - x_5\right)$$

$$\dot{x}_6 = \frac{1}{I_{Hs}}\left(\frac{1}{n}\cdot \bar{x} - \gamma_{Hs}\cdot x_6 - u_2\right)$$

where,

$$\bar{x} = \left(\frac{n^2\gamma_2^*}{\gamma_1^* + n^2\gamma_2^*}\right)\left[\gamma_1^*\cdot x_1 + x_2 - \frac{n-1}{n}\gamma_1^*\cdot x_3 + \frac{\gamma_1^*}{n\gamma_2^*}\cdot x_5 - \frac{\gamma_1^*}{n}\cdot x_6\right]$$

Having defined the full state space model, it is extensively used in the following chapters and serves as the basis for the design of all the controllers discussed. The derivation of all the Bode plots linking different inputs and outputs are derived from the above equations.

4 Energy Capture Assessment for Large Wind Turbines

The operational strategy in below rated operation of a variable speed wind turbine is frequently chosen to maximise the energy capture. To do so the operating state of the wind turbine is caused to track the maximum aerodynamic efficiency curve, the so-called Cp-max curve. Whether it does so accurately depends on the wind turbine controller. It is sometimes claimed that the energy capture can be increased by better design of this controller. This claim is thoroughly examined in the present Chapter. The energy capture per year achieved by different control algorithms and strategies is assessed as a percentage of the total energy available with an ideal strategy. These estimates are obtained using a Simulink simulation of a large 1.7MW commercial wind turbine that enables the latter to be determined. The results from the Simulink model imply that the energy capture is very weakly dependent on the control algorithm. There is more dependence on the choice of control strategy but even here the potential gains are limited. As is thoroughly discussed here the Simulink simulation enables the use of an effective wind speed as an input to the wind turbine. To support the use of Simulink to investigate the energy capture, the model is validated against a GH Bladed model of the same wind turbine. This validation also supports the claim that the Simulink model of the wind turbine described here provides an accurate guide for tuning the controller.

4.1 Introduction

The aim of this chapter is to assess the effectiveness of a MW scale wind turbine in extracting energy from the wind, and to examine the claim that better design of the below rated controller would increase the energy capture. Much research has been done on the hunt for new methods of control to maximize the energy captured by the wind turbine. Different approaches are present in the literature concerning the issue of energy capture.

In general modern large machines have $C_p - \lambda$ curves with a broad flat peak. This is further flattened through the "averaging" of the variation in wind speed over the rotor disc. In studies on rotors with sharper $C_p - \lambda$ curves and large rotor inertia, there are cases when energy capture may be increased by better tuning of the controller. For example, in [1] it is suggested that by modifying the controller gain by 10% an increase of 0.5% in energy capture may be achieved. The issue of determining the optimum controller gain is also discussed in [1], and an adaptive controller is proposed that seeks the best gain that maximizes energy capture, catering for changes to the optimal operating point because of turbulence. The effect of different rotor characteristics and their corresponding $C_p - \lambda$ curves, together with the tracking errors associated with these characteristics, is thoroughly analysed in [6]. Different approaches have also been analysed, such as the one proposed in [7], presenting a complete fuzzy logic control based generation system, one component of which checks online for the desired generator speed for optimal aerodynamic efficiency. An adaptive fuzzy controller approach is presented in [8] to maximise energy capture, by continuously optimizing the internal parameters and adapting them to the system. A self optimizing controlled scheme called "Extremum Seeking Control (ESC)" is presented in [9], promising better practical implementation of the controller, to achieve a significant increase in power output. Other approaches include Nonlinear robust control, as in [10], optimizing the blade pitch for a better tracking of the maximum coefficient curve, and Neural network solutions, as in [11], to compensate for the fluctuations of the generator speed from Cp maximum curve. All these different control methods seek to maximise energy capture from the wind. In contrast, the more basic question of whether the controller has a significant impact on energy capture is conducted here.

The present Chapter is organised as follows. In section 2, a brief description (the detailed description is given in Chapter 3) is given of the Simulink model and the controllers used for the aerodynamic efficiency analysis of this research. Section 3, provides a description and the reasoning for use of the effective wind model used in the Simulink simulation. Section 4, presents a detailed validation of the Simulink model, which is given through extensive comparisons with the commercially and industrially accepted software GH Bladed. These comparisons are presented through

normalized energy capture plots of the two models for a range of different controller gains and wind seeds. Section 5, provides the detailed aerodynamic efficiency analysis and presents the results as a percentage of the total energy capture that would have been possible through an ideal operating strategy. Finally the last section summarises the work done and conclusions are drawn.

4.2 Description of Simulink model and Controller

In order to conduct the research concerning the aerodynamic efficiency of the rotor of the wind turbine, a Simulink model of the wind turbine and its controller is used. This is done because the Simulink model provides with the ability to test a wind turbine using an effective wind speed as an input. Effective wind speed, see Figure 4.2, is the uniform wind speed over the rotor area producing the same aerodynamic effects as the stochastic non-uniform wind field, and is thoroughly discussed in the following section.

Bladed uses a non-uniform wind field; see Figure 4.1 and Figure 4.3, in which wind speed has different values across the rotor area. Therefore, the exact calculation of the energy extracted from the wind and the power output at a specific time is not straightforward. On the other hand, using effective wind speed, enables the exact calculation of power output for a specific input wind speed. This power output can be then compared to the ideal value of power that could have theoretically been extracted.

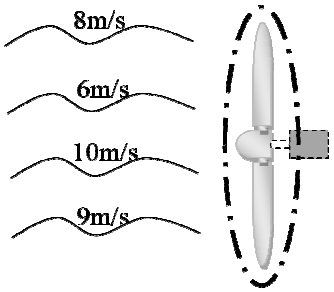

Figure 4.1: Point wind speed

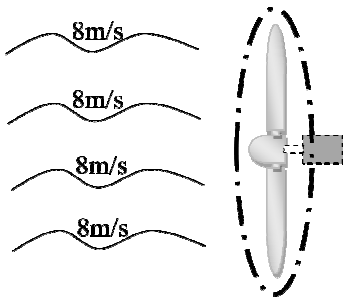

Figure 4.2: Effective wind speed

The power captured by a wind turbine is determined by the aerodynamic efficiency of its rotor. The way the rotor operates in order to maximize the power captured, is mainly determined by the control strategy of the wind turbine. The rotor of the wind

turbine continuously interacts with a complex wind field which is responsible for causing lift on the blades and therefore rotor torque that drives the machine.

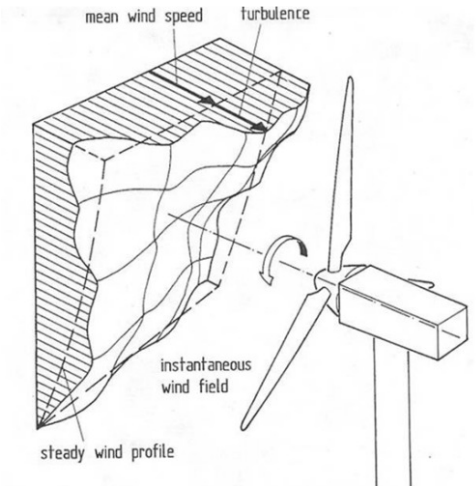

Figure 4.3: Non-uniform wind field representation [72]

The power coefficient is the main quantification of efficiency and depends on pitch angle β, the wind speed v, and the rotor speed Ω. In the below rated operating region the rotor is regulated to achieve constant speed for the first and third operating regions, and maximization of energy capture by tracking the optimum power coefficient curve for region two (see Figure 4.15). This is a region in which the torque value at each time corresponds to the maximum value of the power coefficient curve and is given by (10).

$$T = K_{opt}\omega^2 \tag{10}$$

where, T is the generator reaction torque, K_{opt} is the controller gain for tracking the power coefficient curve and ω the generator speed.

As far as the controller is concerned, torque is used for below rated wind speeds to control the rotor speed. In above rated wind speeds, pitch is used to control the rotor speed and torque is used to control the power of the wind turbine. The torque controller includes a classical controller for the two constant speed regions shown in Figure 4.15, whereas the Cp_{max} region is tracked through (10) with no active control being involved. Of course a full envelope switching scheme is embedded in the controller to achieve smooth switching between the different modes (described in Section 5.9). In above rated wind speeds, the pitch controller deploys “gain

scheduling" techniques, to compensate for the aerodynamic nonlinearities arising from the dependence of aerodynamic torque on the rotor speed, pitch angle and the wind speed. The detailed design and analysis of the controller is presented in Chapter 5.

4.3 Effective Wind Speed Model

Effective wind speed is the uniform wind speed over the rotor area that induces the same aerodynamic forces as the non-uniform wind field [14]. This effective wind speed model, see Figure 4.4, may be produced by filtering the point wind speed.

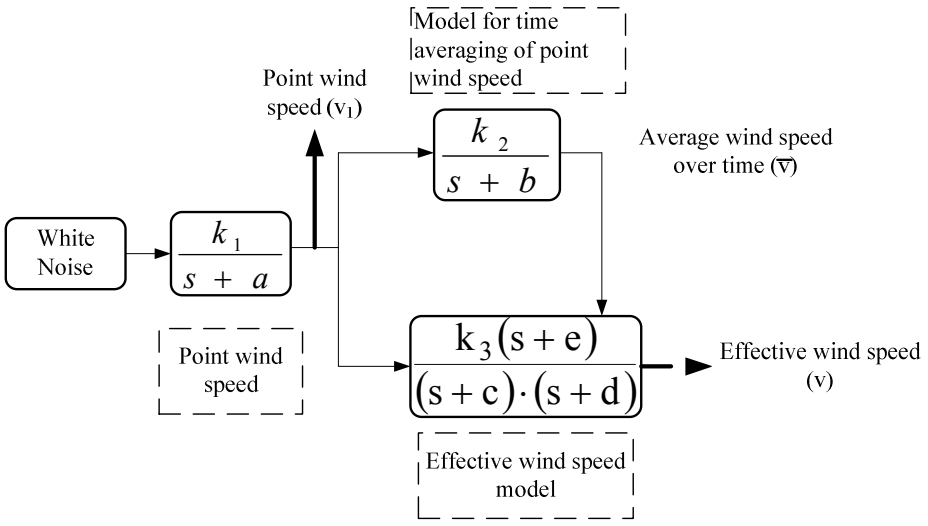

Figure 4.4: Effective wind speed model

The effective wind speed spectrum, in contrast to the point wind speed, has its power enhanced at integer multiples of the rotational angular velocity Ω_0, but power is depleted elsewhere as described in [14], [15], [16].

The dynamics of the "spatial filter" applied to the wind speed in Figure 4.4 are given by (11), which represents the rotational averaging of the wind speed.

$$\frac{k_3(s+e)}{(s+c)(s+d)} = \frac{\frac{1}{\sigma}\left(s+\frac{\sqrt{2}}{\sigma}\right)}{\left(s+\frac{\sqrt{2}}{\sqrt{\alpha'}\sigma}\right)\left(s+\frac{\sqrt{\alpha'}}{\sigma}\right)} \tag{11}$$

Where:

$$\sigma = \frac{\gamma R}{\hat{V}} \tag{12}$$

γ being the turbulent wind speed decay factor, $\hat{V}$ the short term mean wind speed and suggested values $\gamma = 1.3$ and $\alpha' = 0.55$.

The input to the spatial filter is a point wind speed. Quite a few models have been presented for wind speed fluctuations. Their general form is given by (13).

$$S_u(\omega) = \frac{K_u|\omega|^k}{[1 + (\omega T_u)^a]^\delta} \tag{13}$$

In the model of equation (13), K_u and T_u, are constants mainly affected by the turbulence of the wind, the surface roughness and the mean wind speed. The parameters α, δ and k, are powers depending on the spectrum in question. Examples of widely used models for point wind speeds are the Von Karman, Dresden, Kaimal and the Davenport. The one that was used for the simulations included here in both Bladed and Simulink (before the spatial filtering) is the Von Karman spectrum, which is said to be the most appropriate for a few minutes duration of simulations of point wind speed, and is given by (14).

$$S_{VK}(\omega) = 0.475\sigma_u^2 \frac{(L/\hat{V})}{(1 + (\omega L/\hat{V})^2)^{5/6}} \tag{14}$$

Where, σ_u is the wind turbulence intensity, $\hat{V}$ is the 10 minute mean wind speed and L is the length scale of the turbulence. The spectra of the point and spatially filtered wind speeds are depicted in Figure 4.5.

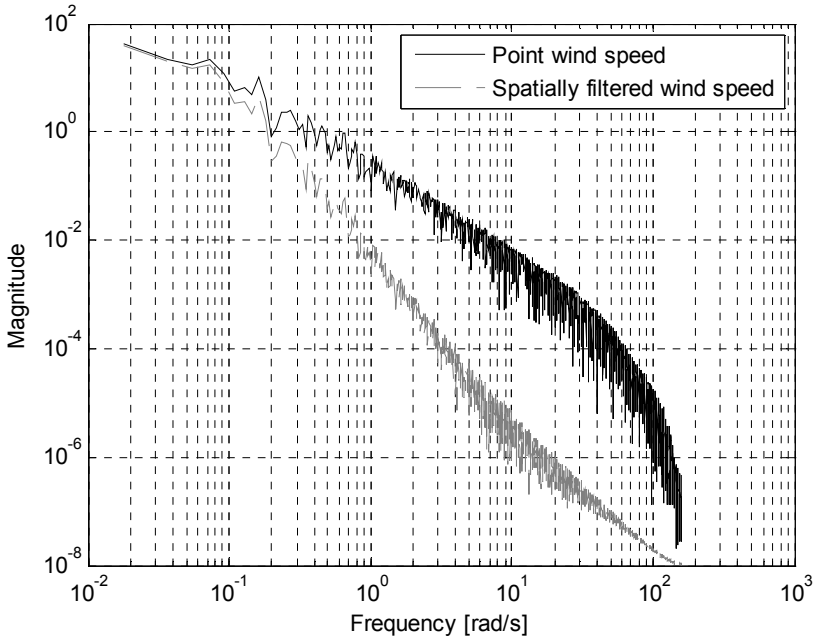

Figure 4.5: Power spectral density of point and spatially filtered wind speed

4.4 Validation of the Model

Amongst others, one software package that is widely accepted in the wind energy community is GH Bladed. Therefore, the Simulink model that is being used for the assessment of the aerodynamic efficiency of the wind turbine is compared with Bladed. This is done in order to verify that by conducting the aerodynamic efficiency analysis using the Simulink model, similar results and operational behaviour would have been acquired by using Bladed. For the purpose of this study the wind turbine is extensively tested using the same controller but different controller gains for the tracking of the below rated Cp curve. The simulations are conducted for uniform wind speeds, as well as for turbulent wind for turbulences of 5% and 10%. The vertical axis of Figure 4.6 through Figure 4.8 depict the normalised energy capture for the two models compared for seven different controller gains and three different seeds of wind.

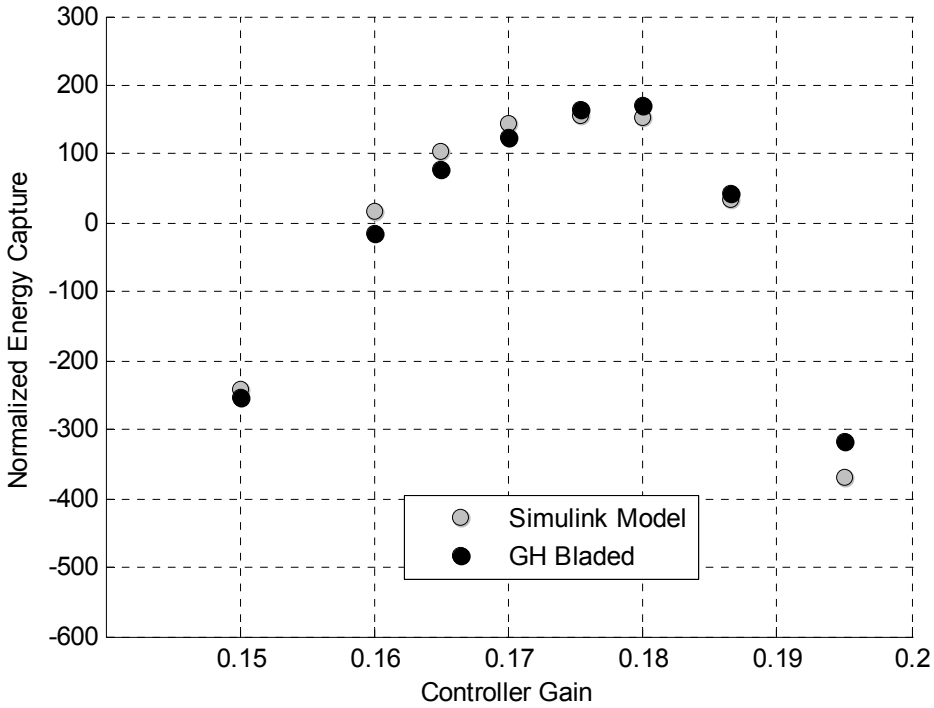

Figure 4.6: Comparison of Bladed Vs Simulink for different controller gains for uniform wind speed

Each of the two models is run for wind speeds from cut-in (4m/s) to cut-out (24m/s) and for the controller gain values shown on the plots. After obtaining and averaging the results from all the runs, they where normalized. This is done by subtracting the average value of all the runs, from each individual run. This allows the two models to be brought to the same scale for comparison reasons. Wind is stochastic; therefore three different seeds are averaged for the accurate presentation of the results. As may be observed from Figure 4.6 through Figure 4.8 there is significant agreement between the trends that the two models follow. The peaks of all the graphs, which shows the maximum energy capture possible and the associated controller gain, coincides for the two models, as does the overall nature of the curves. Moreover, it can be inferred that the Simulink simulation model can be effectively used to tune the wind turbine controller with, similar results to Bladed.

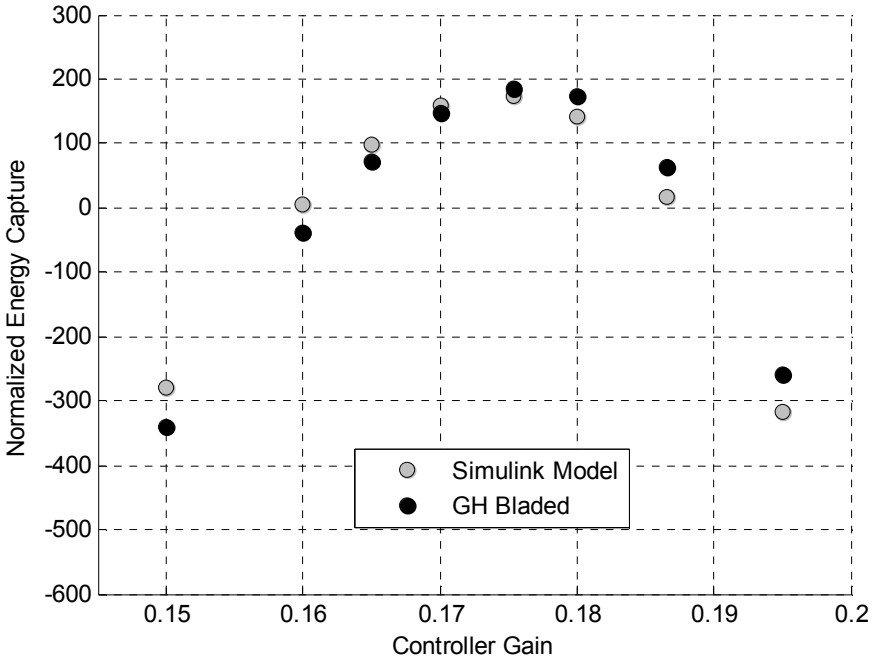

Figure 4.7: Comparison of Bladed Vs Simulink for different controller gains and 5% turbulence intensity.

Moreover, in addition to the previous comparisons for validation of the Simulink model, the power spectral density functions of the hub torque for both Bladed and Simulink models are also compared in Figure 4.9. As previously mentioned GH Bladed uses a 3D turbulent wind field whereas in the Simulink effective wind speed filter only the 3P and 6P components of the spectrum are enabled. Even in this case an accurate match is observed between the two models.

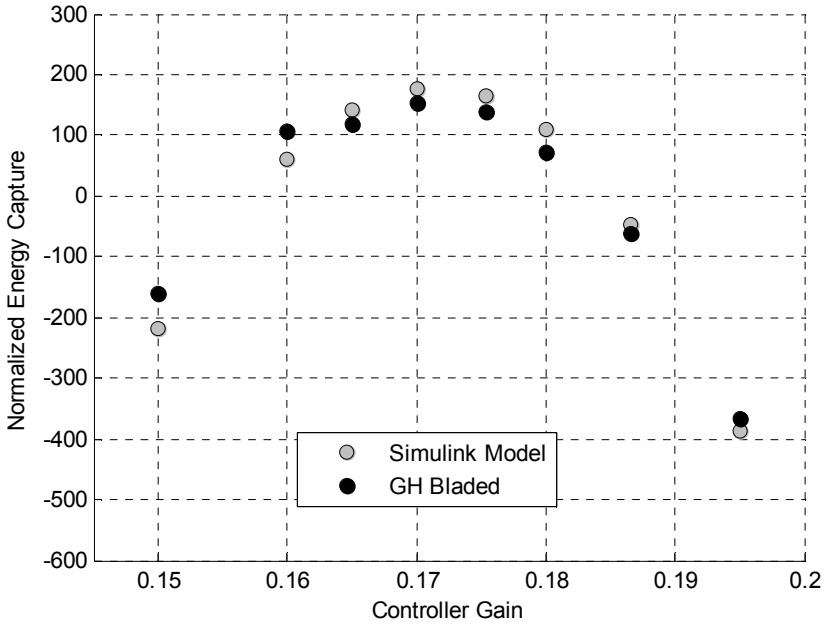

Figure 4.8: Comparison of Bladed Vs Simulink for different controller gains and 10% turbulence intensity.

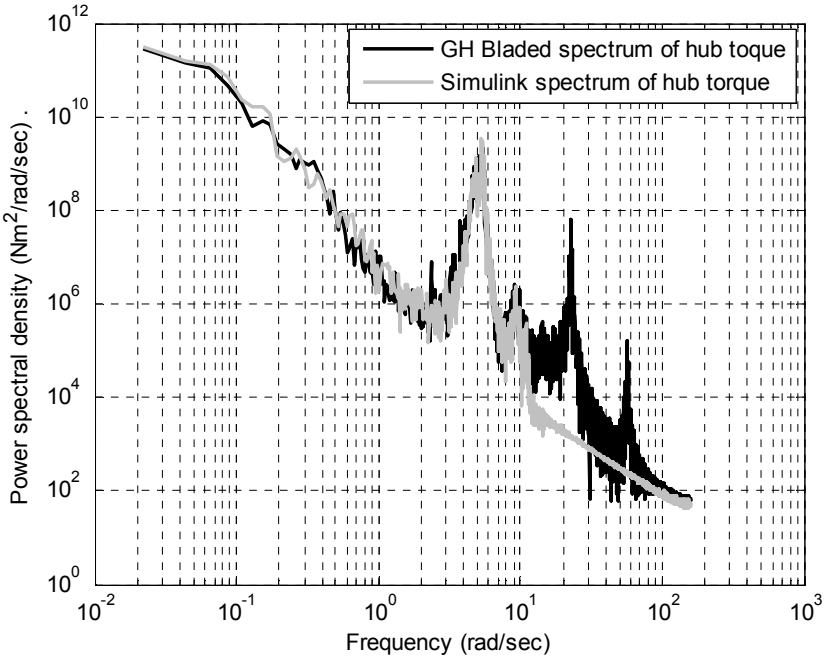

Figure 4.9: Power spectral density of hub torque for both the Simulink and the Bladed model

4.5 Efficiency Analysis

The potential energy capture capability of a wind turbine is dependent on the aerodynamic properties of the rotor, and its operating mode. The purpose of the efficiency analysis done here is to compare the actual input power extracted from the wind by the wind turbine rotor with the ideal maximum input power that theoretically could be extracted from the wind. The actual input power curve is combined with the wind speed probability distribution function to obtain the yearly energy capture and thereby the aerodynamic efficiency. The optimum gain for the controller, as obtained in Section 4.4, is used for this assessment and full runs for wind speeds from cut-in to cut-out are conducted. The results are then compared to results from runs, using controller gains others than the optimum one. This is done to investigate the extent to which maximizing the energy capture of a wind turbine depends on the chosen operating strategy of the turbine. The rotor efficiency is given by the following ratio:

$$\text{Rotor efficiency} = \frac{\text{Actual Input Power}}{\text{Ideal Input Power}}$$

For the efficiency plots shown below the ideal Input power is calculated directly from the steady state characteristics of the wind turbine. Note, this is only possible due to using the effective wind speed in the Simulink wind turbine model. Input power is defined as the product of the Aerodynamic torque on the rotor times the rotor speed. A full set of simulation runs is conducted and the Bin method is used to obtain the dependence of input power on wind speed.

The Bin method refers to the procedure whereby data (in this case input power) is sorted into discrete groups (Bins) for a set of wind speed intervals. Each bin (interval) is allocated the average of the input power values allocated by wind speed to that Bin for a particular time series. The full efficiency envelopes for wind turbulences of 5%, 10% and 15% are presented in Figure 4.10 through Figure 4.12.

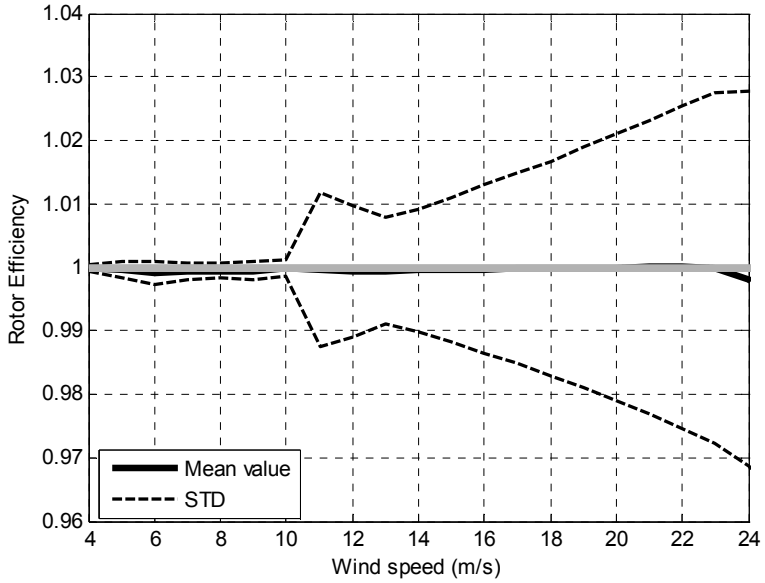

Figure 4.10: Efficiency plot for 5% turbulent wind

It is obvious from the plots (Figure 4.10 through Figure 4.12) that the efficiency is very close to one, with one being the theoretical maximum efficiency. As expected, as turbulence increases the rotor gets disturbed further from its operating strategy curve, resulting in a slight loss of energy. This energy loss occurs in the below rated region between the wind speeds of 4m/s and 12m/s, in which the rotor is controlled to extract as much energy from the wind as possible.

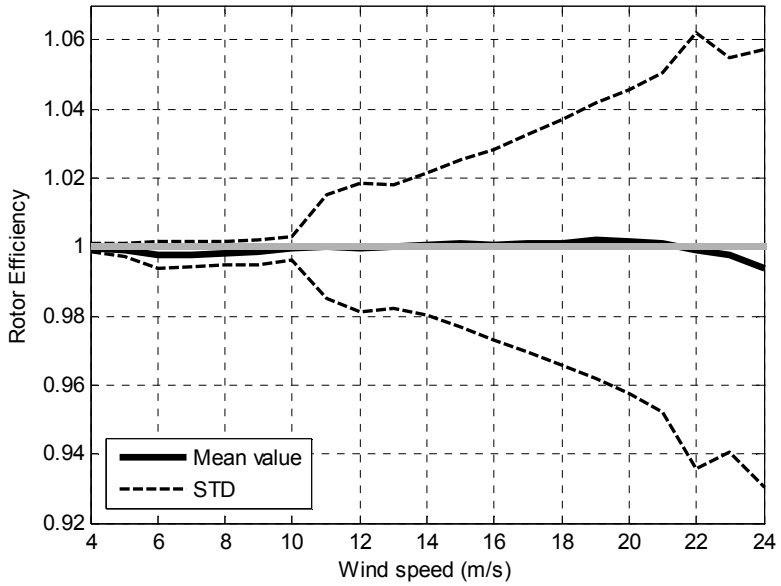

Figure 4.11: Efficiency plot for 10% turbulent wind

During the above rated operating region, the blades of the wind turbine pitch in order to discard wind disturbances, while the rotor speed and consequently the generator speed is constant, maintaining the power output to its nominal (rated) value. Therefore energy capture depends on rotor efficiency and is relevant in the below rated operation of the wind turbine.

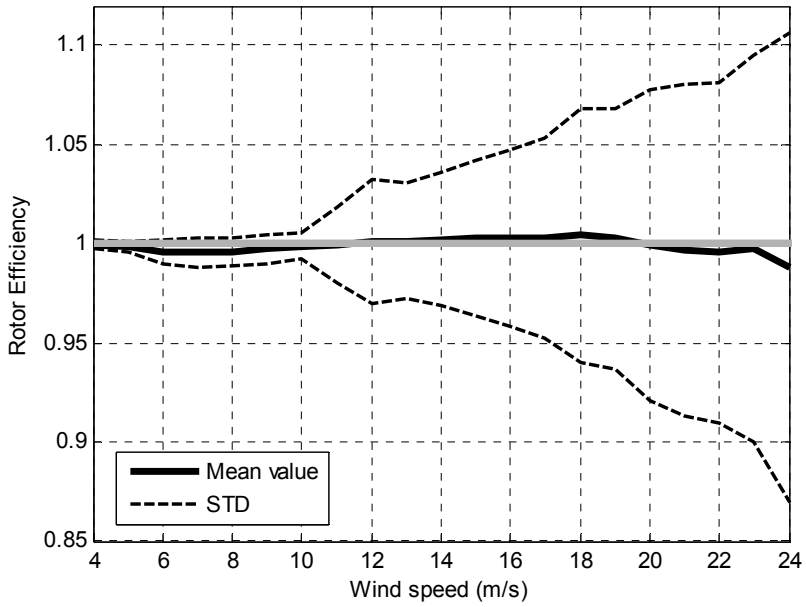

Figure 4.12: Efficiency plot for 15% turbulent wind

In the Weibull distribution the wind speed and its variations are described by two functions. The first one is the probability density function which indicates the probability each wind speed lies at a certain speed. The second one is the probability function, which is the integral of the probability density function. The Weibull distribution [71] used is given by (15).

$$f(V) = \frac{k}{c}\left(\frac{V}{c}\right)^{k-1} e^{-\left(\frac{V}{c}\right)^{k}} \tag{15}$$

where k is the Weibull shape factor and c is the Weibull scale factor. The mean wind speed at any site following the Weibull distribution is given by (16).

$$\bar{V} = \int_{0}^{\infty} V f(V) dV \tag{16}$$

Once the Weibull probability distribution is determined for specific site conditions, it

is multiplied by the mean values of the input power values for each wind speed obtained from the simulation, giving the annual energy distribution of the specific site.

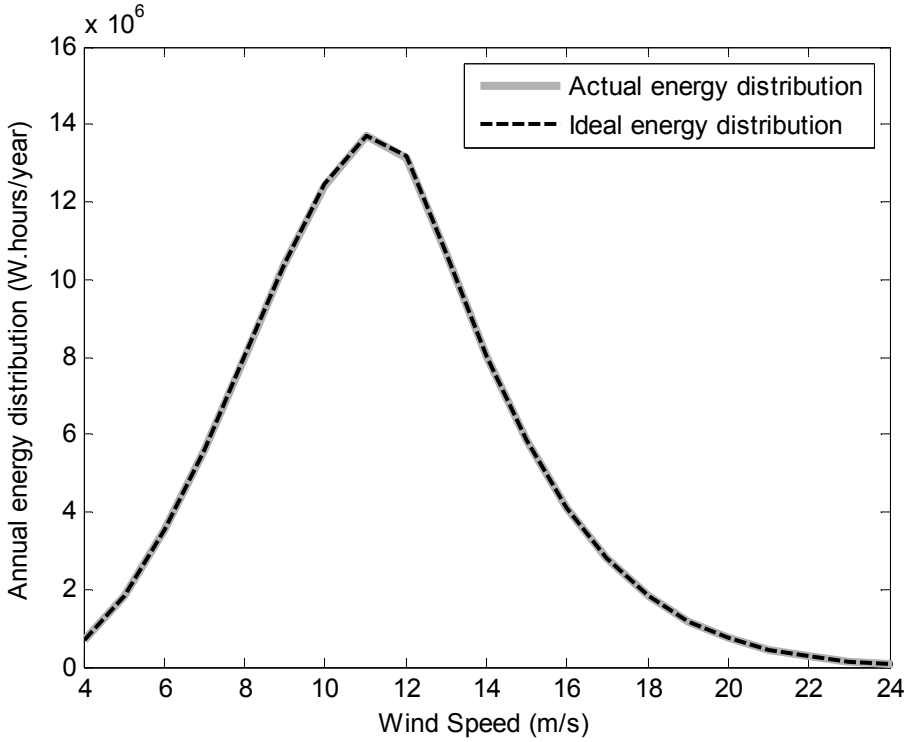

Figure 4.13: Annual energy distribution

The annual distribution shown in Figure 4.13 is for site conditions with an annual mean wind speed of 7.5m/s and a shape factor of $k = 2$.

The annual energy capture of the wind turbine assessed, is given by the integration of the product of the mean of the input power values, times the probability distribution and is shown in Figure 4.14.

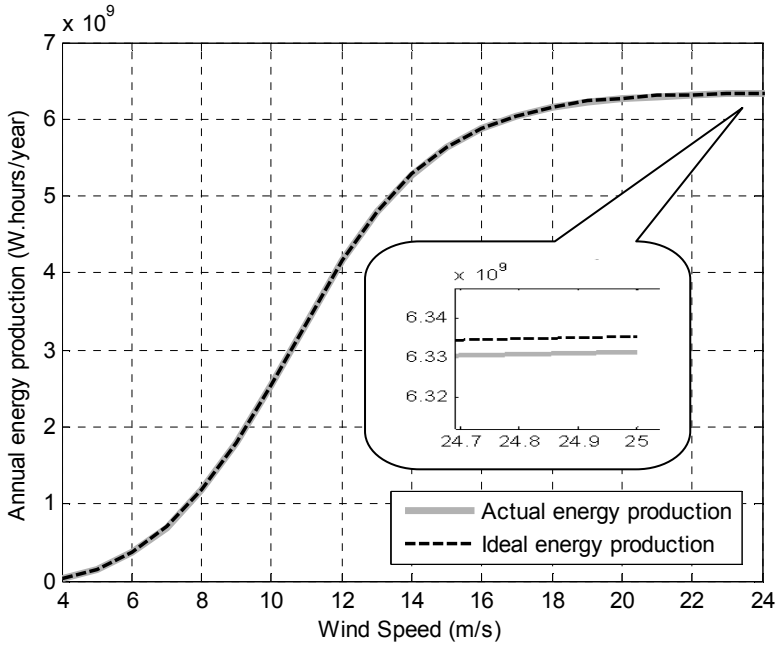

Figure 4.14: Annual energy capture curve

The ratio of the end values of the actual over the ideal annual energy capture curve, provides the annual efficiency of the rotor of the wind turbine.

The results for turbulences of 5%, 10% and 15% are tabulated altogether in two tables. Table 1, considers a site with an annual mean wind speed of 7.5 m/s and Table 2, a site with an annual mean wind speed of 8.5m/s. Both sites record consistent results.

Table 1: Aerodynamic efficiency results for a mean wind speed of 7.5m/s for different turbulence and different controller gains

Turbulence intensity (%)	Controller Gain	Aerodynamic efficiency (%)
5%	0.2	**99.75%**
	0.1753	**99.93%**
	0.15	**99.79%**
	0.12	**99.33%**
10%	0.2	**99.68%**
	0.1753	**99.87%**
	0.15	**99.74%**
	0.12	**99.29%**
15%	0.2	**99.57%**
	0.1753	**99.77%**
	0.15	**99.66%**
	0.12	**99.22%**

The results from the aerodynamic assessment are significant as they reveal almost no energy losses if the operating strategy of the wind turbine is chosen carefully, namely, the simple control law, (10), with optimal gain, $k = 0{,}1753$. Changing the operating strategy, i.e. changing the below rated maximum power coefficient tracking curve, results in losses in energy capture but these are still small. The ideal and desired operating strategy curve for the wind turbine is presented in Figure 4.15, and the objective of the controller is to track this curve as closely as possible. There is little significance on the control method used to achieve this objective.

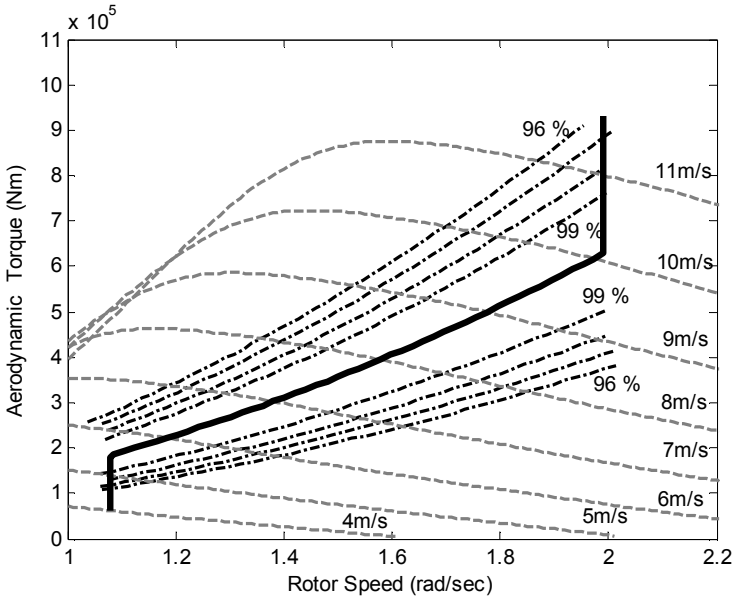

Figure 4.15: Ideal Operating Strategy of the wind turbine

Table 2: Aerodynamic efficiency results for a mean wind speed of 8.5m/s for different turbulence and different controller gains

Turbulence intensity (%)	**Controller Gain**	**Aerodynamic efficiency (%)**
5%	0.2	**99.79%**
	0.1753	**99.93%**
	0.15	**99.82%**
	0.12	**99.46%**
10%	0.2	**99.70%**
	0.1753	**99.88%**
	0.15	**99.78%**
	0.12	**99.42%**
15%	0.2	**99.62%**
	0.1753	**99.79%**
	0.15	**99.71%**
	0.12	**99.30%**

By choosing the optimum controller gain it is observed from Figure 4.16, that the wind turbine operates as desired and from Table 1 & 2, a 99.93% of rotor efficiency is the efficiency in this case. When using a slightly different controller gain, see Figure 4.17 and Figure 4.18, an obvious deviation in the tracking of the ideal curve is recorded. Tracking a curve above or below the ideal one, both result in losses in energy capture.

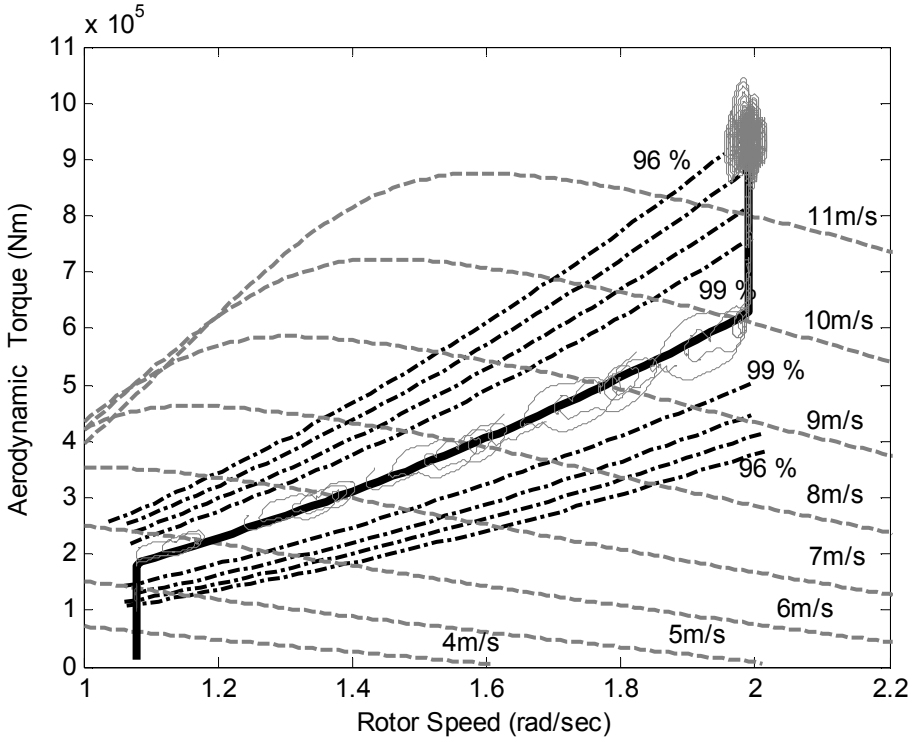

Figure 4.16: Actual Vs Ideal Operating Strategy of the wind turbine 5% turbulent wind and the optimum controller gain.

The same trend of results also appears when the investigation is done using higher turbulences. This is verified in the results presented earlier in the two tables 1 & 2.

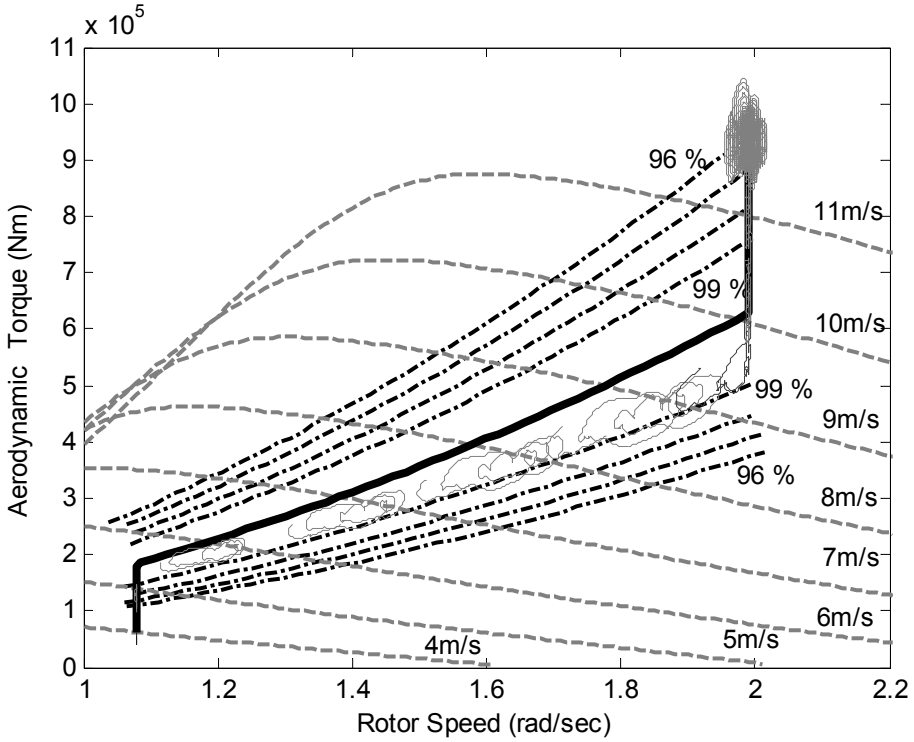

Figure 4.17: Actual Vs Ideal Operating Strategy of the wind turbine 5% turbulent wind, and decreased controller gain.

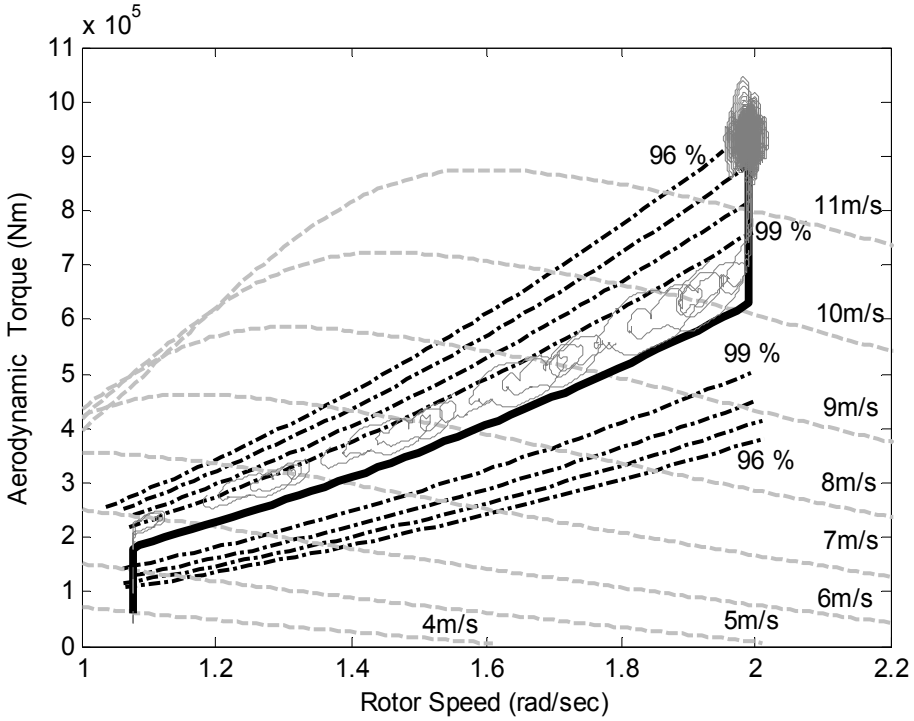

Figure 4.18: Actual Vs Ideal Operating Strategy of the wind turbine 5% turbulent wind, and increased controller gain.

4.6 Concluding Discussion

A thorough analysis of a Simulink simulation of a large wind turbine is presented in this Chapter using spatially filtered wind speed as an input. A comparison with the industrially accepted software GH Bladed is done, in support of the claim that the Simulink model may be used to tune a wind turbine controller and assess its energy capture. The results for a wind turbine with aerodynamic characteristics typical of a modern multi-MW design, reveal that, even with a basic controller that tracks the correct operating strategy curve, the efficiency is very high. There is only very marginal gains to be obtained by improving the controllers thus little dependence on the control methodology used. More dependence is on the operating strategy adopted and how close this is to the ideal strategy but the losses incurred by deviating from the latter are still small.

5 Baseline Controller Design for the 2MW Supergen Exemplar Wind Turbine

5.1 Introduction

This Chapter discusses the design of a full envelope controller for the 2MW Supergen exemplar wind turbine. This controller is used as a benchmark for the newly developed controllers described in the succeeding chapter. It is a new full envelope controller for this wind turbine. All the design information is obtained from a GH Bladed model of the 2MW Supergen exemplar wind turbine. The first step of the design process is to gather all the parameter values available for the wind turbine, see Appendix A, as well as the aerodynamic power and thrust coefficients. This is essential information needed at the beginning of a controller design process as these values define the blades, rotor, drive train, tower, operating points and pitch actuator of the wind turbine. The next step is to extract the linear models in order to validate them with the control models and begin the design process.

The present Chapter is organised as follows:

The first section presents the validation of the control models (referred to as "Simulink" in the legends) against the GH Bladed ones (referred to as "Bladed" in the legends) used for the design of the controller. All the comparison plots, mainly consisting of Bode diagrams, are provided and good agreement between the two models is required for the efficient design of the controller. The next section provides all the steady state operational curves of the wind turbine i.e. the ideal power curve, ideal pitch angle curve, operating strategy etc. Section 5.4 discusses the nonlinear global gain scheduled controller and its design, used to effectively compensate for the aerodynamic nonlinearities that are naturally inherent to the wind turbine. A comparison between the scheduled and the non-scheduled plant is provided in order to illustrate its effectiveness. The next sections involve the design of the Drive train filter, the Tower Feedback Loop, the below and above rated linear controllers, the

phase advance strategy for switching between above and below rated, as well as the complete switching strategy. The tuning of the controller is done using a Simulink version of the designed controller and wind turbine, described in Chapter 3. The full evaluation of the designed controller, consisting of time series, frequency plots and fatigue load results, for different wind speeds is presented in Appendix B.

5.2 Model Validation for Linear Models and Bladed linear Models

The parameters for the linear models used for the full envelope controller design are assigned for the specific wind turbine and the linear control models are validated against linearised models extracted from GH Bladed. The first step in this task is to extract the linear models of the wind turbine from GH Bladed. At the same time the power coefficient and thrust coefficient tables must be extracted from Bladed for a relatively wide range of pitch angles. The Cp and Ct tables for the current wind turbine model are obtained for the range of pitch angles between -5 and 60 degrees. All the parameters and data defining the 2MW wind turbine model are given in Appendix A. The controller here is designed using classical control theory combined with feedback and feedforward control methods, and nonlinear "gain-scheduling" techniques. In the design process, loop-shaping in the frequency domain using Bode plots is mostly employed.

The validation is done by comparing the linear models to the GH Bladed ones. This is done by producing the open loop Bode plots for different inputs and outputs critical to the control design, and comparing them for the two models. Such inputs and outputs are Torque demand to Generator speed, Pitch demand to Generator Speed and Pitch demand to tower acceleration. The objective of this comparison is to ensure that the dynamic modes coincide for the two models.

5.2.1 Torque Demand to Generator Speed

The first comparison is for Torque demand to Generator Speed. The Bode plots are presented in Figure 5.1 and Figure 5.2 for below rated wind speeds. As may be observed, there is good agreement sufficient for control design between the two models. Spikes that exist in the GH Bladed linear models that do not coincide with the linear models correspond to dynamics that are not modelled, and are not

necessary for designing and tuning of the controller. The same also holds true for the following validation sections.

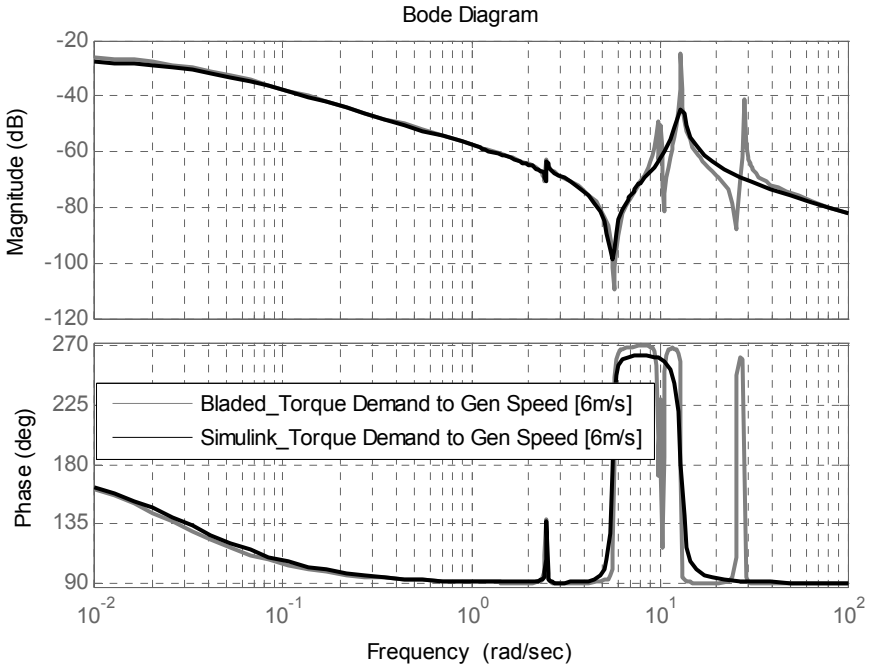

Figure 5.1: Plant Bode plot, Torque Demand to Generator Speed for 6m/sec

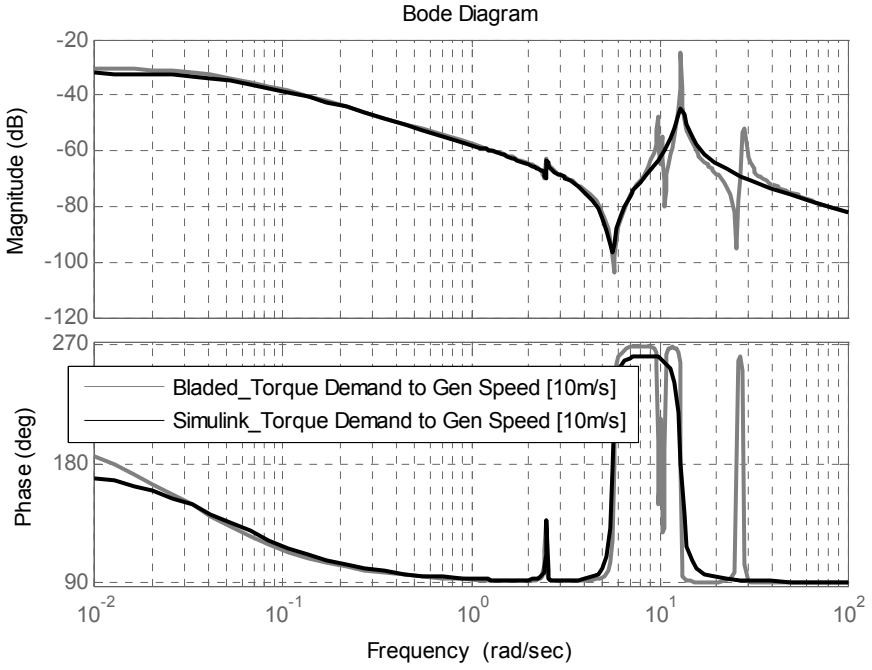

Figure 5.2: Plant Bode plot, Torque Demand to Generator Speed for 10m/sec

5.2.2 Pitch Demand to Generator Speed

The second comparison involves comparison of input/output Bode plots for Pitch Demand to Generator speed. Once again as it may be seen from the open loop Bode plots, see Figure 5.3 to Figure 5.5, there is sufficient agreement between the two models and the linear control models can be therefore used for control design purposes.

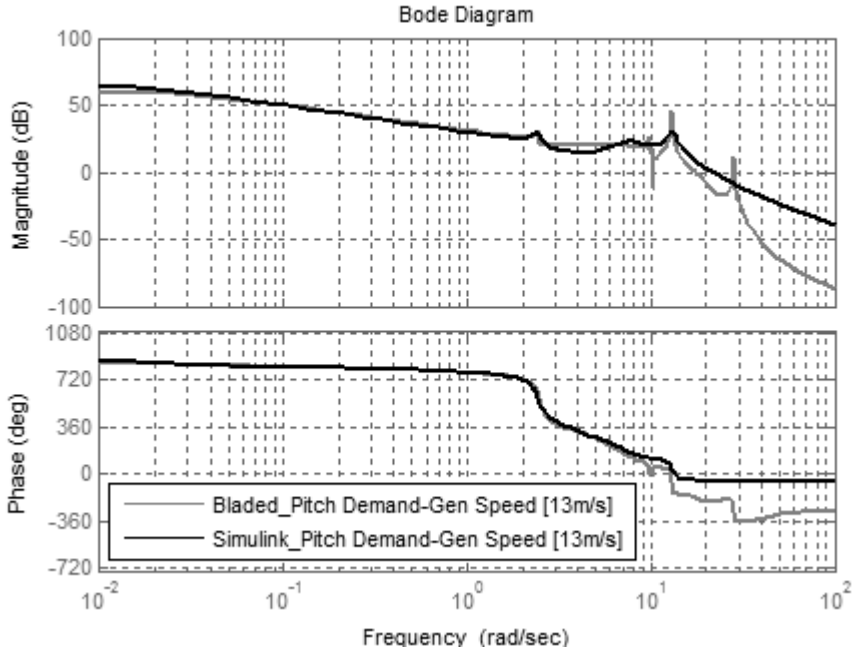

Figure 5.3: Plant Bode plot, Pitch demand to Generator Speed for 13m/sec

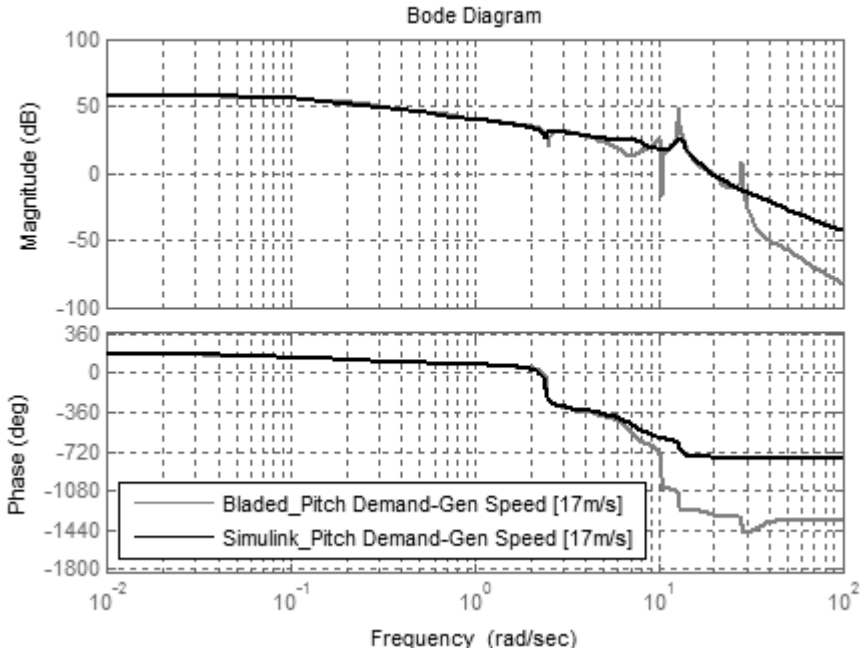

Figure 5.4: Plant Bode plot, Pitch demand to Generator Speed for 17m/sec

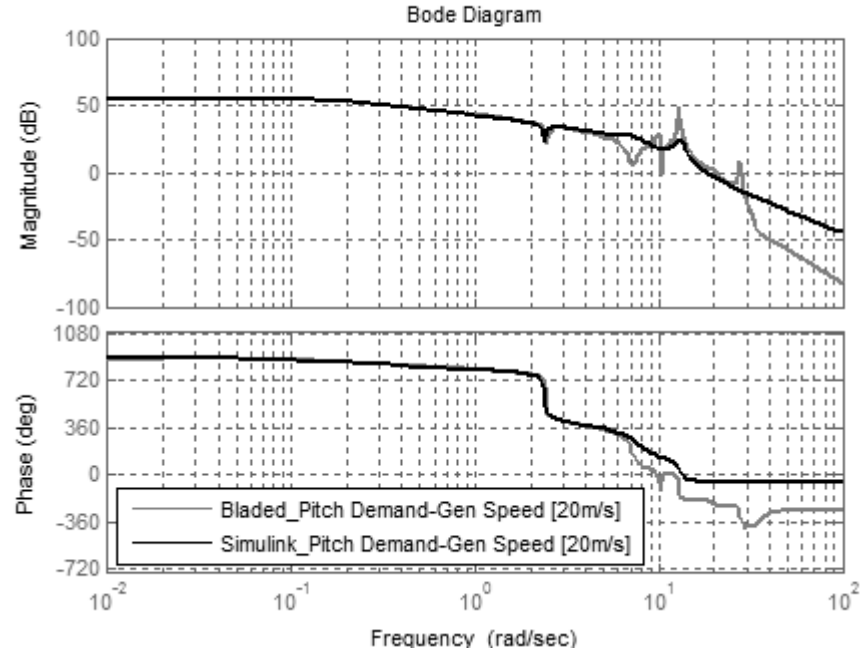

Figure 5.5: Plant Bode plot, Pitch demand to Generator Speed for 20m/sec

5.2.3 Pitch Demand to Tower Acceleration

The third part of the validation compares Bode plots of the two linear models with Pitch Demand as the input and Tower Acceleration as the output, see Figure 5.6 through Figure 5.8. This is required for the design of the Tower Damper (Tower Feedback Loop) later in this Chapter.

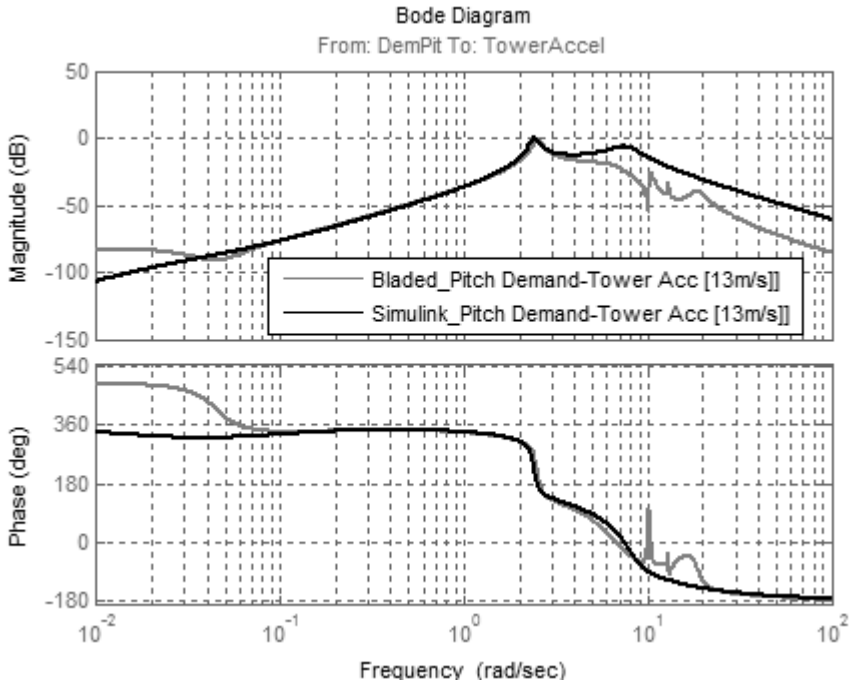

Figure 5.6: Bode plots from Pitch Demand to Tower acceleration for13m/s

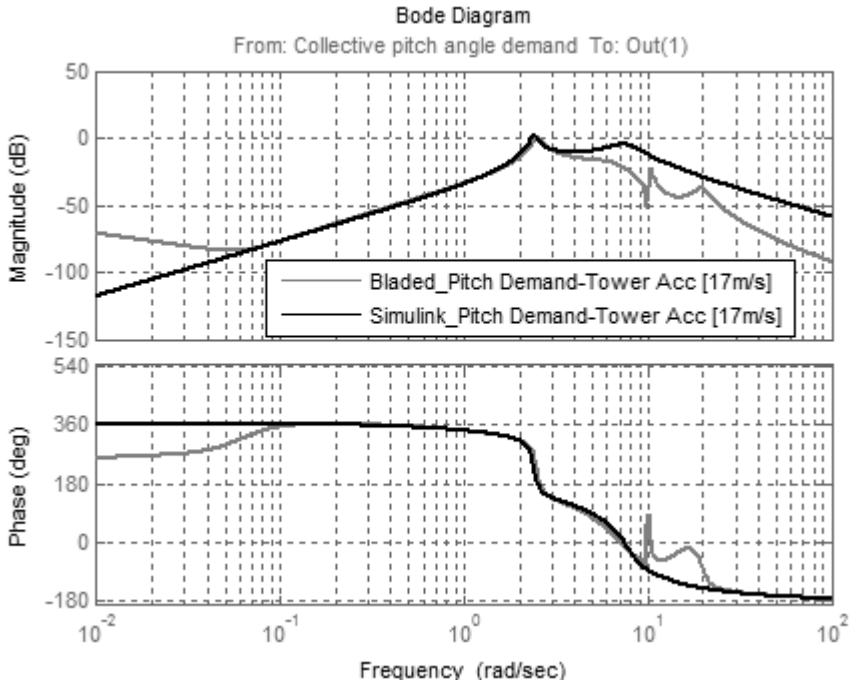

Figure 5.7: Bode plots from Pitch Demand to Tower acceleration for 17m/s

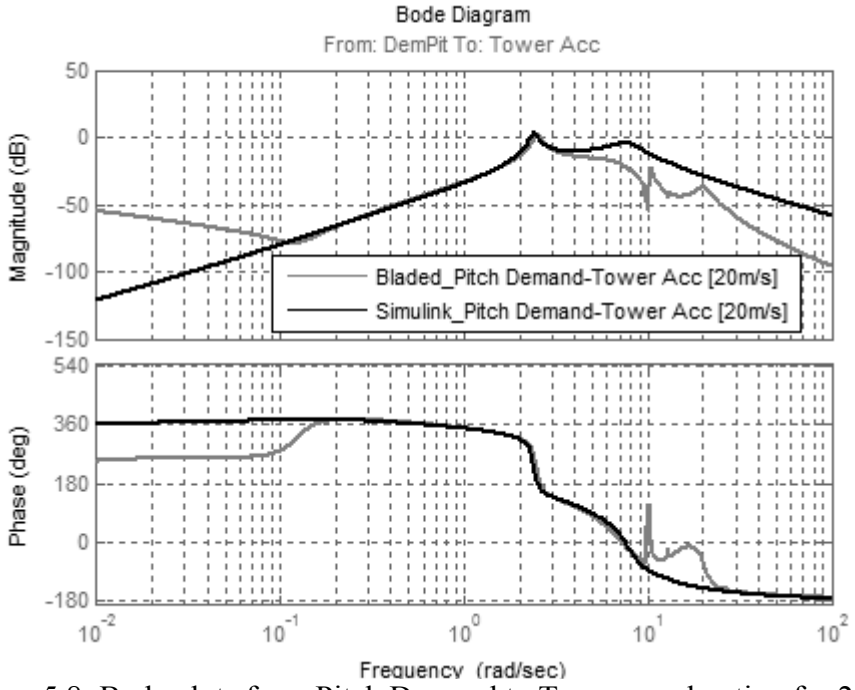

Figure 5.8: Bode plots from Pitch Demand to Tower acceleration for 20m/s

5.3 Operational Curves of the wind turbine

Having available all the parameters that define the linear control models of the wind turbine, all the steady state operating points and the ideal strategies may now be defined.

5.3.1 Operating Strategy

The operating strategy for a wind turbine can be defined in many different ways [25]. The one adopted here is by means of the Torque/Speed plane. Wind turbines have different modes of operation in different wind speeds. The control system is required to ensure the wind turbine operates in the appropriate mode with wind speed. There are four modes consisting of two constant speed modes, power coefficient tracking mode (Cp max tracking) and blade pitching mode. From cut-in wind speed which is the speed that the wind turbine starts to operate, until the aerodynamic torque reaches some value T_0, the generator speed is kept constant at a value of ω_0, see Figure 2.4. When the aerodynamic torque reaches T_0 then the controller changes its mode so that the turbine tracks the maximum power coefficient curve.

In this mode, Cp is maintained at its maximum value such as in eq. (10). Little control is required in this region. As also discussed in Chapter 4, the purpose is to extract as much power from the wind as possible. When the generator speed reaches a value, ω_1, the controller keeps it at that value allowing the torque values to vary according to wind speed. When the wind speed has reached the rated value the blades begin to pitch, to keep the output power at a maximum constant safe level.

5.3.2 Ideal Power curve

The power curve is the graph that indicates the relationship of generated electrical power to wind speed. Actual power curves are found through field testing measurements. These are done for several reasons, one of them being the validation of wind turbine models and to establish its performance for benchmarking reasons. The IEC has developed specific standards for wind turbines that must be used by manufacturers. These standards include power performance, fatigue loads, blade testing etc. Given the characteristics of the 2MW wind turbine under study, which are detailed in Appendix A, its ideal (theoretical) power curve is depicted in Figure 5.9.

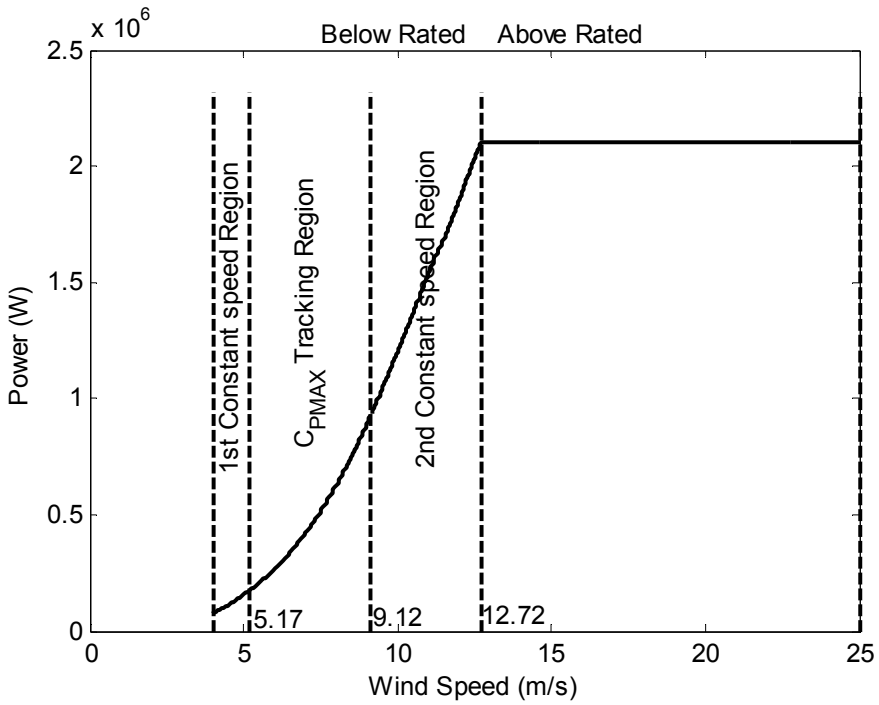

Figure 5.9: Ideal Power curve

According to the type of wind turbine (pitch regulated, stall controlled etc) the shape of the power curve may vary significantly. The wind turbine investigated here is variable speed and pitch regulated to maintain the rated power at 2MW. The modes previously discussed in the operating strategy section are shown by dashed-lines in Figure 5.9.

5.3.3 Cp-lambda (λ) curve

One common method of presenting power performance is the non-dimensional Cp-λ curve [65]. Figure 5.10 presents the Cp-λ of the 2MW wind turbine which represents a modern 3-bladed machine. The Cp-λ curve is plotted using Matlab. Once the Cp table of the wind turbine is loaded into Matlab, the interpolation method is used to interpolate the values of available pitch angles and tip speed ratios of the Cp table to find the ones associated to their steady state values.

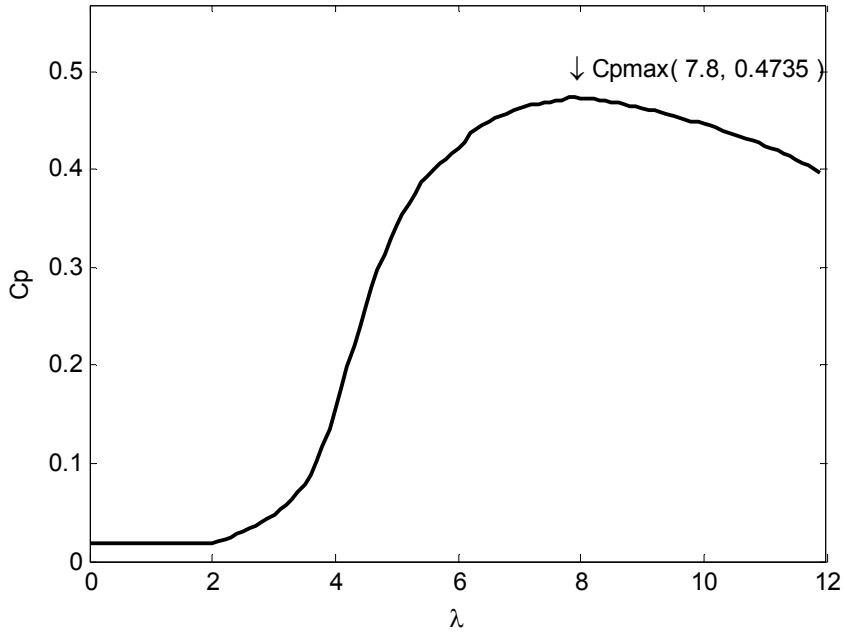

Figure 5.10: Cp-λ curve

It is worth noting that this machine has a maximum power coefficient of 0.47 which is lower than the Betz limit which was discussed in Chapter 3 of this thesis. This is typical for a machine of this size and the reduction from the Betz limit is caused by imperfect blade design, drag and tip losses or a combination of those. In [65] it is shown how drag, tip and stall losses may affect the shape of such curves.

5.3.4 Ideal Pitch Angle versus Wind Speed

The ideal pitch angle strategy sets the ideal pitch angle that the wind turbine blades should have in each wind speed in order to achieve maximum performance. The 2MW wind turbine for which the controller is designed in the present chapter, follows the theoretical strategy presented in Figure 5.11. To obtain this curve the steady state values of pitch angles associated with wind speeds are calculated with the help of Matlab and these pitch angles are plotted against wind speed.

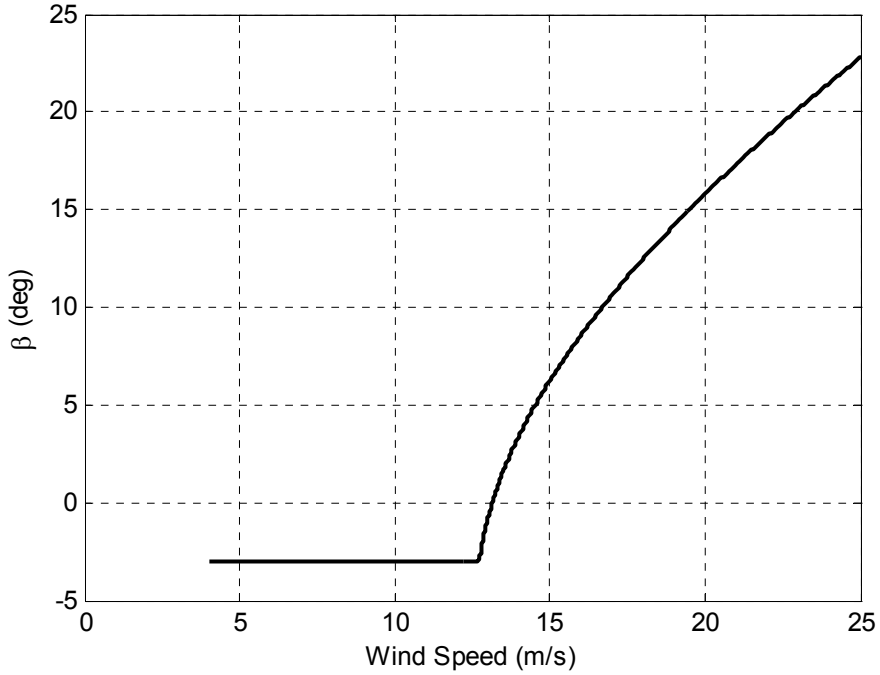

Figure 5.11: Ideal pitch angle strategy

A close look at Figure 5.11 reveals important aspects of the characteristics of the wind turbine. The first important piece of information that we get that is also seen in the ideal power curve is the rated wind speed. The moment the controller starts pitching the blades of the wind turbine, it has reached rated power and the task is to maintain it while discarding excess power. By observing Figure 5.11 it can be seen that in high wind speeds there is much less effort made by the blades pitching in order to maintain rated power. This may be seen by comparing the gradients of the curve in wind speeds just above rated to the ones close to cut-out. In other words pitching the blades slightly in high wind speeds produces the same aerodynamic result as pitching the blades significantly in lower wind speeds close to rated. This plays an important role when compensating for the aerodynamic nonlinearities described in the next section.

5.4 Nonlinear Control Design – Global Gain Scheduling

The "Gain Scheduling" nonlinear control design technique may be successfully applied in controller design cases where severe nonlinearities appear. It is not easy to

formally assign a definition for this technique as it is used in different ways according to the engineering practice applied to. Nevertheless, it may be inferred, that it is the act of exploiting a state of the system, for example the pitch demand to get information as to how the controller must change as the wind speed varies [17], [18].

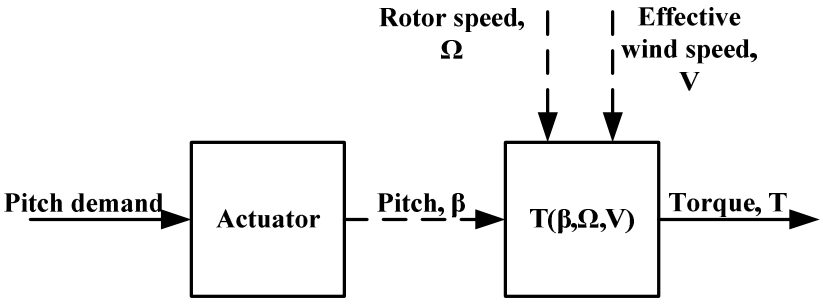

Figure 5.12: Dynamic relationship of pitch, wind and torque [17]

This technique is able to accommodate nonlinearities by continuously changing the structure of the controller according to some local set points. In this context, for the dynamics of a pitch regulated variable speed wind turbine, the controller must be able to cater for the nonlinearities existing between the aerodynamic torque, the rotor speed as well as the pitch angle of the blades [68]. Figure 5.14, depicts the nonlinearity of the plant dynamics in above rated wind speeds 13-24 m/s (the pitch angle has a specific associated value for every wind speed [18], [19]).

Although we may not say that the wind turbine experiences the actual wind speed, as it is impossible for it to be directly measured on the rotor, it may be stated that the wind turbine experiences an effective wind speed which is simply an average of the wind speed over the rotor disc (as discussed earlier in Chapter 4). The nonlinear dependence of the aerodynamic torque (T) on the rotor speed (Ω), pitch angle (β) and effective wind speed (V) is described by (17).

The nonlinearity can be separated as seen in Figure 5.12, thus it is possible to include the inverse of h in the controller, cancelling it [17], see Figure 5.13.

$$T = T(\beta, \Omega, V) = h(\beta, \Omega) - g(V) \tag{17}$$

For every set of (Ω_0, V_0) the rated aerodynamic torque T_0 is accomplished at a unique pitch angle β. By using the Taylor expansion series the nonlinearity described in the above equation may be linearised within these specific operating points as described in [17], [18].

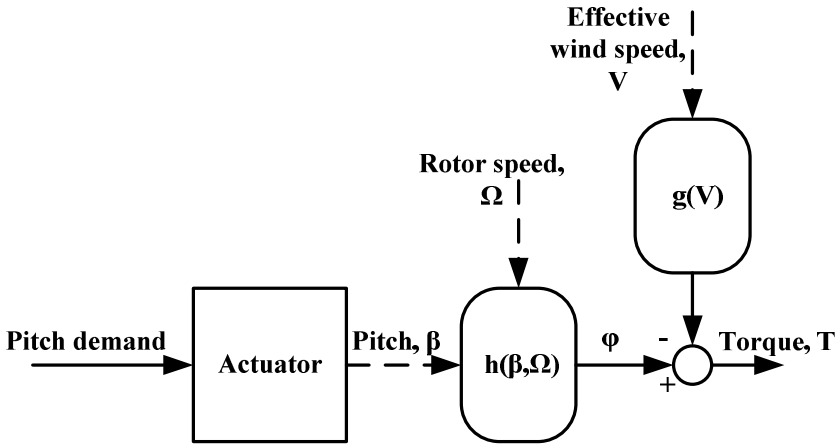

Figure 5.13: Global (separable) reformulation of aerodynamic nonlinearity [17]

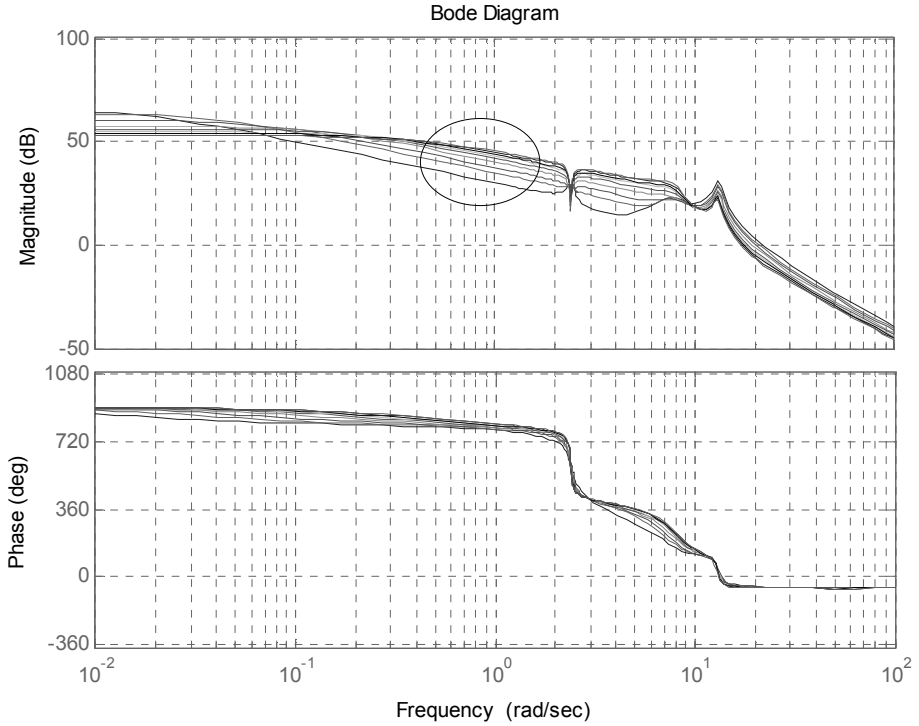

Figure 5.14: Plant dynamics before applying gain scheduling 13-24m/s

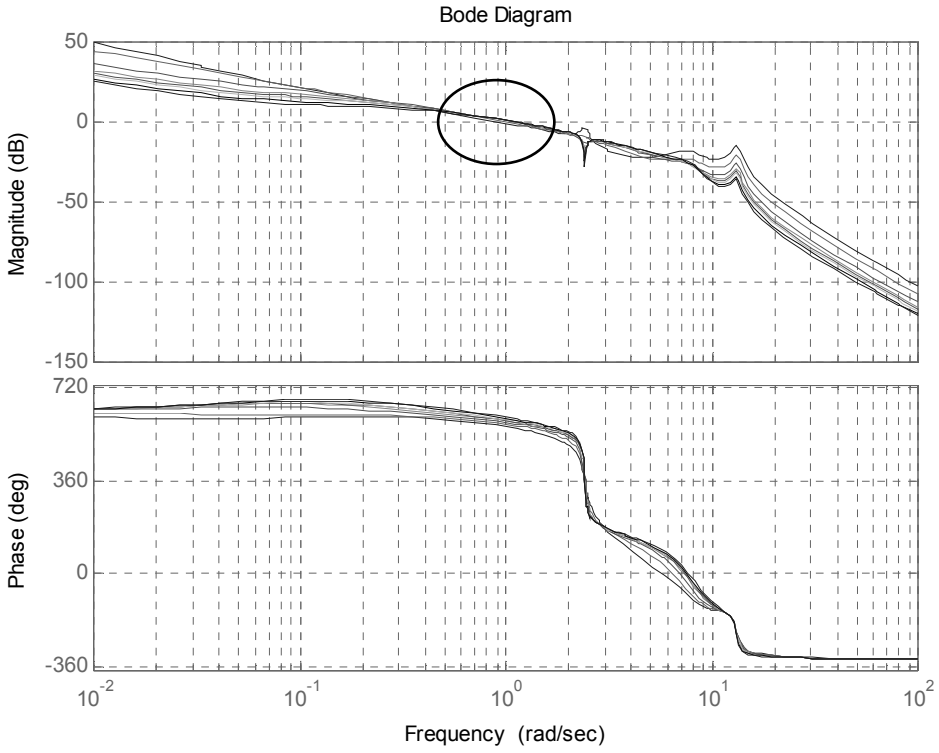

Figure 5.15: Plant dynamics after gain scheduling 13-24m/s

The in-plane partial derivative of aerodynamic torque is derived, see Figure 5.16, and then a linear fit to this curve is found. This is obtained by using the Aerodynamic torque expression of (4). Then the partial derivatives are calculated with the help of Matlab by calculating the gradient of the torque with respect to pitch angle, and finally the steady state values for the partial derivatives are obtained through interpolating the steady state values of wind speed, pitch angle and rotor speed within the calculated gradient.

$$y = 1.3688 + 14.1635 * (pi/180) * x \quad (18)$$

The straight line fit, best describing the gradient, is depicted by the grey line in Figure 5.16 and its equation is given by (18) which is the gain scheduling function which is implemented in the controller. The slope (before conversion to radians) and the offset are then expressed as a constant and a slope parameter for implementation in the controller.

The Bode plots for the "gain-scheduled" dynamics are depicted in Figure 5.15. For comparison the Bode plots before gain scheduling are depicted in Figure 5.14.

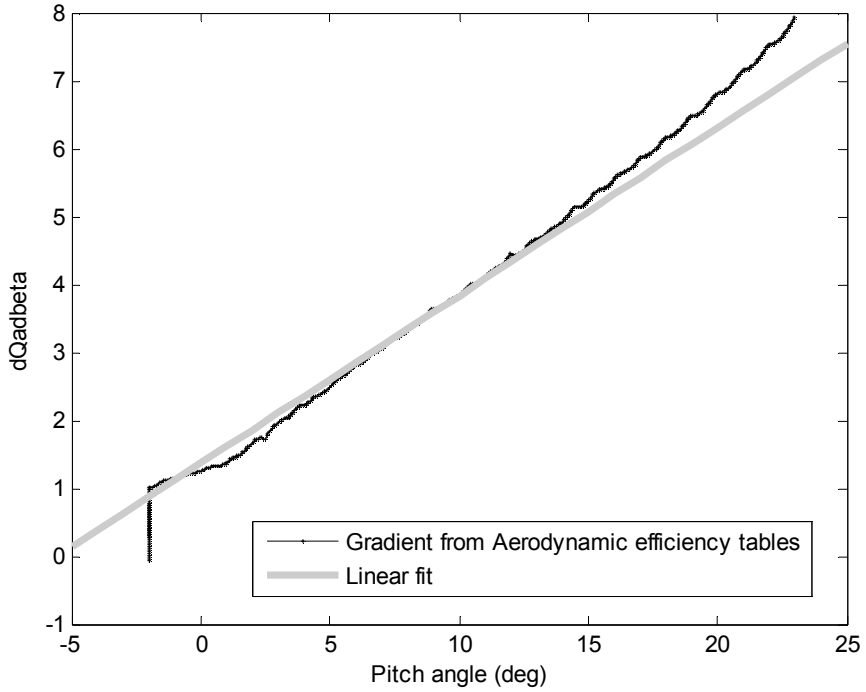

Figure 5.16: dQa/dβ against pitch angle – Linear fit

5.5 Drive Train Filter Design

In variable speed pitch regulated wind turbines like the one under study, there are serious risks of damage caused by the vibrations of the components of the drive train. Methods to mitigate these loads are widely used most of which are discussed in [48], [49], [58], [41]. From the Bode plot in Figure 5.17, depicting the dynamics from Torque demand to Generator speed of the 2MW Supergen exemplar wind turbine it is obvious that the first Drive train mode is lightly damped. This is the general case for variable speed wind turbines and it may lead to large variations in the generator speed and fatigue, which need to be actively damped. The large peak at 13rad/sec of Figure 5.17, which is the drive train frequency of this wind turbine, is indicative of this very low damping that may cause large torque transients and eventually lead to component damage. From the spectrum of Generator speed as well as its cumulative spectrum in Figure 5.18, the same damaging pattern is seen. In order to alleviate this effect, there is a need to increase the damping at this frequency by adding a term proportional to the Generator speed, internally to the model.

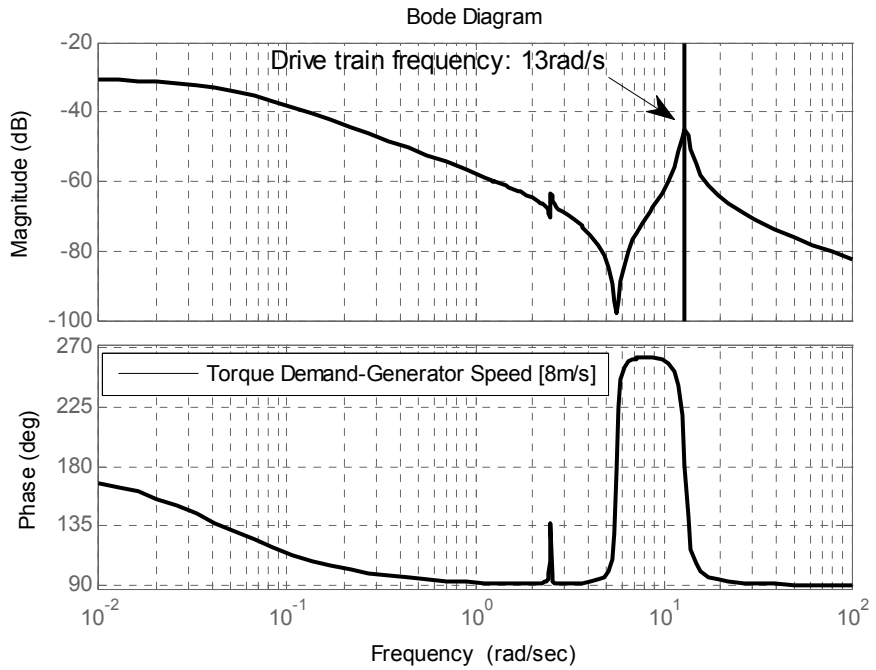

Figure 5.17: Bode Plot depicting the dynamics from Torque demand to Generator speed

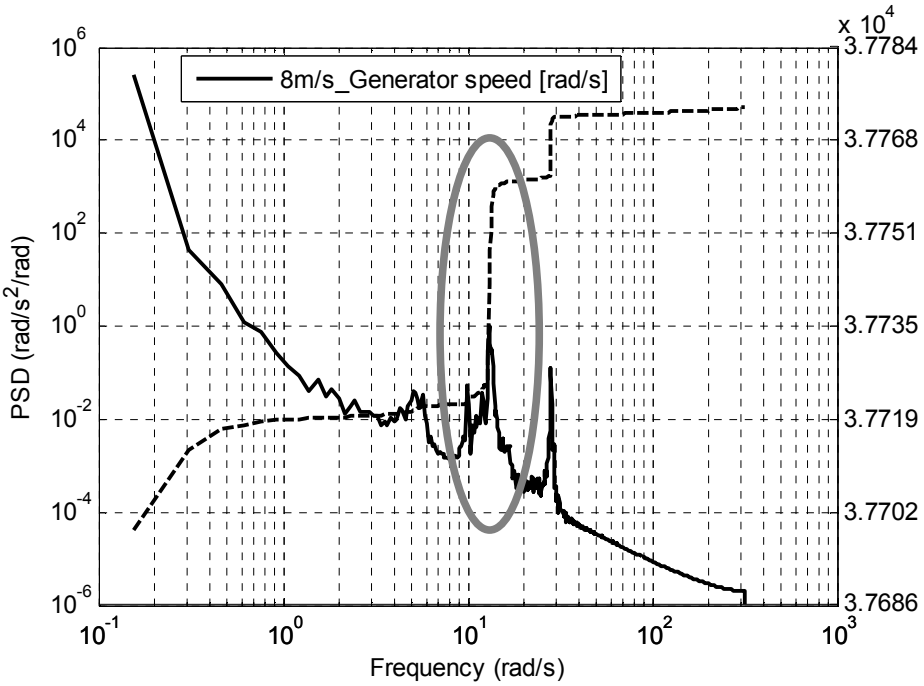

Figure 5.18: Spectrum and Cumulative spectrum of Generator speed at 8m/s wind speed

The approach adopted here, as discussed in [41], is to select a filter of the form of (19) centered at the frequency of the dominant Drive train mode.

$$G_{dtr}(s) = K_{dtr}\frac{2\zeta\omega s}{s^2 + 2\zeta\omega s + \omega^2} \tag{19}$$

This filter feeds back only the oscillations at the resonant frequency and does not affect any other modes. The block diagram of the modification to the system is depicted in Figure 5.19.

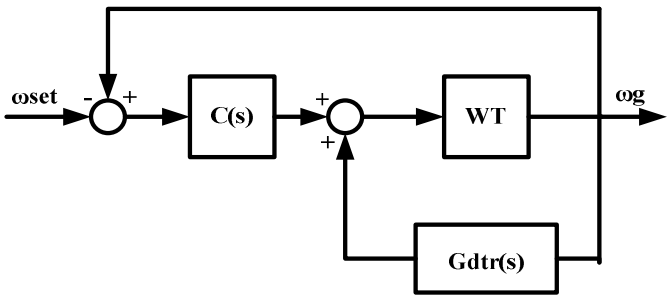

Figure 5.19: Plant with the below rated controller and the drive train damping filter

The transfer function for the controller $G_{dtr}(s)$ designed to damp the oscillations of the drive train of the 2MW exemplar wind turbine, is shown in equation (20), and its Bode plot is depicted in Figure 5.20. To obtain this transfer function the design starts with the general form of a band pass filter of the form of (19) centered at the frequency of the first drive train mode, i.e. 13rad/sec. The purpose is to suppress the "peak" at the frequency of the first drive train mode by managing to bring the peak of the dynamics of $WT * G_{dtr}$ well above 0dB, see Figure 5.21. The dynamics linking Torque Demand to Generator Speed are continuously monitored using Matlab until the result shown in Figure 5.22 is obtained.

$$Gdtr(s) = \frac{5721.6831\text{s}}{s^2 + 10.09942\text{s} + 180.2924} \tag{20}$$

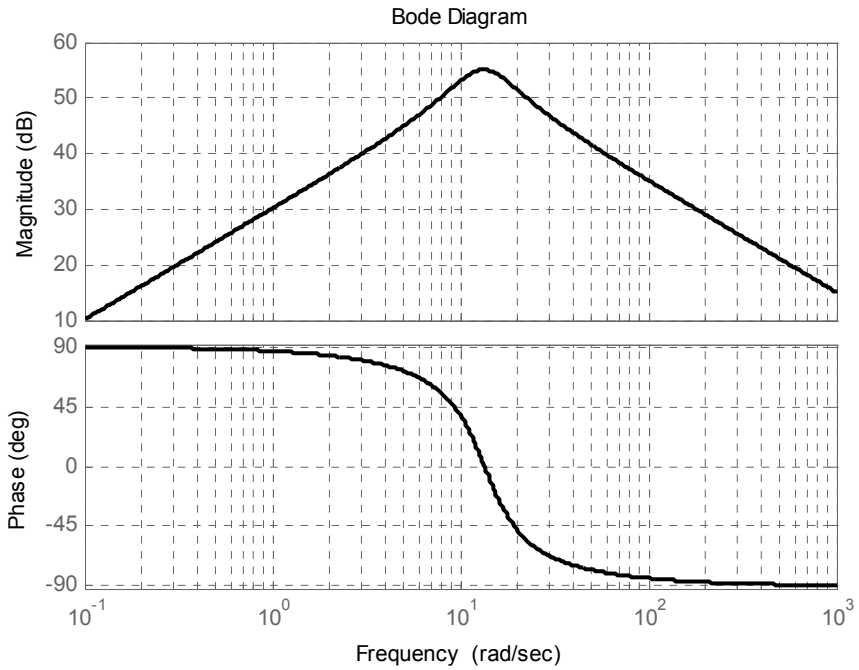

Figure 5.20: Bode plot of drive train filter

Having applied this filter, the dynamics of the Wind turbine from Torque demand to Generator speed, compared to the dynamics before the application of the filter, are depicted in the Bode plot of Figure 5.22. Moreover the spectra of the Generator speed signal comparing "before and after" application of the damper is shown in Figure 5.23. The damping of the drive train mode is significantly increased and the oscillations caused to the generator speed signal are dramatically reduced as well, see Figure 5.24, depicting the time series of the Bladed simulation run, for before and after the application of the damper.

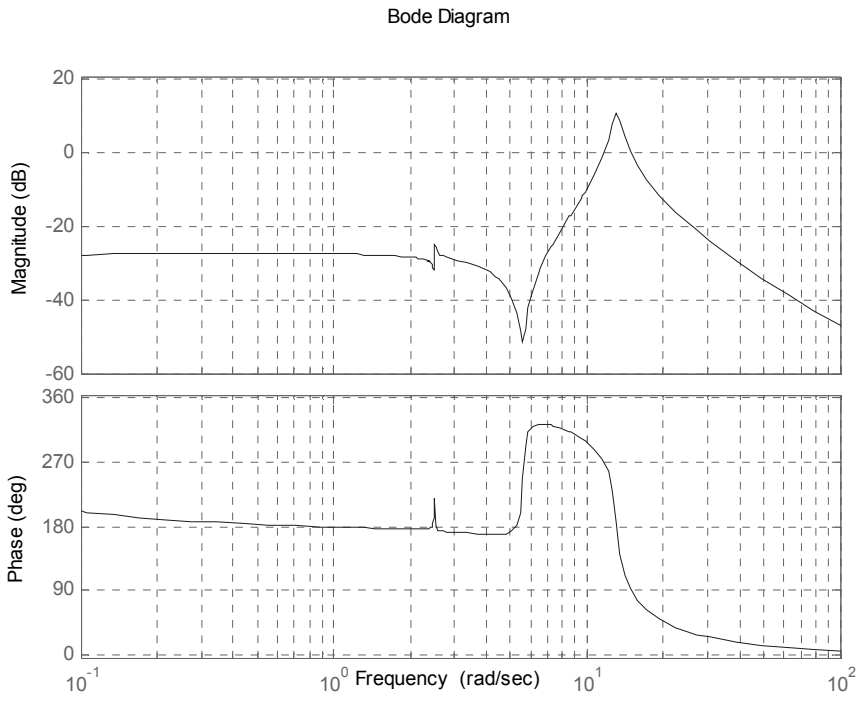

Figure 5.21: Bode plot from Pitch Demand to Drive Train Filter Output at (8m/s)

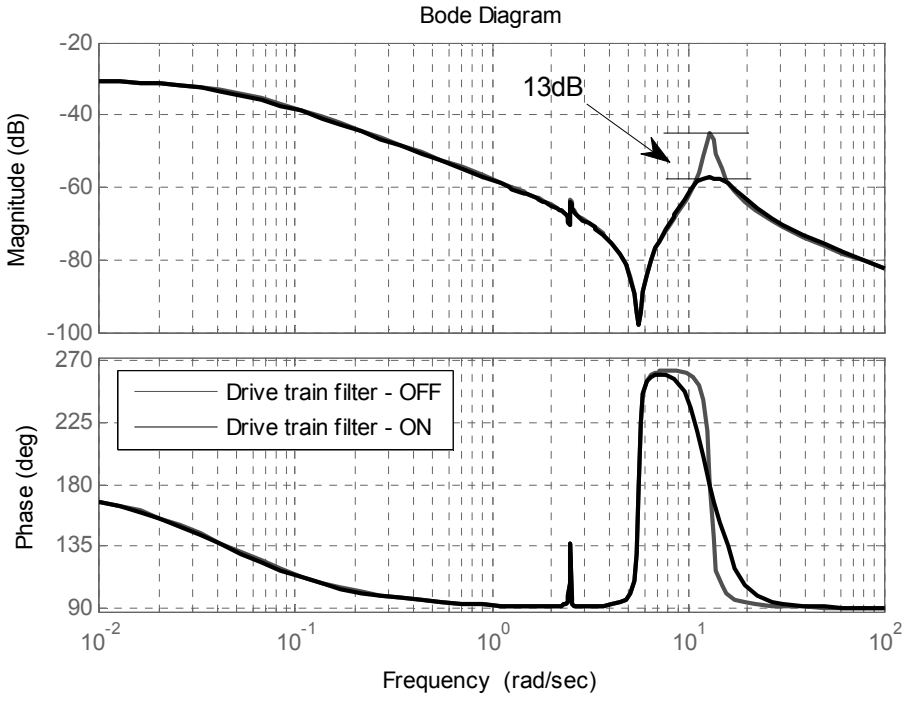

Figure 5.22: Torque demand to Generator speed at 8m/s

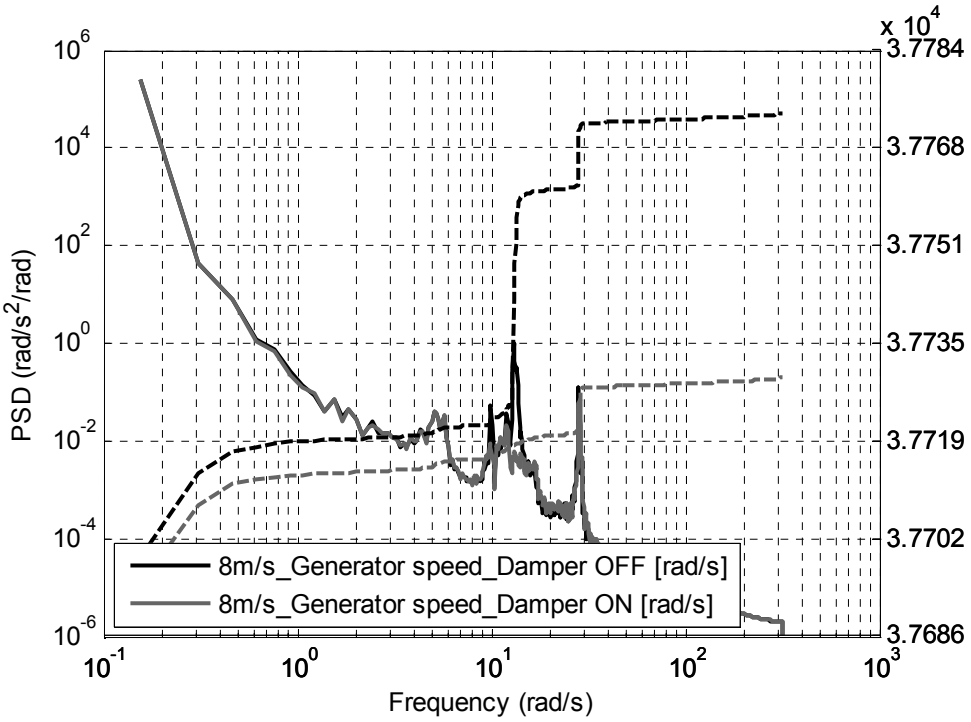

Figure 5.23: Spectra of the Generator speed signal, with and without the Drive train filter

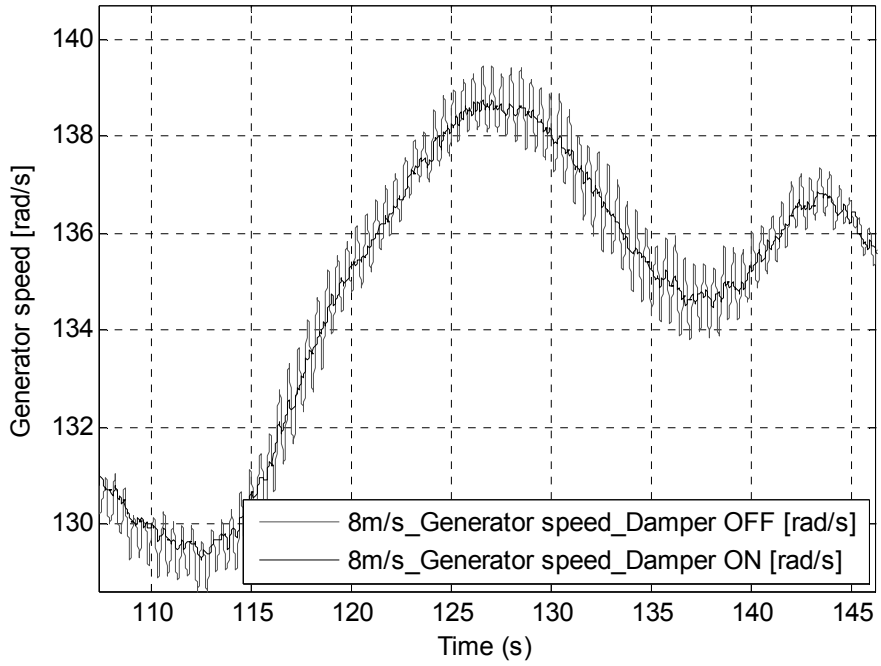

Figure 5.24: Time series of the Generator speed signal before and after the application of the Damper

5.6 Tower Feedback Loop Design

The approach adopted in the last few years for the cancellation of the fore-aft mode of the tower, is the augmentation of the pitch demand by an additive adjustment in response to a measurement of the tower head velocity or acceleration [21]. In [42] similar results are obtained using linear eigenvalue stability estimations in combination with the non-linear simulations. Another similar approach is that discussed in [43], in which the rotor thrust is varied to account for tower vibrations. Individual pitch control methods for mitigating tower vibrations are also proposed in the literature as the two algorithms of [44]. In the first one all blades have different angle of attack and the second one uses de-rating to eliminate the forcing function that causes the instability. They are both proposed for active stall machines and they help in minimising the number of shutdowns caused by excessive tower vibrations.

The method adopted here is that of [21]. Consequently, there are two pitch feedback loops; an inner tower feedback loop and an outer rotor speed feedback loop. The block diagram of the system augmented by the tower feedback loop is depicted in Figure 5.25.

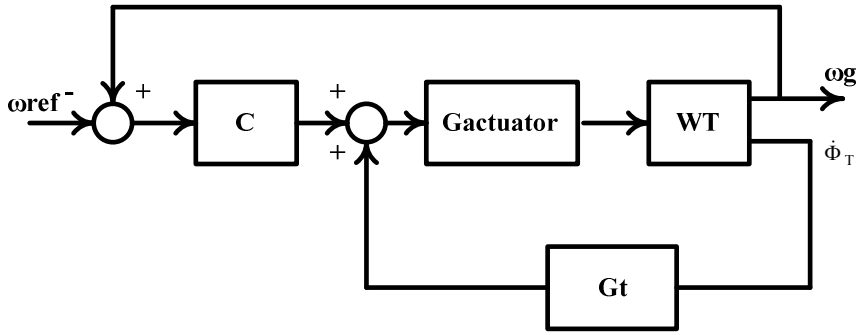

Figure 5.25: Block diagram of system with Tower feedback loop

Acceleration is easily measurable, and speed may be derived from that by simple integration. Therefore, the tower head speed is fed back to improve the damping [21]. The goal of the Tower Feedback Loop (TFL) is to reduce the first tower frequency mode. If the additional pitch coming from the TFL is added onto the demanded pitch, see Figure 5.25, when the Anti-Windup scheme is limiting the variation of the pitch angle, the pitch rate exceeds its maximum value. In order to

prevent this from occurring, the implementation must be done so that the TFL signal is added before the anti-windup scheme. The transfer function of the tower feedback loop of this 2MW wind turbine is given by (21).

$$G_{tfl}(s) = 7.11\frac{s^2 + s + 6.24}{s^2 + 0.71s + 5.74} \cdot \frac{1}{s + 0.61} \tag{21}$$

The design of this controller begins with a filter to raise the gain of the tower relative to the frequency of the blade flapwise mode. Then the phase should be fixed to 180º and the overall gain should be raised so that the dynamics from Pitch to the filter output is above 0dB, see Figure 5.29. To achieve this, loop-shaping (moving, adding the poles and zeros) is partially employed by continuously monitoring the dynamics of the system from Pitch Demand to Tower Acceleration, the poles and zeros are modified in a way so that the resonant peak of the tower is suppressed as much as possible without exciting any frequencies important to the overall operation of the wind turbine. The sensitivity function of the system from Pitch Demand to Tower Acceleration is also monitored to ensure that no damage is done to any important mode of the wind turbine. The dynamics of the wind turbine form Pitch Demand to Tower acceleration, with and without the feedback loop are depicted in Figure 5.26 and Figure 5.27. The region where the dominant Tower mode lies at the frequency of 2.45rad/sec is distinct and marked with a dashed vertical line. The purpose of the TFL is to alter the dynamics in such a way, so that the mode is as much dampened as possible without compromising the performance of the wind turbine. The sensitivity function of the system is depicted in Figure 5.28 and the Bode plot from Pitch demand to the Tower acceleration filter output in Figure 5.29 and Figure 5.30 which shows that the peak at tower frequency is well above 0dB, which means that control will be effective in reducing it. Results of the effectiveness of the Tower Feedback Controller are presented in Chapter 6, as well as in Appendix B.

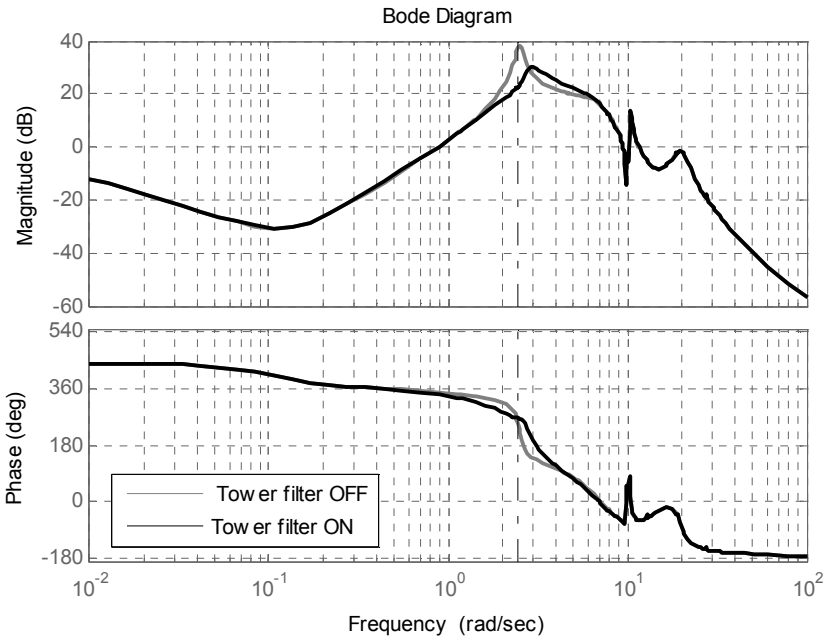

Figure 5.26: Open-loop Bode plot from Pitch demand to Nacelle acceleration for 18m/s (Aeroelastic linearised model)

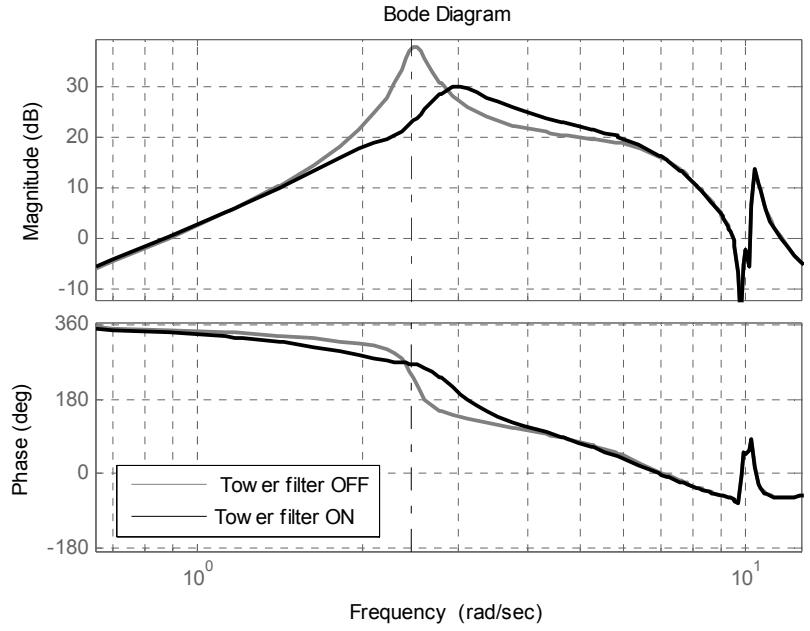

Figure 5.27: Zoomed-in, Open-loop Bode plot from Pitch demand to Nacelle acceleration for 18m/s (Aeroelastic linearised model)

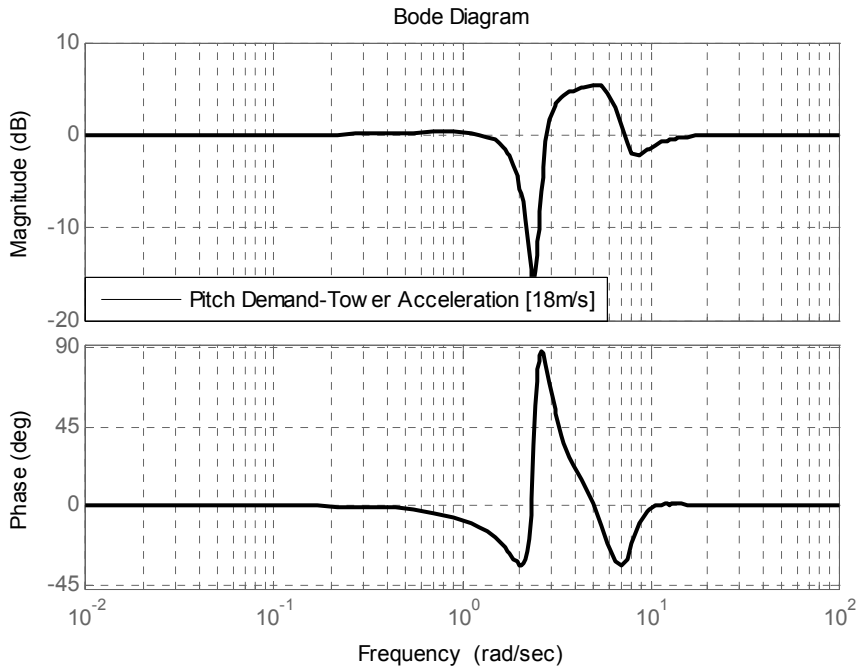

Figure 5.28: Sensitivity function of system with Tower filter, from Pitch Demand to Tower acceleration for 18m/s

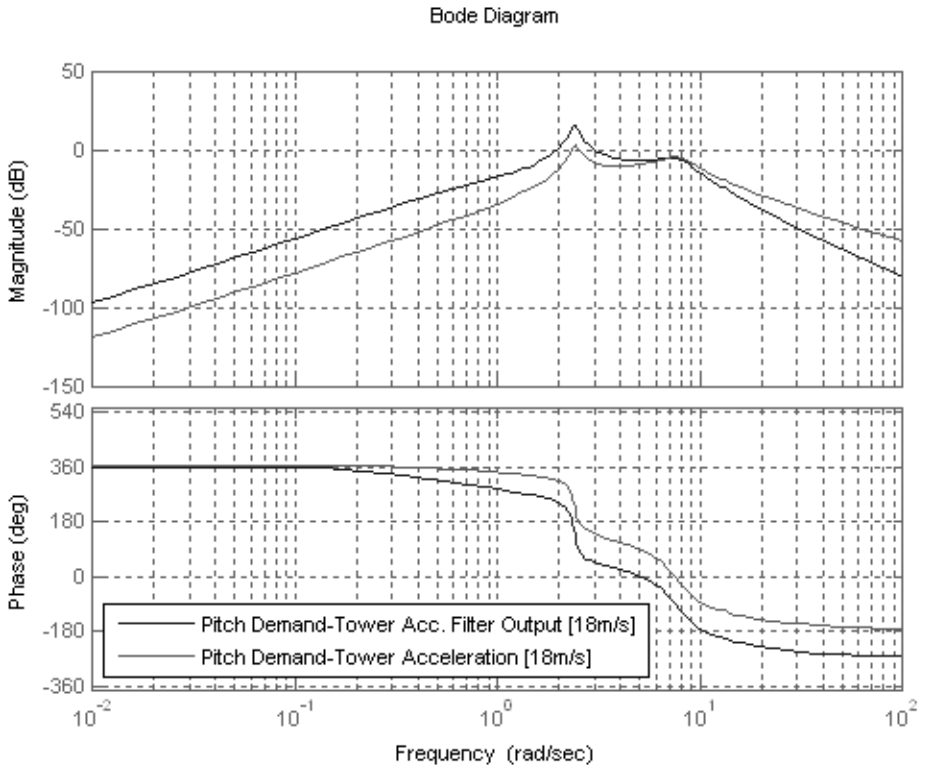

Figure 5.29: Dynamics from Pitch demand to Tower acceleration and Pitch Demand to the designed Tower Acceleration filter output at 18m/s

Figure 5.30: Pitch Demand to Tower Acc. filter output at 18m/s

5.7 Phase Advance Design

The issue discussed in this paragraph concerns the lag that exists in the pitching of the blades when switching from torque control (below rated wind speeds), to pitch control (above rated wind speeds). The idea for the Phase advance addition to the controller arose from the need for a solution for sudden changes in the wind when the blade does not pitch fast enough to satisfy the operating strategy's demand and prevent overspeed [18], [19]. The addition implemented to the controller is depicted in Figure 5.31 and it will enable the blade to pitch earlier, see Figure 5.33 and Figure 5.34, in order to prevent the problem described earlier, and achieve the desired control in time [46].

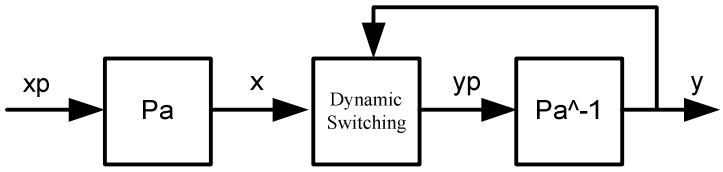

Figure 5.31: Phase advance controller addition mechanism

In the block diagram shown in Figure 5.31, P_a is a phase advance transfer function, given by eq. (22), P_a^{-1} is the inverse of P_a and at the point y both are cancelled out. If the phase advance scheme did not exist, switching would occur at point x. Having implemented the phase advance scheme the switching from torque control to pitch control is done at point x_p which is ahead of x. Between these two points there is the transfer function of eq. (22) which enables the switching to be ahead by approximately 0.5sec. Then the controller returns to the initial configuration at point y, where the two transfer functions are cancelled out. The same activity is repeated when switching from above rated to below rated. The decay in pitch is anticipated and smoothly implemented.

$$P_a = \frac{s + 0.6}{s + 1.6} \tag{22}$$

Expression (22) is a simple lead transfer function, see Figure 5.32, acting only at the moment of pitching from below rated to above rated and vice versa. It is designed to ensure that the blades will pitch about 1 second later in the case of a sudden gust. To test the efficiency of this pitch predicting mechanism, simulations both in Simulink and Bladed are run and compared in Figure 5.33 and Figure 5.34. In both it is observed that whenever the blades are about to pitch and the Phase advance mechanism is turned on, the blades pitch about 1sec earlier. More simulations assessing the performance of this mechanism can be found in Appendix B, in the section where the Basic controller is compared with controllers containing the addition of components such as the tower damper, anti-windup and phase advance (referred to as Basic+ALL).

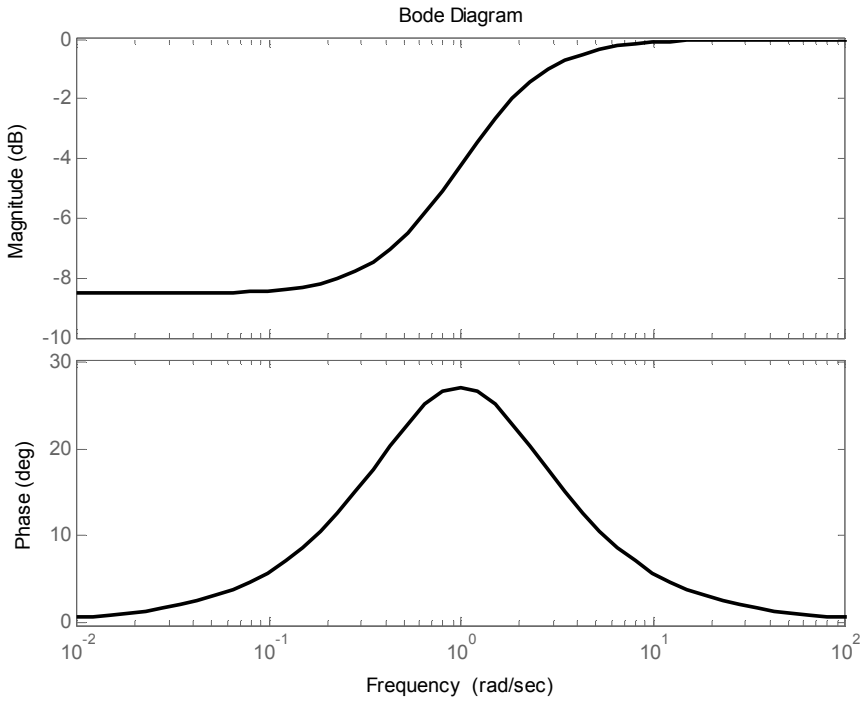

Figure 5.32: Lead Transfer function for Phase Advance Design

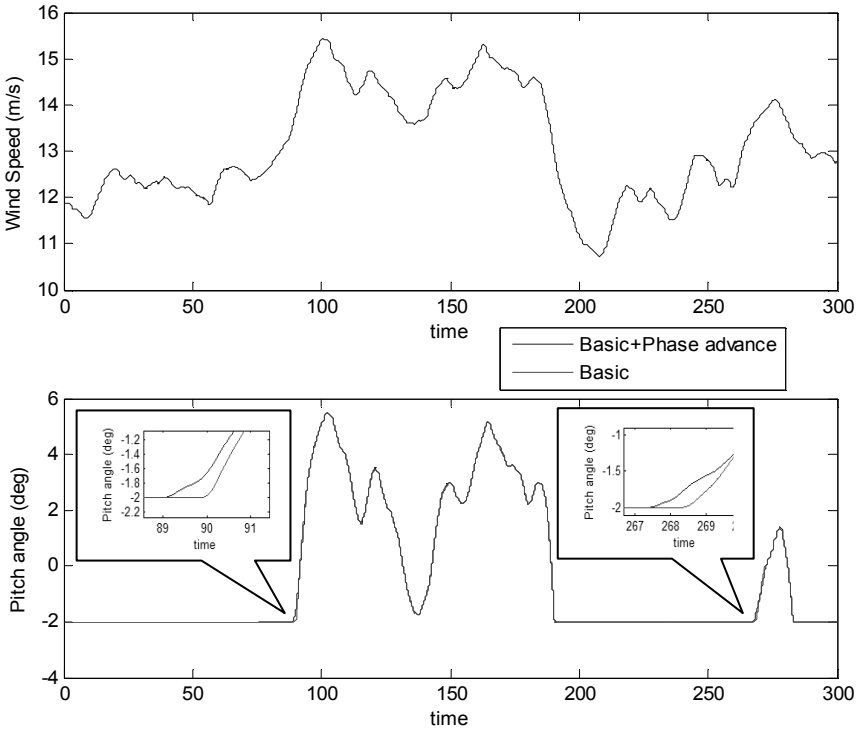

Figure 5.33: Phase advance demonstration using effective wind speed (Simulink simulation)

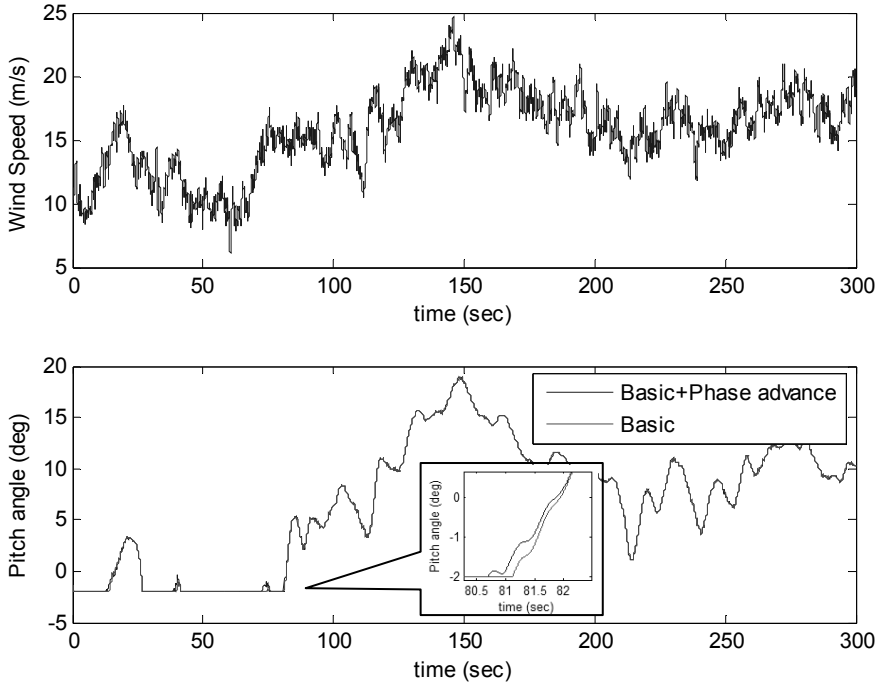

Figure 5.34: Demonstration of the Phase advance addition using point wind speed (GH Bladed simulation)

5.8 Linear Control Design

Apart from nonlinear global "gain-scheduling" techniques the controller design is carried out using classical control employing loop-shaping in the frequency domain to obtain the required dynamics for the overall system. Nowadays the industrial standard for designing commercial wind turbine controllers is the classical PID. Ideally the controller design procedure should be strongly integrated with the overall design of the wind turbine. The general objectives of the controller are to maximize energy capture in below rated wind speeds and to regulate power in above rated wind speeds.

5.8.1 Below Rated Controller (Torque Control)

Torque is used for below rated wind speed to control the rotor speed. The transfer function of the controller used for below rated operation is given by eq. (23) which is designed using loop shaping having in mind that it needs to provide very good disturbance rejection at low frequencies, the required 1rad/sec bandwidth and good

high frequency roll-off, see the open loop bode plot of Figure 5.35, and the sensitivity function of Figure 5.38.

$$C_{br}(s) = \frac{-1762.6146s - 163.98337}{s^2 + 2.2s} \tag{23}$$

The torque controller is a classical controller for the two constant speed regions shown in the operating strategy of Figure 2.4, whereas the Cp_{max} region is tracked through eq. (10) with no active control being involved. The closed loop Bode plots for two below rated wind speeds, see Figure 5.37, indicate the frequencies for which the controller is most effective. In general closed loop Bode plots are used to identify how disturbances dampen or propagate at different frequencies. In this case it is observed that there is no need for any extra control action as the controller dampens the disturbances very effectively; this fact is also verified from the sensitivity plot of Figure 5.38. The Nyquist plot is also depicted in Figure 5.36 indicating satisfactory stability margins.

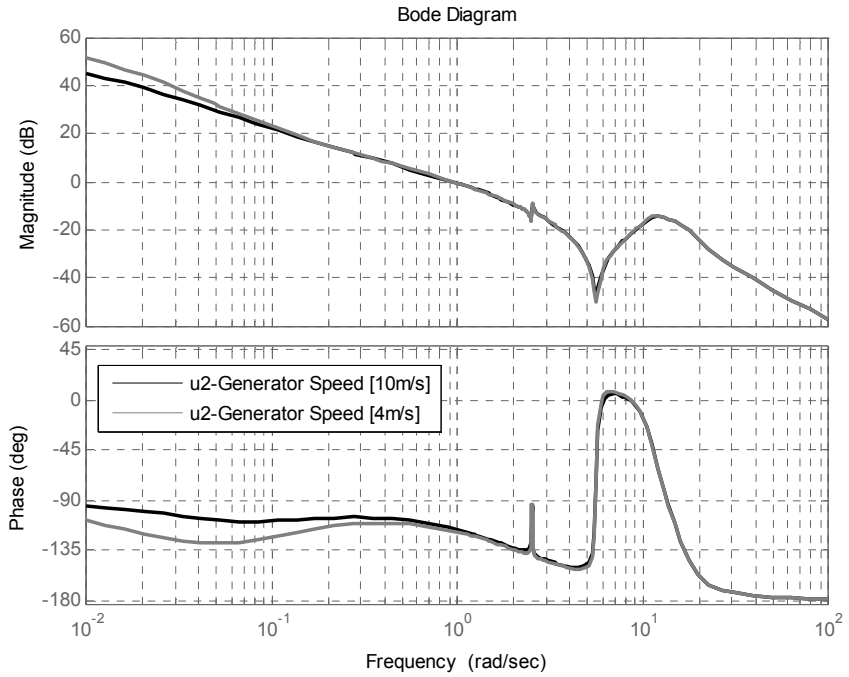

Figure 5.35: Open loop Bode plot of Reference torque demand to Generator Speed for 4m/s and 10m/s

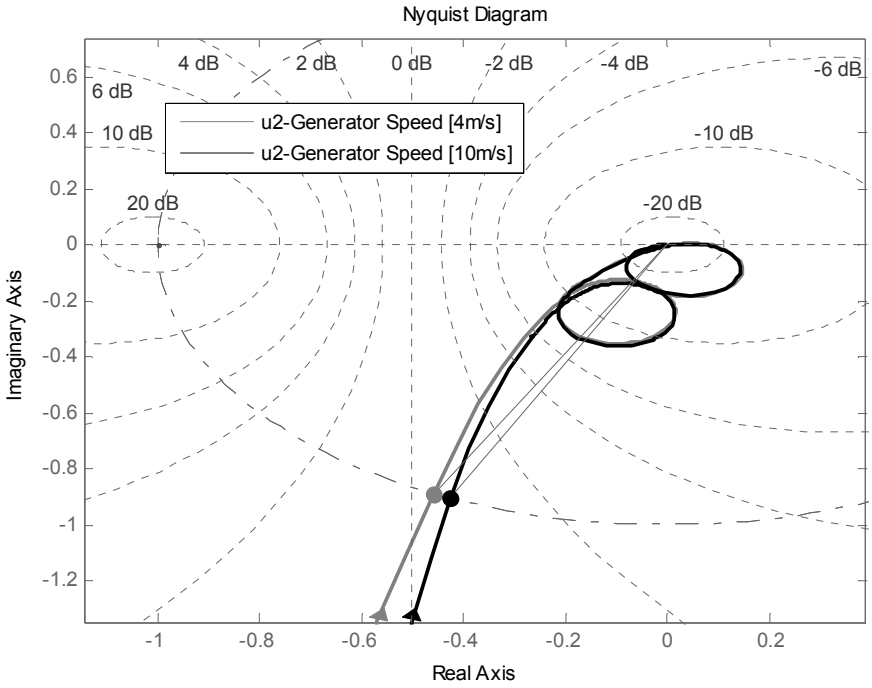

Figure 5.36: Open loop Nyquist plot of Reference torque demand to Generator speed for 4m/s and 10m/s

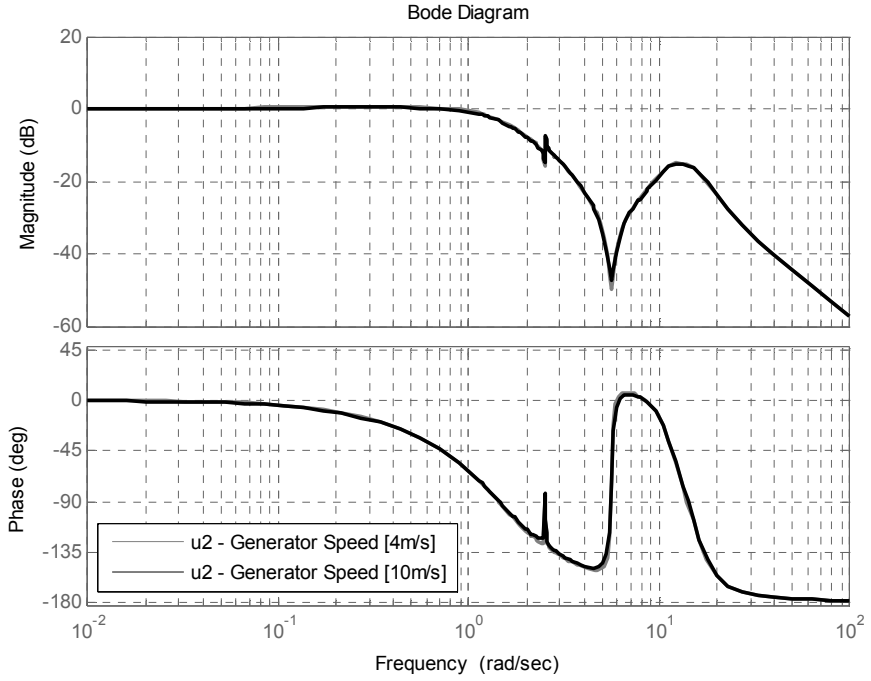

Figure 5.37: Closed loop Bode of Reference torque demand to Generator speed for 4m/s and 10m/s

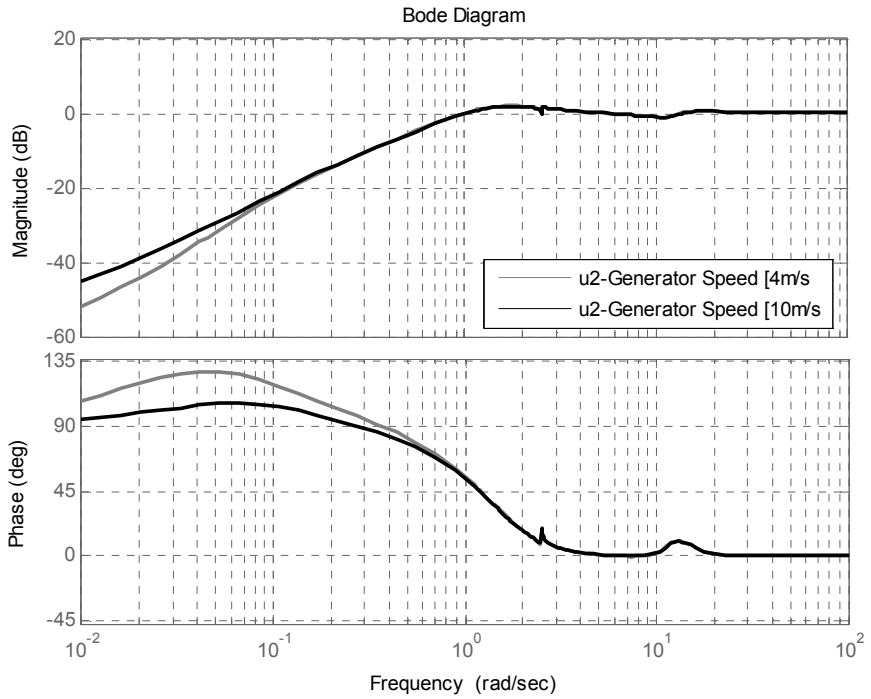

Figure 5.38: Sensitivity function Bode plot of Reference torque demand to Generator speed for 4m/s and 10m/s

5.8.2 Above Rated Controller (Pitch Control)

Pitch is used to control the rotor speed and torque is used to control the power of the wind turbine in above rated wind speeds. A complete switching system, which is described later in this Chapter, is used in the controller, for smooth switching between the different modes. In above rated wind speeds, the pitch-PI controller includes "gain scheduling" techniques as described in the non-linear design section, for the compensation of the aerodynamic nonlinearities occurring from the dependency of aerodynamic torque on the pitch angle, rotor speed and the wind speed. The transfer function implemented in the controller for the above rated operation is given by eq. (24). This is again a classical controller tuned using again loop shaping and aiming to achieve the low frequency disturbance rejection, high frequency roll-off and the required 1rad/sec bandwidth.

$$C_{ar}(s) = \frac{-0.098689s - 0.0054599}{s^2 + 2.2s} \tag{24}$$

As previously mentioned in section 5.4, the wind turbine aerodynamic behaviour is dependent on wind speed and is naturally highly non-linear. The usual approach to designing a controller involves performing the design at one wind speed and applying it for the full envelope using global "gain-scheduling". For the specific controller design, the wind speed chosen for the controller design is 15m/s. Good stability margins should always be aimed for in the design of the controller, otherwise the system might destabilize (not necessarily become unstable), and cause excessive load fluctuations [2]. Because the rotor continuously interacts with a very complex wind field, it is impossible to quantify the aerodynamic model uncertainty and is therefore impossible to establish a rule about the specific values of gain and phase margins that should be achieved in the design. However, practical experience suggests that a close to 10dB gain margin and close to 60 degrees phase margin is known to be sufficient [2], [46]. As the wind turbine increases in size these margins tend to become impossible to achieve, as the structural elements of the wind turbine get bigger, more flexible and dynamically more active. This does not mean that the controller for bigger wind turbines becomes unstable; however it suggests that the stability margins are reduced and the controllers need to be tuned more carefully.

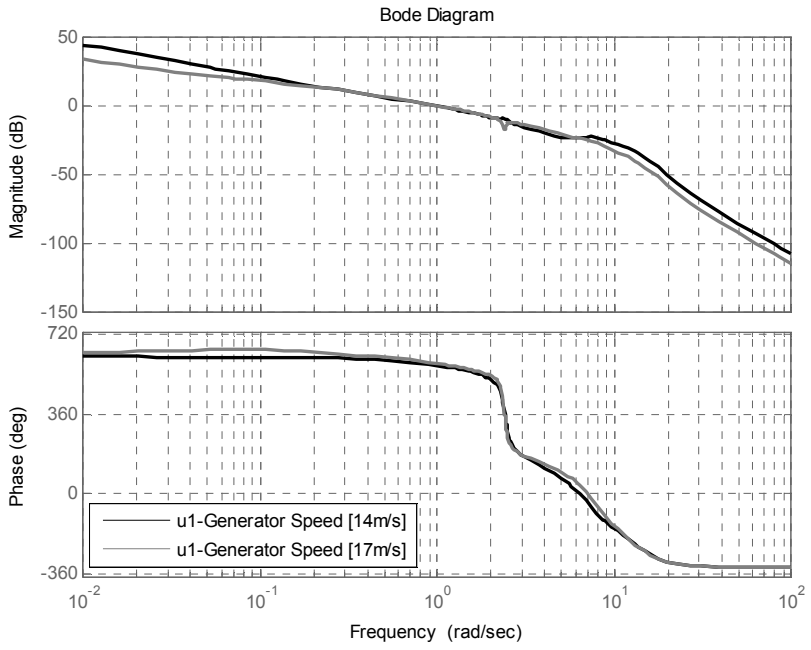

Figure 5.39: Open loop Bode plot of reference Generator speed to Generator speed for 14m/s and 17m/s wind speeds

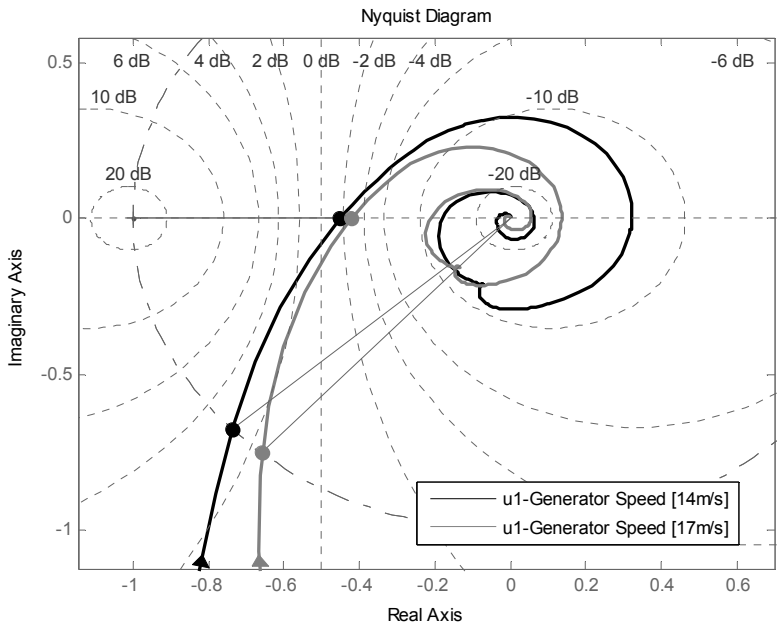

Figure 5.40: Nyquist plot of reference Generator speed to Generator speed for 14m/s and 17m/s wind speeds

In this case, it may be inferred from Figure 5.39, that stability margins of 7.1dB gain margin and 45 degrees of phase margin are achieved which give a satisfactory performance in conjunction with the 1rad/sec of bandwidth. Moreover, the closed loop Bode plot of Figure 5.41, along with the sensitivity function assessment of Figure 5.42, suggests that the design of the controller meets the requirements. Moreover, Figure 5.39 demonstrates very good low frequency disturbance rejection for the rejection of wind speed gusts and significant high frequency roll-off helping the reduction of the actuator activity.

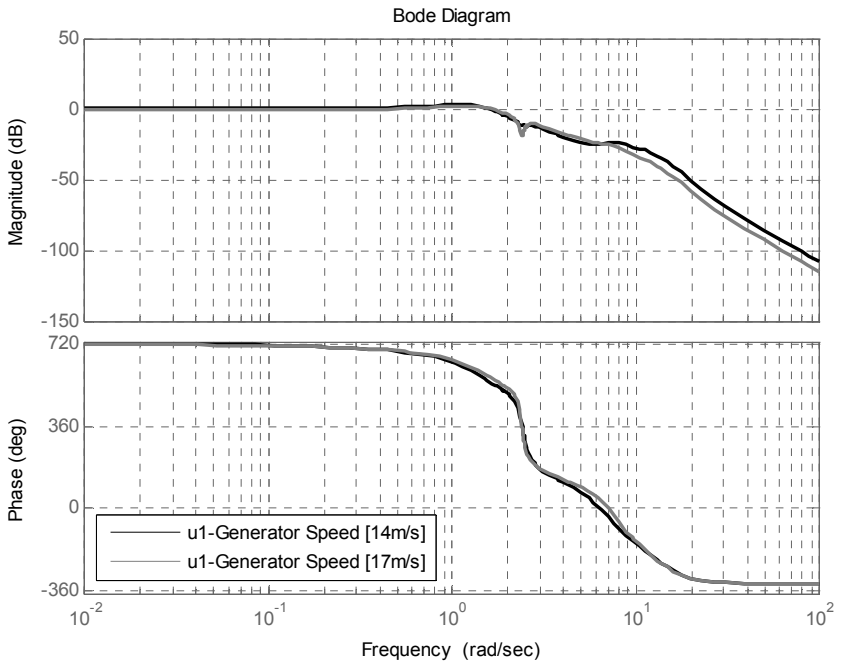

Figure 5.41: Closed loop Bode plots of reference Generator speed to Generator speed for 14m/s and 17m/s wind speeds

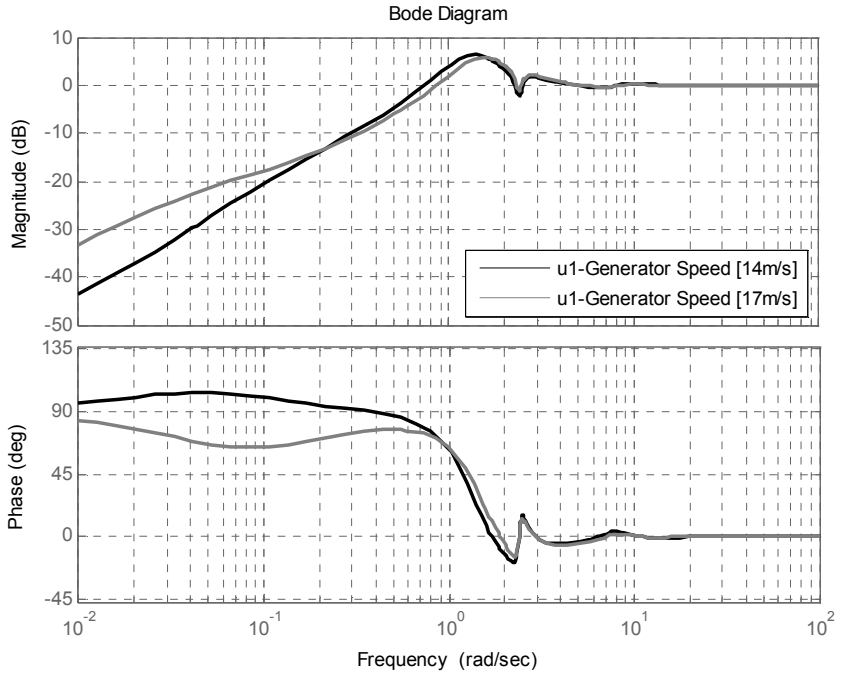

Figure 5.42: Sensitivity function Bode plots of reference Generator speed to Generator speed for 14m/s and 17m/s wind speeds

5.9 Switching Strategy

The switching strategy used here for the design of the controller of the wind turbine was developed by [46]. However, the full scheme description is given here for the sake of completeness, as it was tailored and applied to the 2MW exemplar wind turbine under study.

In order to achieve the desired operating strategy depicted in Figure 2.4, a series of events must be embedded into the controller through gains, switches, comparators and offsets. The switching strategy is perhaps the most important component of the controller. Switching is responsible for the selection of which parts of the controller are active at a given time and ensures smooth operation while minimising possible transient loads [26]. The schematic representation of the switching strategy used is shown in Figure 5.43. In this figure every signal is passed through the switch only if the condition of the switch is met.

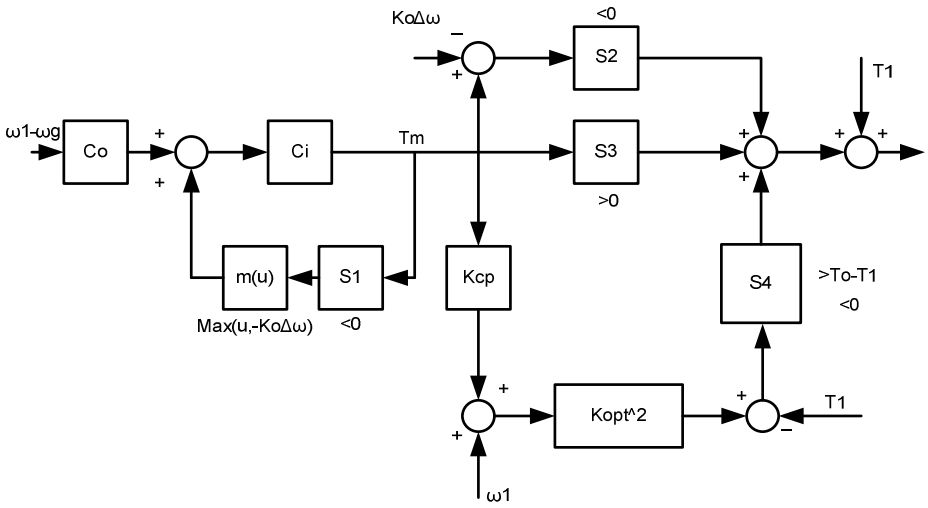

Figure 5.43: Controller switching strategy

The switching in the controller below rated is done on the basis of the value of the demanded torque of the generator which is represented in this case by T_m. The overall switching strategy may be split between above rated and below rated according to:

1. Below rated
    - Mode 0: First constant speed mode
    - Mode 1: Cp_{max} tracking mode
    - Mode 2: Second constant speed mode

2. Above rated

- Pitch control region

The main task of the switching strategy is to tightly follow the operating strategy discussed previously in section 5.3.1, which is depicted in Figure 2.4.

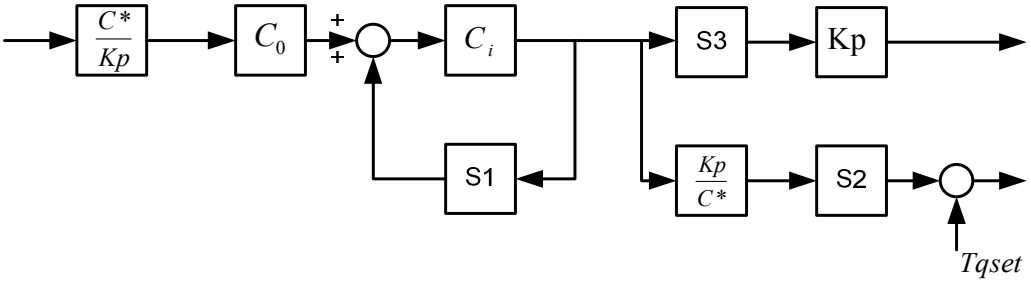

Figure 5.44: Basic switching structure [24]

The linear controller developed in the previous section needs to be split into $C_o(s)$ and $C_i(s)$, the outer and the inner components of the controllers such that $C_{br}(s) = C_o(s)C_i(s)$ as in [24]. The separation is carried out so that $\frac{C_o(s)\cdot C_i(s)}{1-C_i(s)}$ is a low pass filter. From the analysis that follows this split of the controller helps in keeping different parts of the controller active at all times ($C_o(s)$ & $C_i(s)$ are in series) which is essential for maintaining smooth switching without increased dynamic transients. By keeping the controller dynamics active at all times we effectively avoid switching between dynamically active paths which would cause transient loads appearing as spikes in the time series plots every time the controller switches to a different mode.

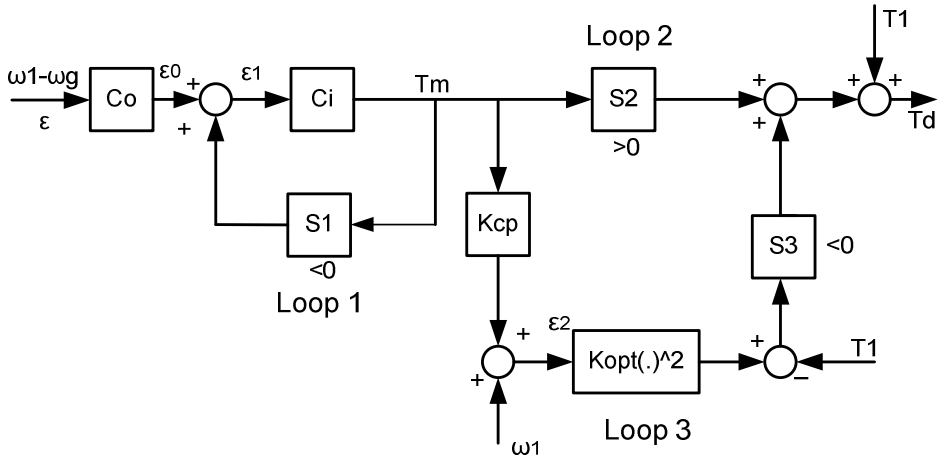

Figure 5.45: Switching between regions 1 and 2

5.9.1 Switching between modes 2 and 1

Mode 2, is a constant speed region, in which constant generator speed needs to be achieved by varying generator torque. In mode 1, the wind turbine is not actively controlled because generator torque is directly determined according to the power coefficient and the generator speed as in eq. (10). The switching from the 2nd constant speed mode to the $\mathrm{Cp_{max}}$ tracking mode is done when the generator torque value is less than the generator torque corresponding to the end of the $\mathrm{Cp_{max}}$ curve, according to the operating strategy of Figure 2.4. A controller structure that is implemented here and achieves smooth switching between these modes is that of Figure 5.45. In mode 1, $\omega_g < \omega_1$, and therefore $\varepsilon > 0$ which implies, given the negative gain of C_i, that $Tm < 0$. Therefore $S1 = 1$, closing that loop, and $S2 = 0$, opening Loop2. Therefore the relationship between Tm and ε is, $Tm = C_0 \frac{C_i}{1-C_i} \varepsilon = H\varepsilon$, H being a constant gain until 3 rad/sec.

To obtain an estimate of the error $-\varepsilon = \omega_g - \omega_1$, we set: $K_{cp} = \frac{1}{H}$ at the output of the K_{cp} block. Therefore adding ω_1, ε_2 is an estimate of the generator speed with the high frequencies removed. Squaring it and multiplying it by K_{opt} the torque for the Cp_{max} tracking region is obtained as in eq. (10). This torque should always be smaller than T_1, which is ensured by subtracting T_1, giving ε_3 which goes through S3 after which T_1 is added. When the rotational speed has reached ω_1, ω_g will be greater than ω_1, changing the sign of T_m and ε_3 which changes the state of all three switches. The relationship between T_m and ε is now: $T_m = C_0 C_i \varepsilon = C_{br} \varepsilon$, being the constant speed controller.

5.9.2 Switching between modes 1 and 0

Similarly, as the wind speed decreases, the rotational speed decreases to ω_0 when the controller must change to the constant speed mode in order to maintain it at that speed. This is done controlling on $\omega_1 - \omega_g$ which introduces the need of the addition of an offset in the first summation of Figure 5.45 in order to correct the output equilibrium set-point. The value of that offset is given by (25).

$$offset = -C_0(0)(\omega_1 - \omega_0) = -K_0 \Delta\omega \tag{25}$$

The low frequency gain of Loop 1, being 1, it can be inferred that at the switching point the value of Tm is precisely $-K_0\Delta\omega$ and therefore, the offset can be implemented as part of the switch S1 as a saturation level so that the output of this loop is never smaller than $-K_0\Delta\omega$, see Figure 5.46. Since the switching in both directions must be done continuously, the value of T_m when controlling in constant generator speed for an output of T_0 , that is when it is about to switch, must be equal to the value of T_m in mode 1.

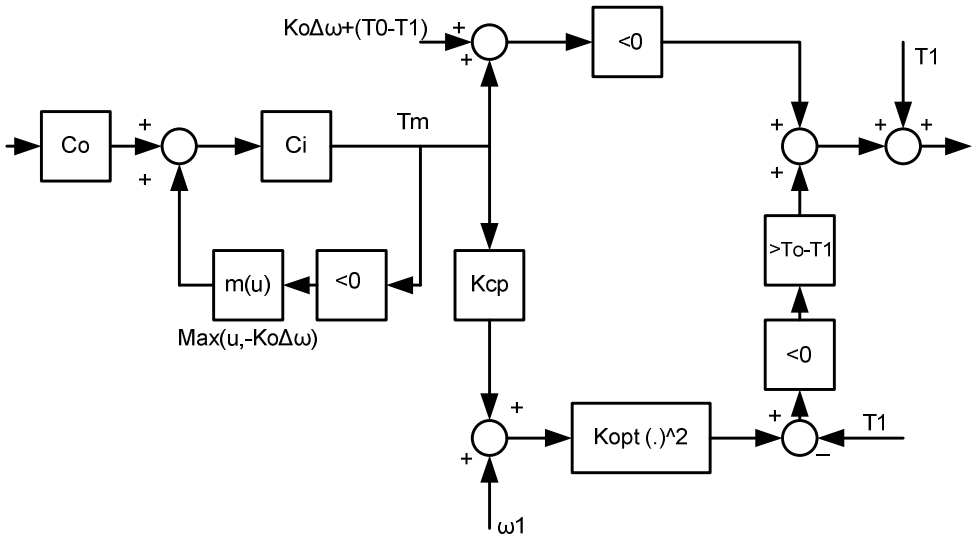

Figure 5.46: Switching between modes 1 and 0

5.9.3 Switching from below rated to above rated

The controller must be active in all modes at all times in order to avoid any switching transients.

First constant speed region

In the first constant speed region, Loop 1 is open since the gain of C_i is negative and $T_m > 0$. S2 is a switch allowing positive signals to pass through.

Since $T_0 = K_{opt}.\omega_{g0}$, and $\omega_g < \omega_{g0}$ it follows that $\varepsilon_3 < 0$, and therefore S3 is open.

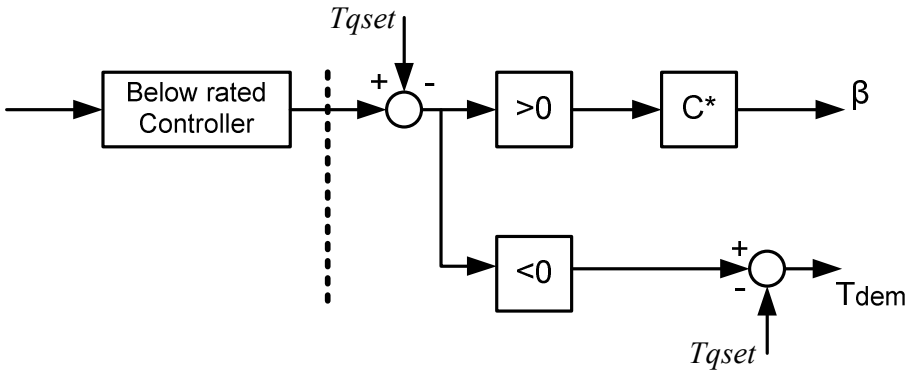

Figure 5.47: switching from below to above rated

When $\omega_g > \omega_{g0}$, $T_m < 0$ and therefore S1 is open, closing Loop 1 which is then described by (26).

$$\frac{C_{br}(s)}{1 - C_{br}(s)} \tag{26}$$

Equation (26) is basically an all pass filter. Since T_m is negative, S2 is open and ε_2 is an estimator of the generator speed. This is because: $\varepsilon_2 = K \cdot T_m + \omega_{g0} \approx \omega_g$ with $K = -1$. In this case $\varepsilon_3 \approx K_{opt}\omega_g^2 - T_0 > 0$ and therefore $T_d \approx K_{opt} \cdot \omega_g^2$.

Representative results from the of the 2MW turbine as given from the GH Bladed simulation are given in Figure 5.48 and Figure 5.49. These demonstrate the accuracy of the switching during moving from 1st constant speed mode to Cpmax tracking, and then switching from Cpmax tracking mode to the 2nd constant speed mode. The data in these two figures represents the buffers placed in the loops monitoring the switching between these modes; see Figure 5.45 and Figure 5.46. The results indicate fast and smooth transition with no overlapping operation of any two modes, i.e., when the buffer of one mode is active, the buffer of the other modes is zero.

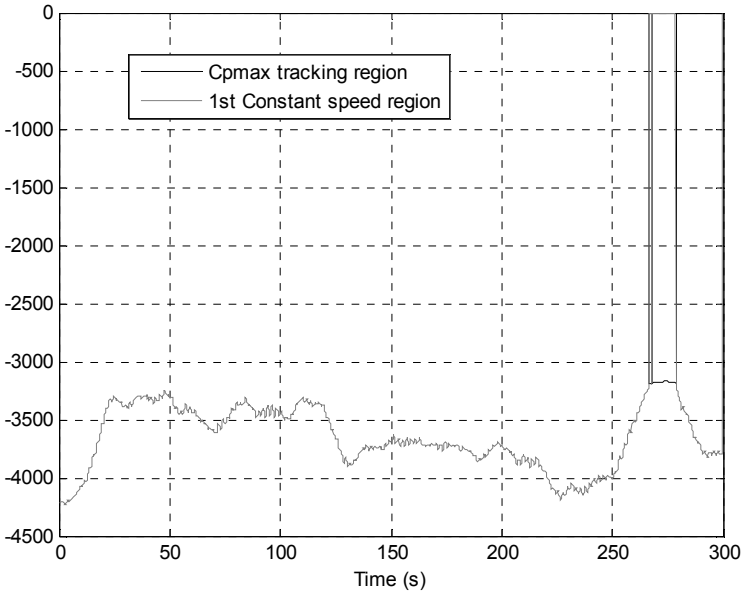

Figure 5.48: 4m/s switching between 1st constant speed and Cpmax tracking

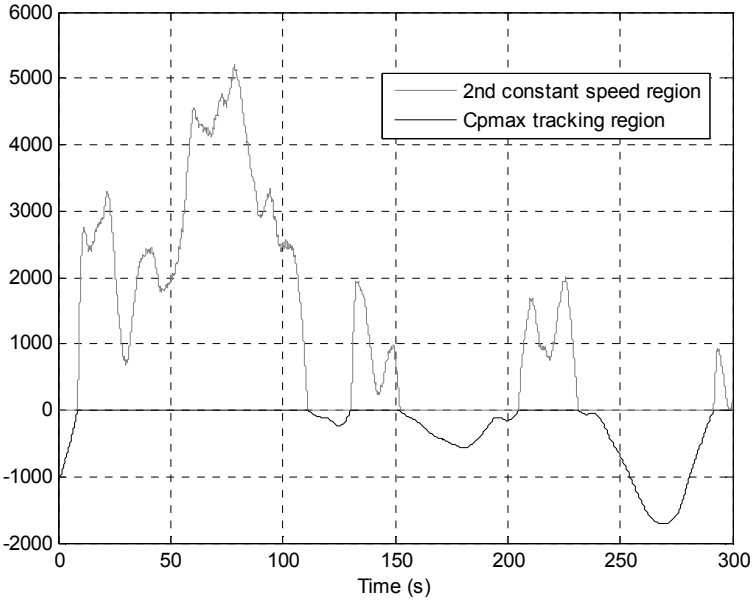

Figure 5.49: 8m/s switching between 2nd constant speed region and Cpmax tracking

5.10 Anti - Windup Scheme

One common possible source of performance degradation of a system is integrator windup effect. All physical systems have some kind of actuator saturation. A typical example is a valve, controlling a flow rate. This can operate between the limits of being open and completely closed. Apart from this simple example, all existing actuators are restricted by some form of hard limits, as seen in Figure 5.50. Usually, in the beginning of a process after a set-point change has been applied to the system, the control variable is likely to quickly reach the actuator limits during the transient response. In such a case the control signal finally reaching the plant is different than the control signal assigned by the controller. The control error decreases slower than it should and the integral term sums up (winding process) becoming unusually large. As a consequence there may be a reduction in stability margins or reach instability [2].

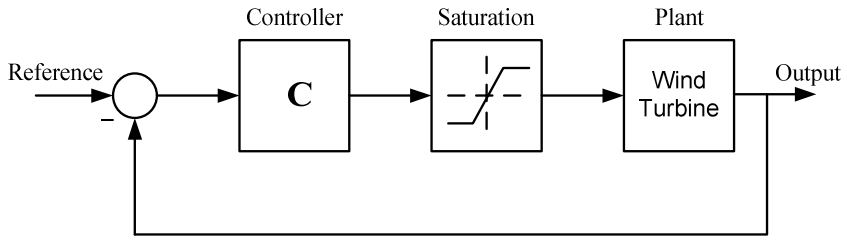

Figure 5.50: Basic system with saturation

The actuator anti-windup prevents the pitch rate from exceeding its maximum value. The estimation of the pitch rate is compared with the maximum value it can reach. In the case the latter is greater than the maximum value, the anti-windup loop is closed.

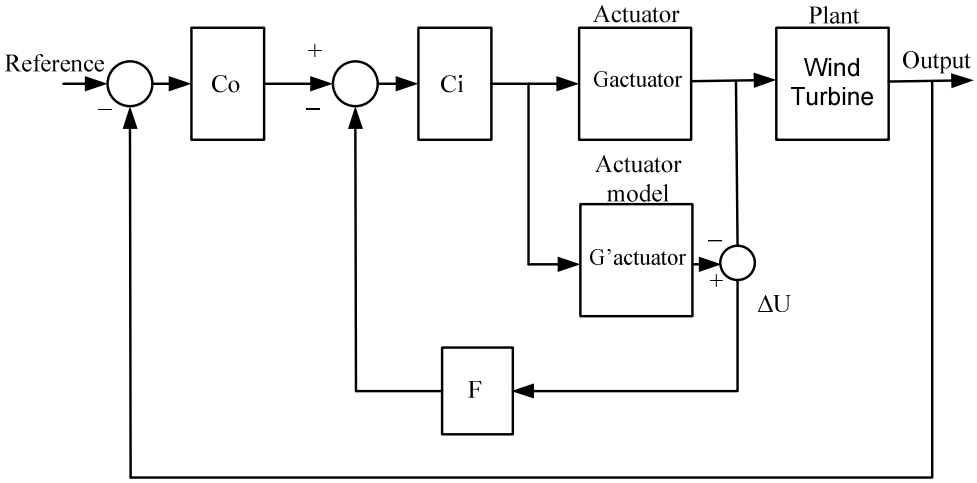

Figure 5.51: Reformulation for controller start-up to avoid the windup effect

The anti-windup strategy adopted here is discussed in [2], [38] and is depicted in Figure 5.51. This approach adopts a dynamic feedback as opposed to other strategies adopting a static approach [5]. The controller here is partitioned into inner and outer loops and the anti-windup feedback only affects the inner dynamics of the controller. The feedback loop measures the difference between the outputs of the actual and a model actuator and the difference is filtered through F, and is fed back. The task of the filter F is to activate or isolate the integrator in order not to "wind up" in the event of actuator saturation. In the case of a wind turbine, apart from the constraint limits existing in the actuators, velocity and acceleration limits may reduce the stability margins by a significant percentage [2].

Since the controller is discrete and in order to avoid the delay in the feedback loop, the transfer functions have been implemented in such a way that its output value depends on the previous input plus the current input times a constant.

5.11 Conclusions and Performance assessment

Having design and discussed all the necessary aspects that the baseline wind turbine controller involves, it is thoroughly tested by full envelope simulation runs in GH Bladed. The results are presented in Appendix B. Initially, the results using the basic SISO controller on its own are presented. This controller is referred to as SISO(Basic) and does not contain a tower feedback loop, a phase advance

mechanism or an anti-windup scheme. Then it is assessed against the same controller but with the addition of a tower feedback loop, referred to as SISO(Basic+TFL). Finally, the SISO(Basic) controller is compared to a controller with the addition of the tower feedback loop, the anti-windup scheme and the phase advance mechanism altogether, referred to as SISO(Basic+ALL). The objective of presenting these results is first of all to verify that these controllers meet the design requirements and secondly to show that there is no compromise in the performance by augmenting the controller with additional loops (e.g. TFL, Phase advance etc.). The outputs presented in the appendix are:

- Wind speed time series
- Generator speed time series and spectrum
- Generator torque time series and spectrum
- Electrical power output time series and spectrum
- Pitch angle time series and spectrum
- Blade root lifetime edgewise bending moment loads
- Blade root lifetime flapwise bending moment loads
- Tower base lifetime side to side moment loads
- Tower base lifetime fore and aft moment loads

The presentation and comparison of the above includes assessment in above and below rated wind speeds and for different seeds of wind.

6 Design of a Co-ordinated controller for Tower Fatigue Load Reduction

As wind turbines increase in size, the tasks being assigned to the controller increase and their design becomes more demanding; in particular, the controller may be required to reduce the tower fatigue loads. The basic approach to tower load fatigue reduction is to employ a tower feedback loop (TFL) as described in Chapter 5. It typically achieves a 4%-7% fatigue load reduction depending on the configuration details of the wind turbine. In this Chapter, two schemes of a Co-ordinated controller, one regarding speed control and the second regarding power control which is an extension-improvement to the first one, are introduced and analysed. They aim to increase the tower fore-aft load reduction whilst simultaneously reducing the pitch activity and circumventing the limiting right-half plane zeros. As there is relatively little literature about new controller designs dealing with tower load reduction, this Chapter serves as a new guideline and framework dealing with this issue.

6.1 Review and problem description

It is a fact that the biggest contribution to the cost of offshore wind turbines is the tower and foundations. Therefore it is clear that addressing the tower loads, and managing to reduce them even by a small percentage is well worthwhile. The exponential increase in the size of wind turbines in recent years has led to more flexible structural elements, thus making the controller design task more demanding and challenging. Apart from the traditional requirements on the controller described earlier, i.e. regulation of rotor speed with pitch to maintain constant power output and maximization of energy capture in below rated wind speeds, more demanding tasks such as tower fatigue load reduction are nowadays of particular interest. Size related issues such as the tower dominant frequency becoming lower as the wind

turbine size increases also need to be taken into account as described in [20]. Moreover the tower fore-aft movement interacts with the drive-train introducing a pair of right half plane zeros causing limitations to the controller design.

The idea for the research done here occurred from the observation that reducing the blade actuator activity effectively reduces the fore-aft loads of the tower. Preliminary results of applying a low pass filter to achieve this are presented in [61], however no attempt is made to develop a complete design approach that would maintain the full performance required of a controller. In order to illustrate this claim a comparison is done using the 2MW exemplar wind turbine under study.

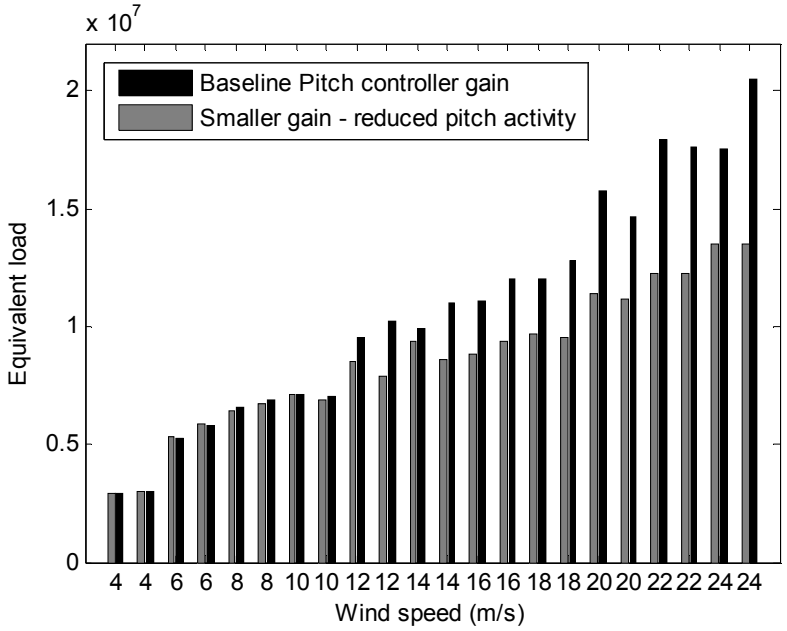

Figure 6.1: Demonstration of load reduction by reducing pitch activity

Firstly, the very basic controller is run for all wind speeds, then the pitch controller gain is reduced by around 50% and the full envelope simulation is repeated. Reducing the actuator activity results in a clear fore-aft moment tower load reduction of about 9%, and this comparison is depicted in Figure 6.1. However, reducing the gain of the pitch controller, results in a significant degradation of the wind turbine performance. The speed control performance and the Power output are greatly compromised, which is clearly observed in Figure 6.2 and Figure 6.3 respectively. This occurs because the bandwidth is dropped significantly and the stability margins are greatly reduced. However, the fact that reducing the actuator activity reduces the

fore-aft moment loads of the tower motivates us to explore new control algorithms that achieve significant reduction of the tower loads without compromising the performance of the wind turbine.

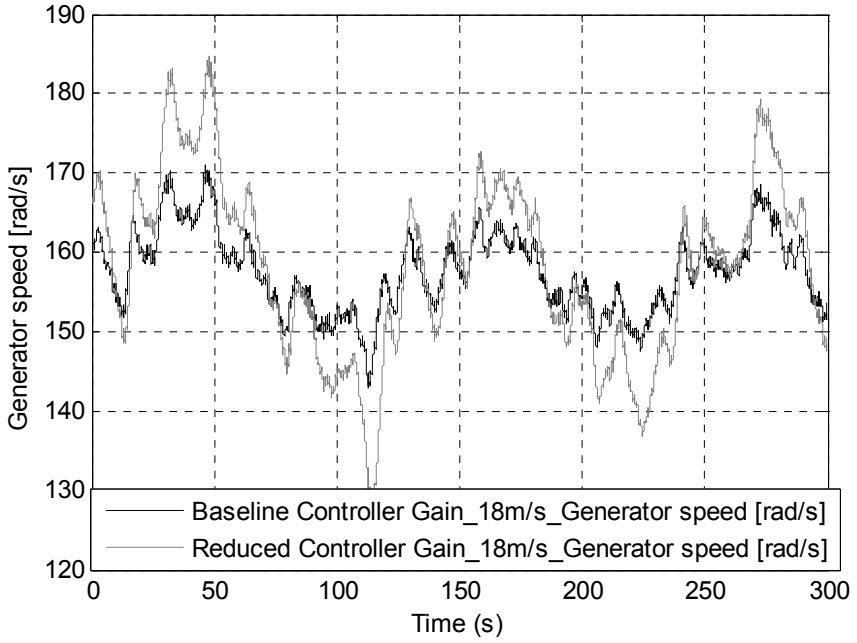

Figure 6.2: Gen. Speed performance comparison for Baseline and Reduced Pitch Controller gain

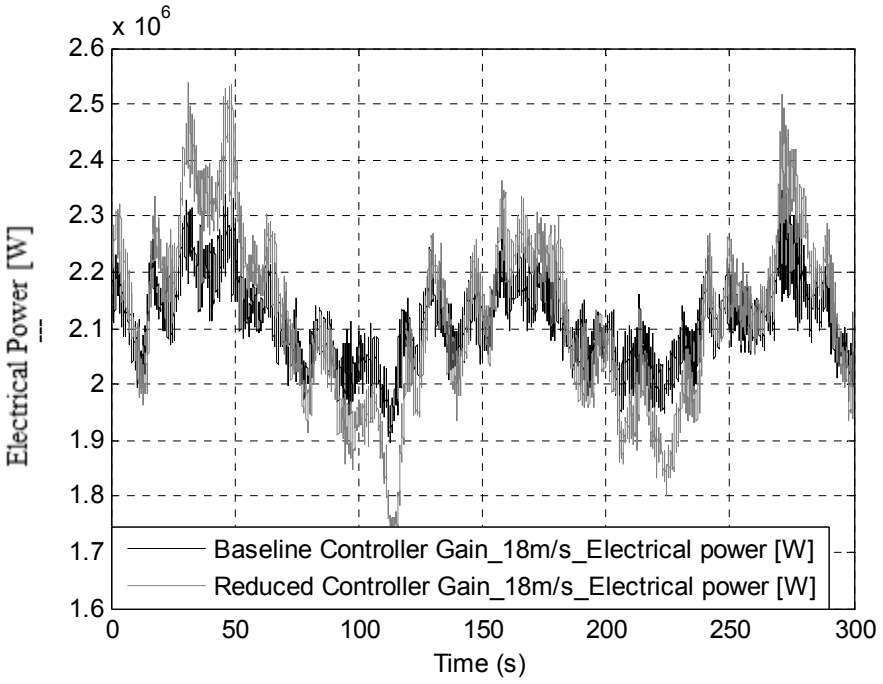

Figure 6.3: Electrical power performance comparison for Baseline and Reduced Pitch Controller gain

A co-ordinated controller design is presented in this Chapter and applied to the 2MW Supergen exemplar wind turbine. This approach introduces an additional parallel path to the controller that takes care of the right half plane zeros, increases the stability margins of the system and gives a substantial reduction in the lifetime loads of the tower, especially when combined with the traditional Tower Feedback Loop.

In the present chapter, a description of the linear models used to design and tune the Co-ordinated controller is given. An assessment of the performance of the traditional approach tower feedback loop to cancelling the fore-aft mode of the tower is presented. This will serve as a benchmark to which the new co-ordinated approach is compared. The problem of right half plane zeros which impose limitations on the traditional controller design is also thoroughly discussed. The approach of the co-ordinated controller design is analysed and all the results regarding its performance assessment are presented. Moreover, the results obtained from the combination of the traditional approach and the Co-ordinated controller approach, are even more significant. However, this scheme has some drawbacks concerning fluctuations that occur in the output power and aerodynamic torque, although speed is controlled sufficiently. To overcome these drawbacks, an improvement to this scheme is presented and designed in Section 6.7, based on power control, while maintaining similar results on tower load reduction.

6.2 Linear Models and Validation

The linear models of the wind turbine which are used for representing the wind turbine dynamics are presented in Chapter 3. These models take into account the tower and blade modes as well as their interaction. The importance of this lies in the fact that the tower and blades may introduce right half plane zeros, which cause restrictions discussed in the following sections. For the context of this research, these linear models are used for the design and tuning of the controller as seen in the previous chapter. The controllers are then compiled in C++ appropriately for use in GH Bladed. All the linear models are validated against the GH Bladed ones, and all the results are obtained from full GH Bladed aeroelastic simulations as done in the previous chapters of this thesis.

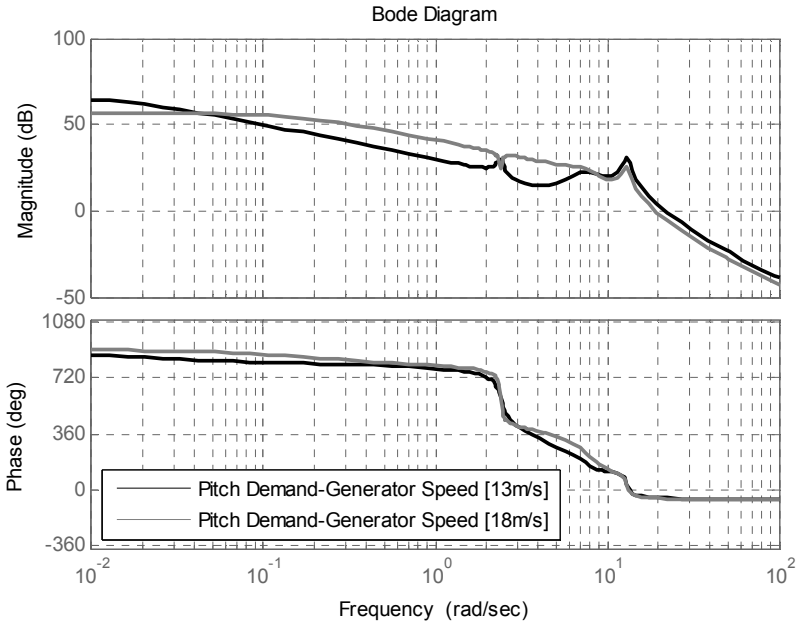

Figure 6.4: Dynamics linking Pitch demand to Generator speed

The dynamics of the 2MW machine linking pitch demand to generator speed, as well as the dynamics linking pitch demand to tower speed are depicted in Figure 6.4 and Figure 6.5.

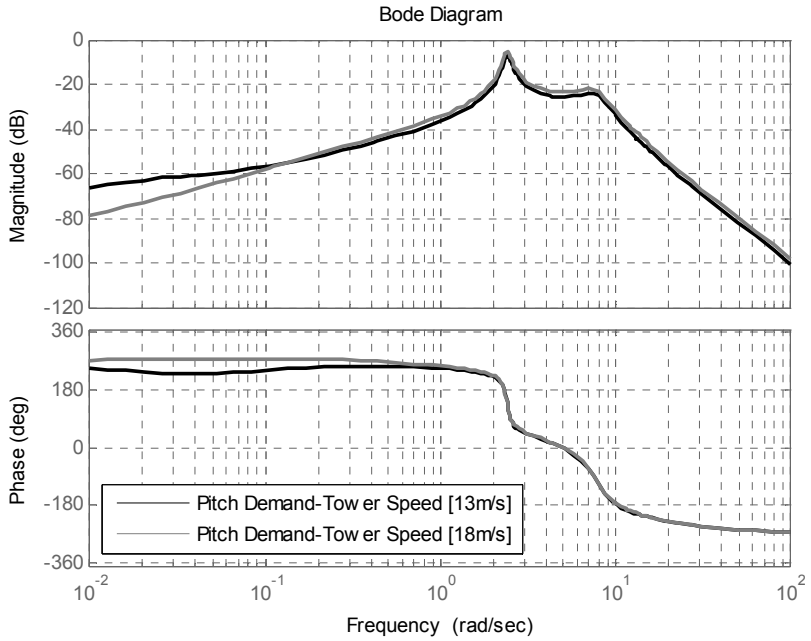

Figure 6.5: Dynamics linking Pitch demand to Tower speed

6.3 Traditional Approach

The usual approach adopted recently for the reduction of the fore-aft mode of the tower, is to augment the pitch demand by an additive adjustment in response to a measurement of the tower head velocity or acceleration as discussed in Chapter 5. In effect there are two pitch feedback loops; an inner tower feedback loop and an outer rotor speed feedback loop. The simplified block diagram of the system augmented by the tower feedback loop is depicted in Figure 5.25.

For benchmarking reasons the results of the usual approach to the tower feedback loop are presented here in terms of fatigue load reduction. The spectra of the tower fore-aft signal for the basic controller and its augmentation with the TFL are depicted in Figure 6.6 and Figure 6.7, for wind speeds of 14m/s and 20m/s respectively. Taking into account the dominant frequency mode of the tower lies at 2.45rad/sec, it can easily be observed that there is a significant amount of reduction of that mode. The integral of the frequency f times the spectrum $S_x(f)$ given by eq. (27), is also given in the same graph, which gives a reasonable first estimate of the fatigue loads of the signal. In eq. (27) U_w is the upper limit of the frequency range of the plot.

$$\int_0^{U_w} f \cdot S_x(f) df \tag{27}$$

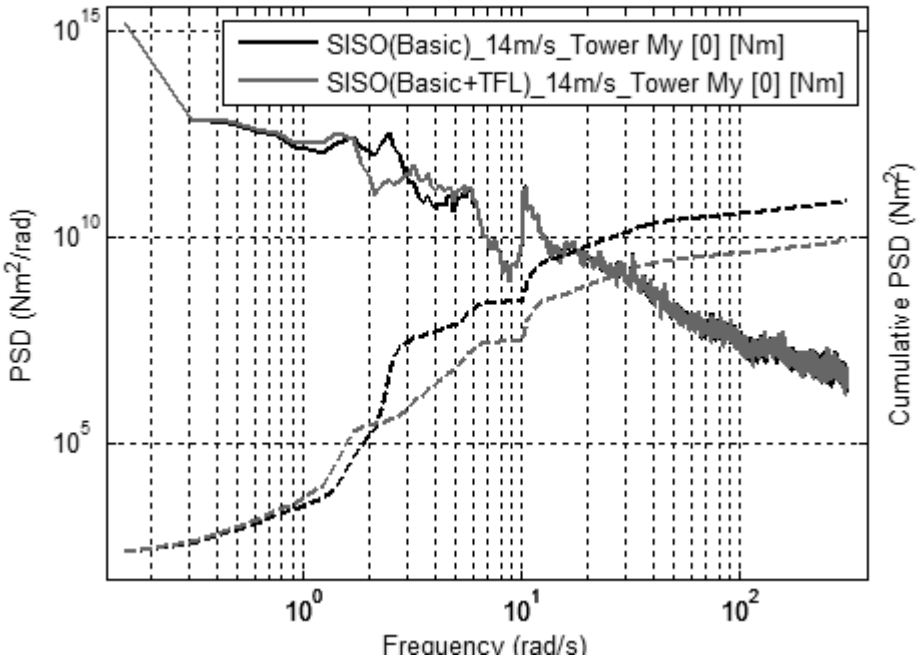

Figure 6.6: Spectra of tower base fore-aft moment for the two SISO controllers at a mean wind speed of 14m/s

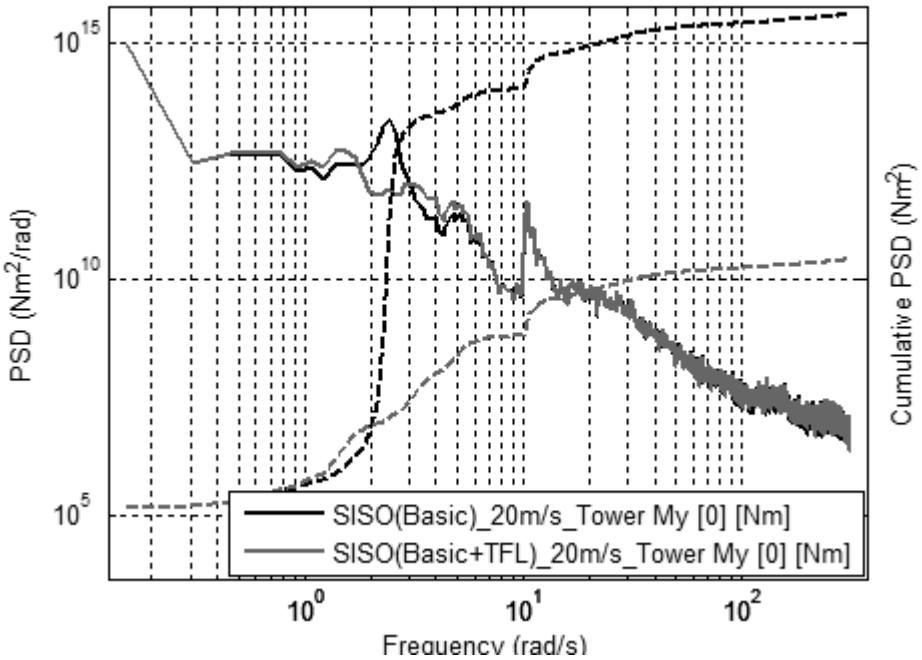

Figure 6.7: Spectra of tower base fore-aft moment for the two SISO controllers at a mean wind speed of 20m/s

The full fatigue load results for all wind speeds and each of the two different wind seeds is given in Figure 6.8. These are obtained by Rainflow counting methods, see Appendix C, which are well established and widely used for fatigue load assessment.

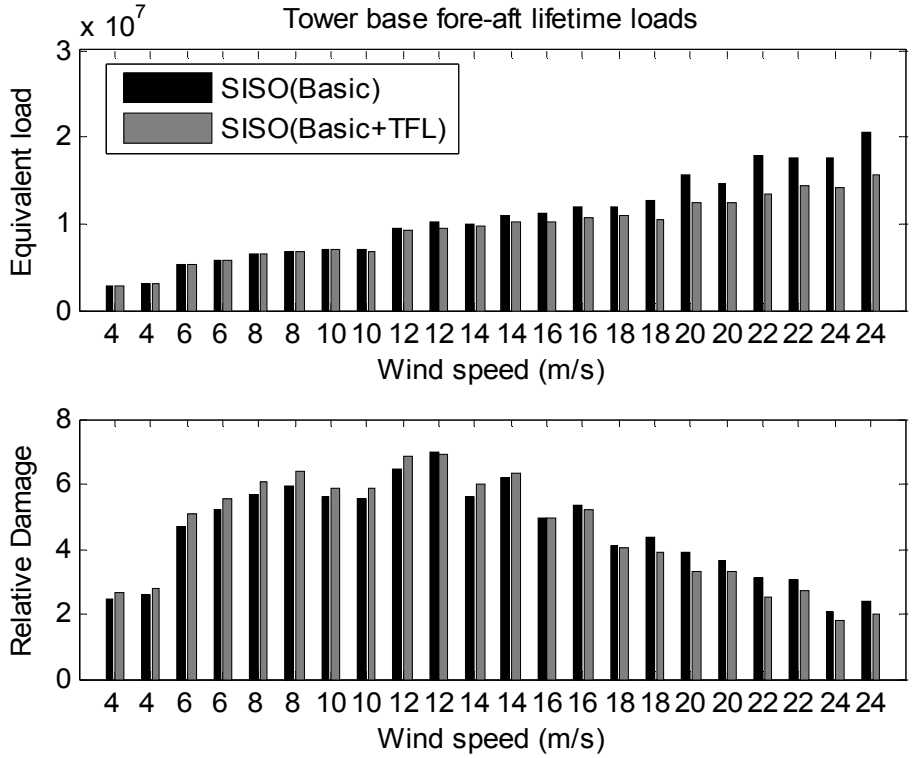

Figure 6.8: Tower lifetime fatigue load comparison of the two SISO controllers for each wind speed

Figure 6.8, along with Table 1, show a reduction of 6.67% in the fore and aft lifetime loads of the tower by augmenting the speed loop with the tower feedback loop.

Table 1: Life time tower fatigue loads for two controllers and two wind seeds

Lifetime Equivalent Tower Fore-Aft Moment Loads	
Controller	**Normalised lifetime loads**
SISO(Basic)	7.2186e+06
SISO(Basic+TFL)	6.7369e+06
6.67% Reduction	

6.4 Right Half Plane Zeros

There is a large category of plants including wind turbines that have naturally occurring right-half plane zeros present in their dynamics, the so called non-minimum phase plants. These zeros can limit the advantages of applying feedback control on the specific system [32], [33]. From the Bode plots linking the dynamics of pitch demand to generator speed, a phase loss of 180° can be observed around the frequency of 2.45rad/sec, the dominant mode frequency of the tower, see Figure 6.9. The limitations that RHPZ's impose on the system and the design of the controller are thoroughly analysed in [22]. These limitations especially affect the bandwidth and stability margins of the system.

There are two pairs of right half plane zeros present in the dynamics of the wind turbine. As mentioned earlier, the first pair linking pitch angle to generator speed is due to the tower, and the second pair is due to blade flapwise mode. They impose limitations on the stability margins of the power loop. The physical interpretation of these zeros is as follows. Given an increase in wind speed, the pitch demand increases in order to decrease the aerodynamic torque captured from the wind. This causes the thrust on the blade to be decreased, and as a result the rotor/nacelle moves forward. The associated increase in the relative wind speed causes a temporary increase in torque. Therefore, the control activity which initially aimed at decreasing the torque causes an initial unwanted increase in the aerodynamic torque. The proposed design of a co-ordinated controller counteracts and removes these zeros as is discussed in the succeeding section.

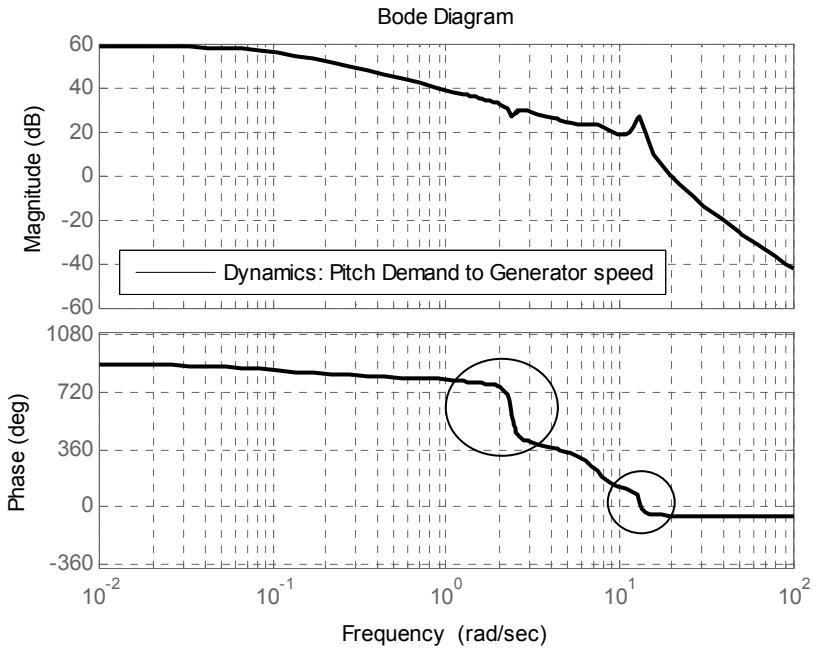

Figure 6.9: Dynamics of the wind turbine linking Pitch demand to Generator speed

6.5 The Coordinated controller

A novel approach to the tower fatigue load reduction is presented here. It addresses the interaction of the controllers for the inner and outer loops; in particular, the rotor speed controller is designed to simultaneously minimise the tower loads. This is achieved by adopting a parallel path structure for the controller, see Figure 6.10. Other than the aerodynamic nonlinearity that can be globally removed by the pitch controller employing gain-scheduling techniques as discussed in the previous Chapter, the plant is essentially linear. Dynamics at different wind speeds are the same in the range of frequencies important to the design of the controller. Therefore there is no need for additional gain-scheduling and the controller may be designed for a single wind speed.

The modification made to the rotor speed controller is such, as to reduce the pitch activity over a region near the frequency of the tower mode, 2.45rad/sec, as well as to remove the right half plane zeros resulting from the tower mode. As discussed earlier the right half plane zeros will make the system instantly perform worse before they perform well again. The fact that by adding a parallel path modification to the system will remove the existing pair of zeros is extremely significant, as the plant is

altered for a specific range of frequencies without compromising the overall operation and performance of the wind turbine. For the context of wind turbines it can be observed from the Nyquist diagram of Figure 6.17 that this gives room for exploiting higher gains that will further improve the speed control loop. Also, as wind turbines get bigger in size these RHPZ's become more restrictive, therefore it is very important to be able to remove them.

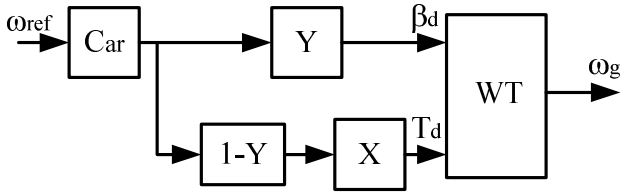

Figure 6.10: Block diagram implementation of the Coordinated controller scheme

A closer view of the dynamics of the plant is given in Figure 6.11 and Figure 6.12, which is helpful when designing the coordinating function later on this chapter. In both figures A is the dynamics from Pitch demand to Generator speed, B the dynamics from Torque demand to Generator speed and C the dynamics from Torque demand to Generator torque.

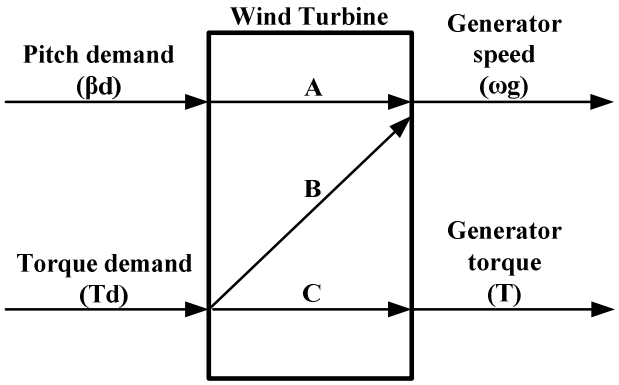

Figure 6.11: Wind turbine internal view

The region of interest for this study is the above rated one, although the simulations are always carried out for the full operational envelope of the wind turbine. The above rated pitch controller transfer function is given by eq. (24), and its design procedure is detailed in Chapter 5.

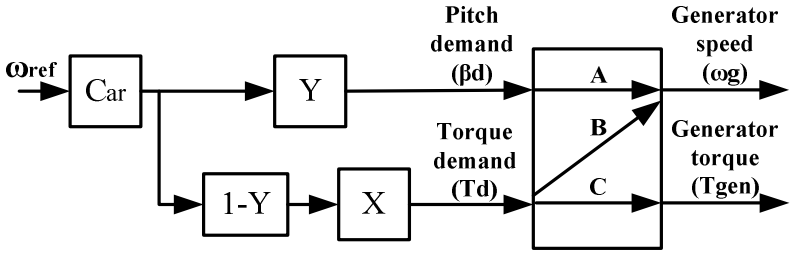

Figure 6.12: Coordinated scheme with internal view of the wind turbine

6.5.1 The Tower Filter Design

The tower filter *Y*, is a filter designed to reduce pitch activity in the vicinity of the frequency of the tower. Two types of filter sets were explored for suitability, one being a high and a low pass filter and the second being a notch and a band pass filter see Figure 6.13 and Figure 6.14.

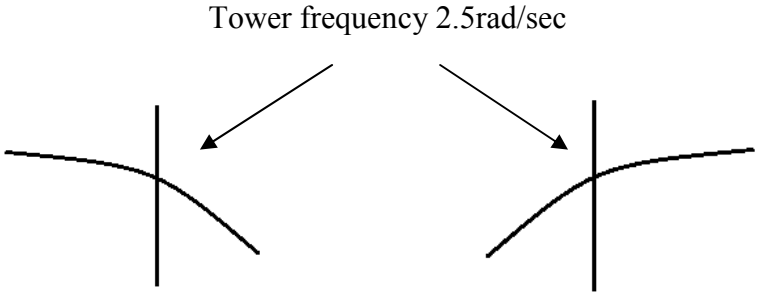

Figure 6.13: Low and high pass filters centred at tower frequency

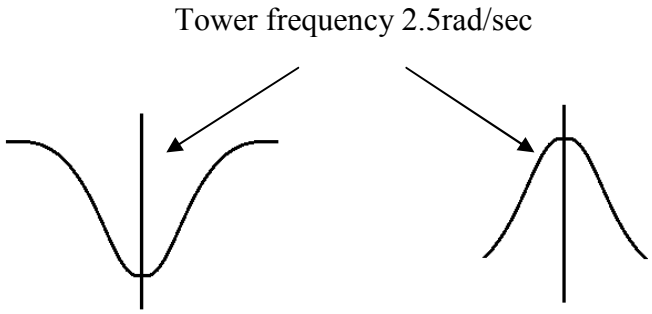

Figure 6.14: Notch and band pass filters centred at tower frequency

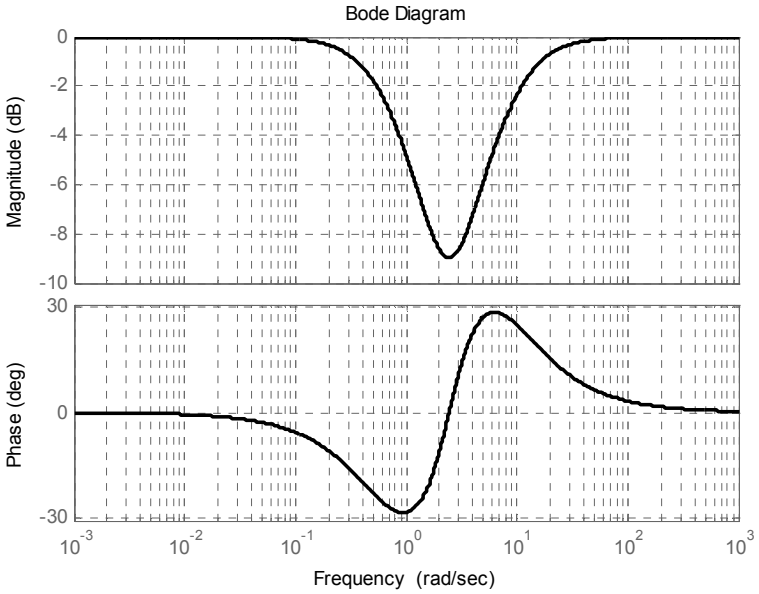

Figure 6.15: Bode plot of notch filtered designed for the CCD scheme

The low and high pass filters are quickly ruled out of the choice palette as they act on a wide range of frequencies, therefore, causing increased variations in the torque and power compared to the notch filter, see Figure 6.26 and Figure 6.27. Moreover, a direct comparison of the two filters in terms of fore-aft moment tower load reduction reveals a clear advantage of using a notch filter, see Figure 6.28 and Table 4. However the results obtained from using both sets of filters is presented here for the sake of completeness. The low pass filter used for the initial tests is given by equation (28).

$$Y_{LP} = \frac{0.3}{s + 0.3} \tag{28}$$

Amongst others tested, the notch filter designed for the specific wind turbine has the transfer function of eq. (29) and is depicted in Figure 6.15. A guideline for designing the appropriate notch filter for a specific wind turbine is given in the conclusions of this Chapter.

$$Y = \frac{s^2 + 3.2s + 6.003}{s^2 + 9s + 6.003} \tag{29}$$

The design of the filter starts with a simple notch filter centred at the frequency of the tower mode i.e. 2.45rad/sec, and is then amended according to the guidelines discussed later on to achieve optimum performance. Designing the notch filter too wide will result in degradation of performance of the speed loop which will lead to unwanted variations in the generator speed signal. On the other hand designing it to be too narrow will not guarantee significant results in tower load reduction. The overall design depends on the configuration of the specific wind turbine. It must be kept in mind that as wind turbines increase in size the frequency of the dominant tower mode becomes lower.

6.5.2 Design of the Coordinating Transfer Function

The co-ordinating function is the function that coordinates the operation between the pitch and the torque control as they are both simultaneously used in this scheme. The co-ordinating transfer function, which is not dependent on wind speed, must be designed in such a way that the overall system dynamics remain unchanged. Taking into account Figure 6.11 through Figure 6.14, the co-ordinating function X and the notch filter Y must be designed so that eq. (30) holds true. The exact implementation of this function contains all the dynamics of the wind turbine and has a very high order. An approximation of these dynamics is necessary for the implementation of the coordinating function and for the specific 2MW wind turbine is given by equation (31).

$$Car * Y * A + Car * (1 - Y) * X * B \equiv Car * A \tag{30}$$

It must be made clear that the function X should be designed on a case to case basis as it depends on the below and above rated dynamics of each wind turbine.

$$X = \frac{4.8027 \cdot 10^6}{(s^3 + 19.17s^2 + 122.5s + 260.9)} \tag{31}$$

6.5.3 Performance Assessment

The open loop dynamics from the reference generator input to the actual generator speed, using the Basic controller, is compared to the co-ordinated one, in Figure 6.16 and Figure 6.17. The Bode plot in Figure 6.16, reveals that the right half plane zeros causing the limitations discussed earlier, have now been removed, whereas the rest of the speed loop dynamics remain relatively unchanged.

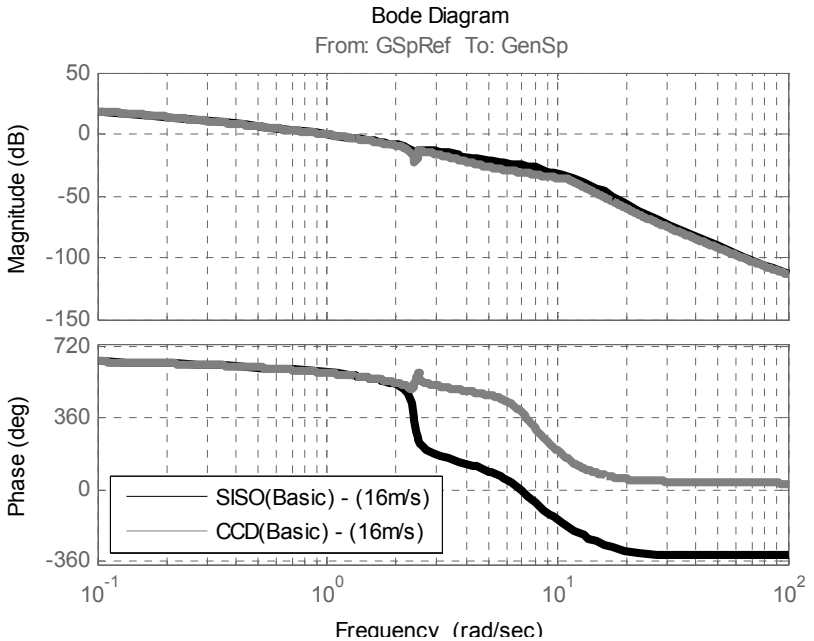

Figure 6.16: Open loop dynamics from generator ref. input to generator speed

The Nyquist plot of Figure 6.17, reveals a clear improvement in the stability margins and the sensitivity of the system. This could be interpreted as providing scope for increase of the bandwidth of the controller, but this is not done here.

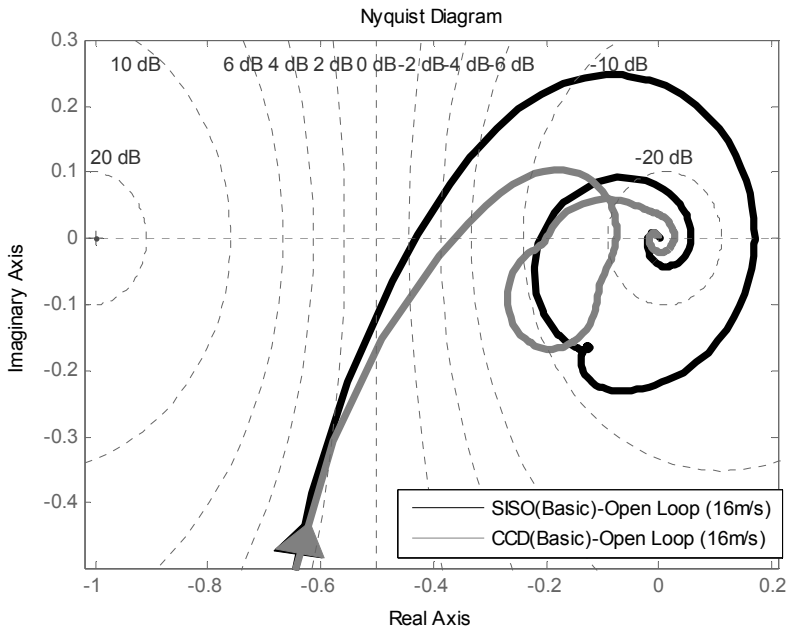

Figure 6.17: Open loop Nyquist plot of the speed loop for 16m/s

The spectra of the fore-aft signal of the tower of the basic controller versus the co-ordinated controller are given in Figure 6.18 and Figure 6.19. Comparing the magnitudes of the spectra around the frequency of 2.45rad/sec (tower frequency), a significant reduction is observed. As the wind speed increases, see Figure 6.19 and Figure 6.20, the reduction in loads becomes more pronounced.

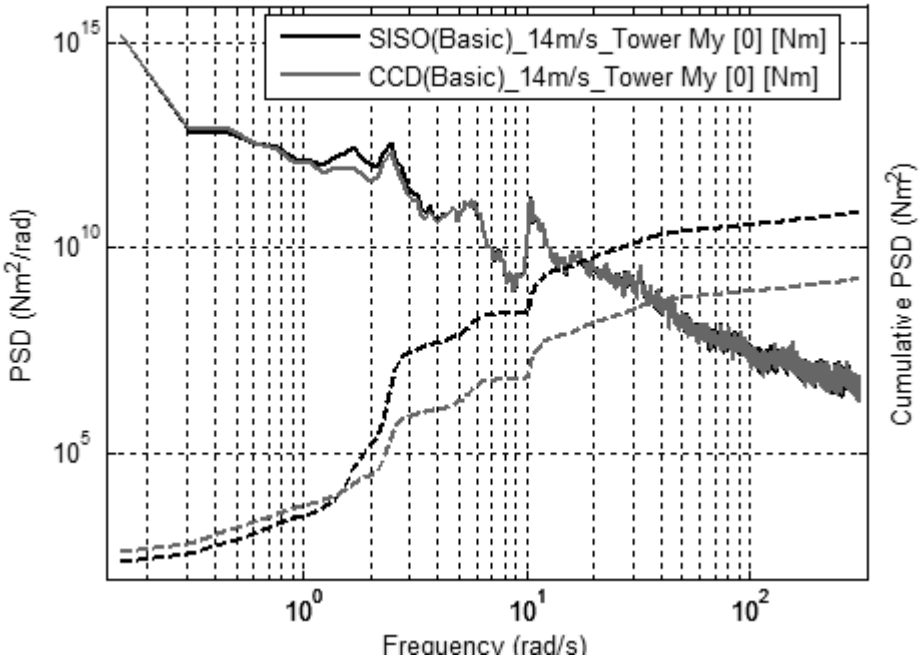

Figure 6.18: Basic SISO vs CCD controller spectra of the fore-aft tower signal for a mean wind speed of 14m/s

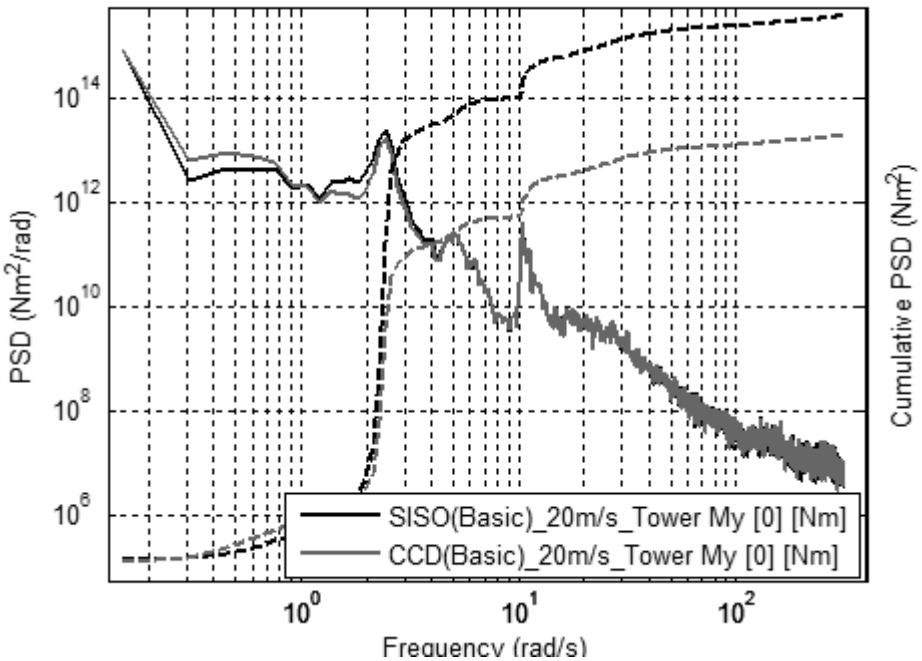

Figure 6.19: Basic SISO vs CCD controller spectra of the fore-aft tower signal for a mean wind speed of 20m/s

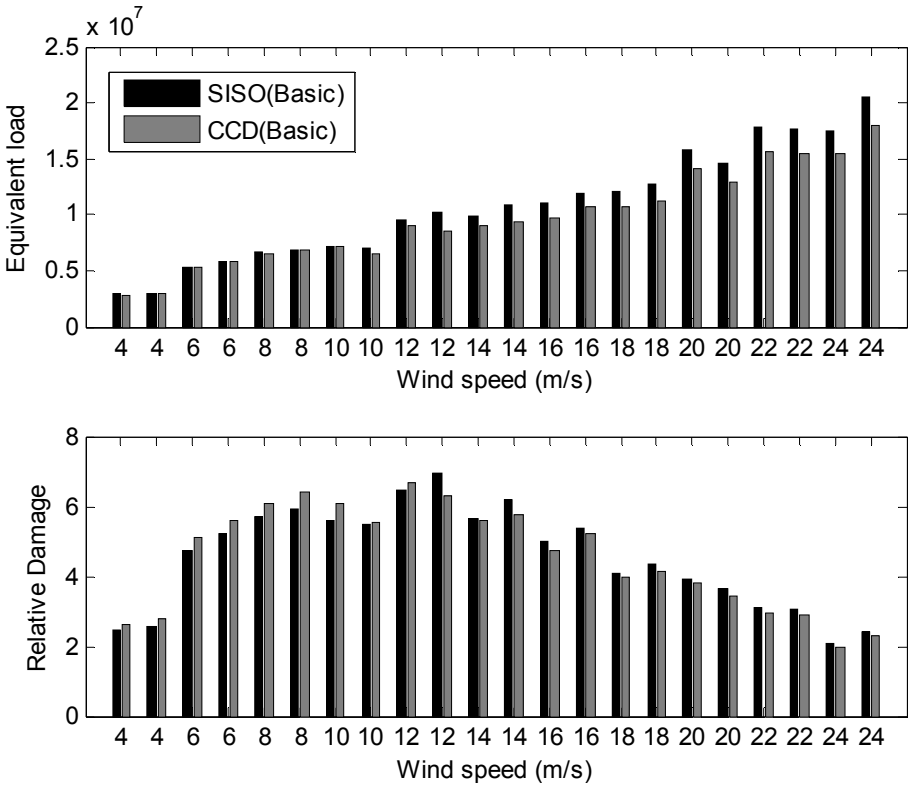

Figure 6.20: Fatigue load comparison the basic SISO with the basic CCD controller for each wind speed

The bar graph depicting the comparison of the basic versions of the SISO and CCD controllers is shown in Figure 6.20, and the values of the full envelope lifetime loads are listed in Table 2.

Table 2: Life time tower fore-aft fatigue loads for two controllers

Lifetime Tower Loads	
Controller	**Lifetime fatigue loads**
SISO(Basic)	7.2186e+06
CCD (Basic)	6.7036e+06
7.13% Reduction – 2 wind seeds	

As mentioned earlier the CCD approach also reduces the activity of the pitch actuator and this is depicted in Figure 6.21. This reduction is done without any compromise in the performance of the generator speed loop. The generator speed time series for the basic SISO and CCD controllers are shown in Figure 6.22, for a wind speed of 16m/s.

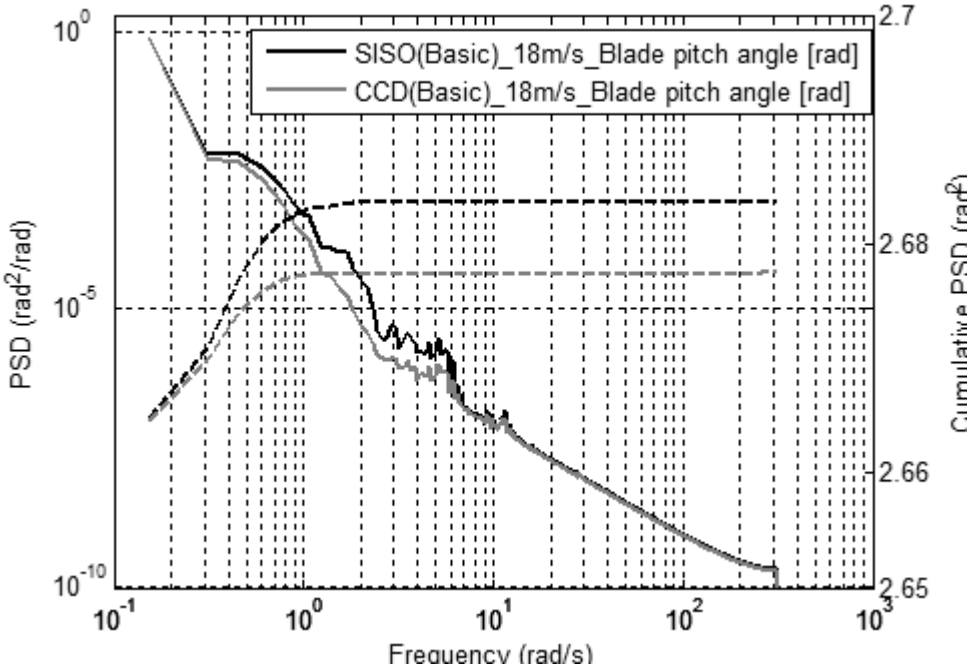

Figure 6.21: Spectra depicting the reduction in pitch activity when using the co-ordinated controller at a mean wind speed of 18m/s

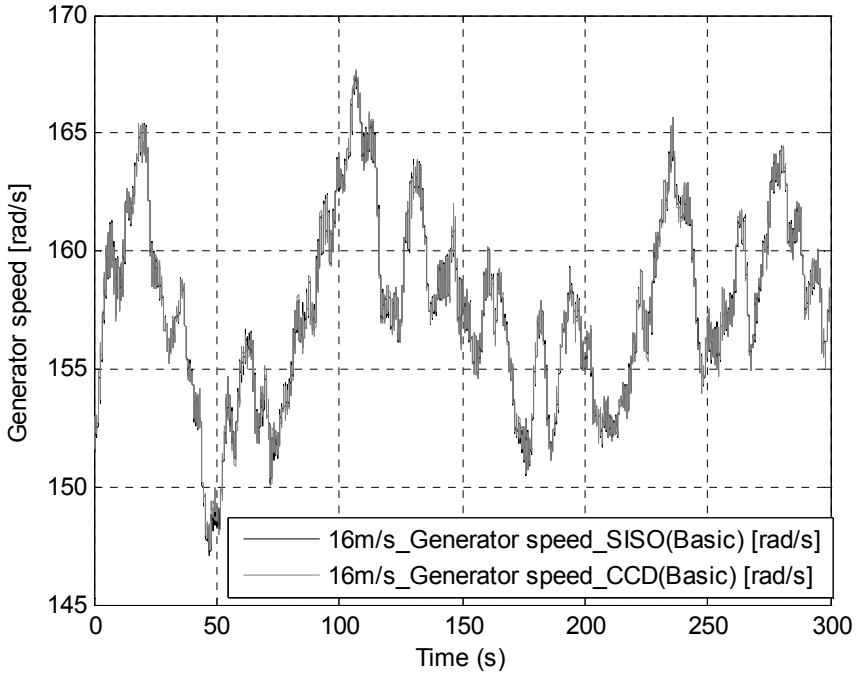

Figure 6.22: Time series of Generator speed for the basic SISO and CCD controllers at a mean wind speed of 16m/s

6.6 Combining co-ordinated controller with the Tower Feedback Loop

In this section an assessment of the loads of the wind turbine is made, when combining the traditional tower feedback loop approach with the alternative coordinated design. The reduction in loads in this case is an improvement in comparison to the two methods on their own, and is up to a value of 10.86%. The spectra of the fore-aft movements of the turbine for the three controllers at two wind speeds are given in Figure 6.23 and Figure 6.24.

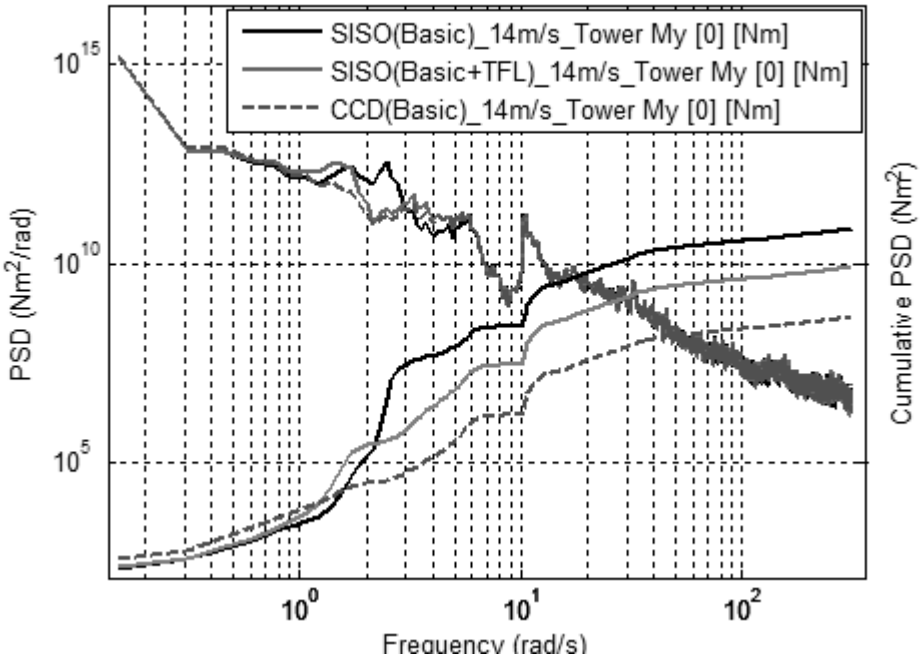

Figure 6.23: Spectra of Fore-aft motion of the tower comparing the three controllers for 14m/s wind speed

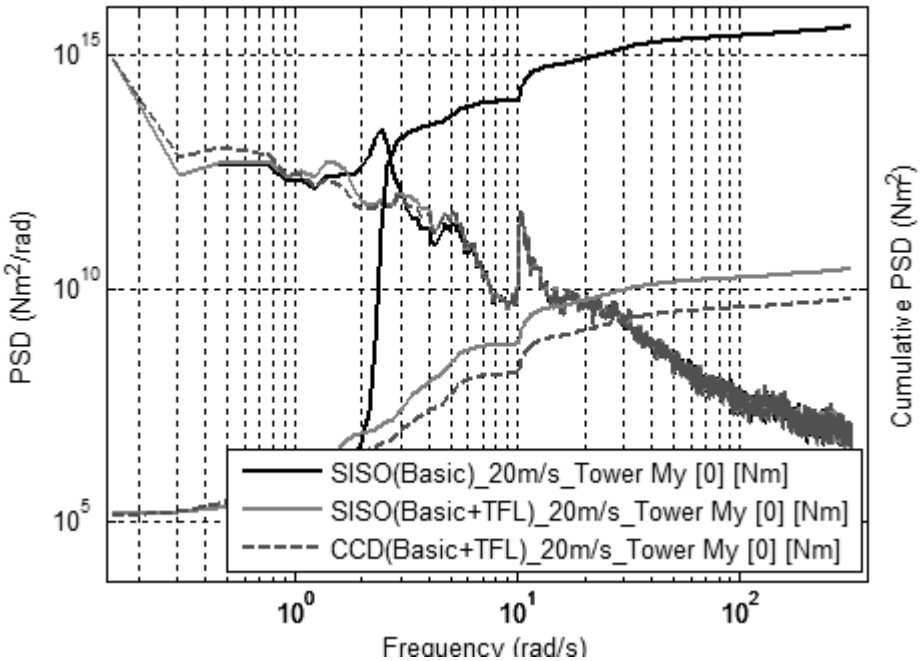

Figure 6.24: Spectra of Fore-aft motion of the tower comparing the three controllers for 20m/s wind speed

The bar graph comparing the loads in this case is given by Figure 6.25, while Table 3 lists the lifetime values of fatigue loads for all three cases.

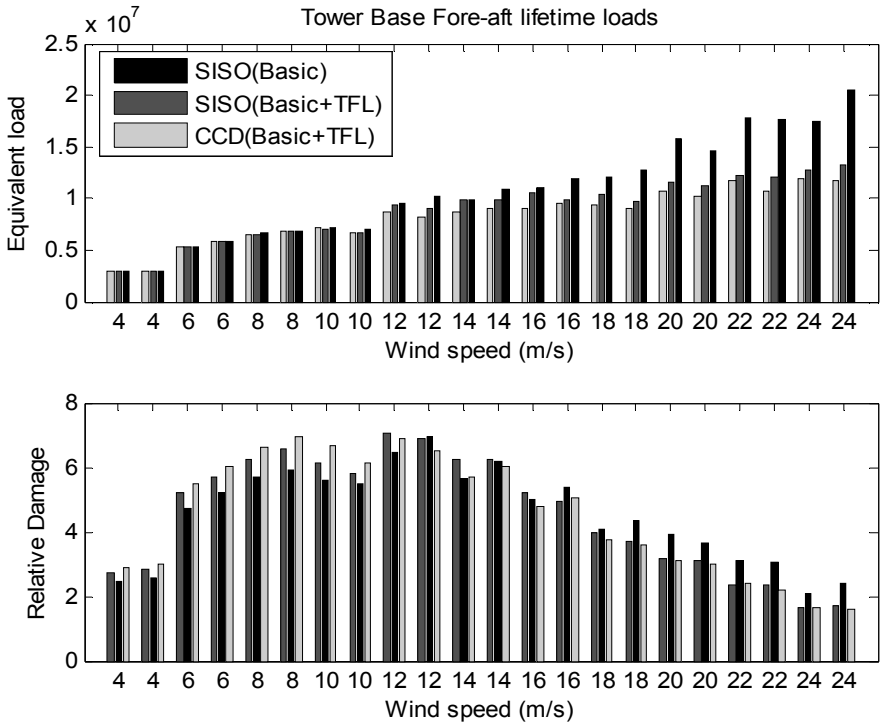

Figure 6.25: Comparison of lifetime fatigue loads for fore-aft movement of the tower for the three controllers

Table 3: Life time tower fore-aft fatigue loads for three controllers

Tower fore-aft moment lifetime loads	
Controller	**Normalised lifetime fatigue loads**
SISO(Basic)	7.2186e+06
SISO(Basic+TFL)	6.7369e+06
CCD(Basic+TFL)	6.4341e+06
10.86% Reduction	

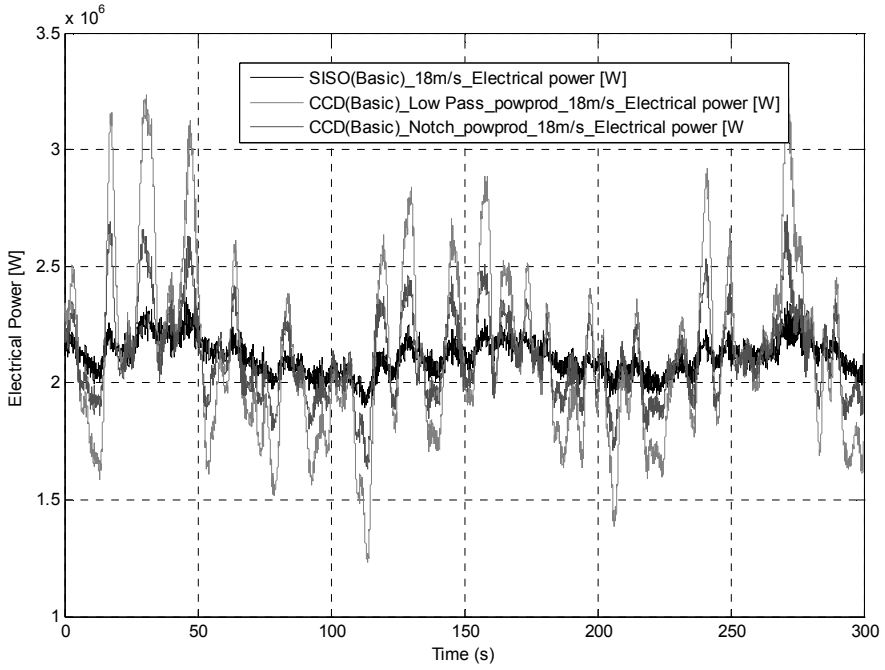

Figure 6.26: Electrical power output comparison for a Low pass and a Notch filter

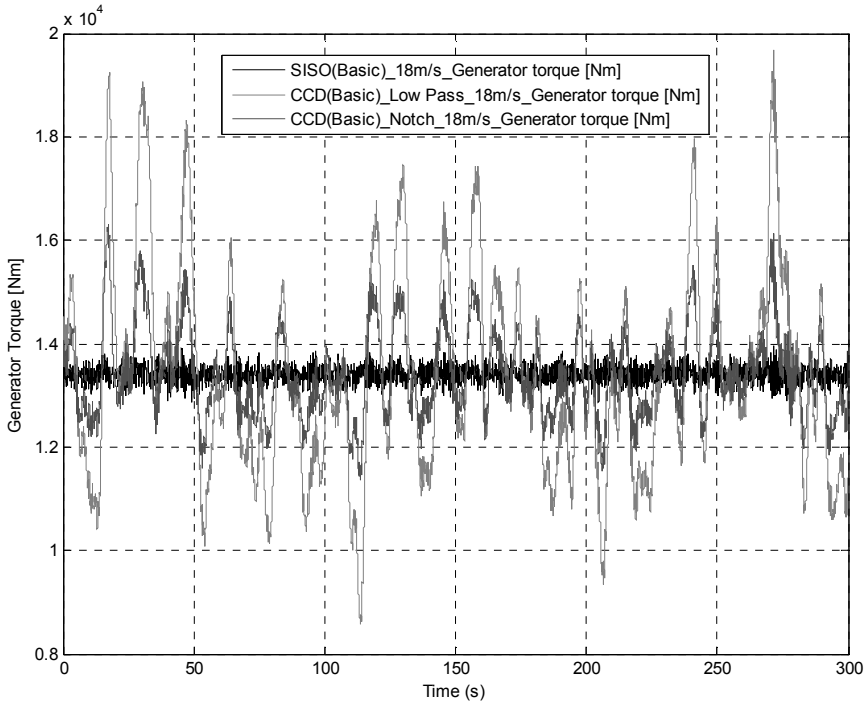

Figure 6.27: Generator torque comparison for a Low pass and a Notch filter

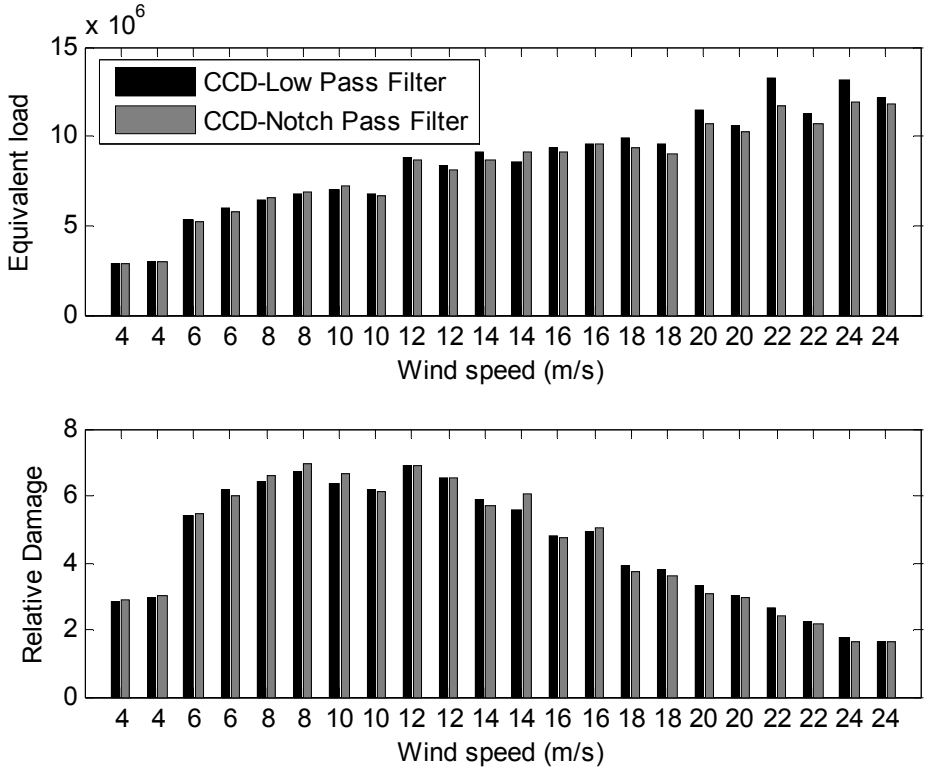

Figure 6.28: Lifetime fore-aft tower load comparison for Low pass and Notch filter options in the context of CCD

Table 4: Comparison of the lifetime fore-aft tower loads for two filters

Lifetime fore-aft tower loads for a Low pass and a High pass filter in the context of CCD	
CCD(Basic+TFL)_High-Low Pass	6.4791e+06
CCD(Basic+TFL)_Notch-Band Pass	6.4341e+06

6.7 Extension to the Power coordinated controller

The results observed by the above scheme are very significant but induce fluctuations to the output power and the torque, see Figure 6.26 and Figure 6.27, because power is not directly controlled by this scheme. A controller is required that gives the same results in terms of tower load reduction but does not compromise the performance of the wind turbine in terms of power, torque or speed.

Because of the fact that the wind disturbance is concentrated at low frequencies such that effective regulation of rotor speed requires a closed loop bandwidth of around 1 rad/sec, as mentioned in Chapter 5, and the fact that the rotor inertia is large and therefore the response of the generator speed to perturbations in the generator reaction torque is weak, little increase in the speed fluctuations are expected to occur but all within acceptable limits that do not compromise the overall performance of the wind turbine.

The approach adopted in the previous sections involved looking at the dynamics of the generator speed loop. The extension of the controller to a power coordinated controller involves looking at the same dynamics but with power as the output as shown in Figure 6.29.

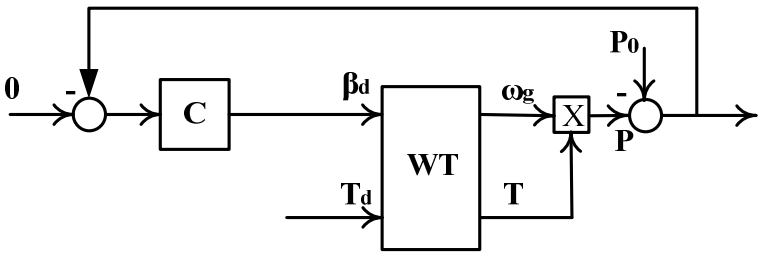

Figure 6.29: Power loop of overall system

Assuming the aerodynamic nonlinearity is counteracted by the controller through the nonlinear gain scheduling control technique described in Chapter 5, the only nonlinearity now present is $\omega_g T$. By considering the attribute that the response of the generator torque to perturbations in demanded pitch angle is very weak, the perturbations in output power arise almost entirely from the perturbations of generator speed. Hence, if output power is controlled well then so is generator speed.

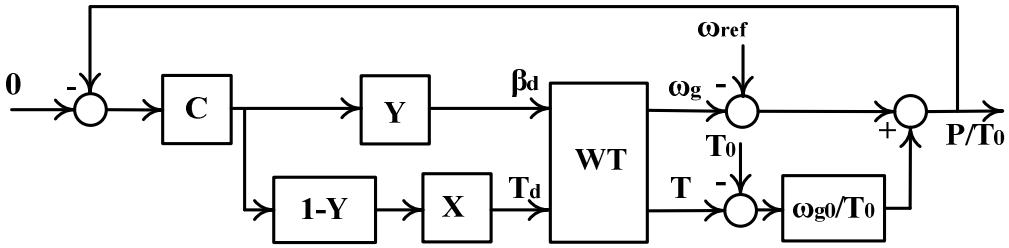

Figure 6.30: Reformulation of System

All the controllers acting through the demanded pitch angle and generator torque may be reformulated as in Figure 6.30, which is finally equivalent to Figure 6.31 and includes the reappearance of speed control. As mentioned earlier the large rotor inertia reduces the fast response of generator speed to perturbations in generator reaction torque and the torque also responds very slowly to perturbations in demanded pitch angle, but there are large fluctuations in generator torque and demanded pitch angle that stem from the demanded torque and pitch (at lower frequencies). Hence, in general it is possible to have good regulation of P/T_0 at low frequency but with large fluctuations in both $(\omega_g - \omega_{ref})$ and $(T - T_0)$ provided they cancel. At higher frequencies, this possibility is excluded by the weak response of ω_g because of the large rotor inertia and P/T_0 could be regulated through demanded torque when generator speed is essentially unregulated. The lack of regulation of ω_g causes little increase in fluctuations in ω_g, since the wind is concentrated at low frequency. Consequently, choosing $Y \approx 0$ at low frequencies and $(1 - Y) \approx 0$ at high frequencies ensures that controlling P/T_0 well, also causes ω_g to be regulated well.

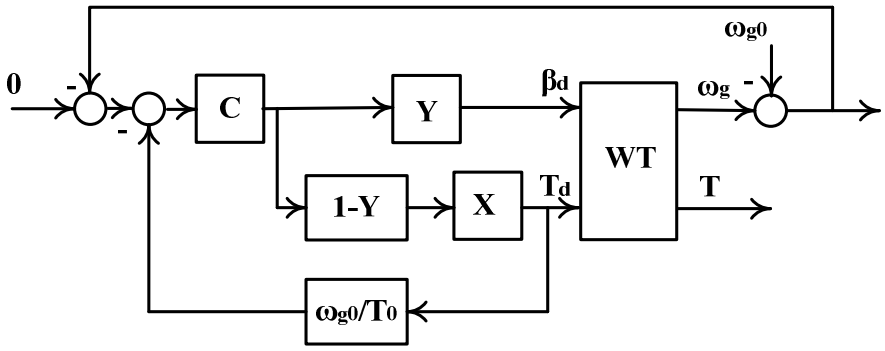

Figure 6.31: Final formulation with the re-appearance of speed control

The same rule applies when designing the coordinating function as with the initial coordinated controller. Since a modification is made so that to regulate power, torque and indirectly generator speed, eq. (32) must now hold true.

$$Car * \tilde{Y} * A + Car * \left(1 - \tilde{Y}\right) * \tilde{X} * (B + \frac{\omega_0}{T_0}) \equiv Car * A \tag{32}$$

Once again the full order of the coordinated function is very high, therefore a low order approximation is designed, see equation (33), that achieves very good results in coordinating the pitch and torque controllers whilst not compromising any aspects of the performance of the wind turbine.

$$\tilde{X} = \frac{-2.504 * 10^6}{s^4 + 30.1s^3 + 303s^2 + 1030s + 100} \tag{33}$$

The dynamics of the exact and approximated coordinating functions are compared in the Bode diagram of Figure 6.32.

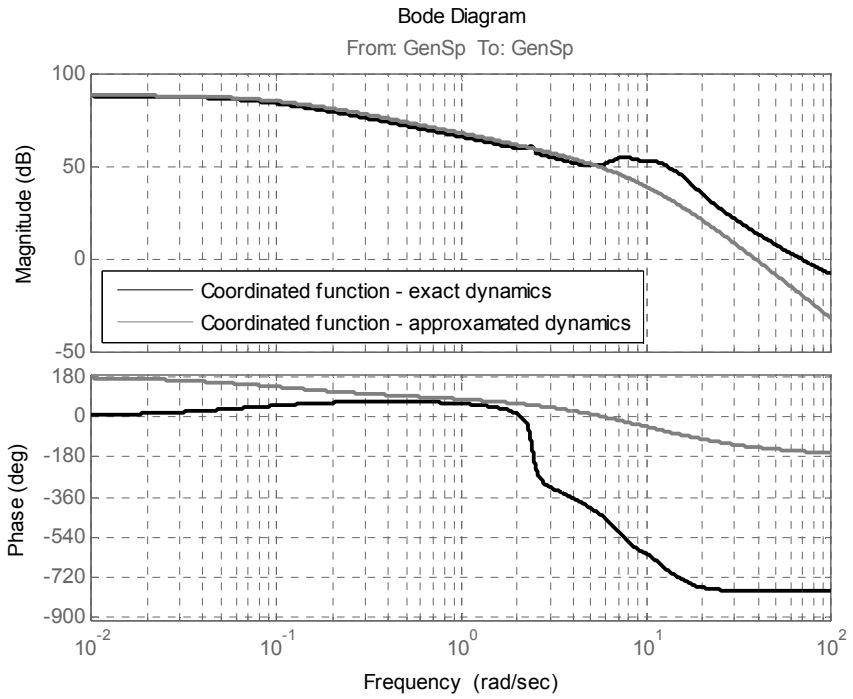

Figure 6.32: Exact vs approximated dynamics of the coordinating function

The localised tower filter $\widetilde{Y}$, which is a notch filter, chosen using the same criteria as earlier, is given by eq (34).

$$\tilde{Y} = \frac{s^2 + 1.4s + 6.1}{s^2 + 3.2s + 6.1} \tag{34}$$

The new open loop dynamics of the overall system by using the basic test-bed controller and the "extended" coordinated one are compared in the Bode plot of Figure 6.33. The Bode plot, spectra and time series plots validating the claim that the performance of the wind turbine is not compromised in any way are provided in Figure 6.34 to Figure 6.44. These comparisons include the signals of: generator speed, electrical power, generator torque and pitch activity.

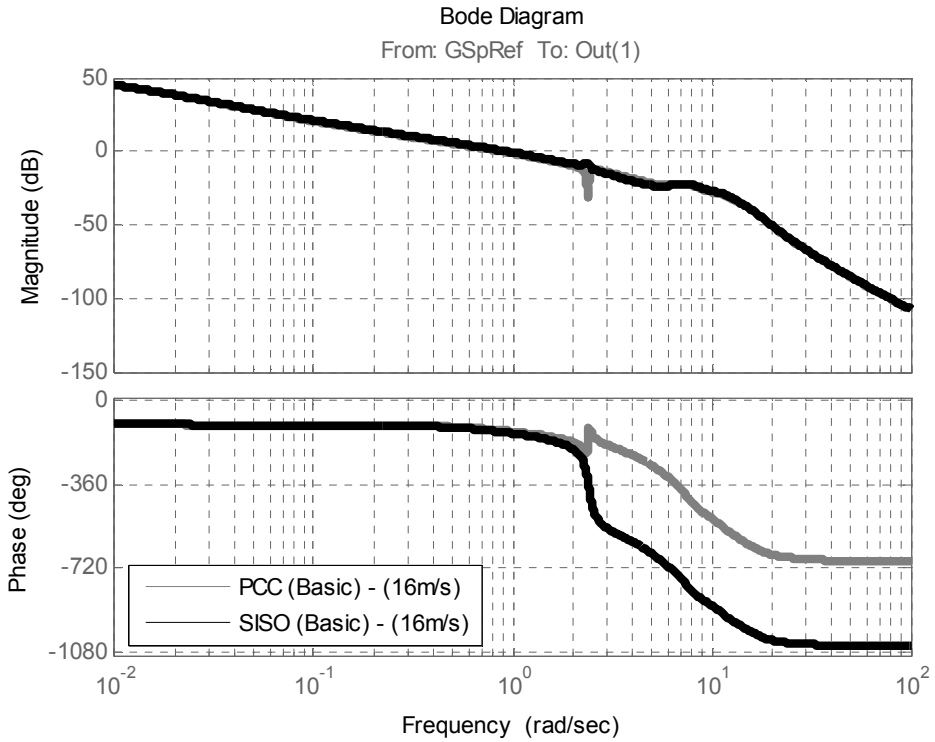

Figure 6.33: Open loop dynamics for the Basic vs Power coordinated controller

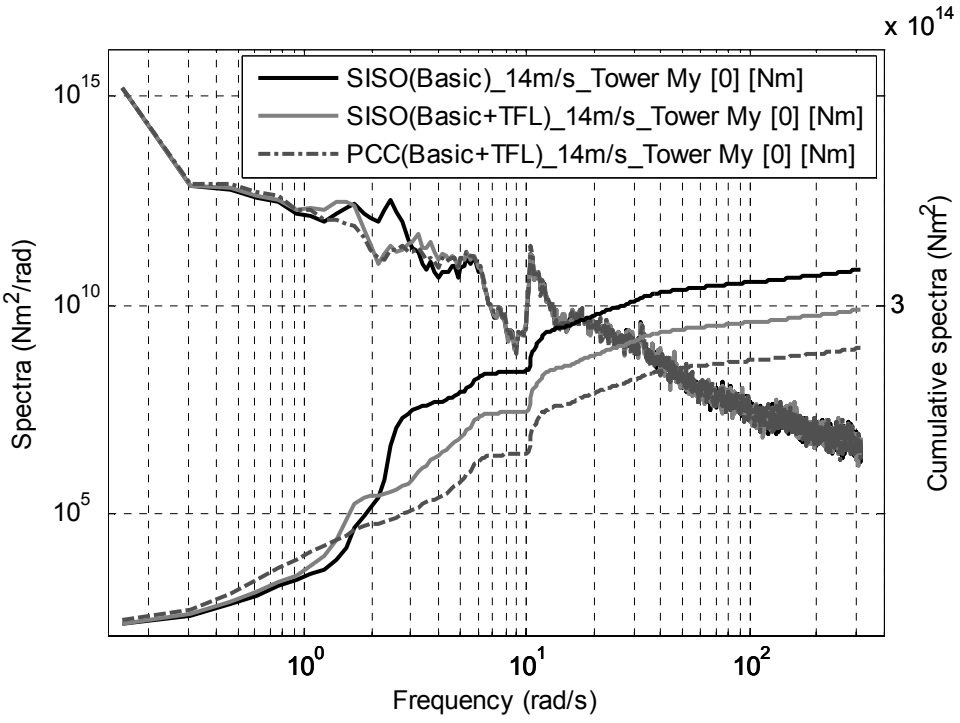

Figure 6.34: Spectra comparison between the Baseline and the Power coordinated controller

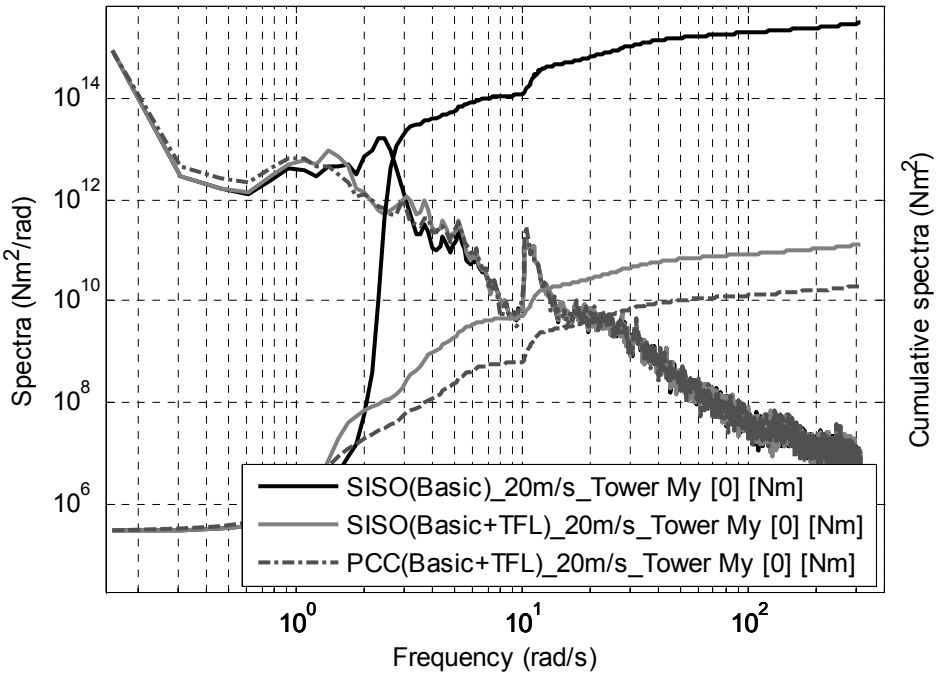

Figure 6.35: Spectra depicting the comparison of the basic versus the power coordinated controller

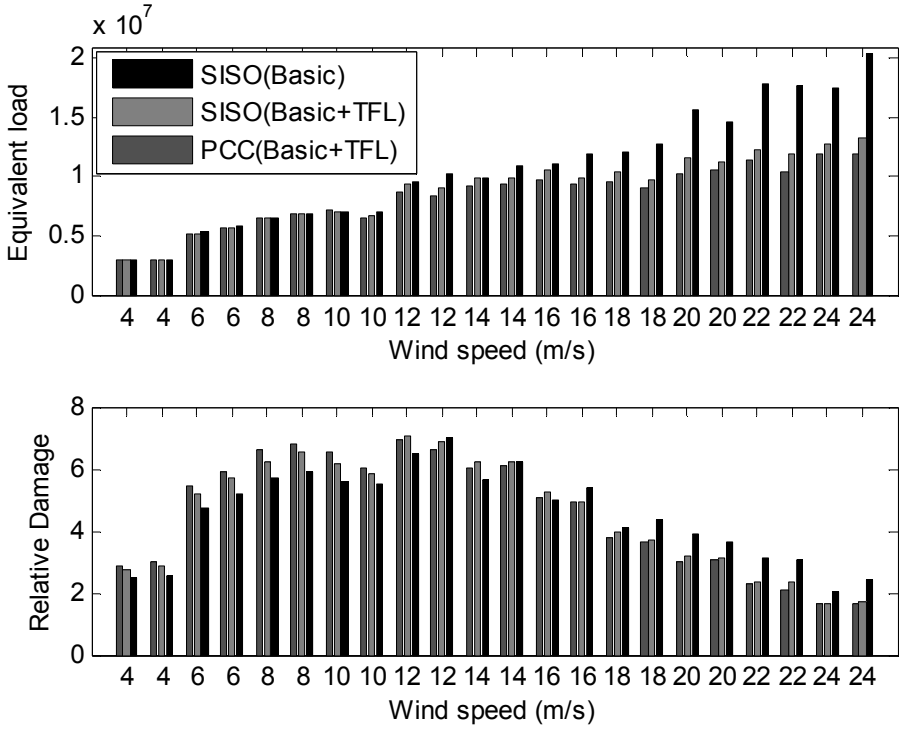

Figure 6.36: Comparison of lifetime fatigue loads for the fore-aft moment of the tower for the three controllers and two seeds of wind

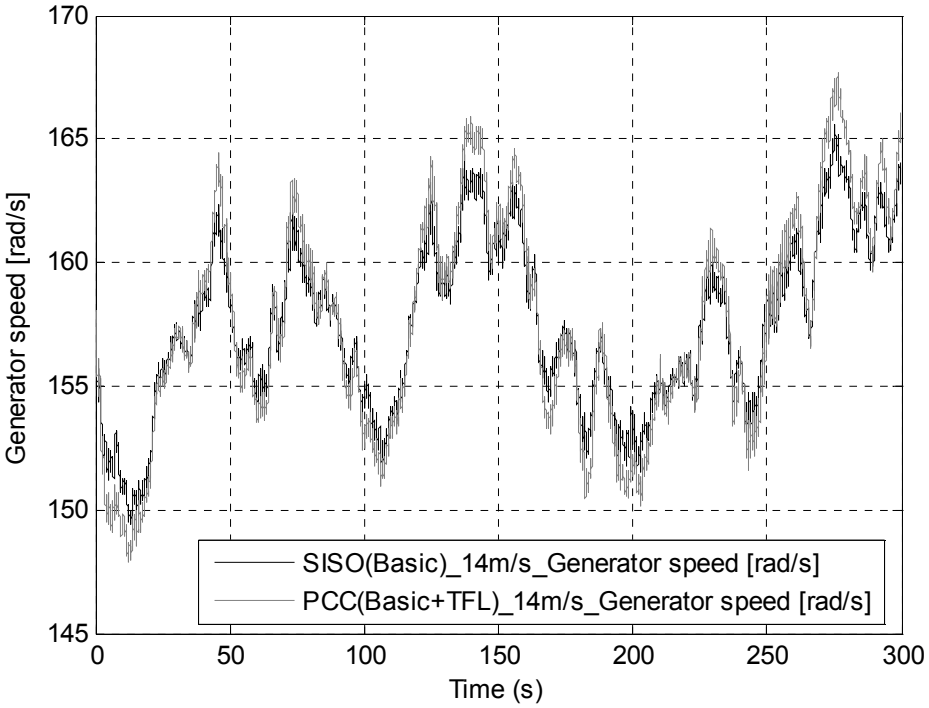

Figure 6.37: Generator speed signal comparison for Basic SISO controller vs Power coordinated controller at a mean wind speed of 14m/s

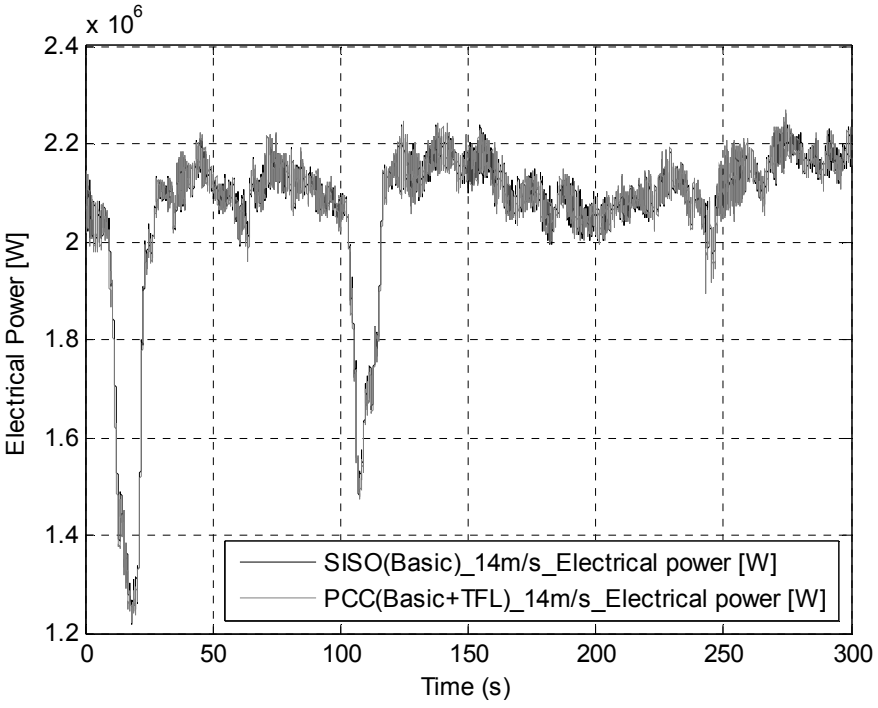

Figure 6.38: Electrical power signal comparison for Basic SISO controller vs Power coordinated controller at a mean wind speed of 14m/s

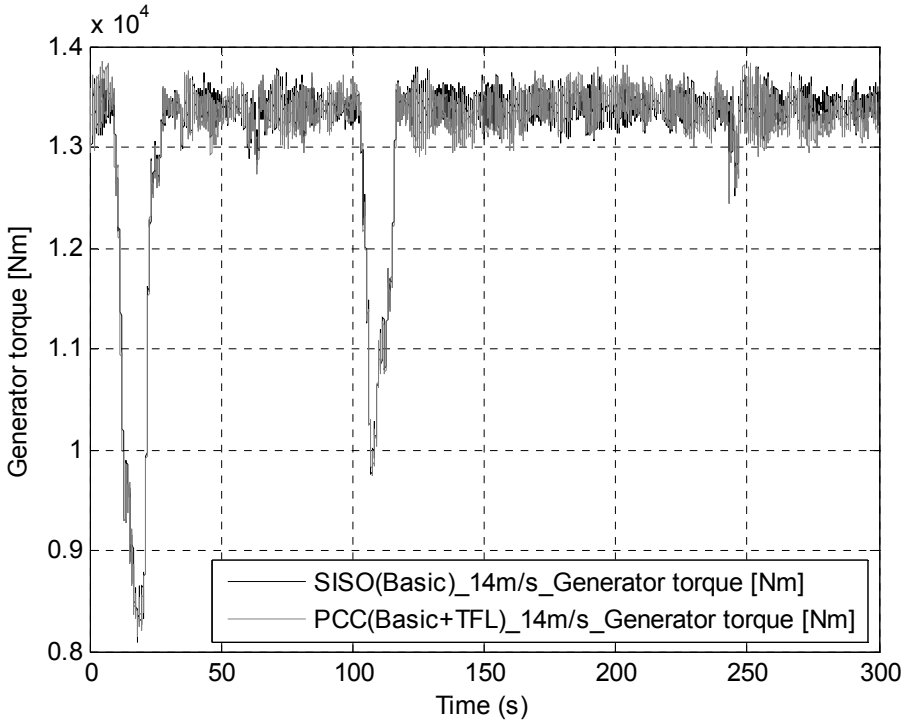

Figure 6.39: Generator torque signal comparison for Basic SISO controller vs Power coordinated controller at a mean wind speed of 14m/s

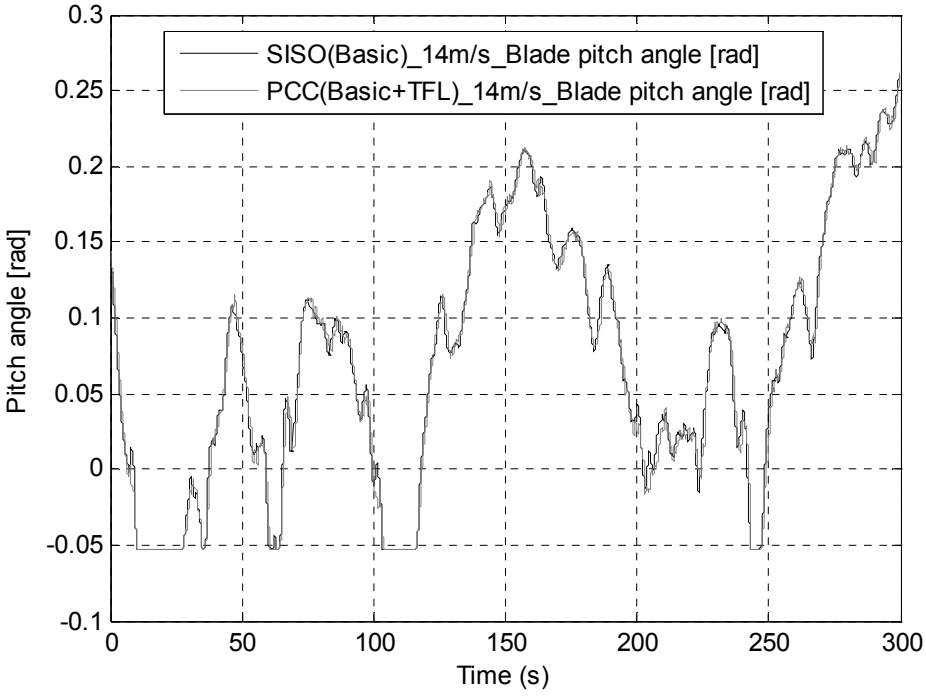

Figure 6.40: Blade pitch angle signal comparison for Basic SISO controller vs Power coordinated controller at a mean wind speed of 14m/s

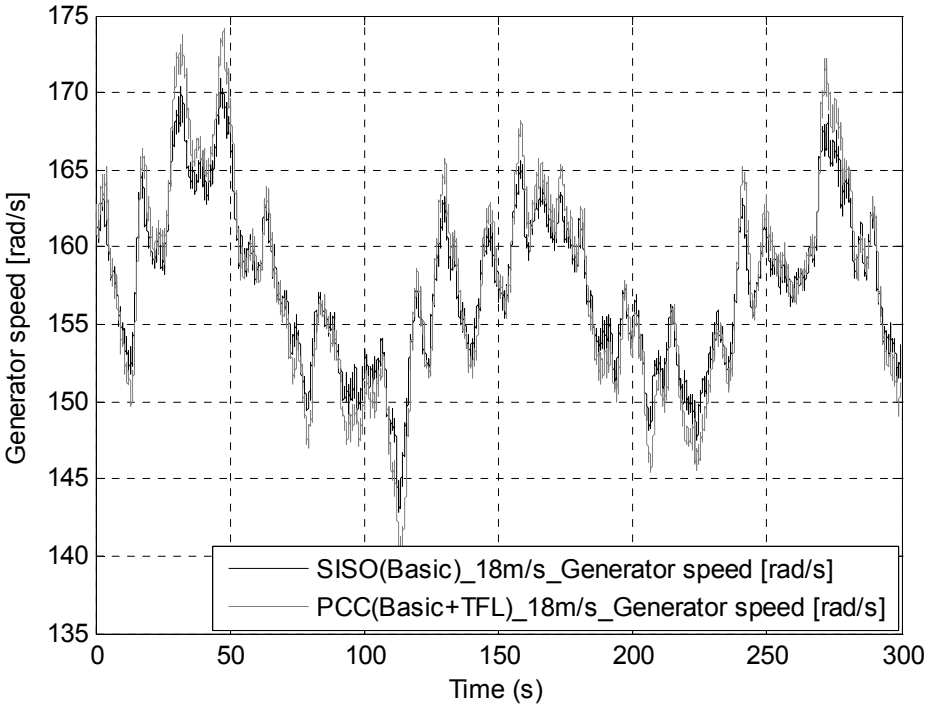

Figure 6.41: Generator speed signal comparison for Basic SISO controller vs Power coordinated controller at a mean wind speed of 18m/s

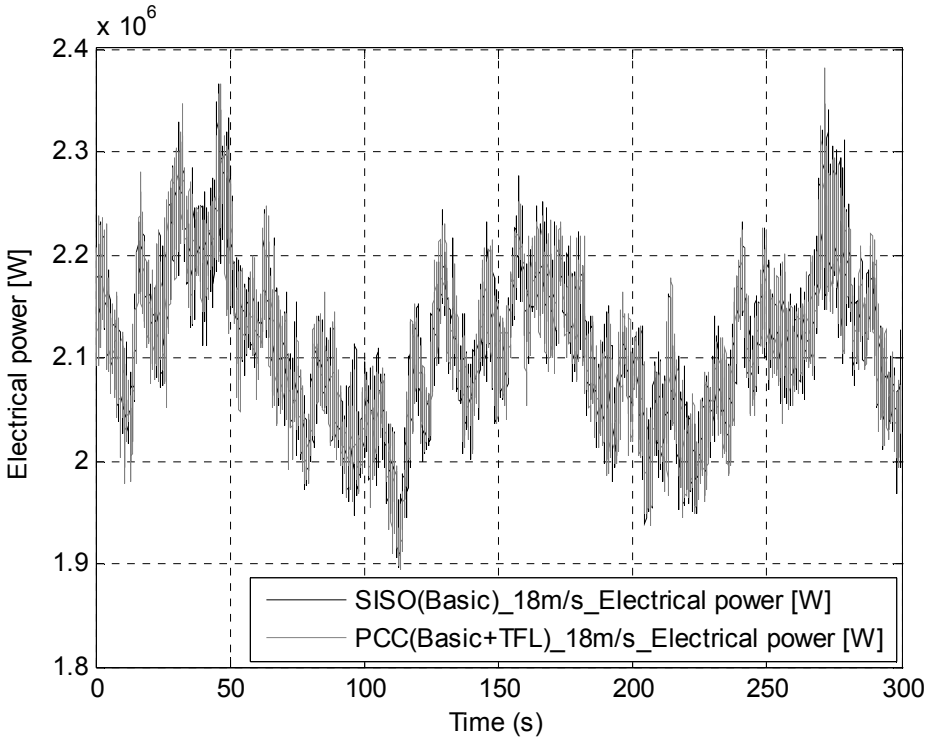

Figure 6.42: Electrical power signal comparison for Basic SISO controller vs Power coordinated controller at a mean wind speed of 18m/s

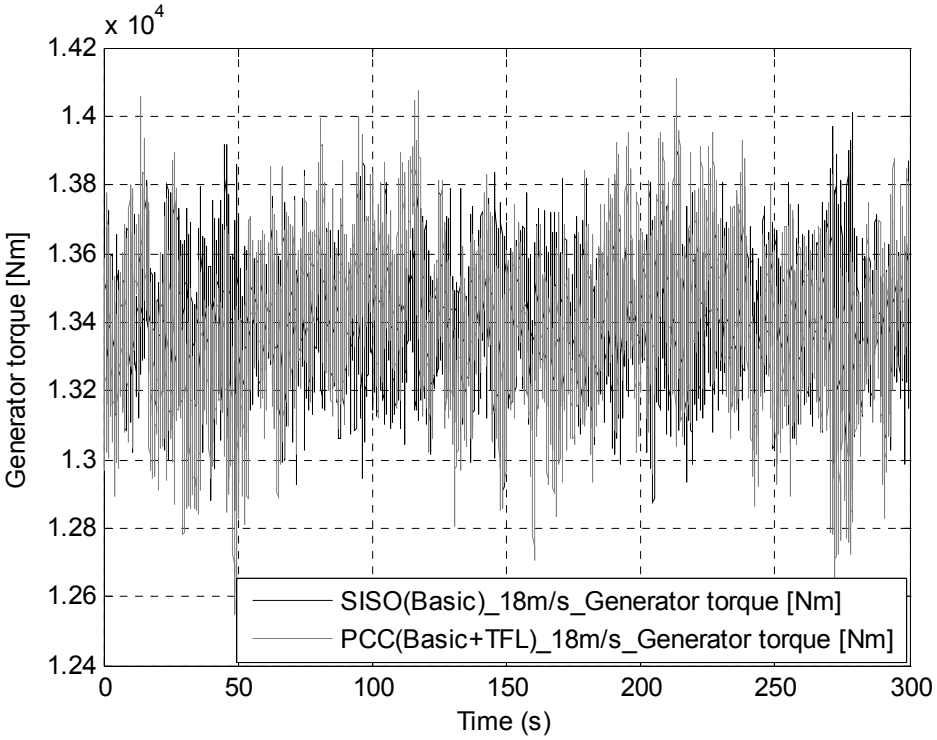

Figure 6.43: Generator torque signal comparison for Basic SISO controller vs Power coordinated controller at a mean wind speed of 18m/s

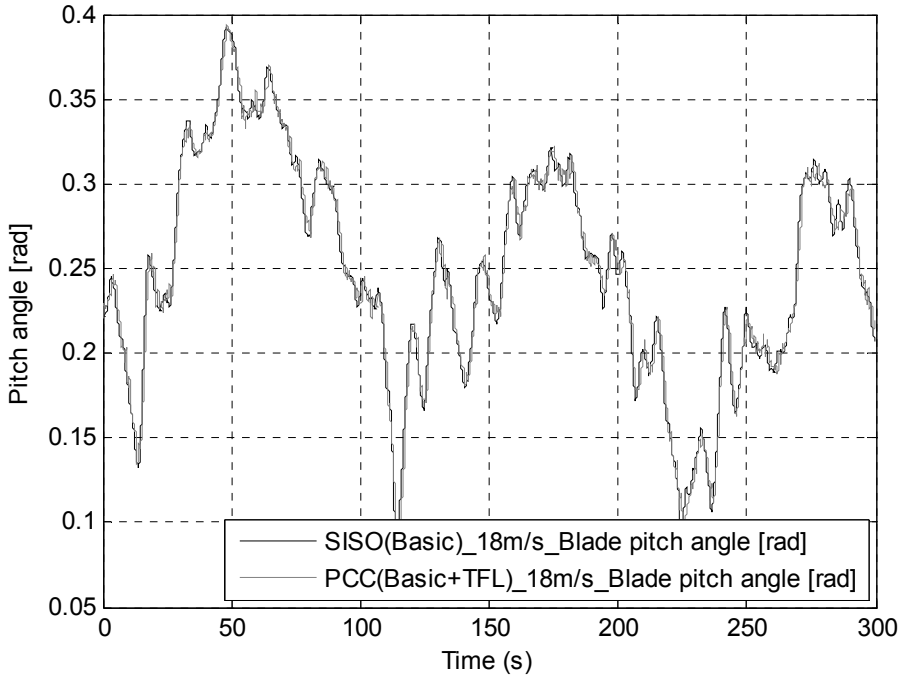

Figure 6.44: Pitch angle signal comparison for Basic SISO controller vs Power coordinated controller at a mean wind speed of 14m/s

6.8 Discussion of results

A co-ordinated controller in the form of a parallel path modification to the existing controller is presented in this chapter. A full assessment of its impact on lifetime fatigue loads of the tower is presented, as well as a comparison to the traditional tower feedback loop approach. Results show that the reduction in loads when using the CCD controller on its own, is 7.13% compared to the 6.67% of the traditional method. The results are significant when combining the two approaches to the controller design. In this case the reduction reaches 10.1% which is clearly better than any of the methods on their own. As a first approach to this scheme might induce some fluctuations in aerodynamic torque and power, a modification of this method controlling power and torque (and generator speed indirectly) was implemented and analysed, giving significantly better results. Additionally, the co-ordinated approach overcomes the limitations in the controller design induced by the presence of a pair of right-half plane zeros in the dynamics linking pitch to generator speed. The results presented in Figure 6.33 through Figure 6.44, which depict a thorough comparison between the basic benchmark controller and the newly designed one, suggest that almost no compromise is being made to the overall performance of the wind turbine whilst achieving the aforementioned results regarding lifetime tower fatigue load reduction. A guideline for designing the notch filter designed earlier in this Chapter is given here.

Having ruled out the use of a low pass filter in order to reduce pitch activity in the region around tower frequency it is worthwhile providing a guideline for designing the notch filter for application in wind turbine. It has to be kept in mind that we aim at minimum impact in generator speed control whilst reducing tower loads as much as possible. Firstly, the notch filter must be wide enough to cover a range of frequencies bigger than the range of frequencies that the dominant mode of the tower lies in. Then the loads and the generator speed must be checked. If the notch filter is too wide, unacceptable variations in the generator speed signal are present. It must be kept in mind that if the notch is too wide its poles are underdamped and can cause undesirable transients due to interfering with the switching. This might also cause dips in the power. Therefore, if such signal behaviour is observed in the time series plots then the notch filter should be narrowed until the variations in generator speed

become acceptable. According to the observations made in the current research, the depth of the filter has a value at which it is most effective. After all it must be kept in mind that the notch filter is responsible for allocating frequencies to the pitch and torque controller respectively. Therefore there is a balance that needs to be found for the optimum result. Initially the depth of the notch filter should match the “bump” of the dominant mode of the tower occurring from the spectrum plot. In the case of the 2MW wind turbine under study an 8dB depth was needed. At some point if the filter becomes too deep, although not increasing them, it does not make a difference in the loads. An initial start point of 10dB is usually appropriate to start testing the filter from.

7 Conclusions and Future Research

The biggest percentage of the lifetime of a wind turbine is spent in below rated wind speed especially in the maximum power coefficient tracking region. Careful design of the controller in that region is important as the results of this thesis demonstrate. Many control design approaches have been proposed in the literature for this region. The research done in Chapter 4 establishes the following:

- The Simulink model based on effective wind speed is sufficiently good to enable the performance to be assessed and controllers to be tuned in this region. The Simulink model is much simpler than the GH Bladed model and enables certain aspects of performance such as efficiency of the energy capture to be estimated much more efficiently.
- The overall energy efficiency is particularly high, up to 99.9% for some cases.
- Only large changes in the choice of the maximum power coefficient tracking curve have significant impact on the energy capture.
- The controller which achieves the tracking does not require high performance.
- The potential improvement in energy capture through advanced control in this region is very modest.

The design task for a wind turbine controller is demanding and as the size of the wind turbine increases the difficulty also increases. The structural elements are more flexible and the stability margins become tighter. The increasing number of tasks that the controller is assigned, makes the design even more complex and the designer needs to assess carefully the trade-offs involved. A full envelope baseline controller is successfully developed for the 2MW exemplar wind turbine addressing all aspects of the design. These aspects include the following:

- Dealing with the transition from below rated to above rated through the phase advance, whilst predicting sudden wind gusts.

- Maintaining smooth switching between different operating modes avoiding transients and frequency excitations using a full envelope switching scheme.
- Avoidance of actuator saturation using an anti-windup scheme.
- Design of controllers for each of the four operating modes i.e. 1st constant speed, Cp_{max} tracking, 2nd constant speed and pitching mode above rated.
- Exploitation of the separation of the aerodynamics through global "gain-scheduling".
- Addition of drive train damping through additional feedback loop in torque.
- Addition of tower damping through additional feedback loop on pitch.
- Regulation according to the operational strategy, the speed and power of the wind turbine over its full operating envelope.

The tower lifetime fatigue loads are a central focus of this research and Chapter 6 presents and analyses the design of a novel coordinated controller, addressing this important issue. Two approaches have been developed; one based on controlling generator speed and the second on controlling power directly and speed indirectly. Both give similar results in terms of tower load reduction. Of course the results depend on the specific wind turbine that the controller is designed for; however the significance here lies in the fact that this wind turbine did not have a very prominent tower mode. The advantages of the approach are the following:

- There is a final lifetime tower fore-aft bending moment reduction of more than 10% for the exemplar 2MW wind turbine which is about 45% improvement on the traditional tower feedback loop.
- The approach does not compromise other aspects of the wind turbine performance such as speed or torque variations as well as loads on other components.
- There is a reduction of actuator activity which further reduces the fatigue of the machine.
- The parallel path modification to the controller improves the dynamics of the pitch control loops through removing the RHPZ's.

One of the important aspects of the coordinated power controller is that it can easily be implemented as an addition to an existing controller that does not already address the issue of reducing the tower loads.

Future research concerning this work involves the further improvement of the performance of the controllers where possible. It is demonstrated in Chapter 6, that by removing the RHPZ's from the dynamics of the wind turbine, the stability margins slightly increase. It is recommended that future work takes advantage of this outcome by increasing the gain, therefore the bandwidth of the controller. This could possibly result in a bigger improvement in the control of the speed loop of the wind turbine. Moreover, it is recommended that the switching strategy is improved further in order to accommodate wider notch filters in the coordinated control scheme. A very interesting piece of work would be to try the coordinated controller scheme in wind turbines with a "dominant" mode less modest than the one of the wind turbine discussed here. Preliminary tests show that the same approach could demonstrate a lifetime tower load reduction of more than 15% on other machines.

Finally, it is recommended that future work addresses issues such as the accommodation of the coordinated scheme in larger machines using individual pitch control as their main strategy. By doing this it is expected that tower loads will be reduced effectively whilst minimising the effect of any existing rotor imbalances.

8 Bibliography

[1] K.E. Johnson, L.J. Fingersh, M.J. Balas, L.Y. Pao, "*Methods for Increasing Region 2 Power Capture on a Variable Speed HAWT*", 23rd ASME Wind Energy Symposium, 2004, January 5-8.

[2] D.J. Leith, W.E. Leithead, "*Implementation of Wind Turbine Controllers*", International Journal of Control, Vol. 66, p. 349-380, February 1997

[3] W.E. Leithead, S.A. De La Salle, D.L. Reardon, "*Classical Control of a Pitch Control System*", Proceedings of the British Wind Energy Association Conference, Norwich, 1990

[4] W.E. Leithead, S.A. De La Salle, D.L. Reardon, "*Classical Control of Active Pitch Regulation of Constant Speed HAWTs*", International Journal of Control, Vol. 55, p. 845-876, 1992

[5] M.V. Kothare, P.J. Campo, M. Morari, C.N. Nett, "*A Unified Framework for the Study of Antiwindup Designs*", Automatica, Vol. 30, p. 1869-1883, 1994

[6] B. Connor, W.E. Leithead, "*The effect of rotor characteristics on the control of pitch regulated variable speed wind turbines*", Wind Energy Conversion, Proceedings of the 16th BWEA conference, Sterling, UK, 1994

[7] J.D. Simoes, B.K. Bose, R.J. Spiegel, "*Fuzzy Logic Based Intelligent Control of a Variable Speed Cage Machine Wind Generation System*", IEEE Transactions on Power Electronics, Vol. 12, No. 1, Jan 1997.

[8] V. Galdi, A. Piccolo, P. Siano, "*Exploiting maximum energy from variable speed wind power generation systems by using an adaptive Takagi–Sugeno–Kang fuzzy model*", Energy Conversion and Management, 413-421, 2009.

[9] L. Yaoyu, J. Creaby, *"Maximizing Wind Power Output Using Multivariable Extremum Seeeking Control"*, Wind Power 2008 Conference, Houston, June 2008.

[10] E. Iyasere, M. Salah, D. Dawson, J. Wagner, "*Nonlinear Robust Control to Maximize Energy Capture in a Variable Speed Wind Turbine"*, American Control Conference, Washington, USA, June 2008.

[11] L. Hui, K.L. Shi, P.G. McLaren, "*Neural-Network-Based Sensorless Maximum Wind Energy Capture With Compensated Power Coefficient"*, IEEE Transactions on industry applications, Vol.41, No.6, November/ December 2005.

[12] W.E. Leithead, M.C.M Rogers, "*Drive-Train Characteristics of Constant Speed HAWT's: Part I – Representation by Simple Dynamic Models, Wind Engineering*", Vol. 20, No. 3, 1996.

[13] W.E. Leithead, M.C.M Rogers, "*Drive-Train Characteristics of Constant Speed HAWT's: Part II – Simple Characterisation of Dynamics*", Vol. 20, No. 3, 1996.

[14] D.M. Robb, W.E. Leithead, "*Derivation and Validation of Simple Corellated Wind Speed Models*", Technical Report, University of Strathclyde, 2000.

[15] J.R. Connell, "*The spectrum of wind speed fluctuations encountered by a rotating blade of a WECS"*, Solar Energy, v. 29(5), 1982, pp.363-375.

[16] J.R. Connell, R.L. George, "*A new look at turbulence as experienced by a rotating wind turbine"*, 2nd ASME Wind Energy Symp., Houston, TX, pp. 455-479, Jan. 1983.

[17] W.E. Leithead, D.J. Leith, F. Hardan, H. Markou, "*Global gain-scheduling control for variable speed wind turbines"*, Proceedings of European Wind Energy Conference,1999, Nice, France.

[18] D.J. Leith & W.E. Leithead, "*Appropriate realisation of gain-scheduled controllers with application to wind turbine regulation"*, International Journal of Control, vol.73 No.11, pp.1001-1025, 1996.

[19] W.E. Leithead, M.C.M. Rogers, "*Design of Wind Turbine Controllers*", Recent Results in Robust and Adaptive Control, EURACO Workshop, Florence – Italy, 11-14 September, 1995

[20] S. Dominguez, W.E. Leithead, "*Size related performance limitations on wind turbine control performance"*, European Wind Energy Conference 2006, Athens, February 27 – March 2, 2006.

[21] W.E. Leithead, S. Dominguez, "*Controller Design for the Cancellation of the Tower Fore-aft Mode in a Wind Turbine"*, Proceedings of the 44th IEEE conference on Decision and Control, and the European Control Conference 2005, Seville, Spain, December 12-15.

[22] J.S. Freudenberg, D.P. Looze, "*Right Half Plane Poles and Zeros and Design Tradeoffs in Feedback Systems"*, IEEE Transactions on Automatic Control, Vol. AC-30, No. 6, June 1985.

[23] W.E. Leithead, "*Effective wind speed models for simple wind turbine simulations*", Proceedings of the 14th British wind energy Assoc. Conf., March 1992, Nottingham, UK, pp. 321-326.

[24] W.E. Leithead, S. Dominguez, "*Active regulation of Multi-MW wind turbines: an overview"*, Power System Technology, Vol. 31, No. 20, pp. 24-34, 2007.

[25] D. Goodfellow, G.A. Smith, "*Control Strategies for Variable Speed Wind Energy Recovery*", Proceedings of the 8th BWEA Conference, p.219-228, Cambridge, 1986

[26] D.J. Leith, R.N. Shorten, W.E. Leithead, O. Mason, P. Curran, "*Issues in the design of switched linear control systems: A benchmark study*", 17:103–118, Int. J. Adapt. Control Signal Process, 2003.

[27] L.N. Freeman, R.E. Wilson, "*The FAST Code*", Proceedings of the 28th IEA Meeting of Experts "State of the Art Aeroelastic Codes for Wind Turbine Calculations", Technical University of Denmark, p.37-56, Lyngby, 11-12 April 1996

[28] M.L. Buhl Jr, A. Manjock, "*A Comparison of Wind Turbine Aeroelastic Codes Used for Certification*", 44th AIAA Aerospace Sciences Meeting and Exhibit, Reno, Nevada, 9 - 12 January 2006

[29] V.A. Riziotis, S. Voutsinas, "*GAST: A General Aerodynamic and Structural Prediction Tool for Wind Turbines*", Proceedings of the European Wind Energy Conference, p. 448-452, Dublin, Ireland, 6-9 October 1997

[30] IEC 61400-12:1998 – Wind Turbine Generator Systems, Part 12: - Wind Turbine Power Performance Testing

[31] E.A. Bossanyi, "*Theory Manual and User Manual for GH Bladed 3.82*", Garrad Hassan and Partners Ltd, 2009

[32] M. Sidi, O. Yaniv, "*Margins and Bandwidth Limitations of NMP SISO Feedback Systems*", Proceedings of the 7th Mediterranean Conference on Control and Automation (MED99), Haifa, Israel, June 28-30, 1999

[33] M. Sidi, "*Gain-bandwidth Limitations of Feedback Systems with Non-Minimum-Phase Plants*", International Journal of Control, Vol. 67 No. 5, p. 731-743, 1997

[34] A. Halfpenny, "*A Frequency Domain Approach for Fatigue Life Estimation From Finite Element Analysis*", Key Engineering Materials, Vol. 167-168, p. 401-410, 1999

[35] DNV and Risø, "*Guidelines for Design of Wind Turbines*", 2nd Edition, Denmark, 2002

[36] S. Sivrioglou, U. Ozbay, E. Zergeroglu, "*Variable Speed Control of Wind Turbines: A Robust Backstepping Approach*", Proceedings of the 17th World Congress, The International Federation of Automatic Control Seoul, Korea, July 6-11, 2008

[37] T. Engelen, P Schaak, C. Lindenburg, "*Control for damping of the fatigue relevant deformation modes of offshore wind turbines*", Rep ECN-RX-03-037, Energy Research Center of the Netherlands, June 2003

[38] W.E. Leithead, B. Connor, "*Control of variable speed wind turbines: design task*", Int. Journal of Control, Vol. 73, No. 13, p. 1189-1212, 2000.

[39] W.E. Leithead, B. Connor, "*Control of variable speed wind turbines: dynamic models*", Int. Journal of Control, Vol. 73, No. 13, p. 1173-1188, 2000

[40] D.J. Leith, W.E. Leithead, "*Application of Nonlinear Control to a HAWT*", Proceedings of the Third IEEE Conference on Control Applications, p. 245 – 250, 24-26 Aug, Glasgow, 1994

[41] C. J. Spruce, H. Markou, W.E. Leithead, S. Domínguez Ruiz, "*Review of Control Algorithms for Offshore Wind Turbines*", ETSU W/35/00629/00/REP, 2004

[42] E. S. Politis, V. A. Riziotis, P. K. Chaviaropoulos, S. G. Voutsinas, "*Assessment of a Control Strategy for Reducing Tower Loads*", Torque 2010: The Science of Making Torque From Wind, Proceedings of 3rd EWEA Conference, p.633-645, 28-30 June 2010, Heraklion, Greece

[43] E. A. Bossanyi, "*Wind Turbine Control for Load Reduction*", Wind Energy, Vol. 6, p. 229-244, 2003

[44] C. J. Spruce, J. K. Turner, "*Control Algorithms for Eliminating Tower Vibration Events on Active Stall Wind Turbines*", Torque 2010: The Science of Making Torque From Wind, Proceedings of 3rd EWEA Conference, p.523-542, 28-30 June 2010, Heraklion, Greece

[45] European Wind Energy Association, "*Wind Energy – The Facts*", Earthscan, 2009

[46] Private communication with Professor W.E. Leithead and S. Dominguez (MLS UK)

[47] D. Veldkamp, *"Chances in Wind Energy, A Probabilistic Approach to Wind Turbine Fatigue Design"*, PhD Thesis, Delft University of Technology, Delft 2006

[48] J. Peeters, *"Simulation of Dynamic Drive Train Loads in a Wind Turbine",* PhD Thesis, Katholieke Universiteit Leuven, Belgium 2006

[49] A. Mathiopoulos, S.J. Watson, *"A methodology for producing a self-tuned wind turbine drive train damper"*, European Wind Energy Conference (EWEC2008), Brussels, Belgium, 31 March - 3 April 2008

[50] H. Camblong, F. Lescher, X. Guillaud, I. Vechiu, *"Comparison of Three Wind Turbine Controller Synthesis Methodologies"*, IEEE ICIT 06, p.1908-1913, Bombay, India, 2006

[51] B. Connor, W. E. Leithead, M. J. Grimble, *"LQG control of a constant speed horizontal axis wind turbine"*, Third IEE Conference on Control Applications 1994, pages 251–252, Glasgow-UK, 1994

[52] T. Ekelund, "*Modeling and linear quadratic optimal control of wind turbines"*, PhD thesis, School of Electrical and Computer Engineering, Chalmers University of Technology, Sweden, 1997

[53] X. Zhang, W. Wang, Y. Liu, *"Fuzzy Control of Variable Speed Wind Turbine"*, The Sixth World Congress on Intelligent Control and Automation, p. 3872 – 3876, China, 2006

[54] P. Ridanpaa, *"Fuzzy control of a wind power plant"*, MSc Thesis, Tampere University of Technology, Dept. of Electrical Engineering, Tampere, Finland, February 1998

[55] D. Robb, *"Model based predictive control with application to renewable energy systems"*, PhD thesis, University of Strathclyde, Glasgow-UK, March 2000

[56] A. Koerber, R. King, *"Model predictive control for wind turbines"*, European Wind Energy Conference 2010, Warsaw - Poland, 2010

[57] F. Lescher, J. Y. Zhao, and A. Martinez, *"Multiobjective H2/H∞ control of a pitch regulated wind turbine for mechanical load reduction"*, International Conference on Renewable Energies and Power Quality, Spain, 2006

[58] A. Wright, M. Balas, *"Design of controls to attenuate loads in the Controls Advanced Research Turbine,"* J. Solar Energy Eng., vol. 126, no. 4, pp. 1083–1091, 2004

[59] T. Thiringer, A. Petersson, *"Control of a variable-speed pitch-regulated wind turbine"*, Technical report, Chalmers University of Technology, 2005

[60] A.G. Dutton, P.A. Bonnet, P. Hogg, Y.L. Lleong, *"Novel materials and modelling for large wind turbine blades"*, Journal of Power and Energy, Vol. 224, No 2, pp 203-210, 2010

[61] W.E. Leithead, S. Dominguez, "*Coordinated Control Design for Wind Turbine Control Systems*", European Wind Energy Conference 2006, Scientific Proceedings, p. 56-59, Athens, 2006

[62] E. Hau, "*Wind Turbines Fundamentals, Technologies, Application,* Economics", 2nd edition, Springer, 2006

[63] S. Mathew, "Wind Energy Explained – Fundamentals, Resource Analysis and Economics", Springer, 2006

[64] T. Ackerman, "Wind Power in *Power Systems"*, Wiley, 2005

[65] T. Burton, D. Sharpe, N. Jenkins, E. Bossanyi, *"Wind Energy Handbook"*, Wiley, 2001

[66] M. O. L. Hansen, *"Aerodynamics of Wind Turbines",* Earthscan, 2008

[67] A. Visioli, "*Practical PID Control*", Springer, 2006

[68] I. Munteanu, A. I. Bratcu, N. A. Cutululis, E. Ceang, "*Optimal Control of Wind Energy Systems*", Springer, 2008

[69] F. D. Bianchi, H. De Battista, "*Wind Turbine Control Systems - Principles, Modelling and Gain Scheduling Design*", Springer, 2007.

[70] D. Molenaar, "*Cost-effective Design and Operation of Variable Speed Wind Turbines*", Delft University Press, 2003

[71] M. Sathyajith, "*Wind Energy, Fundamentals, Resource Analysis and Economics*", Springer, 2006

[72] R. Gasch, J. Twele, "*Wind power plants : fundamentals, design, construction and operation",* Solarpraxis, 2002

[73] O. Anaya-Lara, N. Jenkins, J. Ekanayake, P. Cartwright, M. Hughes, "*Wind Energy Generation – Modelling and Control*", Wiley, 2009

Appendix A: Wind turbine parameters

A.1 Parameters defining the 2MW Supergen Wind turbine

The parameters, which are necessary for the definition and formulation of the Simulink model, as well as the control models, of the exemplar 2MW Supergen wind turbine, are extracted from Bladed and are listed below:

Parameters of the 2MW Supergen Exemplar Wind Turbine	
Blade & Rotor parameters	
Rotor radius [m]	R = 37.5
Effective blade length (for wind speed correction) [m]	L = 26.25
Distance of the centre of mass from the hub axis [m]	Rc = 11.94
One blade mass [Kg]	Mblade = 5320
One blade mass*3 [Kg]	Mbl = Mblade*3
Hub height [m]	h = 65
Tower/Rotor cross-coupling inertia [Kg*m^2]	Jc = Rc*h*Mbl
Flap natural frequency [rad/s]	w_f = 6.66
Rotor inertia [Kg*m^2]	J = 4.26849e+006
Blade flapwise stiffness [Nm/rad]	Kf = w_f^2*J
Edge natural frequency [rad/s]	w_e = 9.99
Blade edgewise stiffness [Nm/rad]	Ke = w_e^2*J
Rotor and nacelle mass [Kg]	Mr_n = 97961
Tower parameters	
Tower fore-aft inertia [Kg*m^2]	Jt = h^2*(Mr_n-Mbl)
Tower fore-aft frequency [rad/s]	w_t = 2.5133

Tower fore-aft damping	Bt_param = 0.005
Tower fore-aft damping moment [Nm]	Bt = 2*Bt_param*w_t*Jt
Tower fore-aft stiffness [Nm/rad]	Kt = w_t^2*Jt
Tower side-side natural frequency [rad/s]	w_ts = 2.5133
Tower side-side inertia [Kg*m^2]	Jts = h^2*Mr_n
Tower side-side stiffness [Nm/rad]	Kts = w_ts^2*Jts
Tower side-side damping	Bts_param = 0.005
Tower side-side damping moment [Nm]	Bts = 2*Bts_param*w_ts*Jts
Coefficient to adjust tower/nacelle displacement	Ka = 1.4
Pitch Actuator parameters	
Pitch actuator transfer function	$G_{pa}(s) = \frac{39.48}{s^2 + 10.05s + 39.48}$
Operational parameters	
Minimum generator speed in generation mode [rad/s]	WMIN = 89.0118
Maximum generator speed in generation mode [rad/s]	WMAX = 157.07
Cut in wind speed [m/s]	WCUTIN = 4
Cut out wind speed [m/s]	WCUTOUT = 25
Nominal generator torque [Nm]	TQSET = 13403
Minimum pitch angle [deg]	PITMIN = -3
Maximum pitch angle [deg]	PITMAX = 90
Sampling time [s]	sample_time = 0.05
Air density [Kg/m^3]	rho = 1.225
Drive-train parameters	
Hub inertia [Kg*m^2]	ILs = 12000
Low speed shaft damping	gls = 1e-007
High speed shaft damping	ghs = 5
Low speed shaft stiffness [Nm/rad]	KLsb = 1.9e+008

Low speed shaft material damping	g1s = 1.6e+006
High speed shaft material damping	g2s = 1000
High speed shaft stiffness [Nm/rad]	KHs = 1e+010
Gearbox ratio	N=n = 84.15
High speed shaft inertia [Kg*m^2]	J_Hs = 5
Generator inertia [Kg*m^2]	J_gen = 130
Drive-train efficiency below rated	EtaFL = 0.96
Drive-train efficiency above rated	EtaVS = 0.96
High speed shaft + generator inertia [Kg*m^2]	IHs = J_Hs+J_gen

Appendix B

B.1 Performance of the SISO controller

Below rated 8m/s

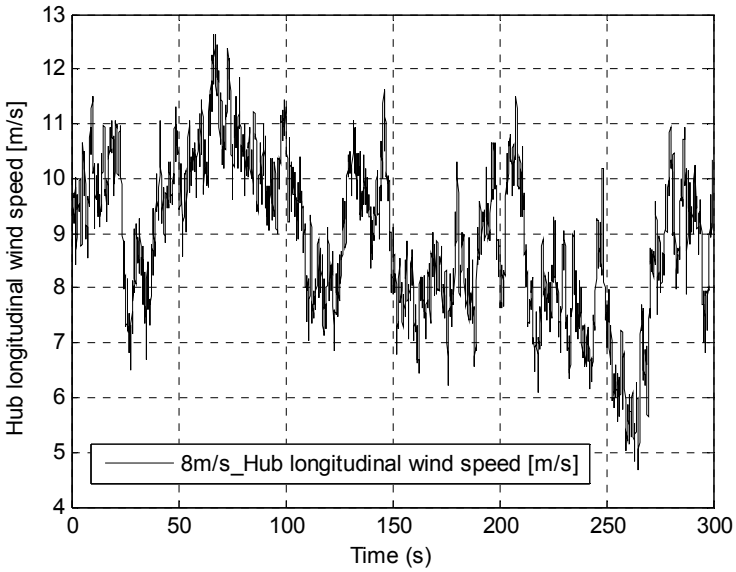

Figure B.1: Wind speed time series for 8m/s

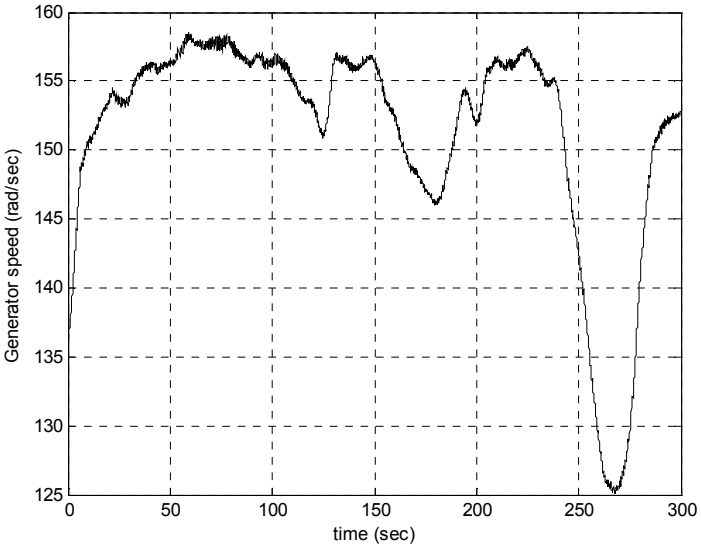

Figure B.2: Generator speed time series for 8m/s

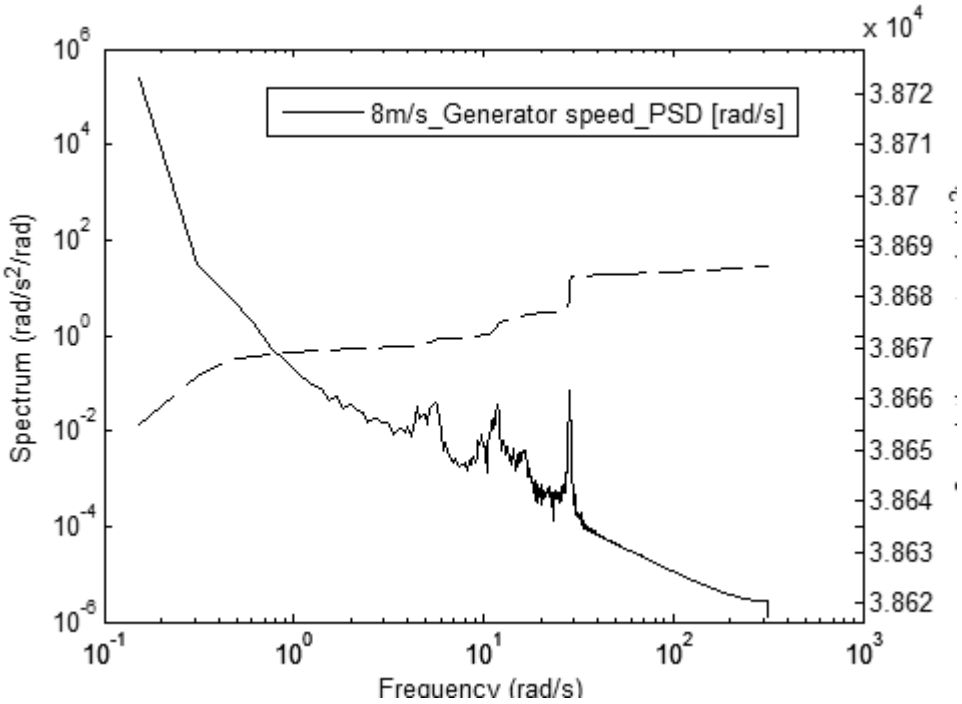

Figure B.3: Generator speed spectrum for 8m/s

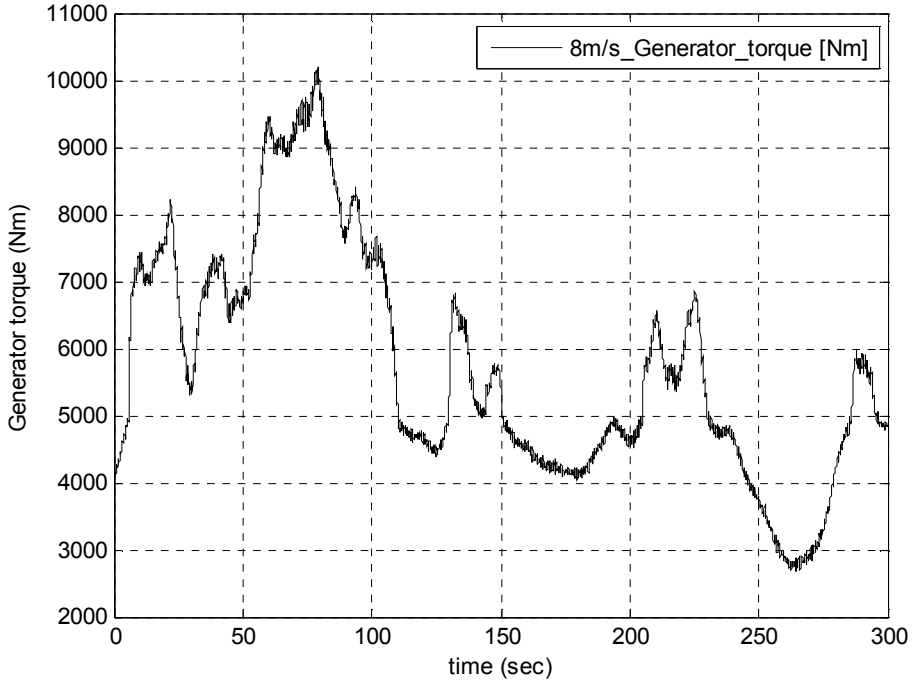

Figure B.4: Generator torque time series for 8m/s

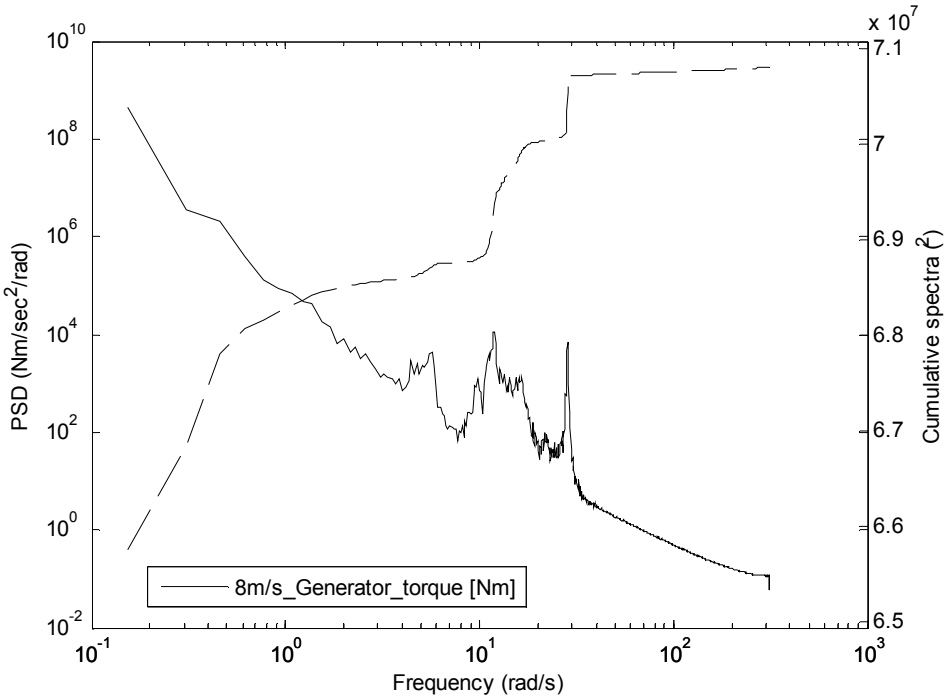

Figure B.5: Generator torque spectrum for 8m/s

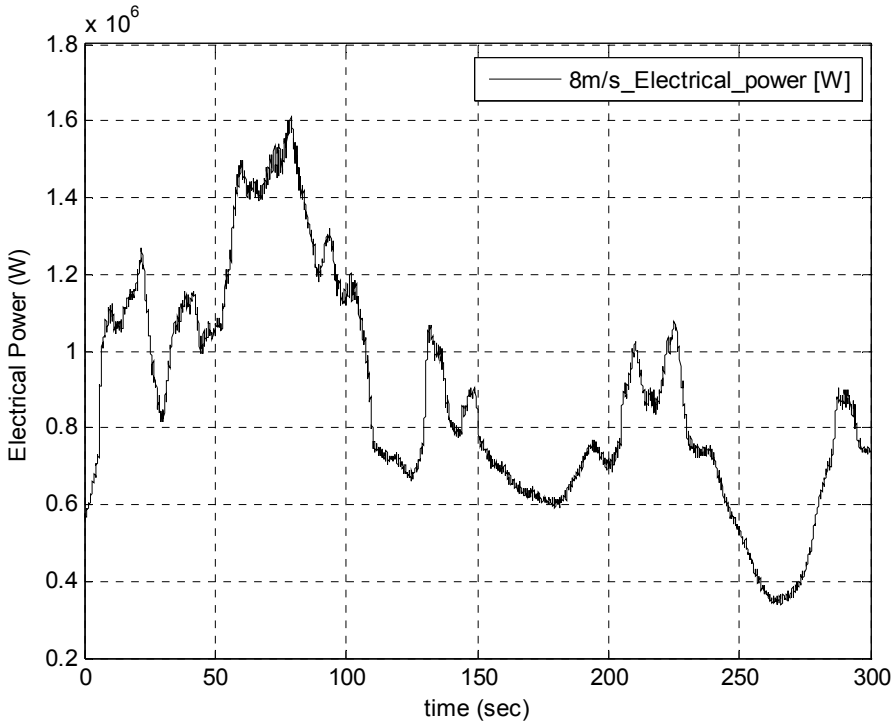

Figure B.6: Electrical power output time series for 8m/s

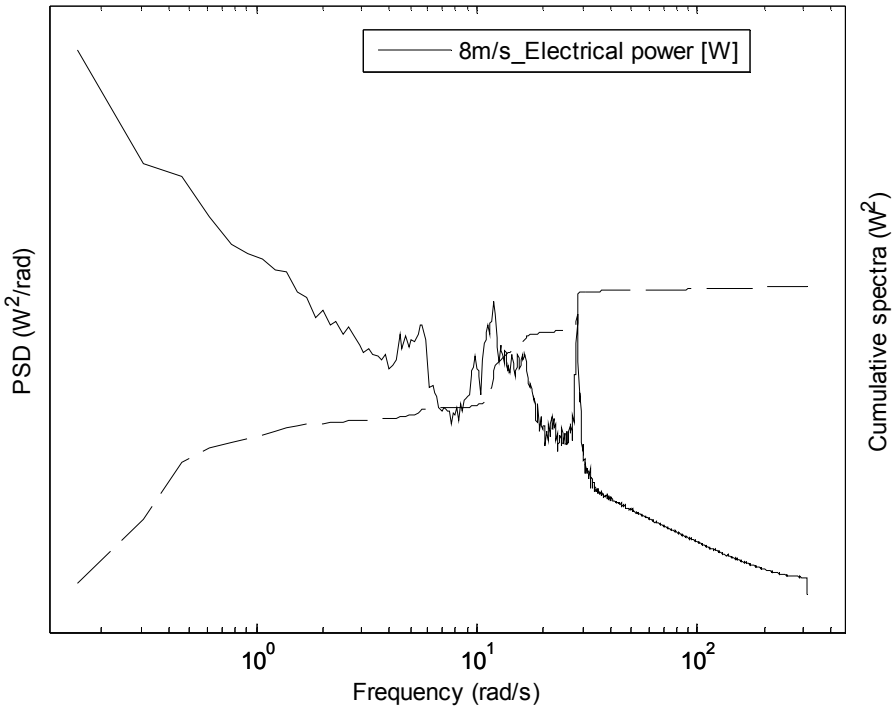

Figure B.7: Electrical power output spectrum for 8m/s

Above rated 14m/s

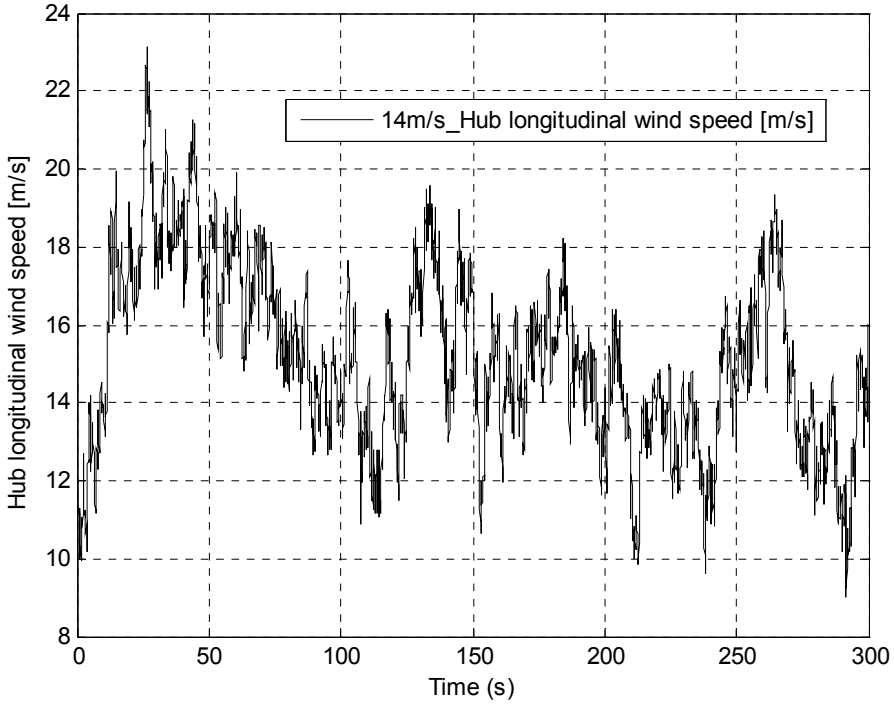

Figure B.8: Wind speed time series for 14m/s

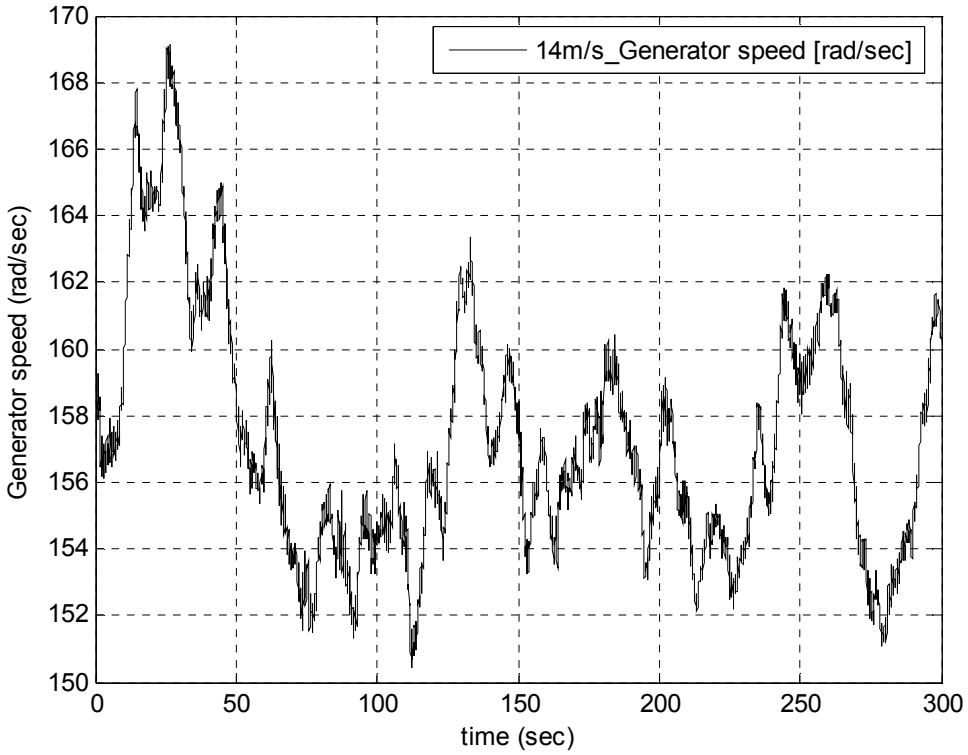

Figure B.9: Generator speed time series for 14m/s

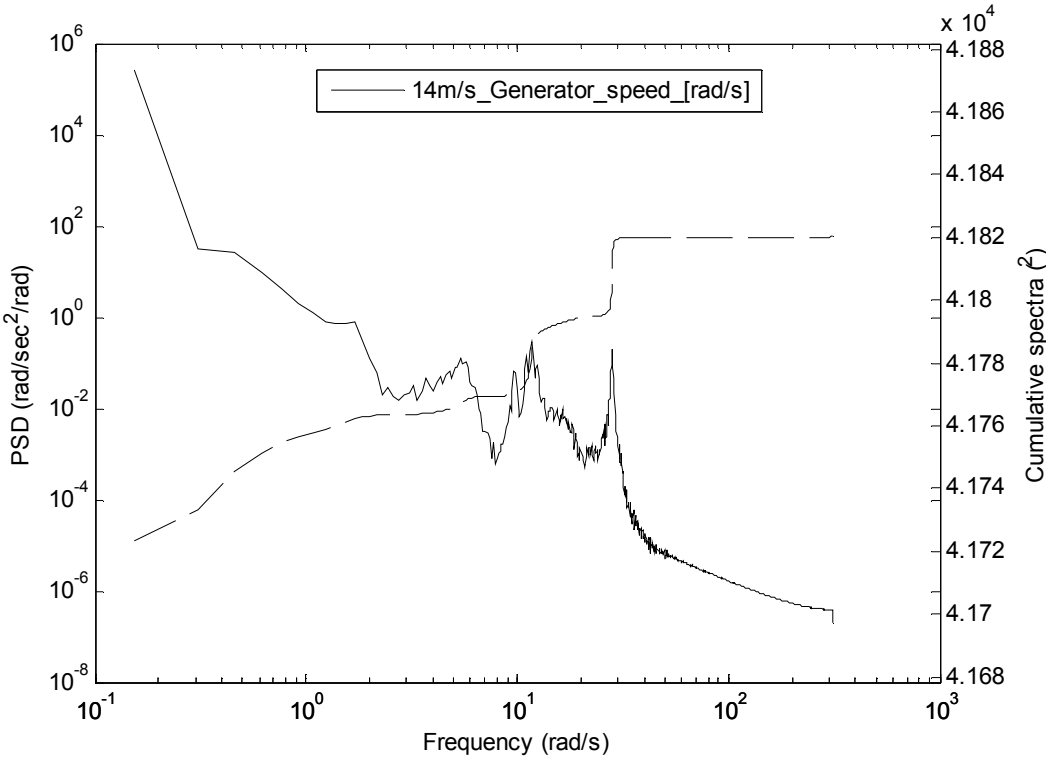

Figure B.10: Generator speed spectrum for 14m/s

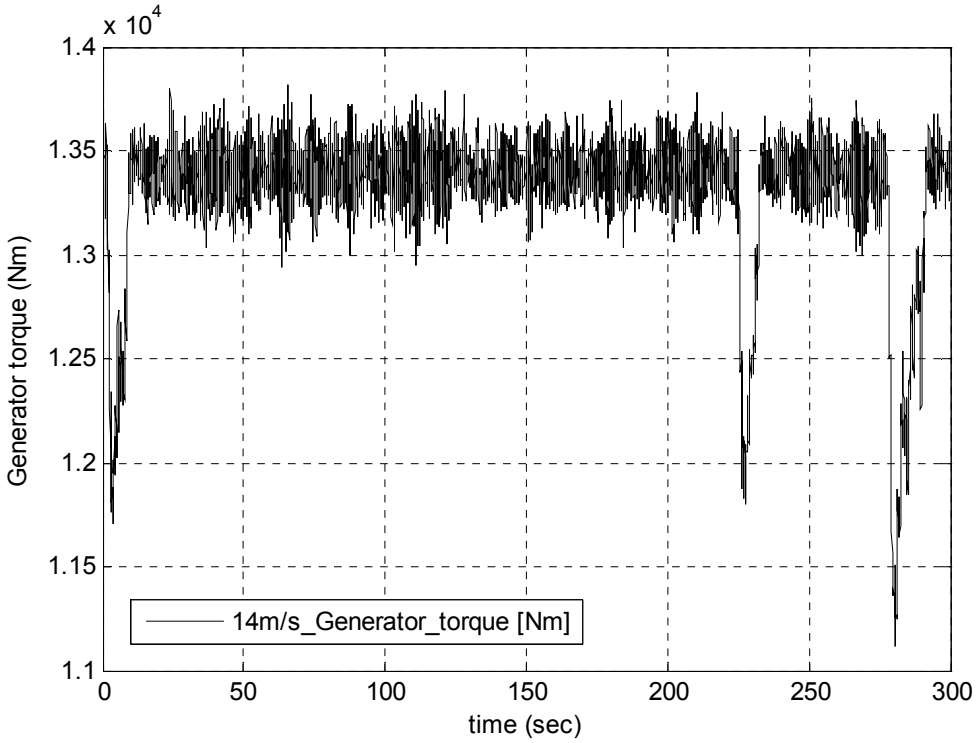

Figure B.11: Generator torque time series for 14m/s

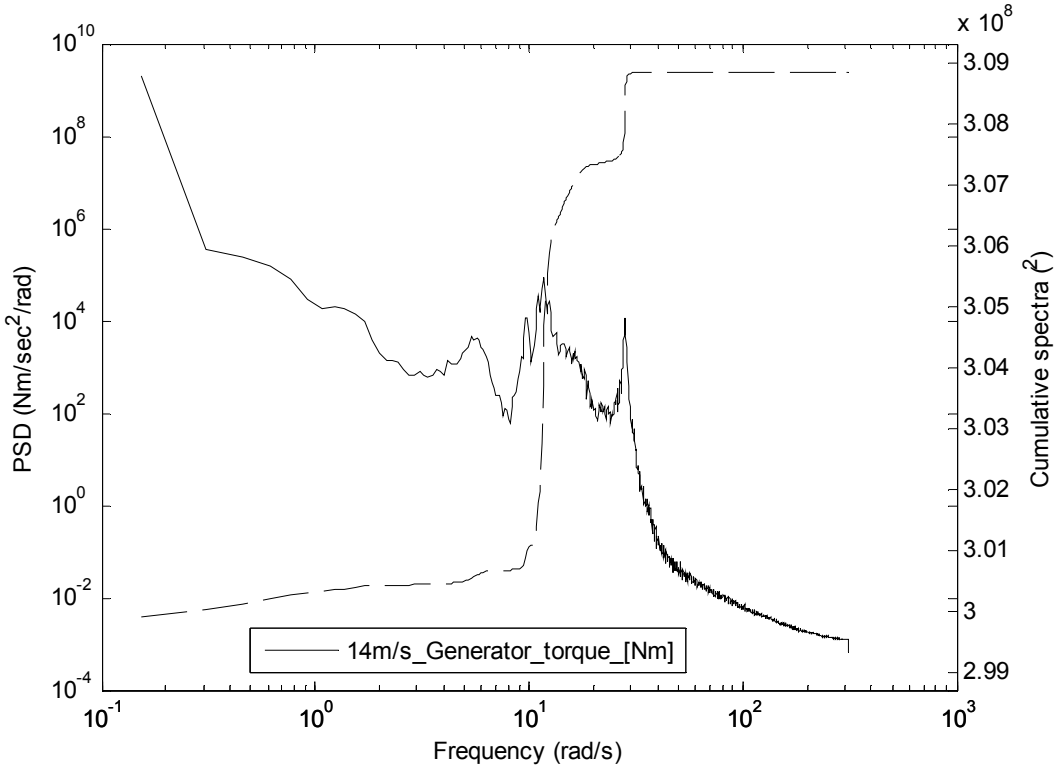

Figure B.12: Generator torque spectrum for 14m/s

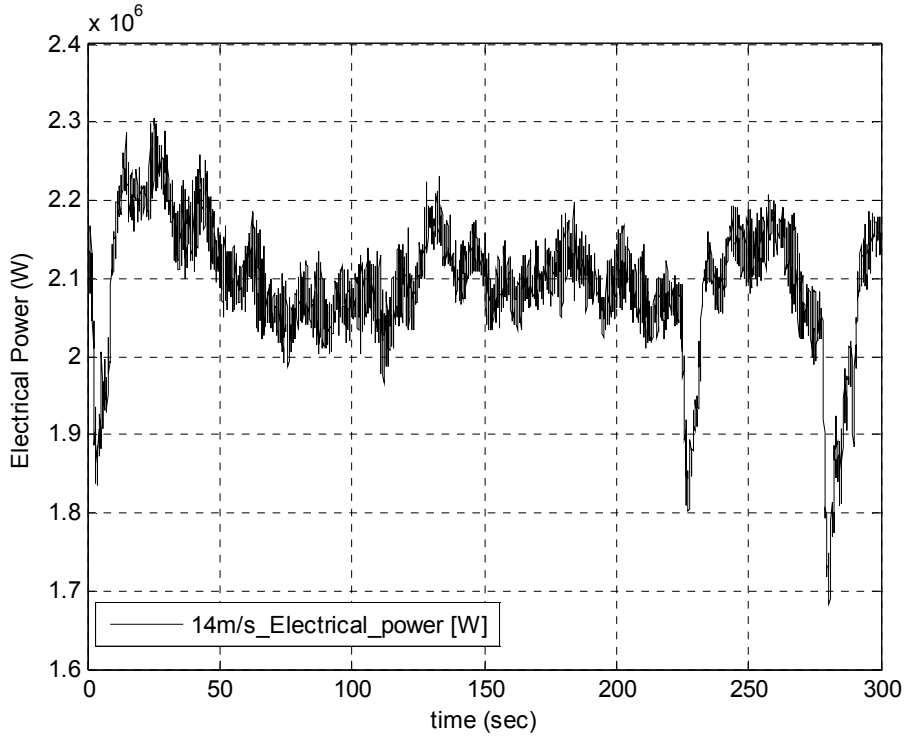

Figure B.13: Electrical power output time series for 14m/s

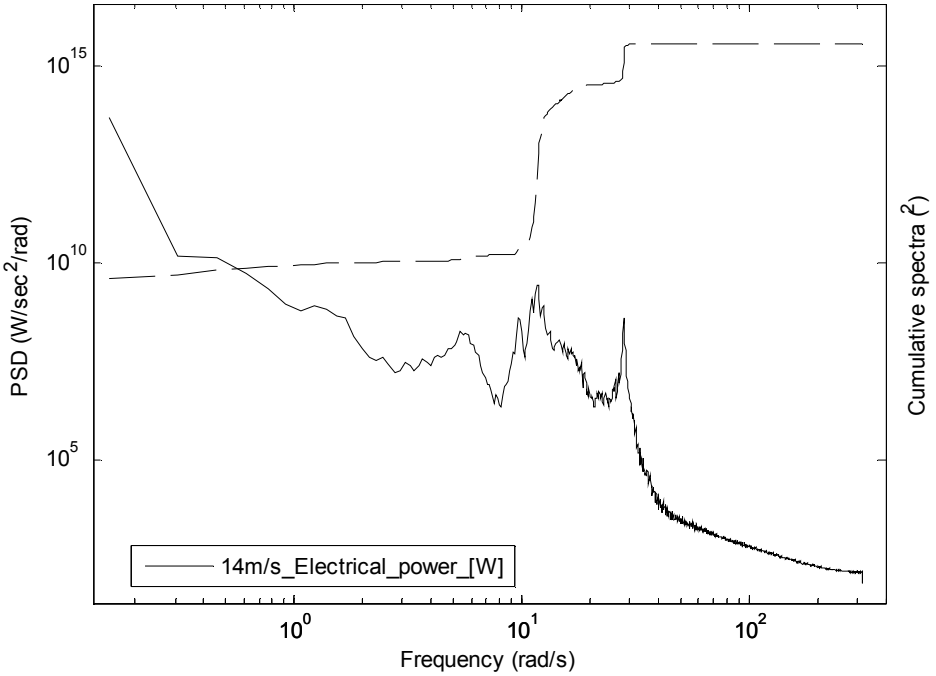

Figure B.14: Electrical power output spectrum for 14m/s

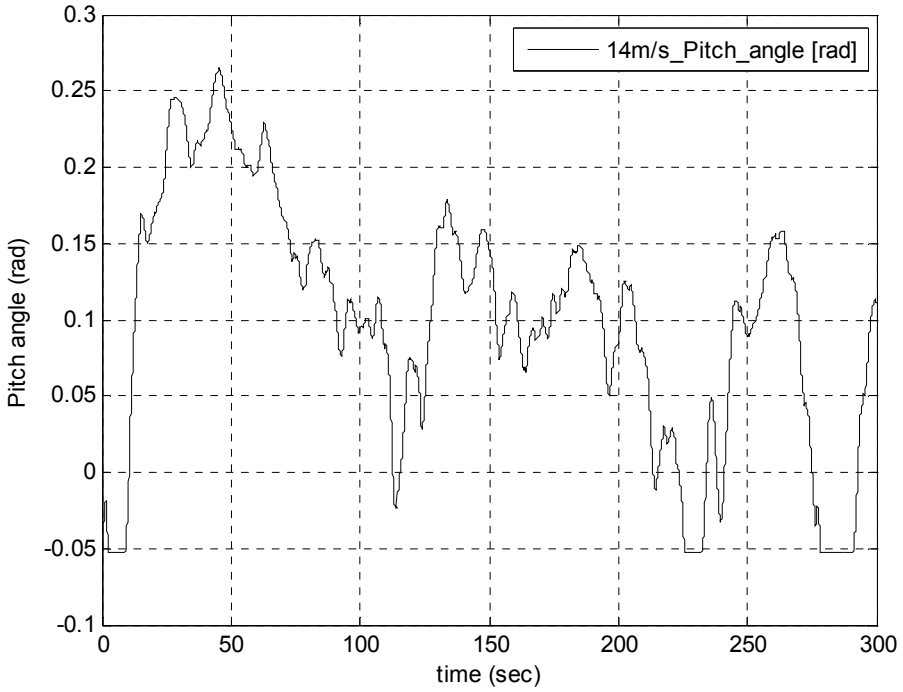

Figure B.15: Pitch angle time series for 14m/s

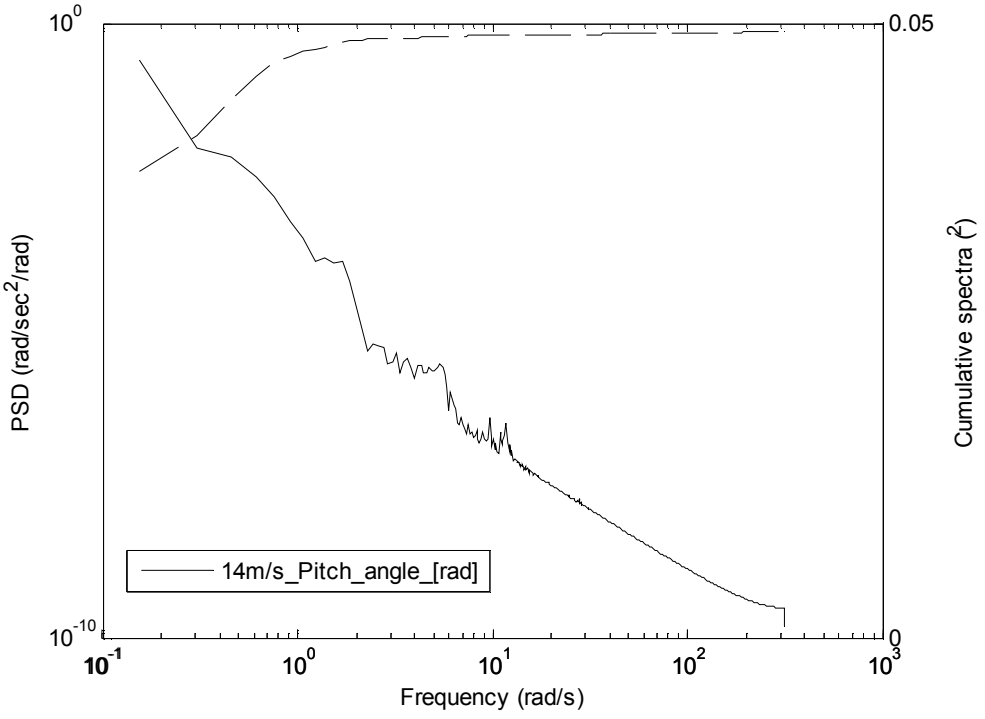

Figure B.16: Pitch angle spectrum for 14m/s

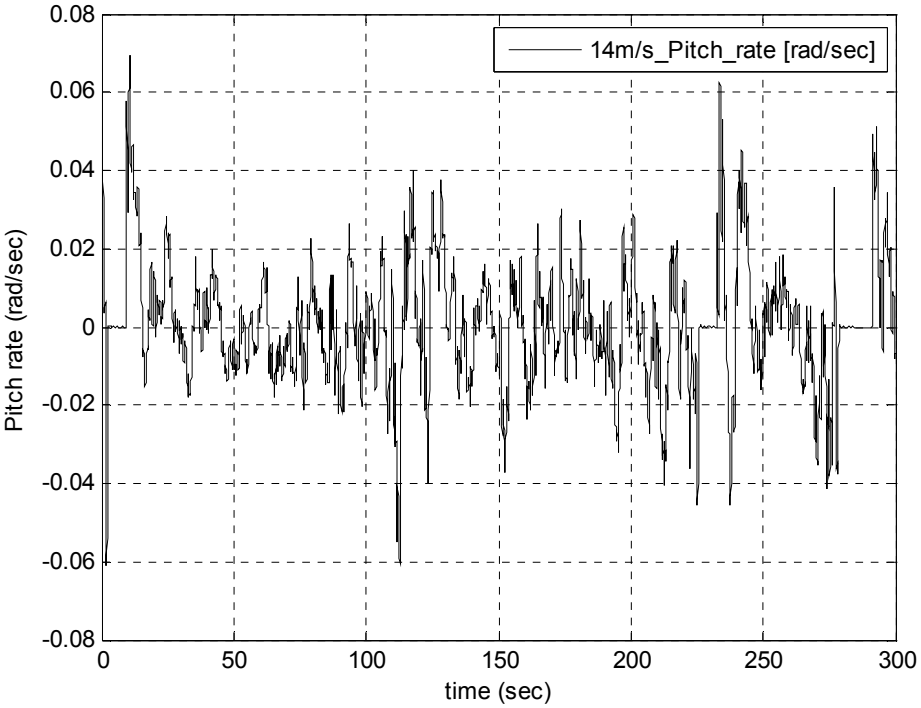

Figure B.17: Pitch rate time series for 14m/s

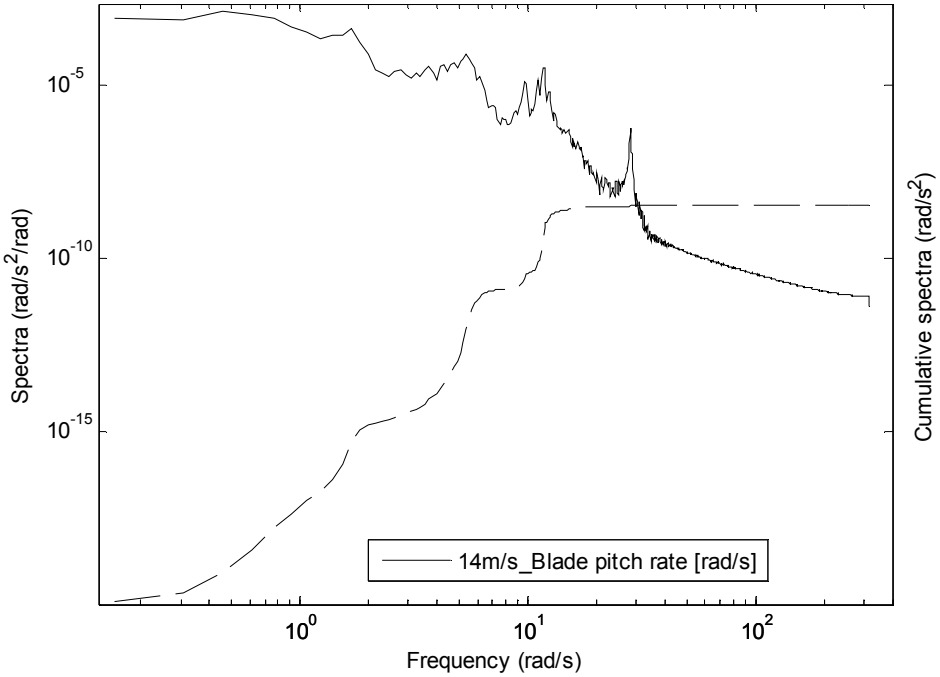

Figure B.18: Pitch rate spectrum for 14m/s

Above rated 20m/s

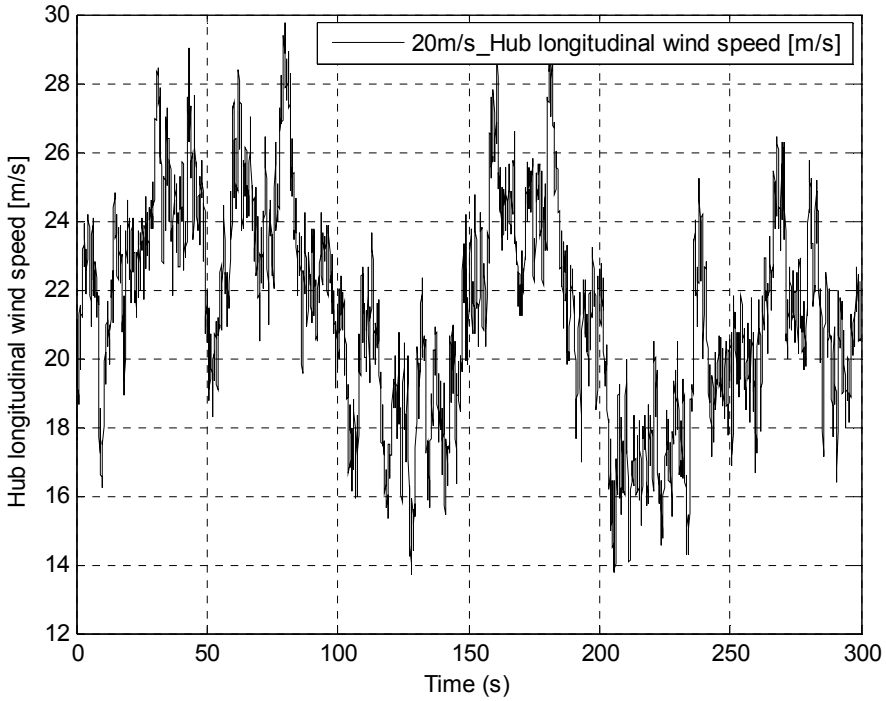

Figure B.19: Wind speed time series for 20m/s

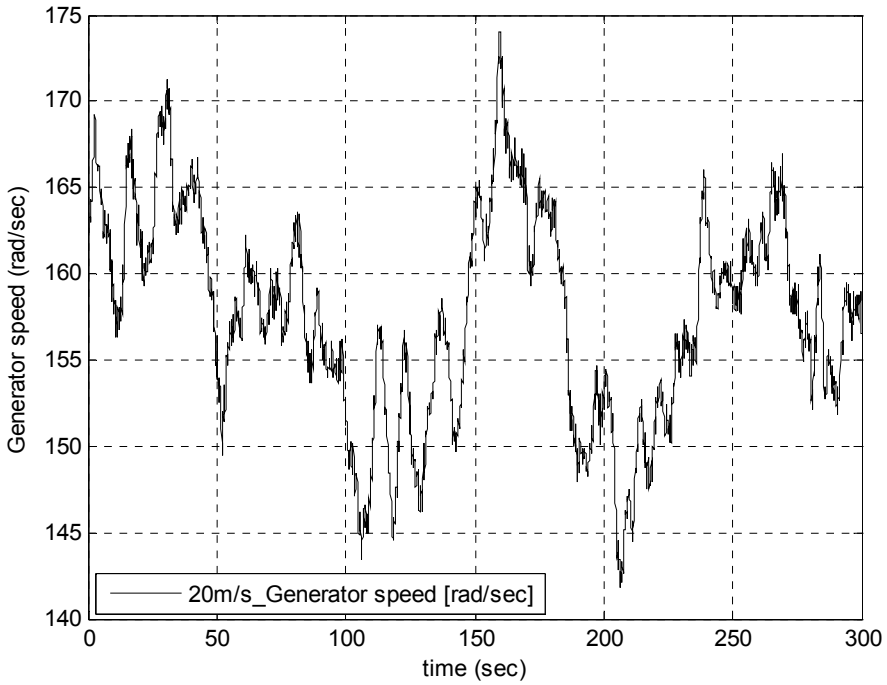

Figure B.20: Generator speed time series for 20m/s

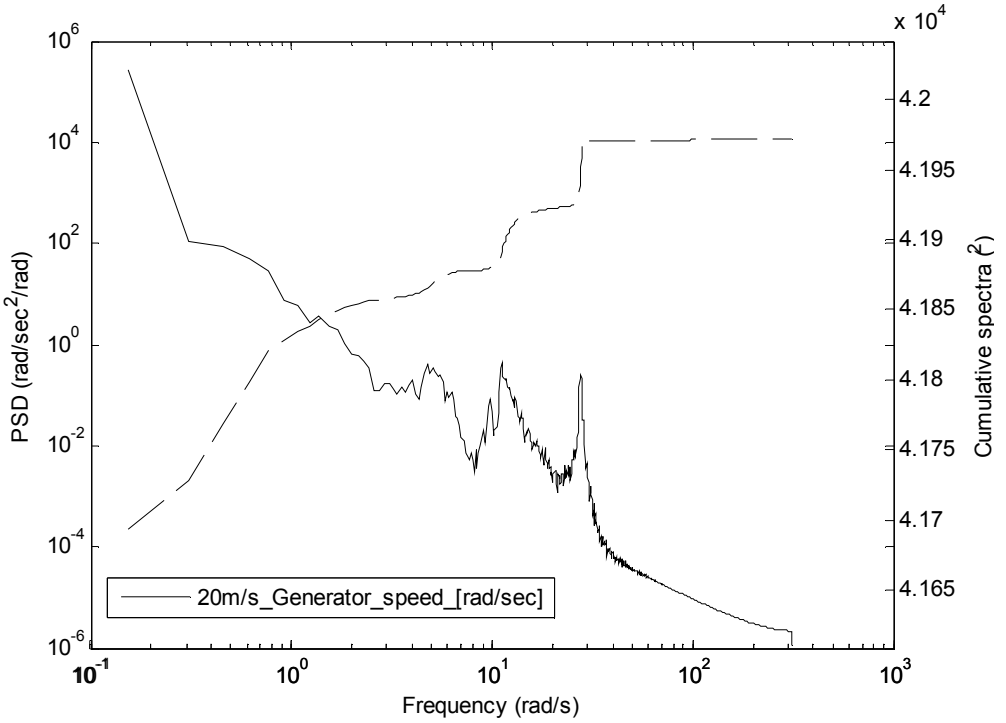

Figure B.21: Generator speed spectrum for 20m/s

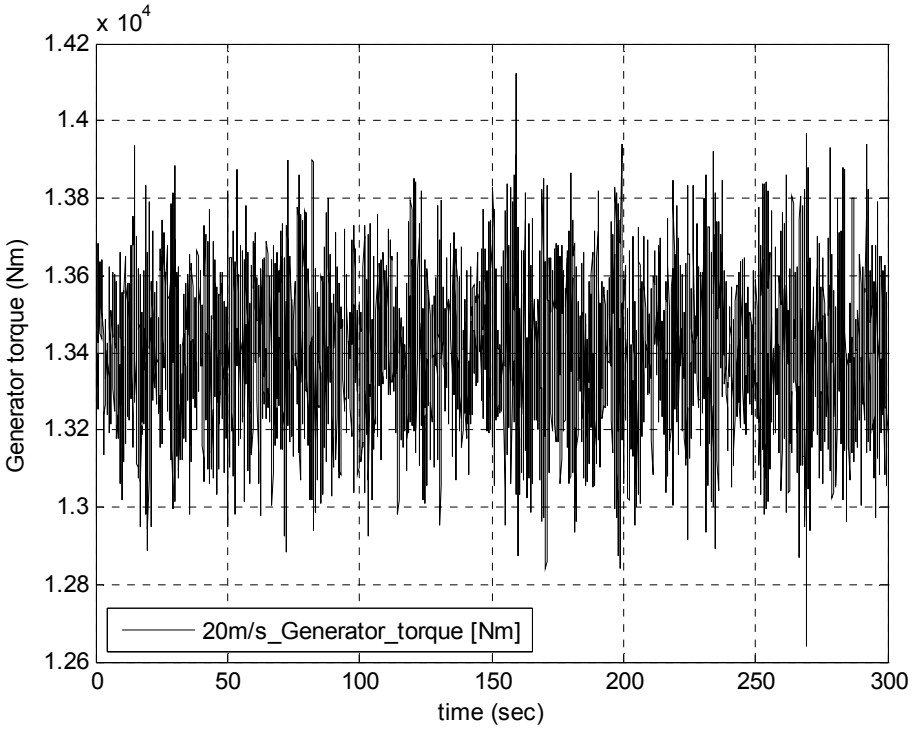

Figure B.22: Generator torque time series for 20m/s

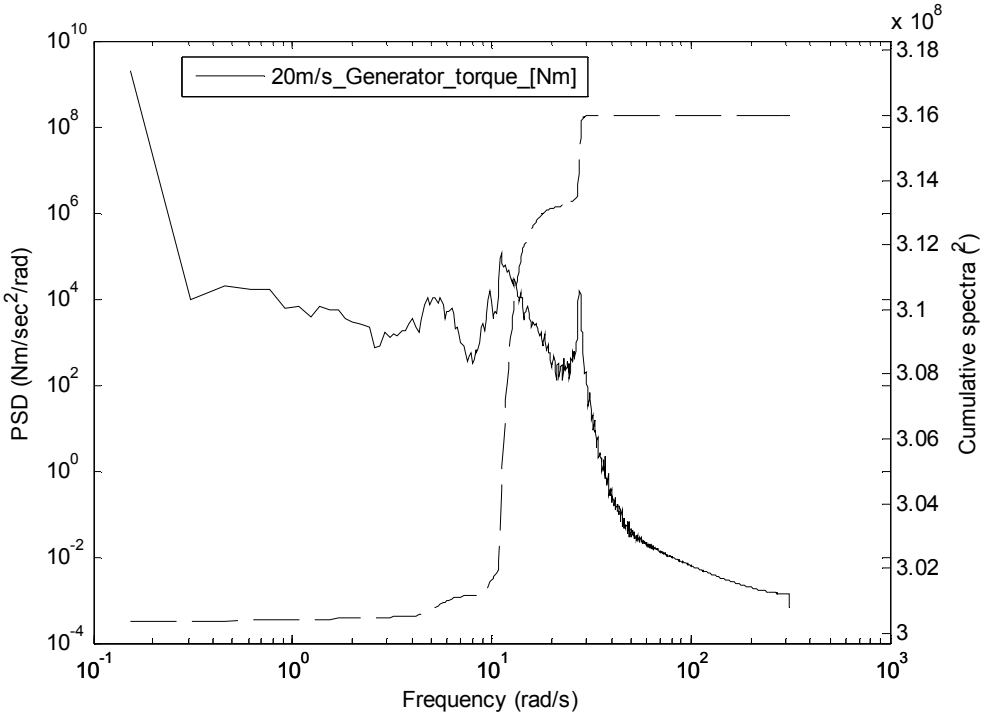

Figure B.23: Generator torque spectrum for 20m/s

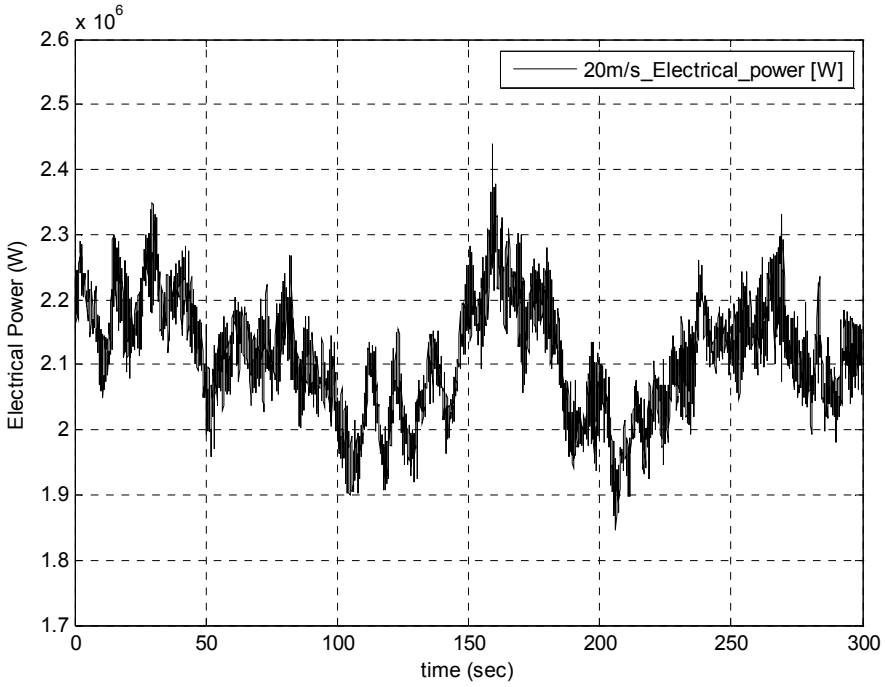

Figure B.24: Electrical power output time series for 20m/s

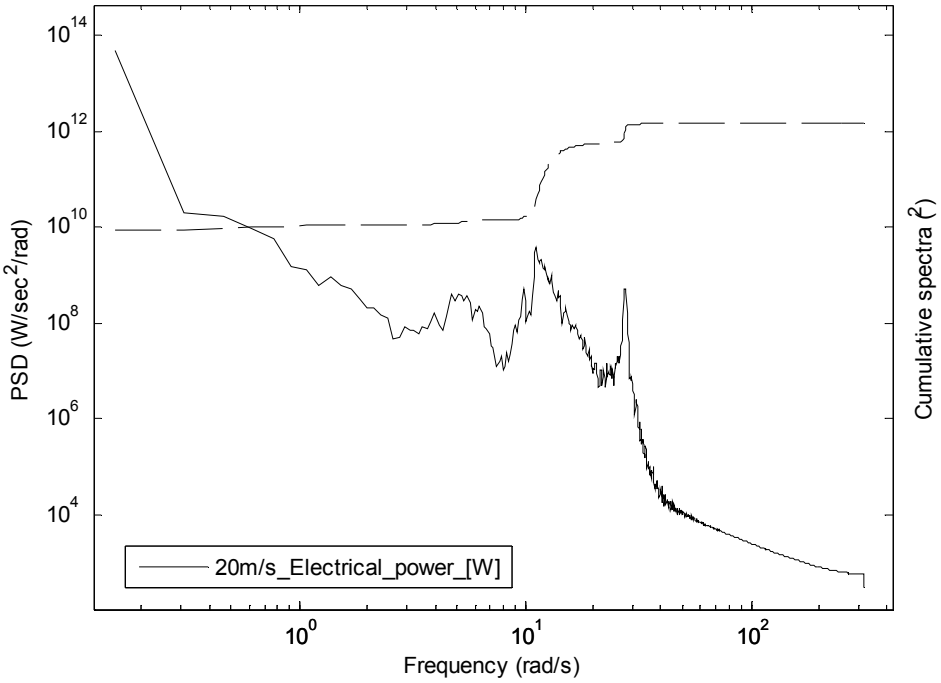

Figure B.25: Electrical power output spectrum for 20m/s

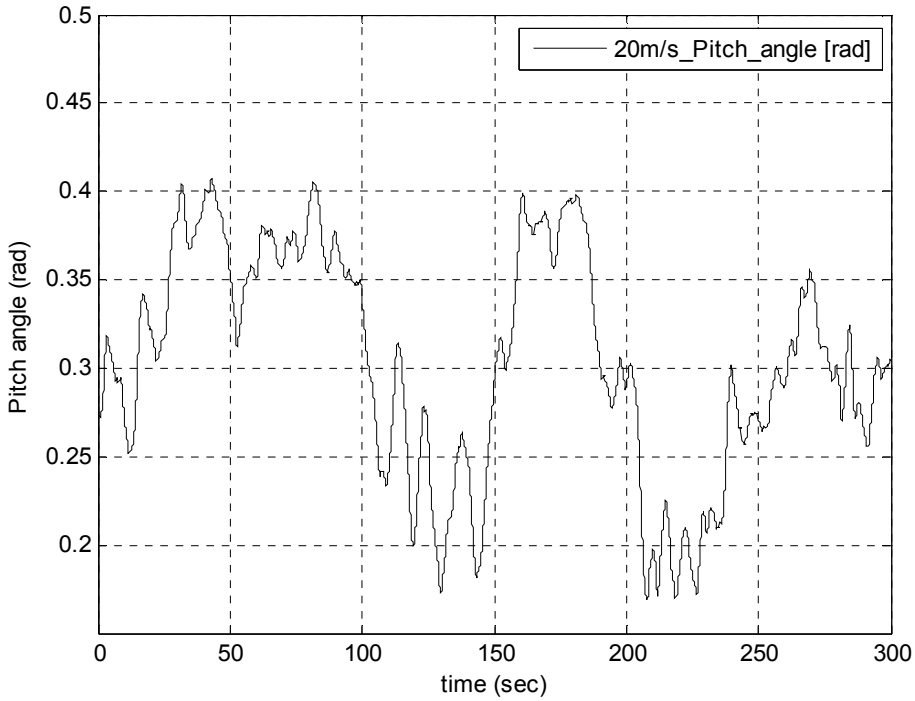

Figure B.26: Pitch angle time series for 20m/s

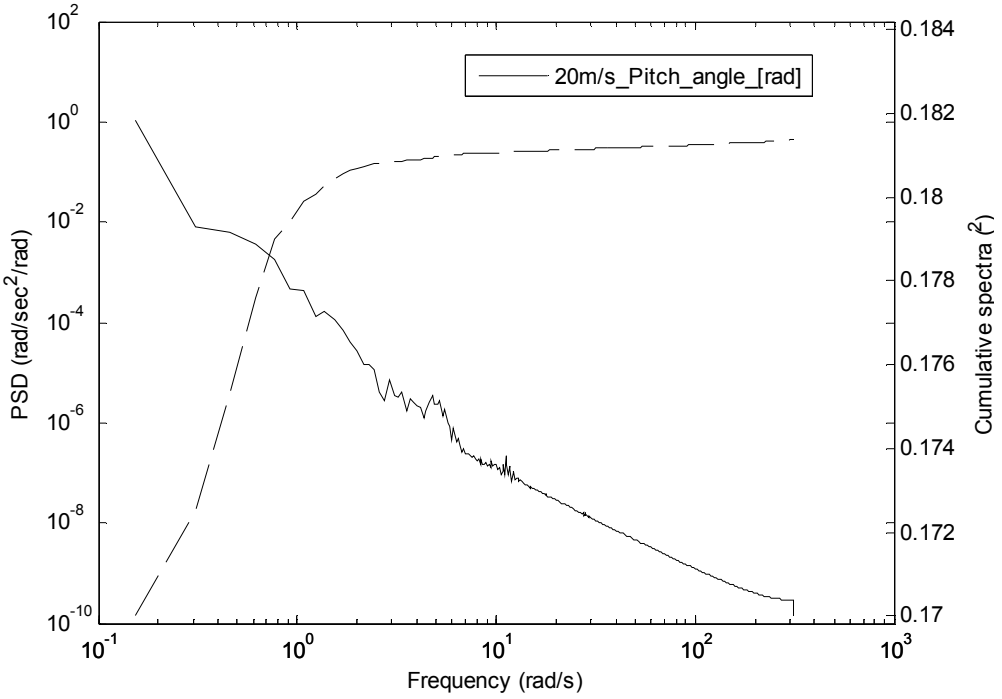

Figure B.27: Pitch angle spectrum for 20m/s

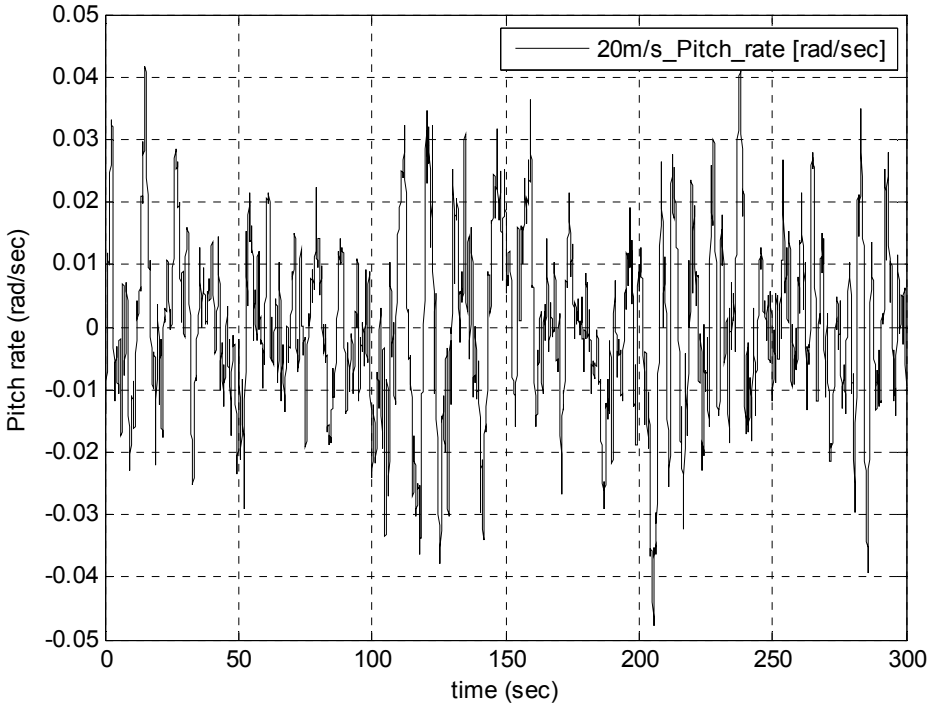

Figure B.28: Pitch rate time series for 20m/s

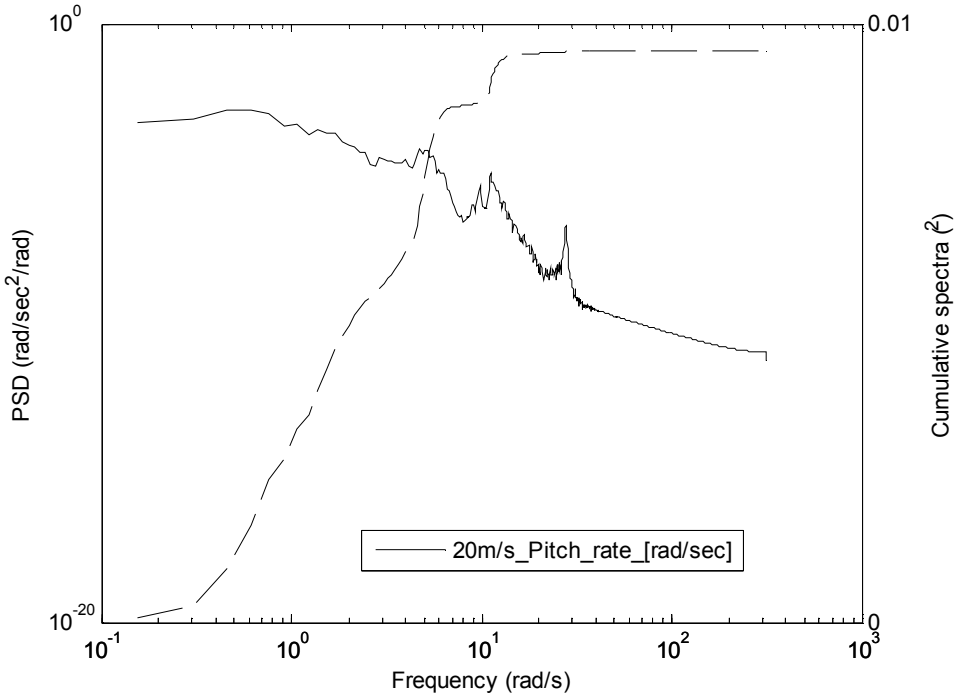

Figure B.29: Pitch rate spectrum for 20m/s

Blade root edgewise moments

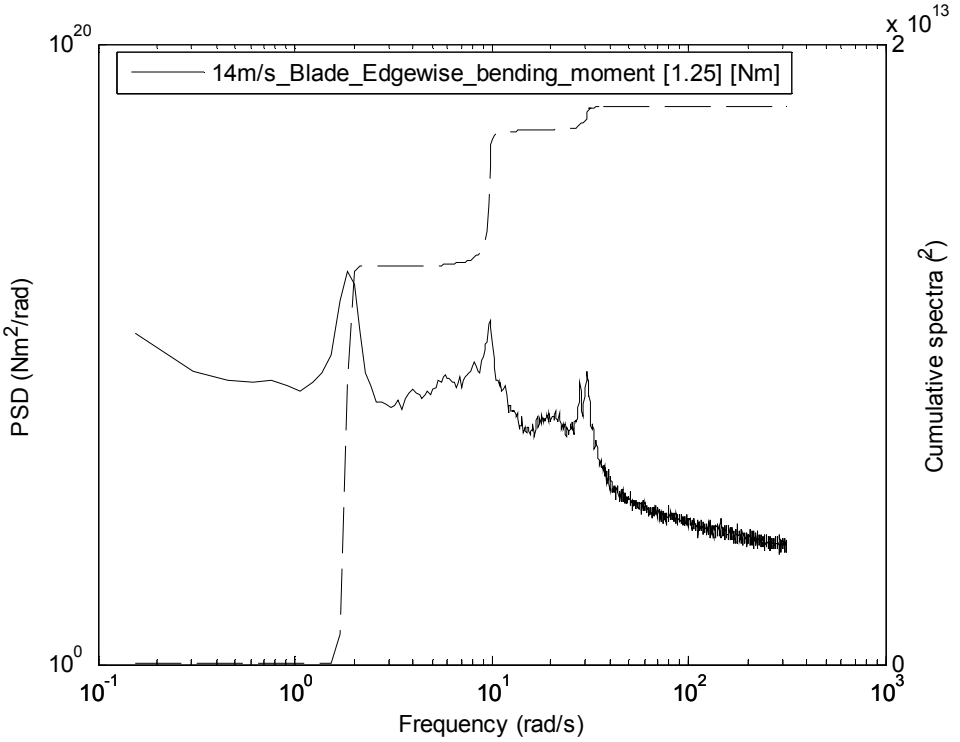

Figure B.30: Blade edgewise bending moment spectrum for 14m/s

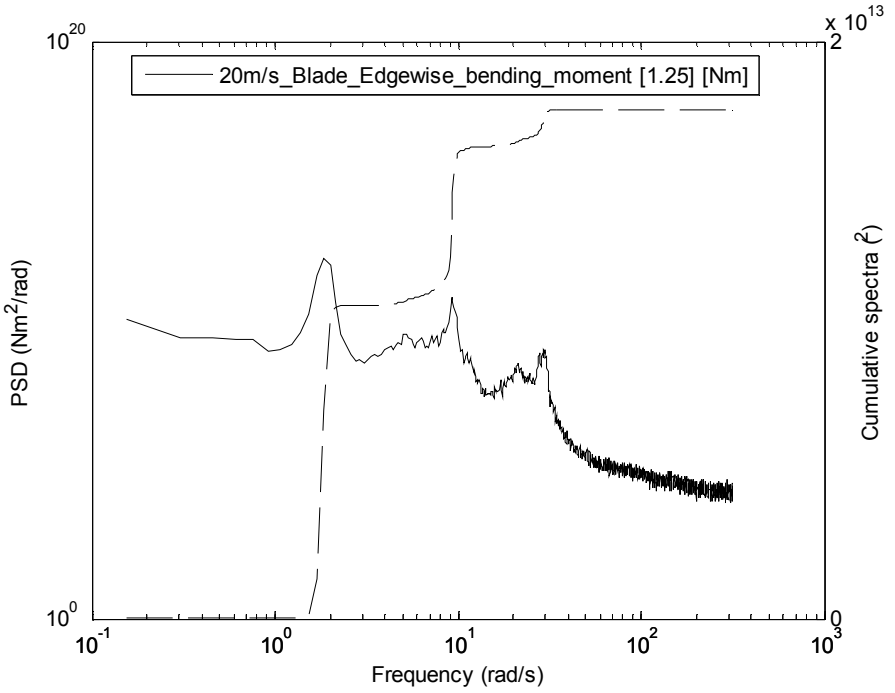

Figure B. 31 Blade edgewise bending moment spectrum for 20m/s

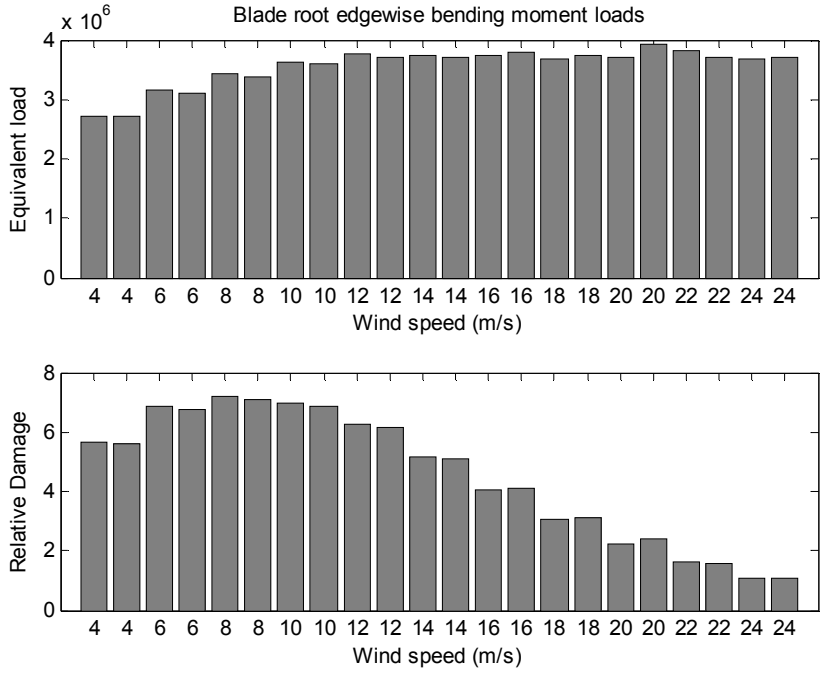

Figure B.32: Blade edgewise bending moment loads

Table 5: Lifetime blade root edgewise bending moment loads

Lifetime blade root edgewise bending moment loads	
Controller type	**Loads**
SISO(Basic)	3.2116e+06

Blade root flapwise moments

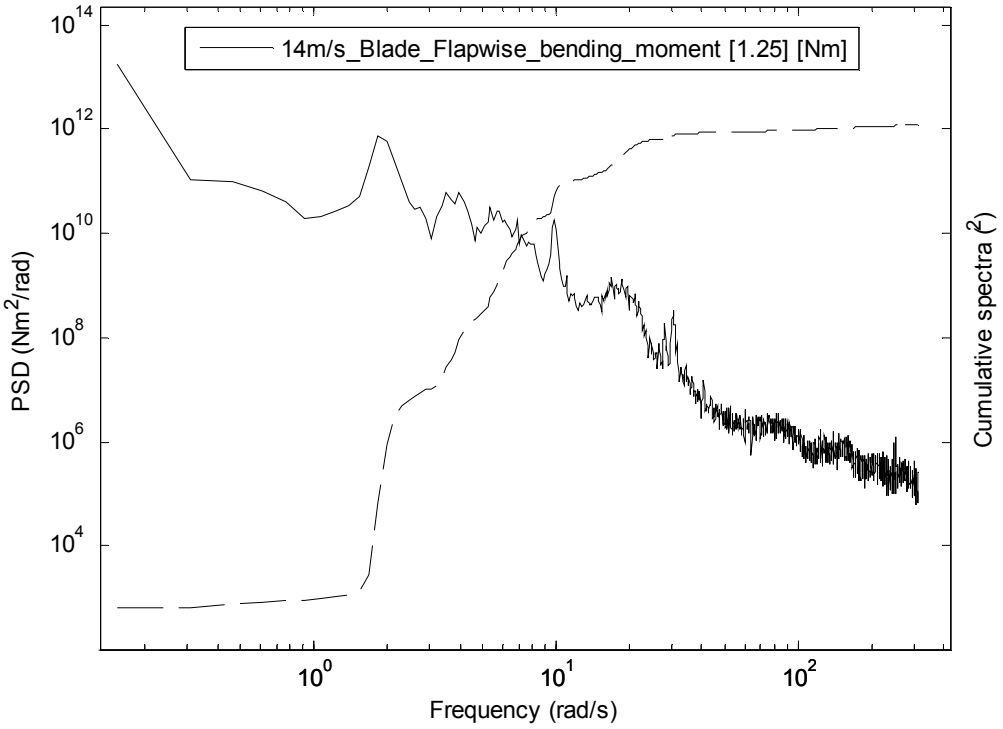

Figure B.33: Blade flapwise bending moment spectrum for 14m/s

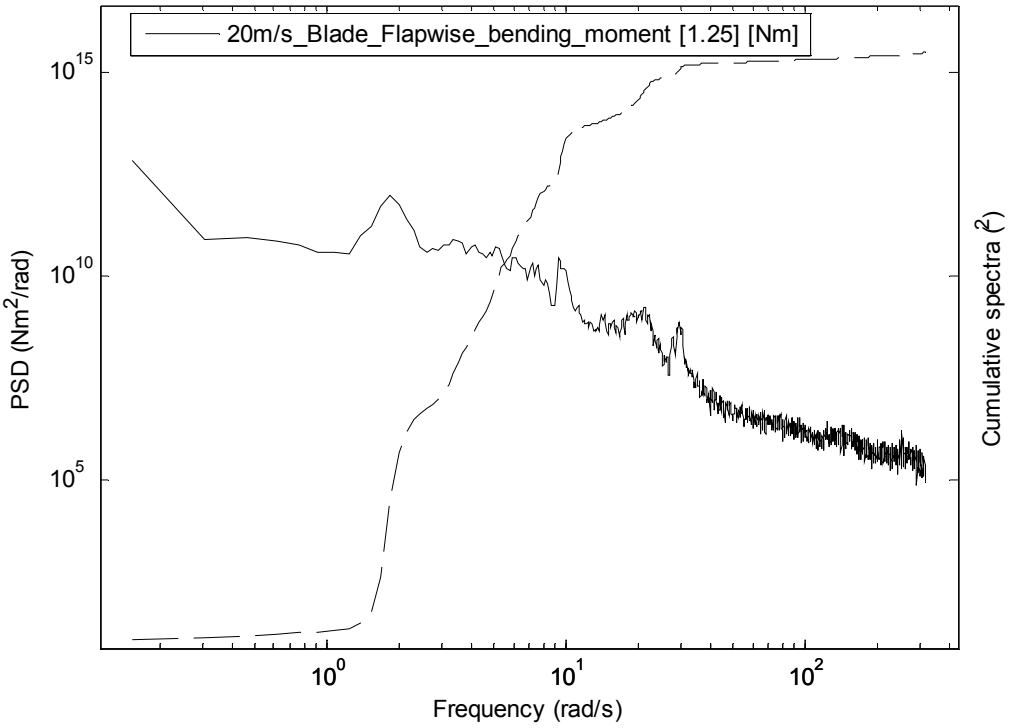

Figure B.34: Blade flapwise bending moment spectrum for 20m/s

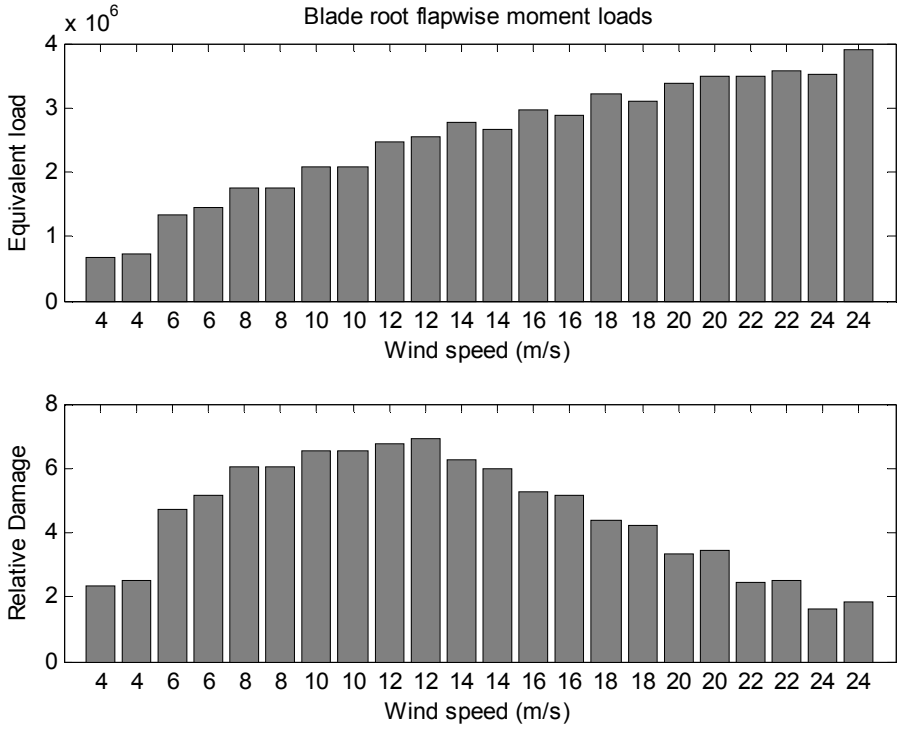

Figure B.35: Lifetime blade root flapwise bending moment loads

Table 6: Lifetime blade root flapwise bending moment loads

Lifetime blade root flapwise bending moment loads	
Controller type	**Loads**
SISO(Basic)	1.8698e+06

Tower base side to side moment loads

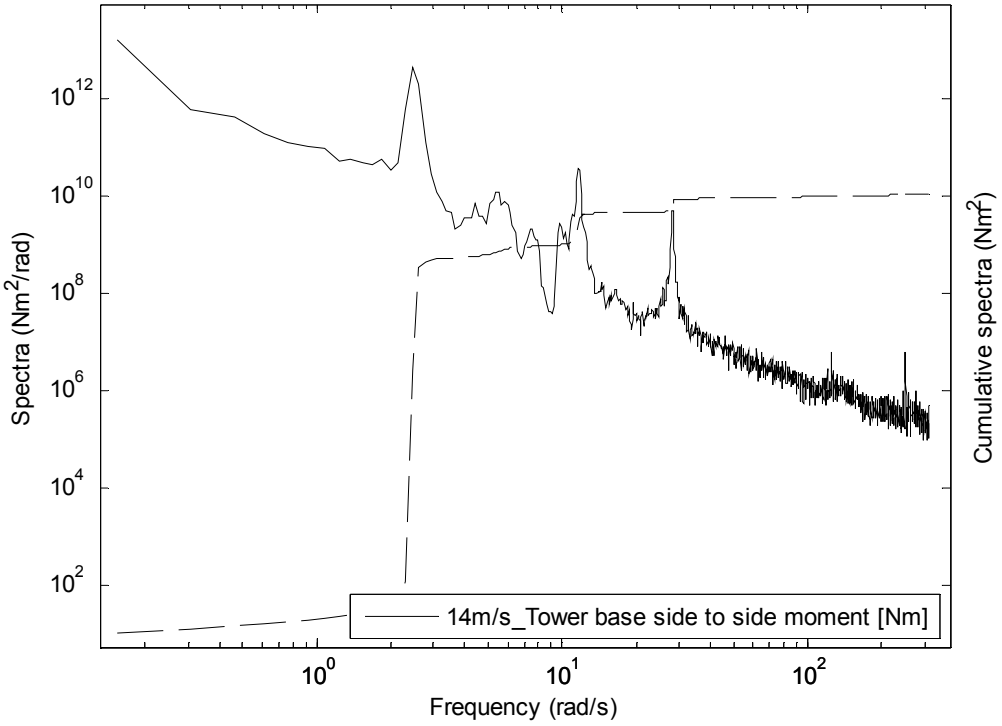

Figure B.36: Tower base side to side moment spectrum for 14m/s

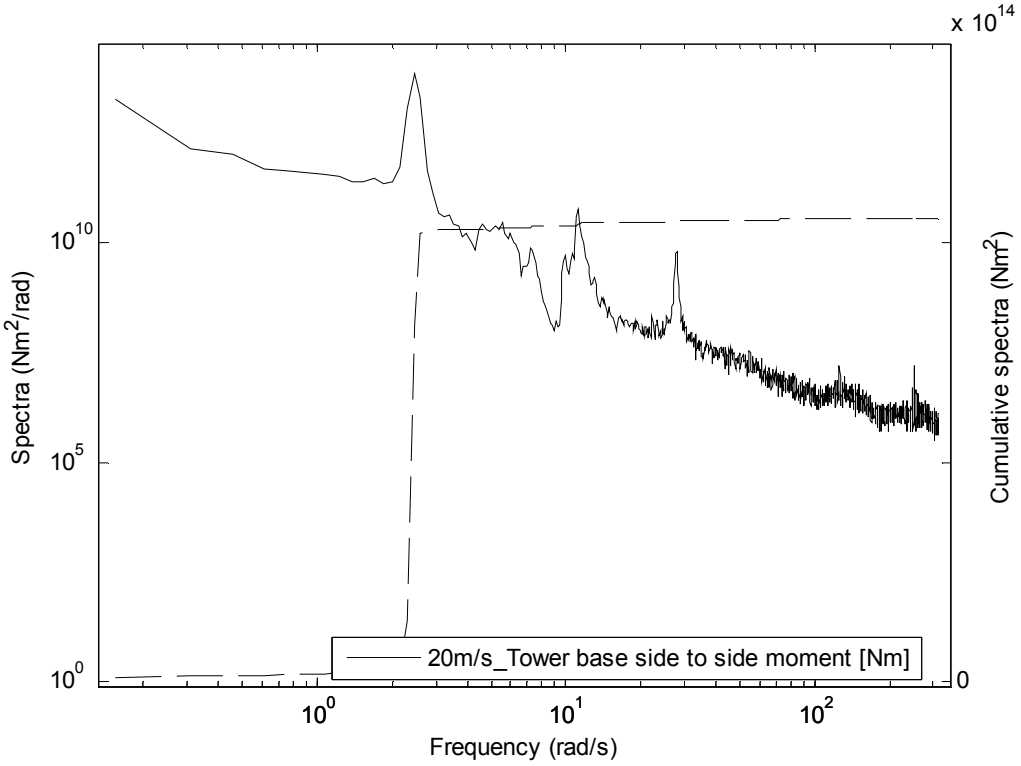

Figure B.37: Tower base side to side moment spectrum for 20m/s

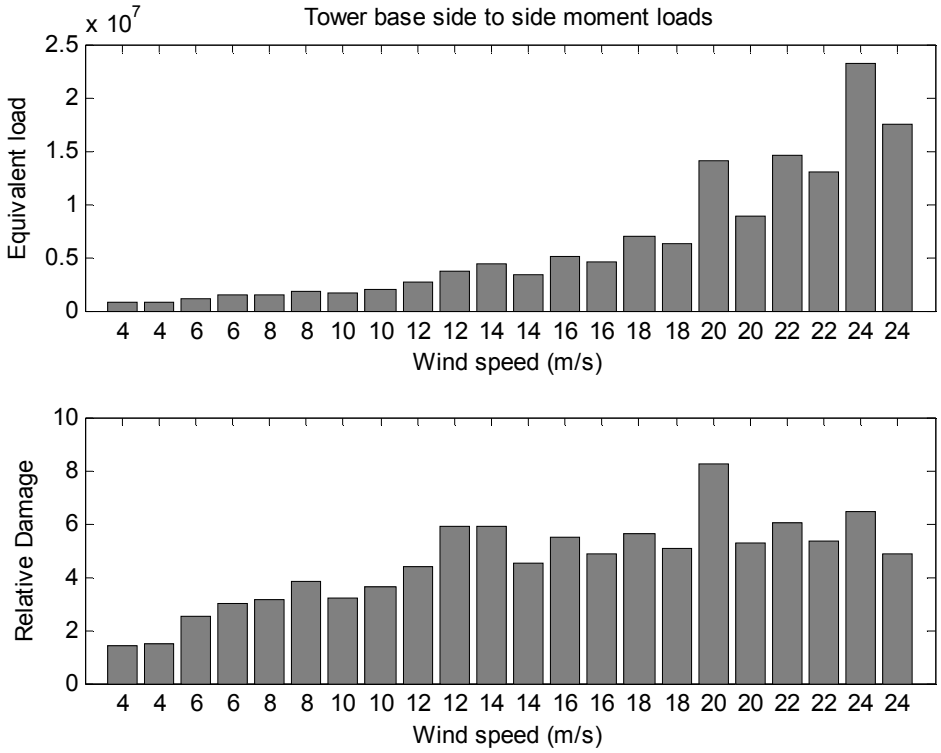

Figure B.38: Lifetime tower base side to side moment loads

Table 7: Lifetime tower base side to side moment loads

Lifetime tower base side to side moment loads	
Controller type	**Loads**
SISO(Basic)	3.1154e+06

Tower base fore-aft moment loads

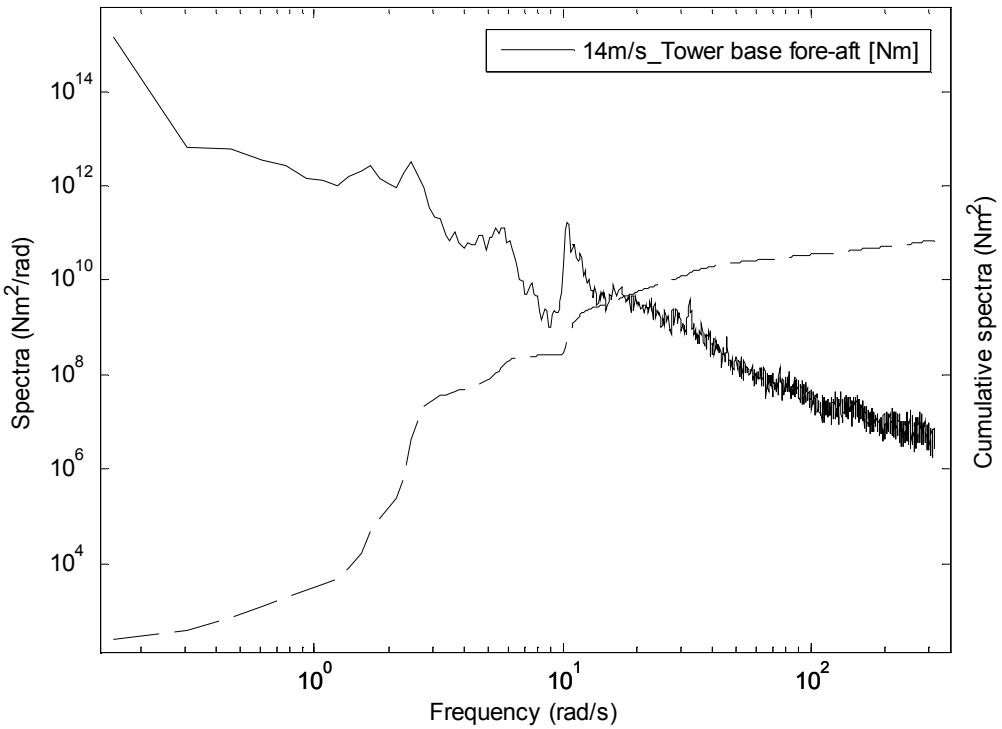

Figure B.39: Tower fore and aft moment spectrum for 14m/s

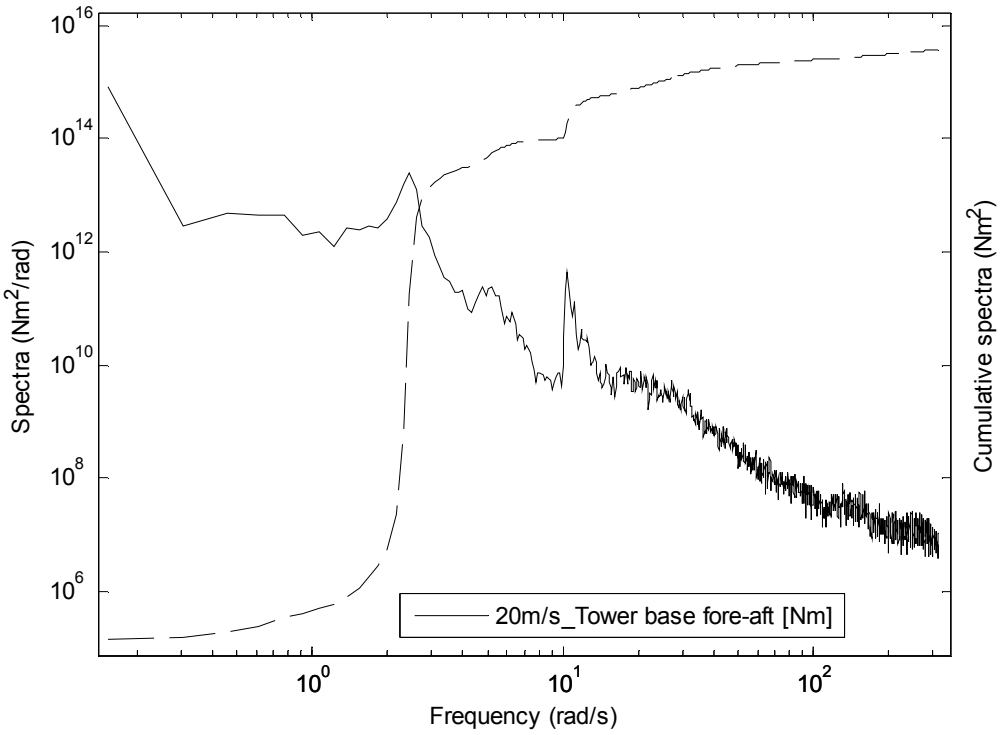

Figure B.40: Tower fore and aft moment spectrum for 20m/s

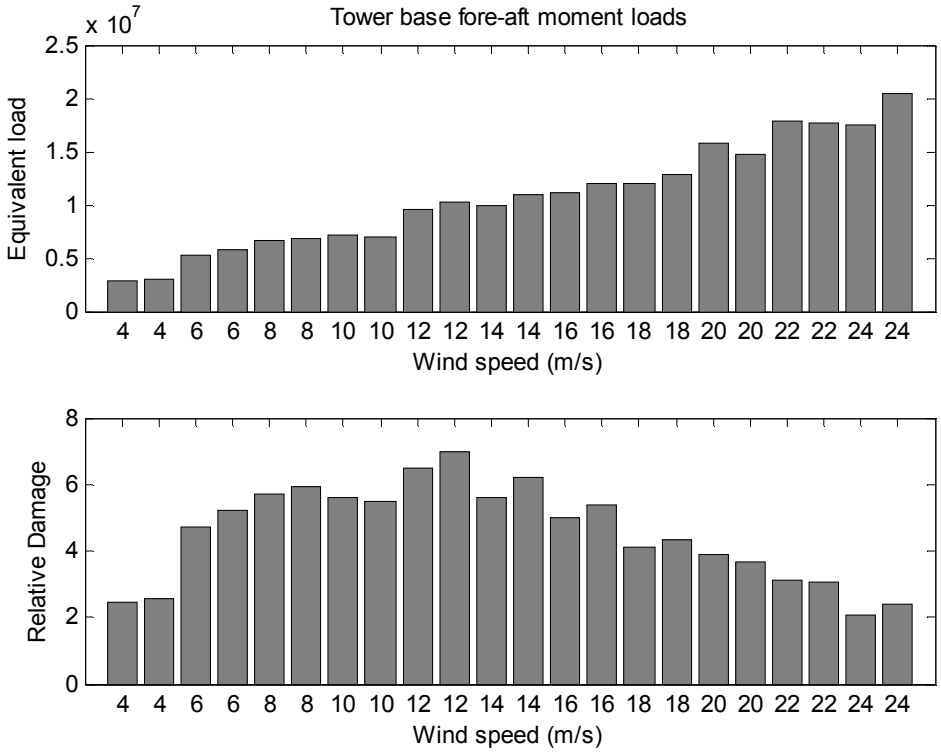

Figure B.41: Lifetime tower base fore and aft moment loads

Table 8: Lifetime tower base fore and aft moment loads

Lifetime tower base fore-aft moment loads	
Controller type	**Loads**
SISO(Basic)	7.2186e+06

B.2 Performance of the SISO controller with TFL

Above rated 14m/s

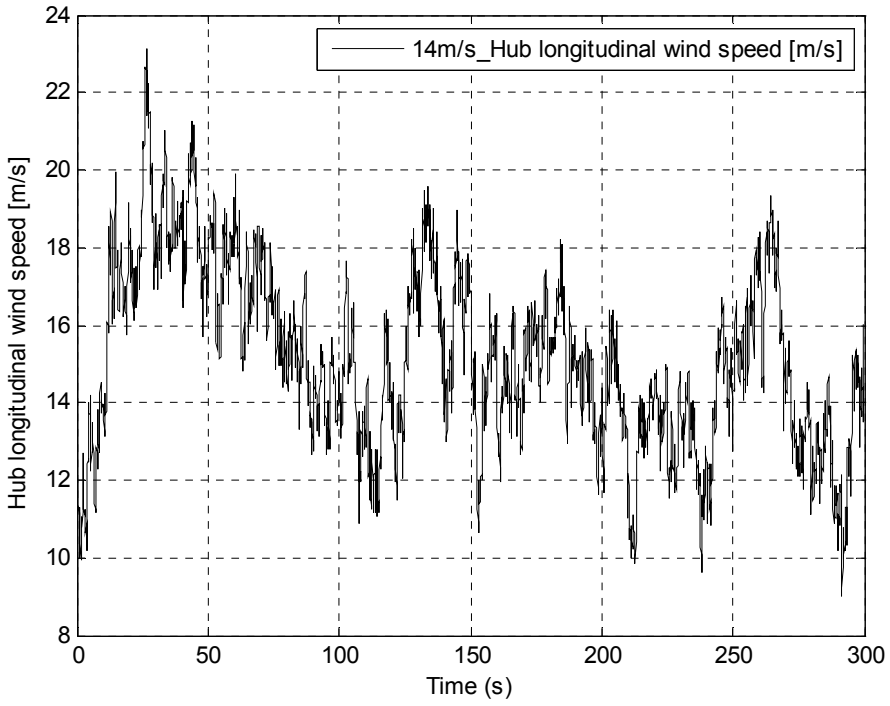

Figure B.42: Wind speed time series for 14m/s

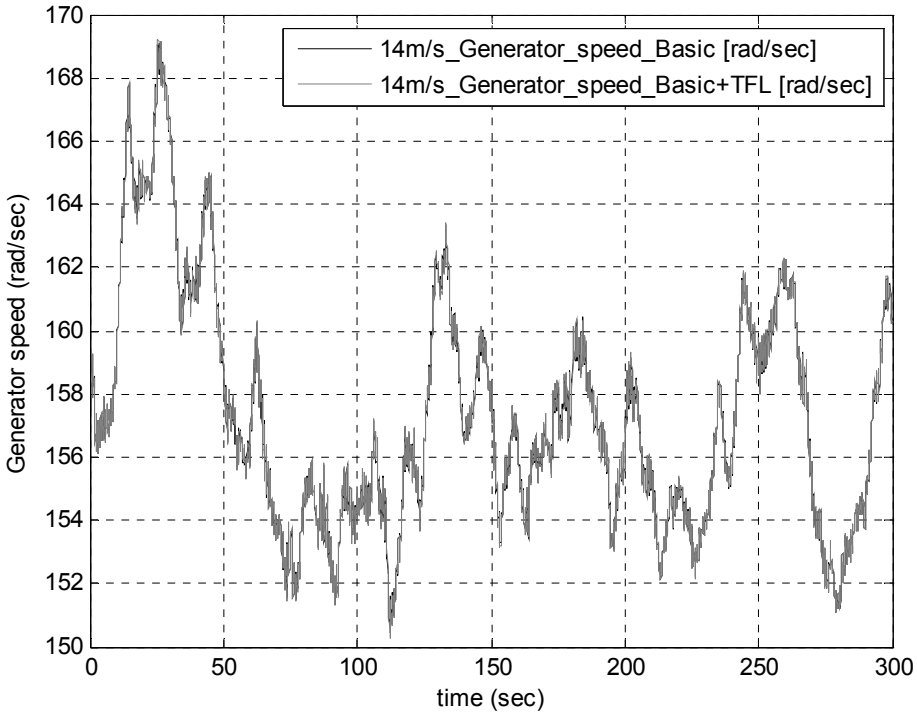

Figure B.43: Generator speed time series for both controllers at a mean wind speed of 14m/s

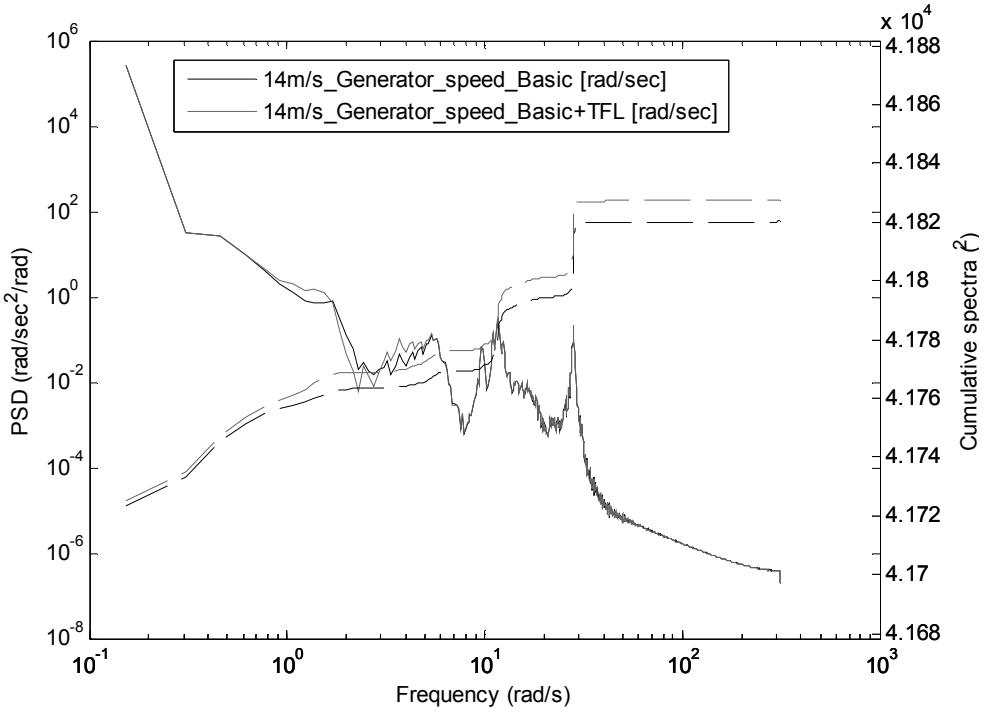

Figure B.44: Generator speed spectra for both controllers at 14m/s

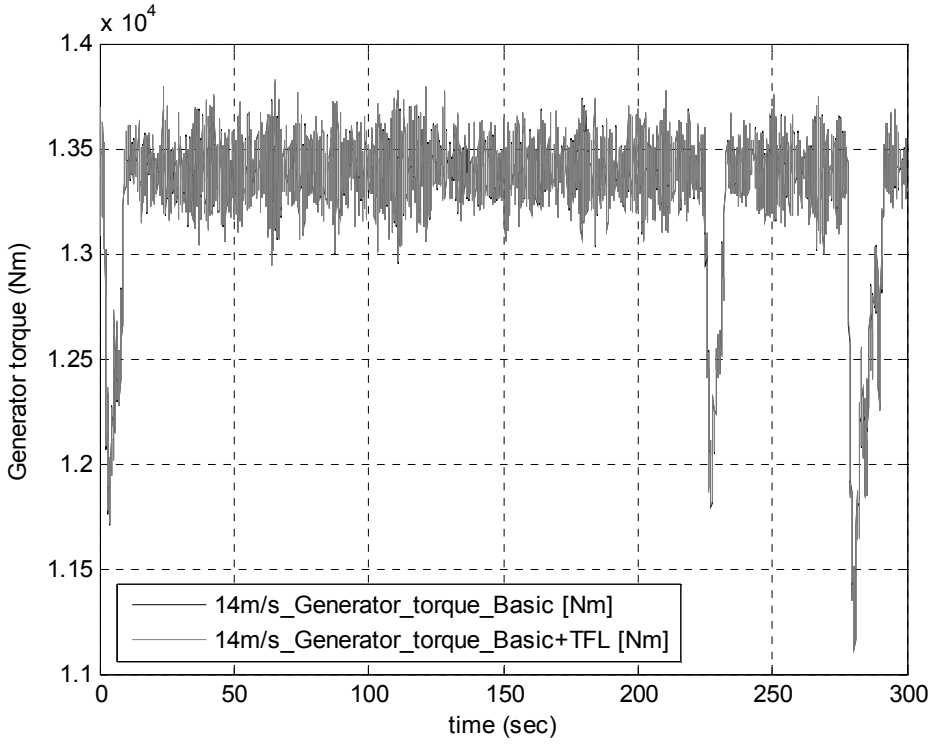

Figure B.45: Generator torque time series for both controllers at a mean wind speed of 14m/s

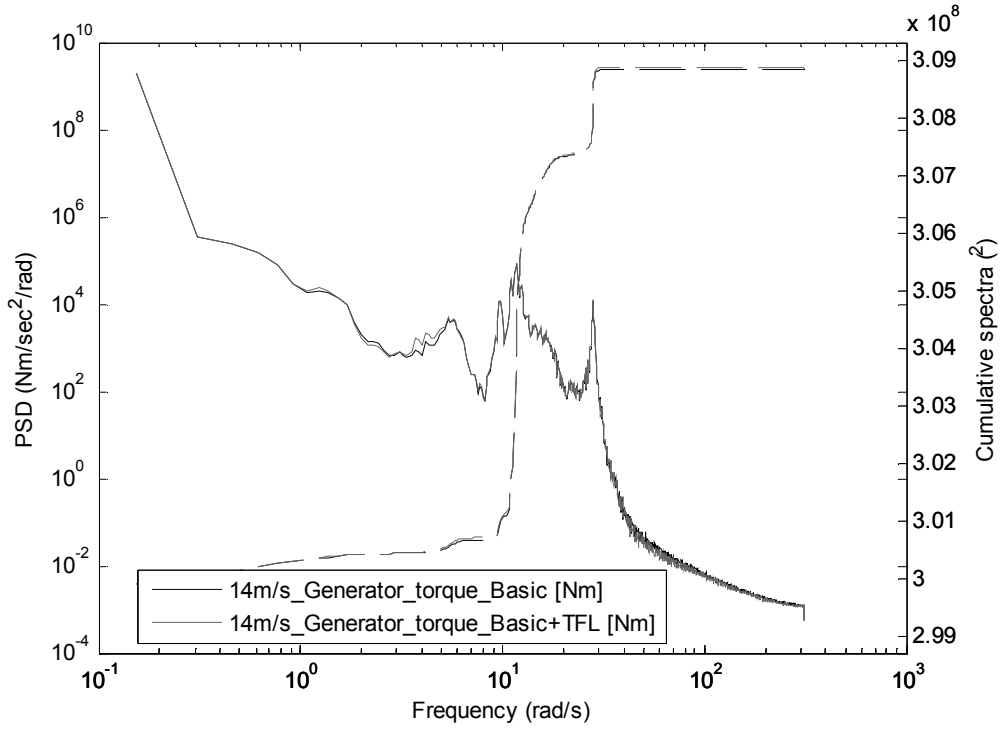

Figure B.46: Generator torque spectra for both controllers at 14m/s

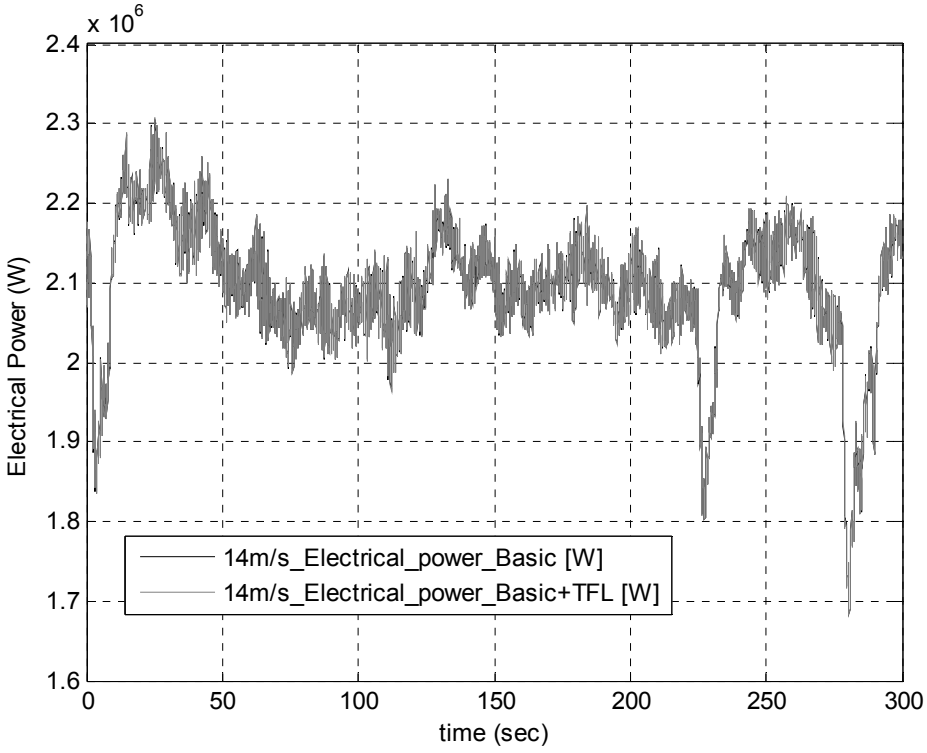

Figure B.47: Electrical power time series for both controllers at a mean wind speed of 14m/s

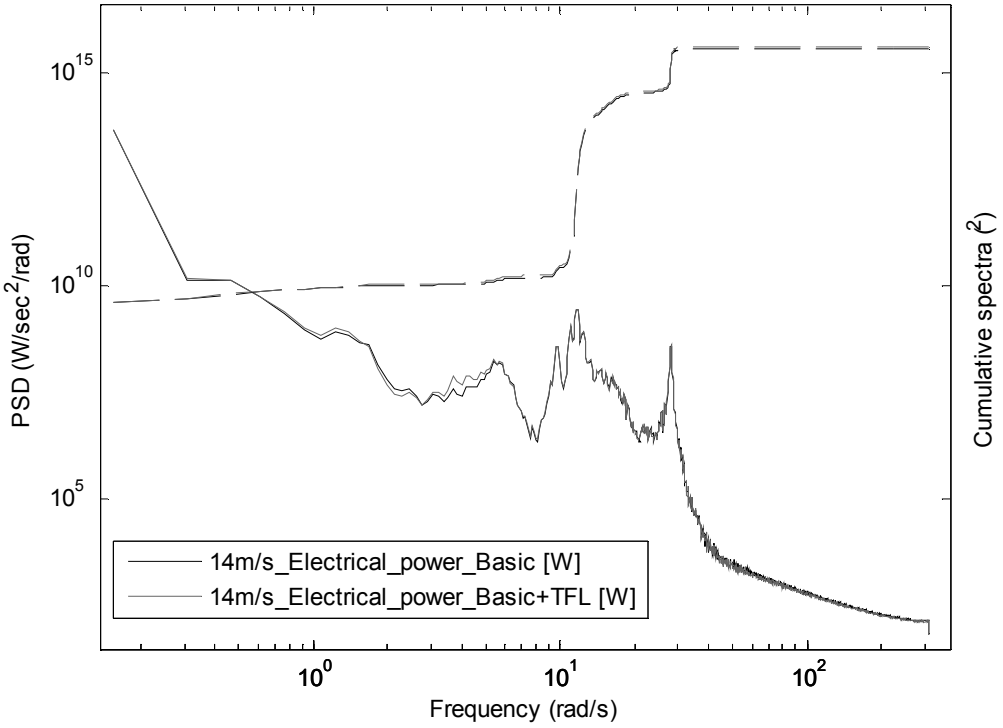

Figure B.48: Electrical power spectra for both controllers at 14m/s

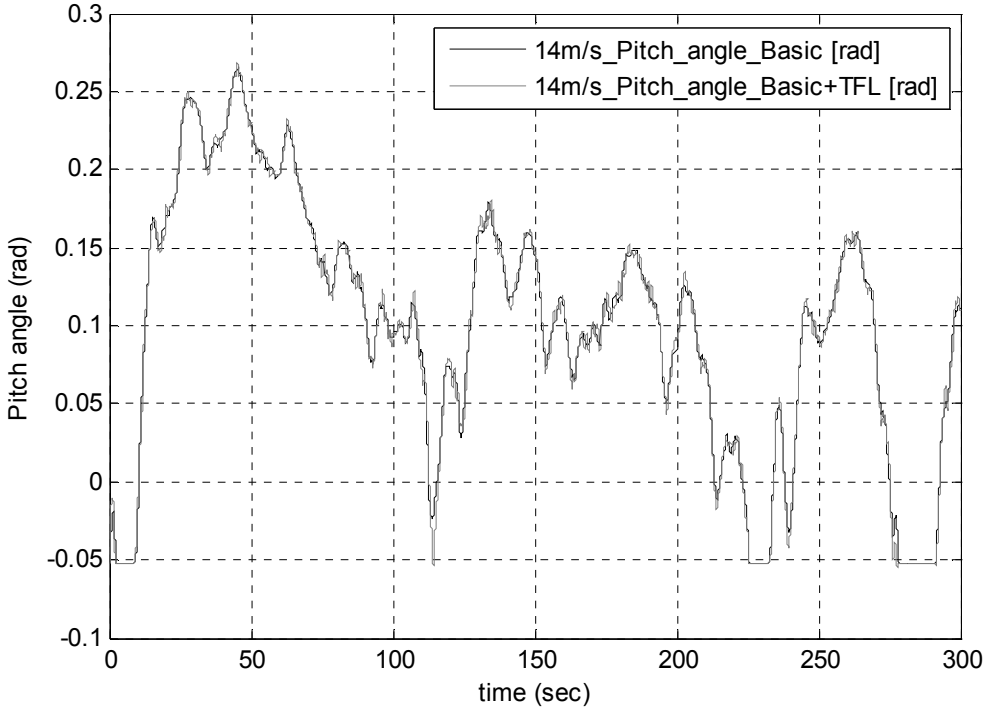

Figure B.49: Pitch angle time series for both controllers at a mean wind speed of 14m/s

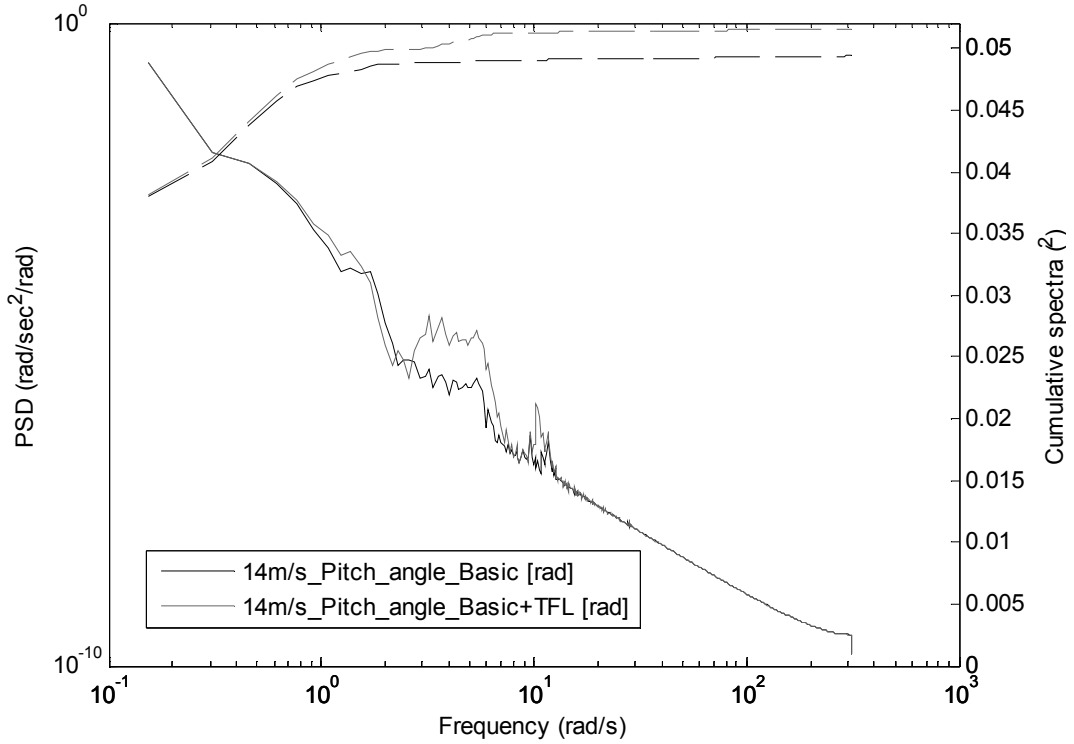

Figure B.50: Pitch angle spectra for both controllers at 14m/s

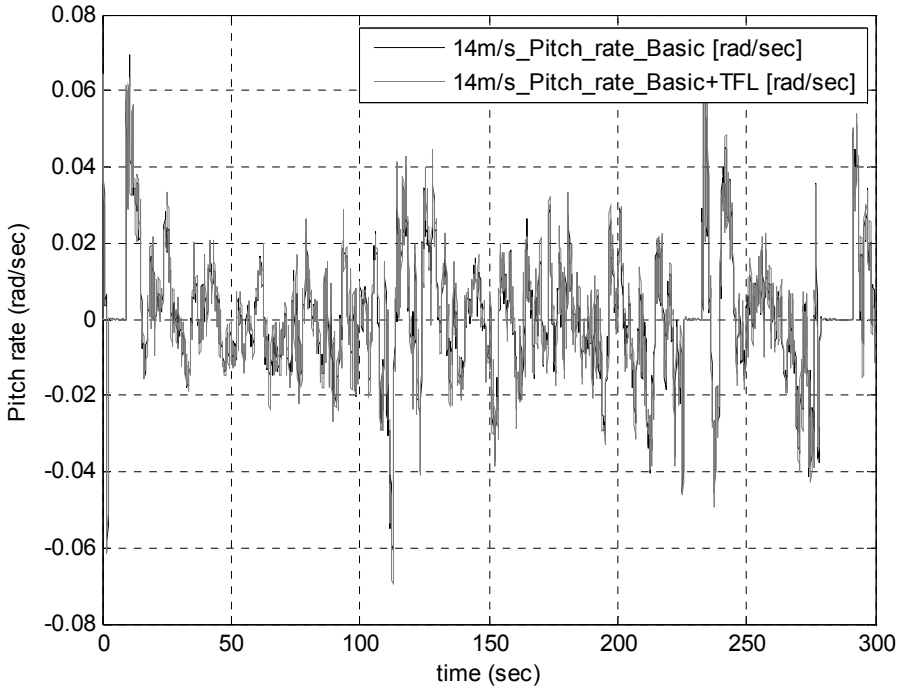

Figure B.51: Pitch rate time series for both controllers at a mean wind speed of 14m/s

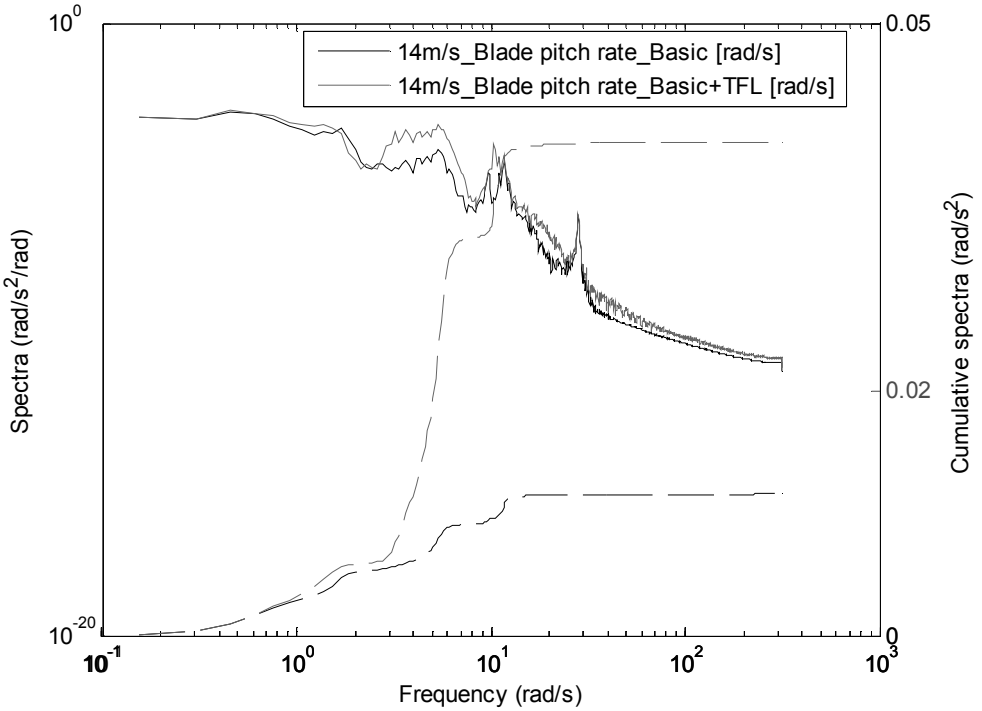

Figure B.52: Pitch rate spectra for both controllers at 14m/s

Above rated 20m/s

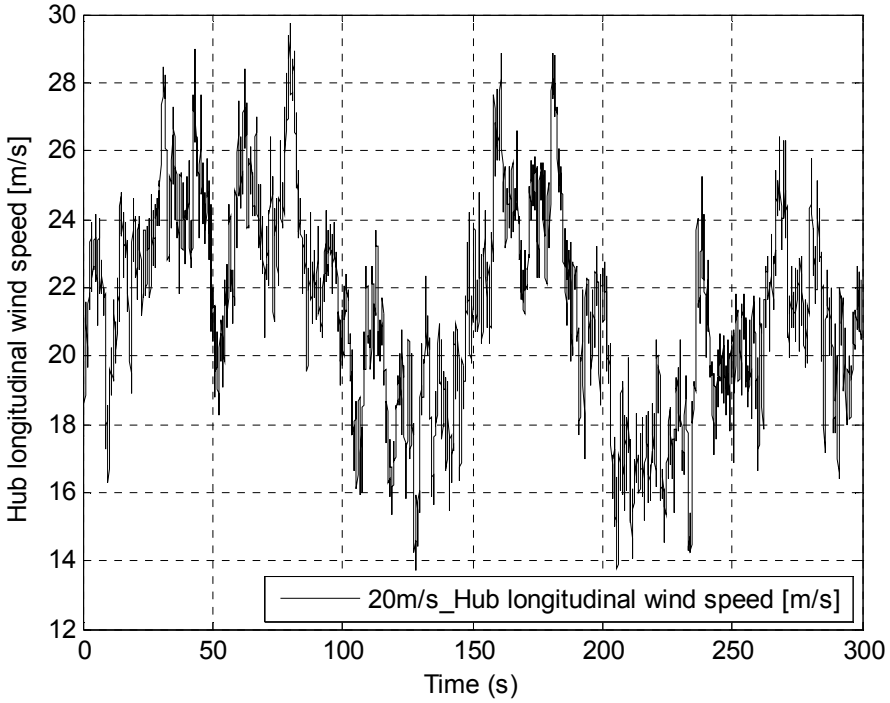

Figure B.53: Wind speed time series for 20m/s

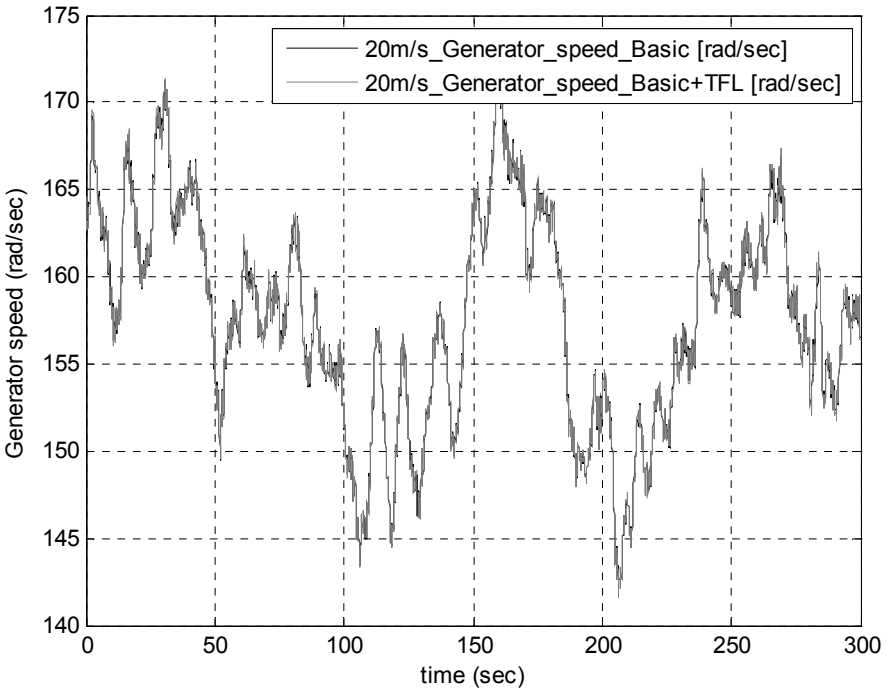

Figure B.54: Generator speed time series for both controllers at a mean wind speed of 20m/s

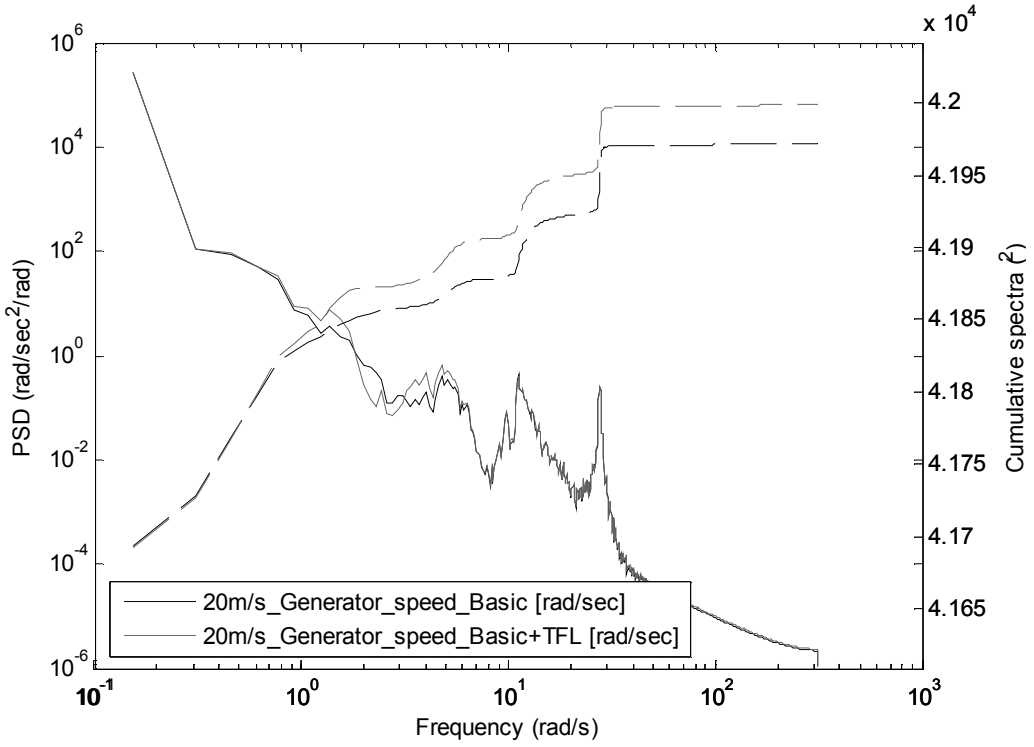

Figure B.55: Generator speed spectra for both controllers at 20m/s

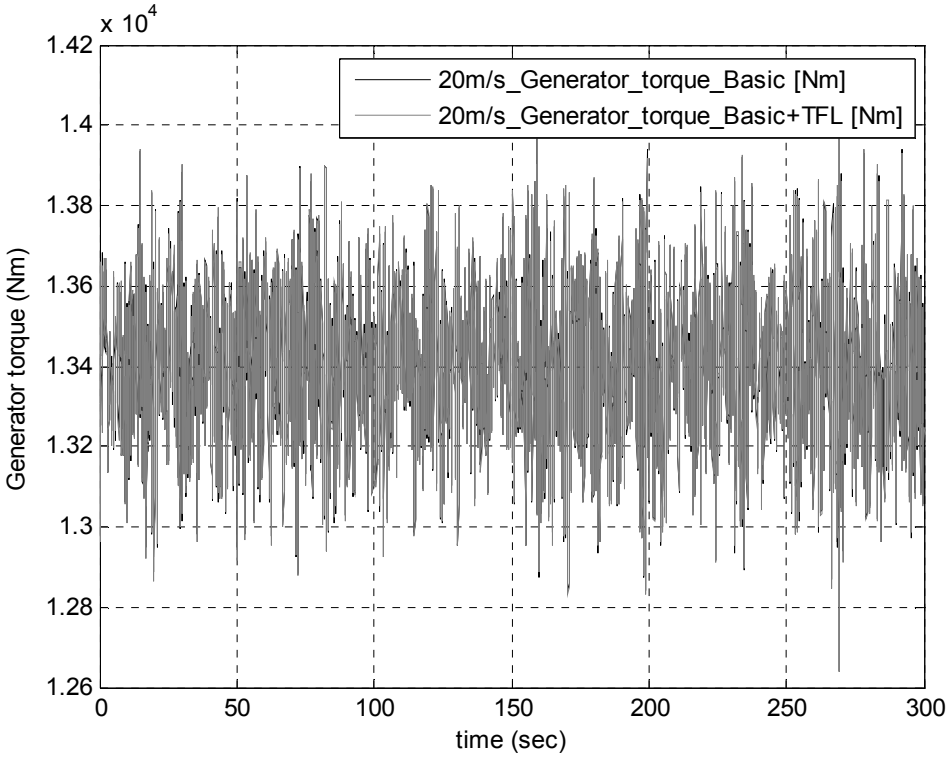

Figure B.56: Generator torque time series for both controllers at a mean wind speed of 20m/s

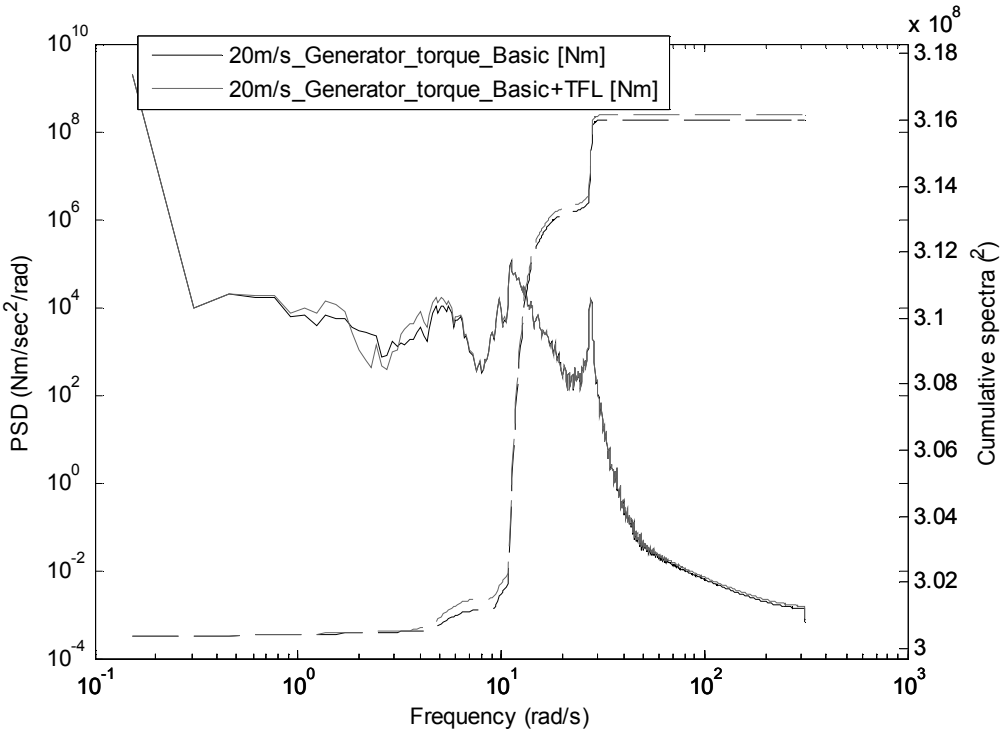

Figure B.57: Generator torque spectra for both controllers at 20m/s

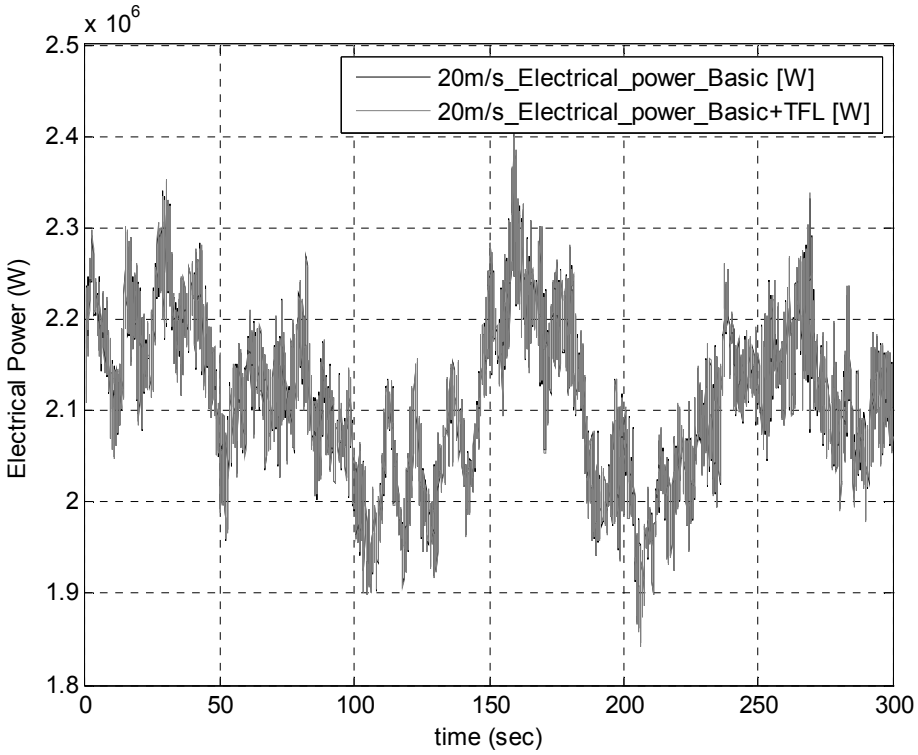

Figure B.58: Electrical power time series for both controllers at a mean wind speed of 20m/s

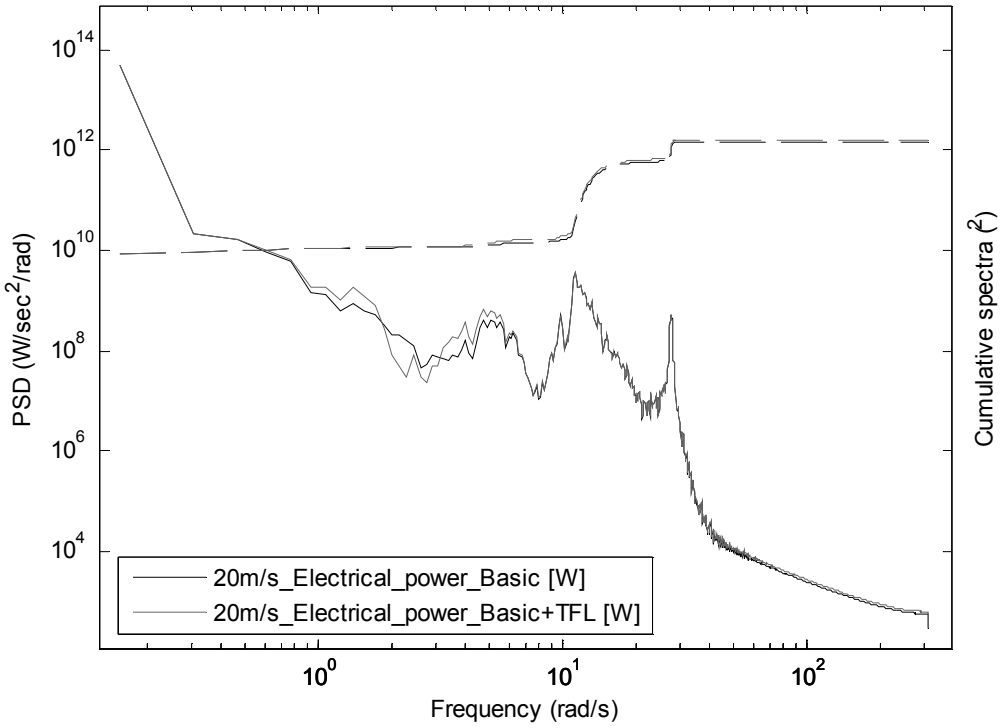

Figure B.59: Electrical power spectra for both controllers at 20m/s

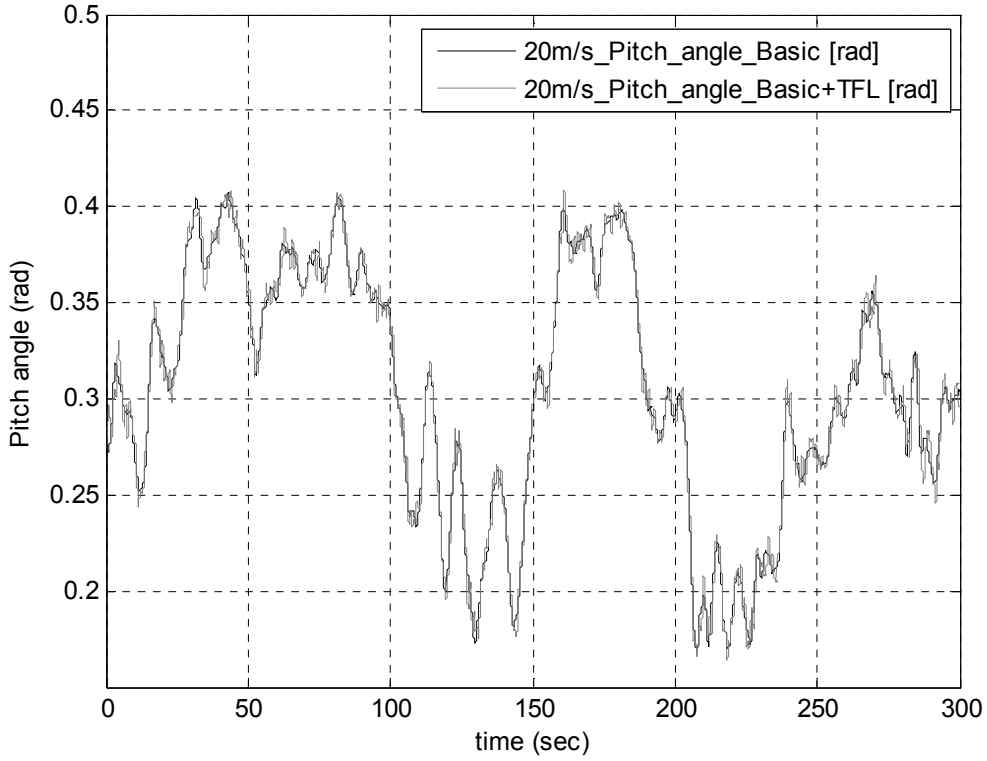

Figure B.60: Pitch angle time series for both controllers at a mean wind speed of 20m/s

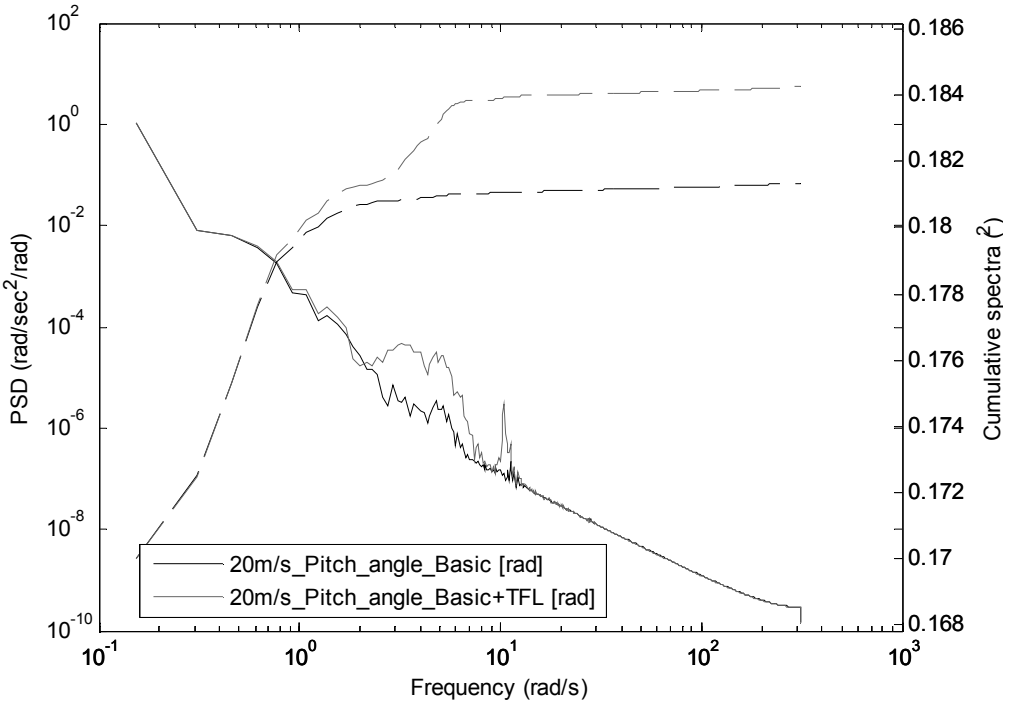

Figure B.61: Pitch angle spectra for both controllers at 20m/s

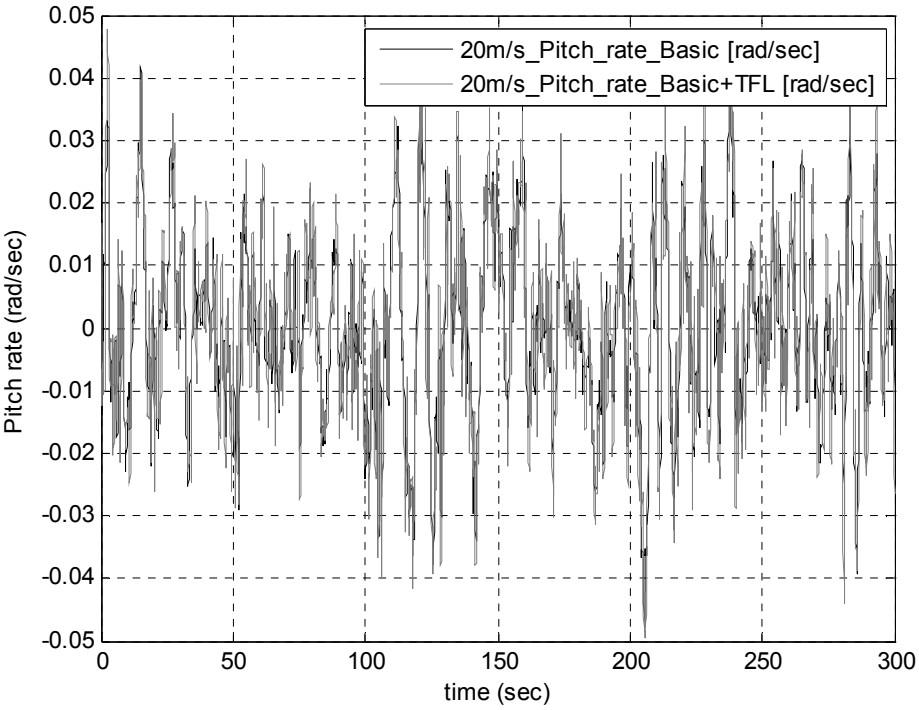

Figure B.62: Pitch rate time series for both controllers at a mean wind speed of 20m/s

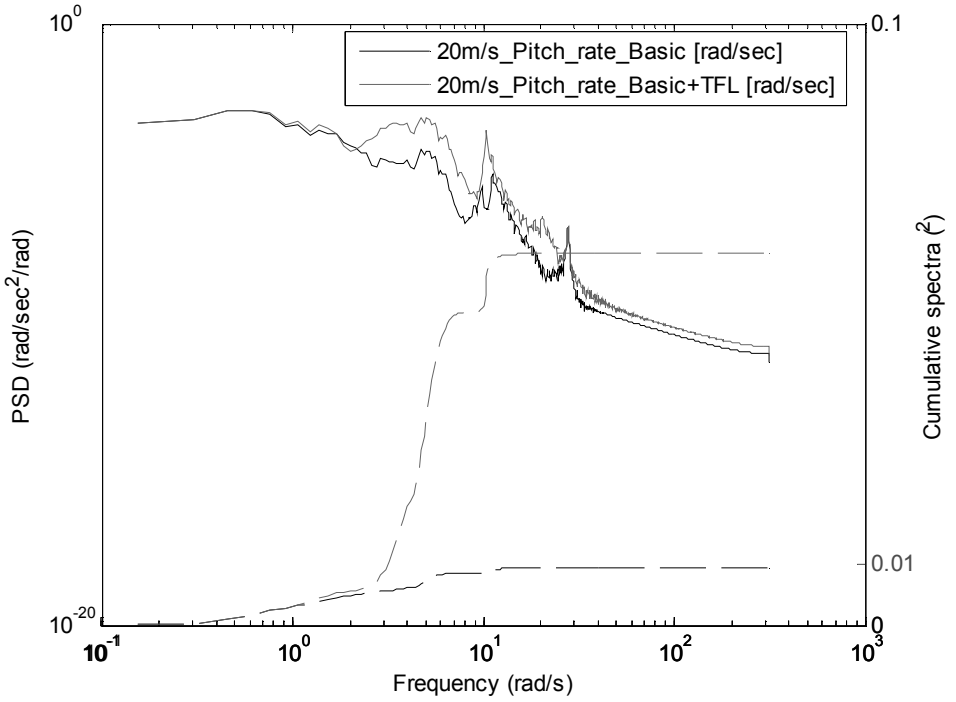

Figure B.63: Pitch rate spectra for both controllers at 20m/s

Fatigue loads

Blade root edgewise moments

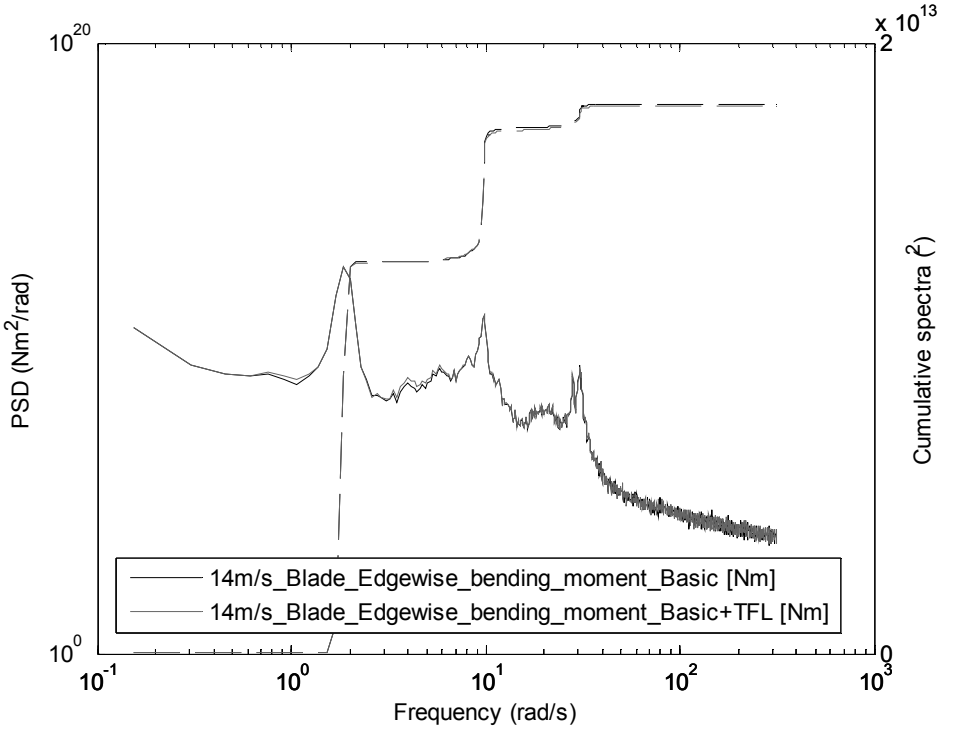

Figure B.64: Blade edgewise bending moment spectra for two controllers at 14m/s

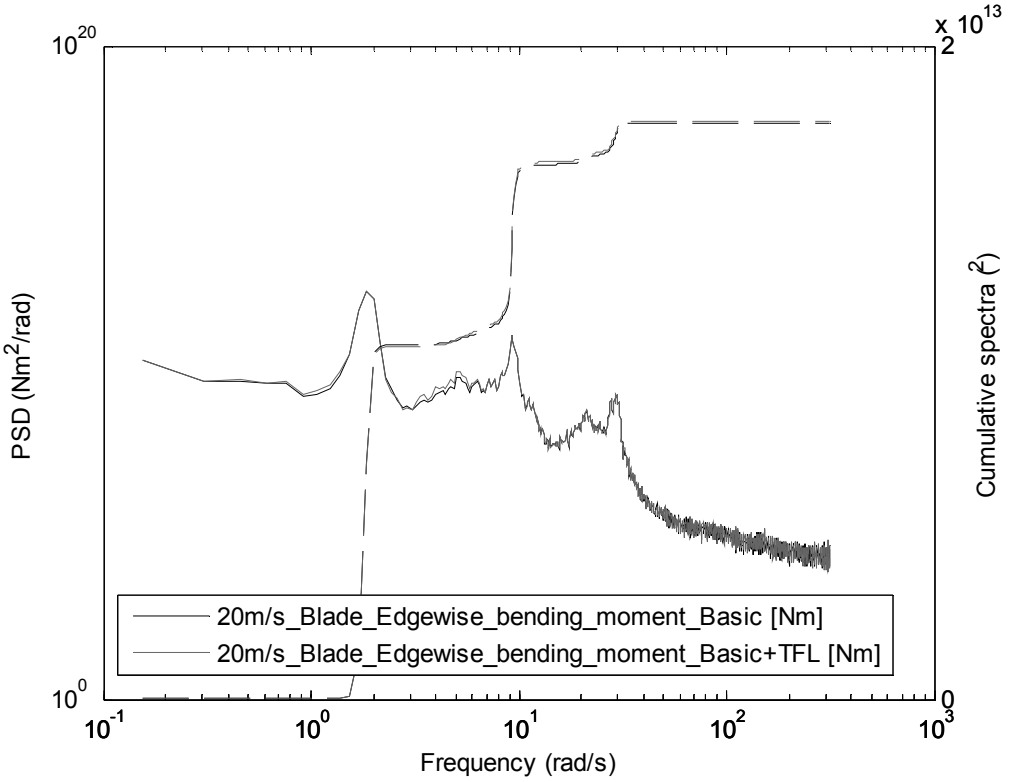

Figure B.65: Blade edgewise bending moment spectra for two controllers at 20m/s

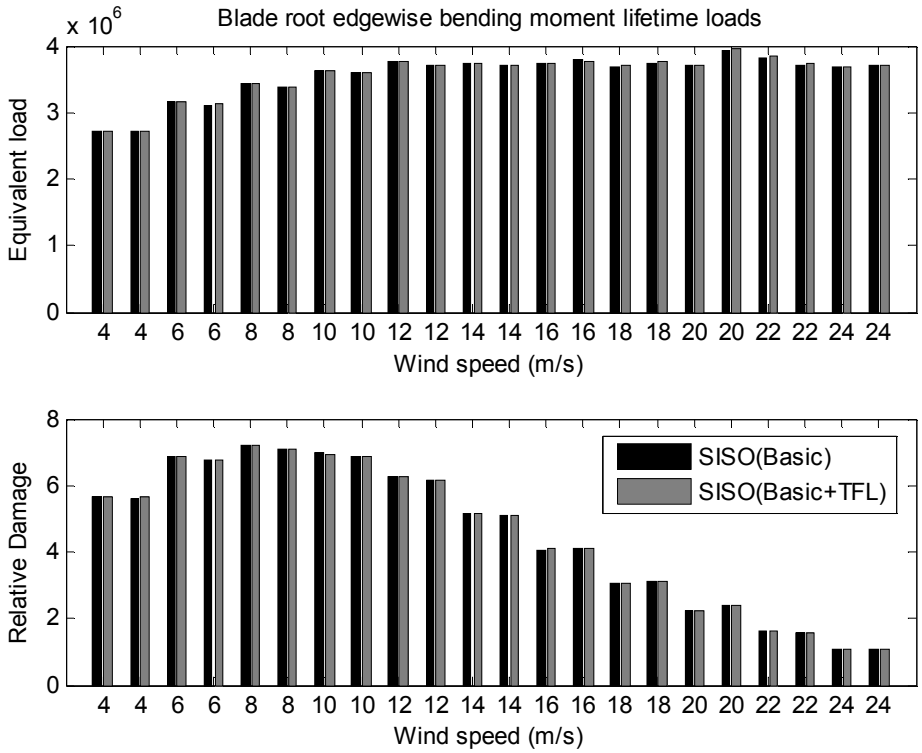

Figure B.66: Lifetime blade root edgewise bending moment loads for the two controllers

Table 9: Blade root edgewise bending moment lifetime loads

Blade root edgewise bending moment lifetime loads	
Controller type	**Loads**
SISO(Basic)	3.2113e+06
SISO(Basic+TFL)	3.2098e+06

Blade root flapwise moments

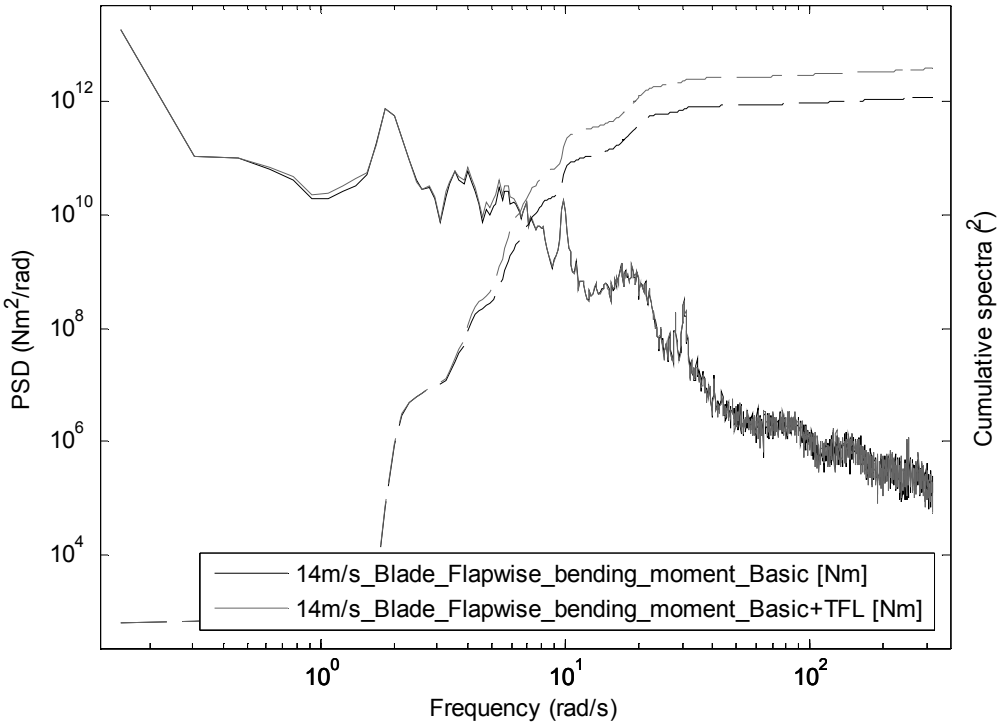

Figure B.67: Figure B.68: Blade flapwise bending moment spectra for two controllers at 14m/s

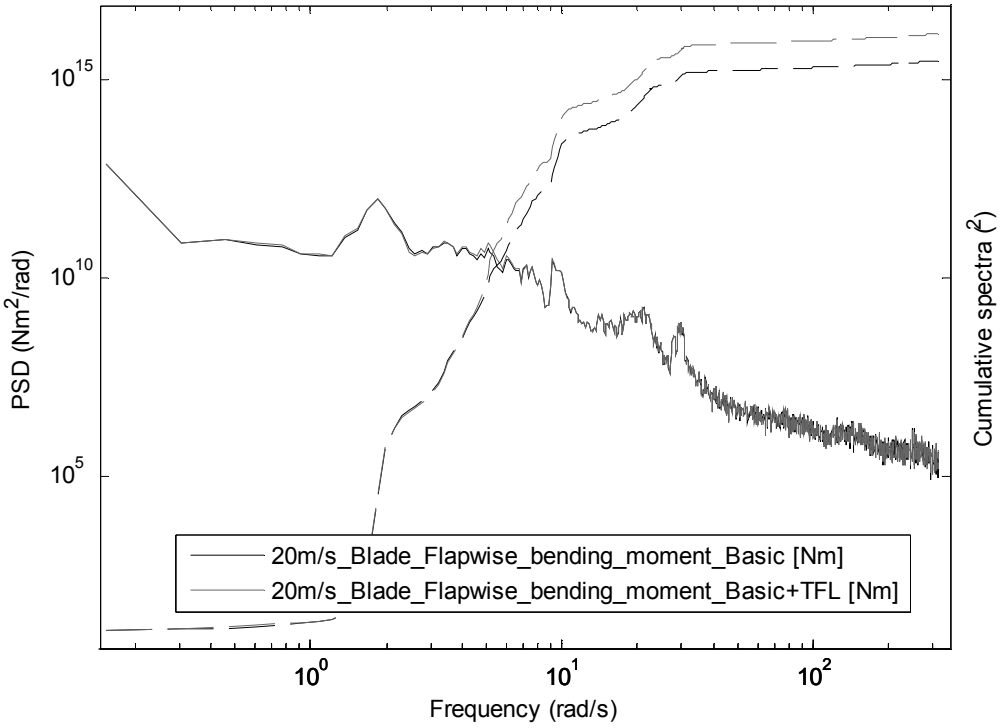

Figure B.69: Blade flapwise bending moment spectra for two controllers at 20m/s

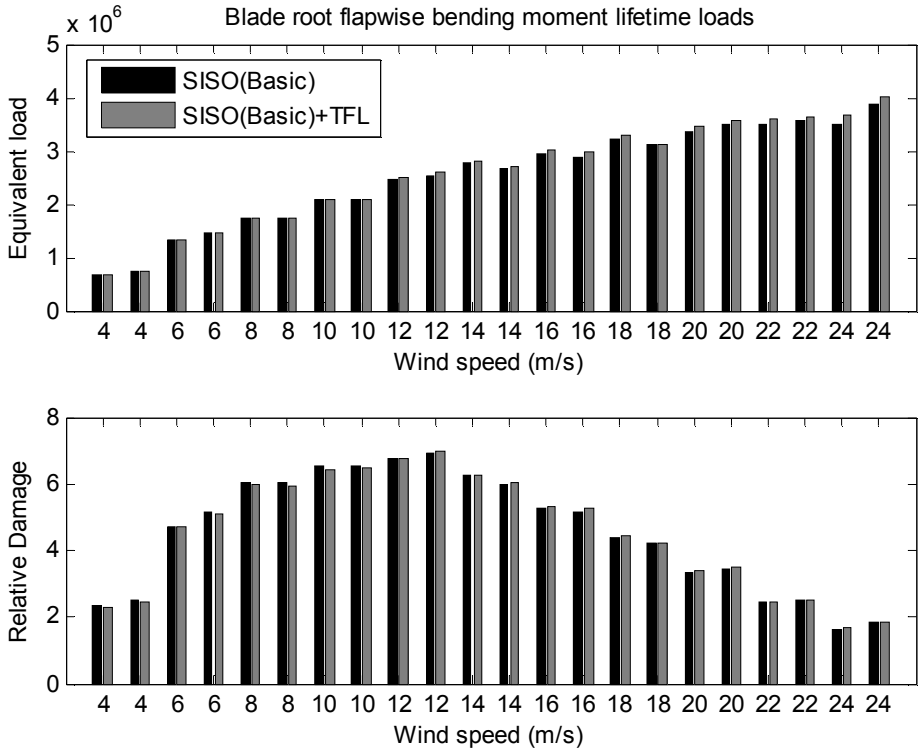

Figure B.70: Lifetime blade root flapwise bending moment loads for the two controllers

Table 10: Blade root flapwise bending moment lifetime loads

Blade root flapwise bending moment lifetime loads	
Controller type	**Loads**
SISO(Basic)	1.8698e+06
SISO(Basic+TFL)	1.8898e+06

Tower base side to side moment loads

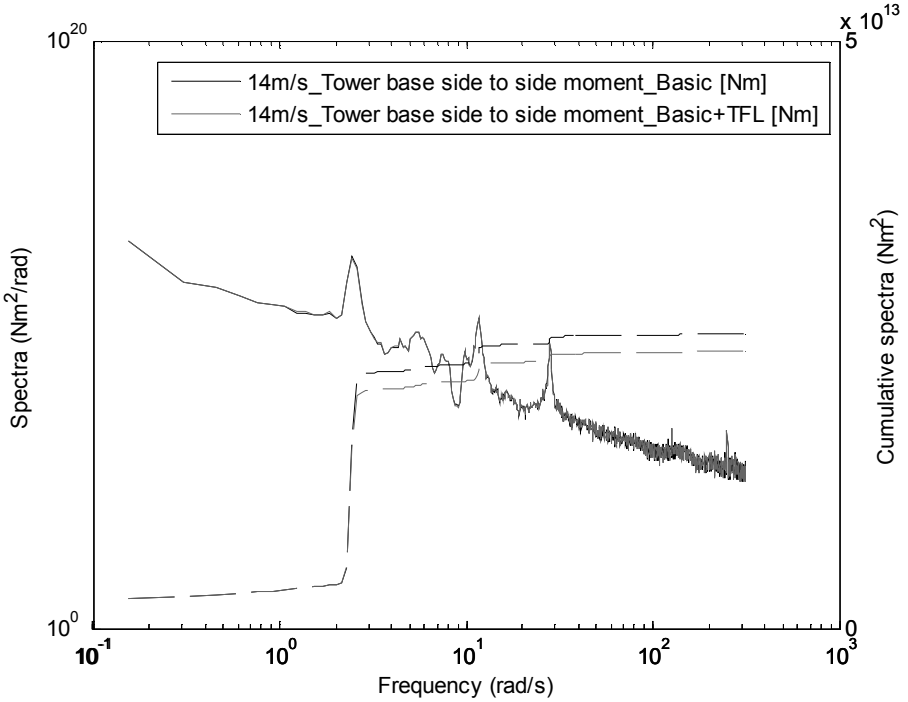

Figure B.71: Tower base side to side moment spectra for both controllers at 14m/s

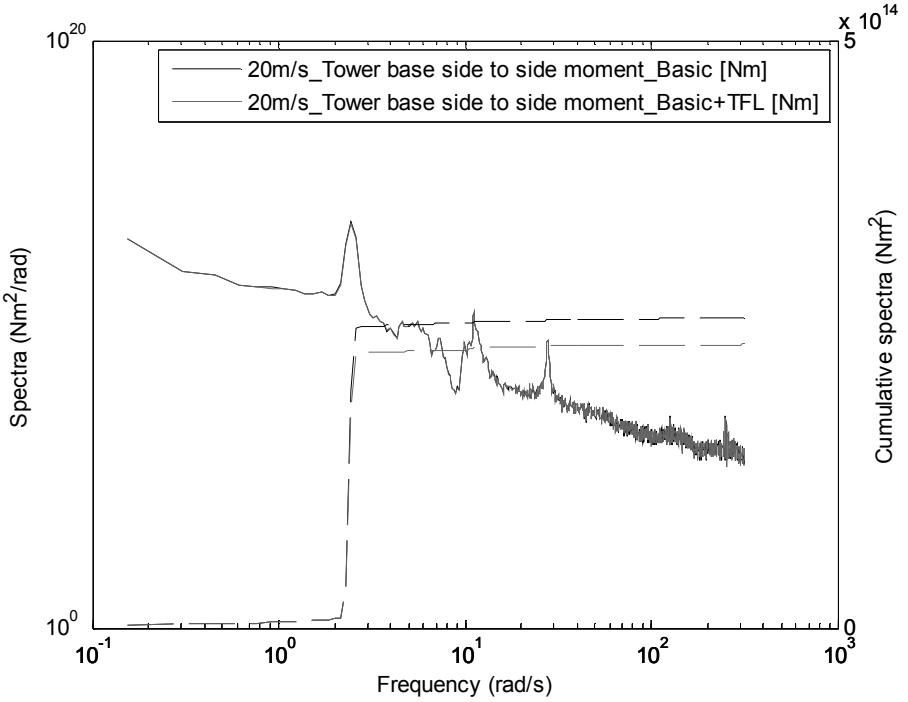

Figure B.72: Tower base side to side moment spectra for both controllers at 20m/s

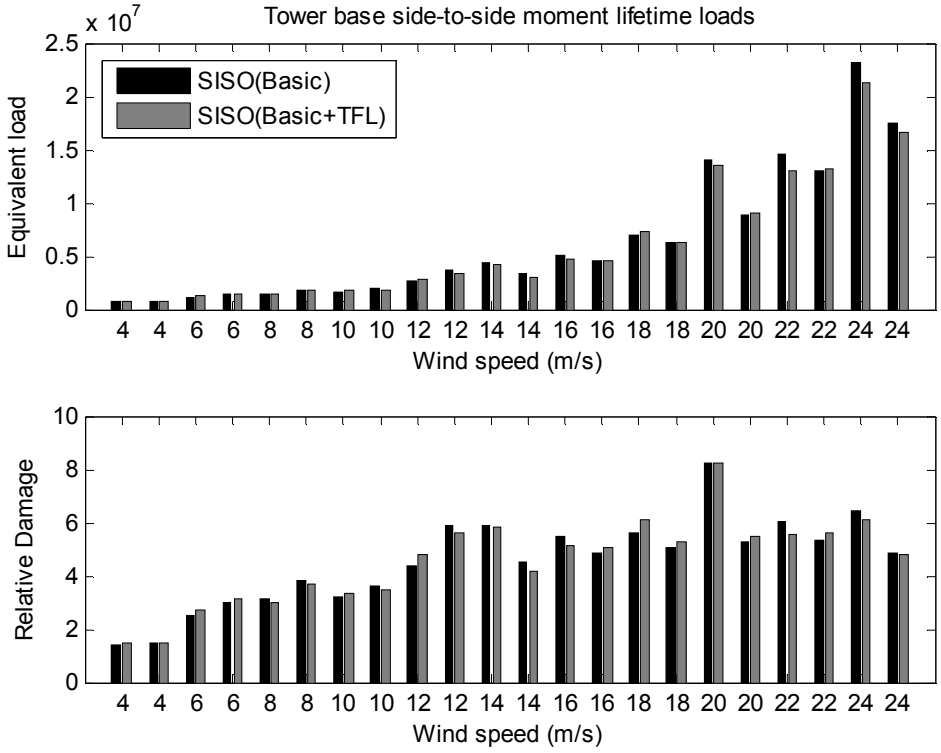

Figure B.73: Lifetime tower base side to side moment loads for the two controllers

Table 11: Tower base side-to-side moment lifetime loads

Tower base side-to-side moment lifetime loads		
Controller type	**Loads**	**Load reduction**
SISO(Basic)	3.1154e+06	
SISO(Basic+TFL)	3.0164e+06	3.17%

Tower base fore-aft moment loads

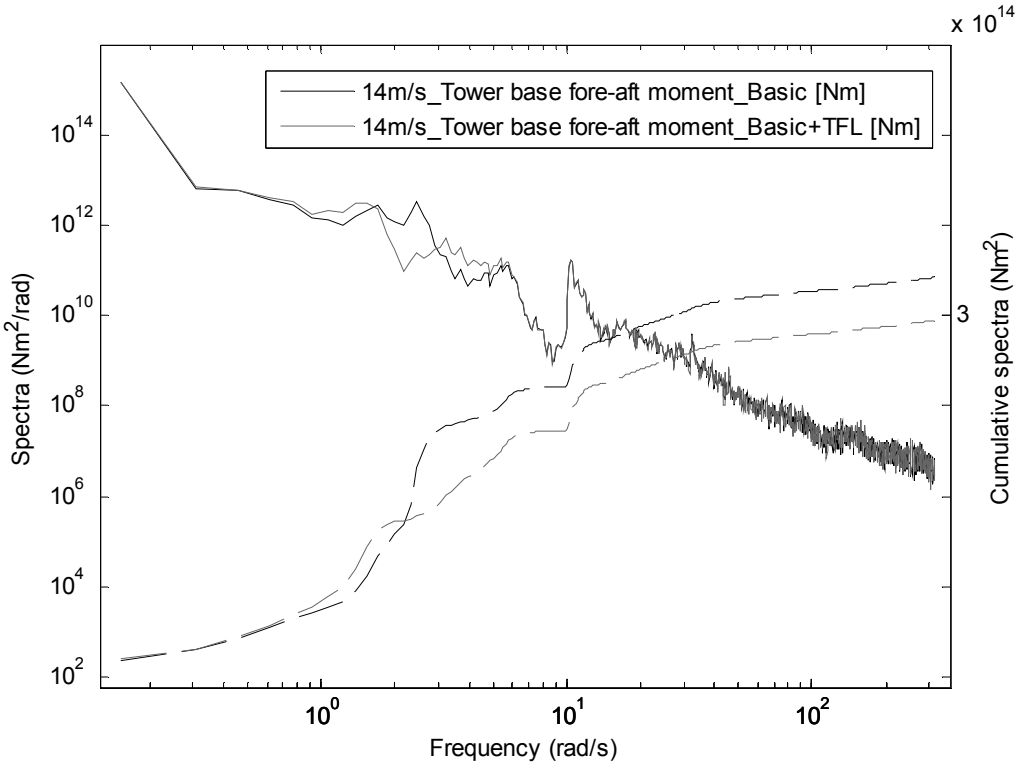

Figure B.74: Tower base fore and aft moment spectra for both controllers at 14m/s

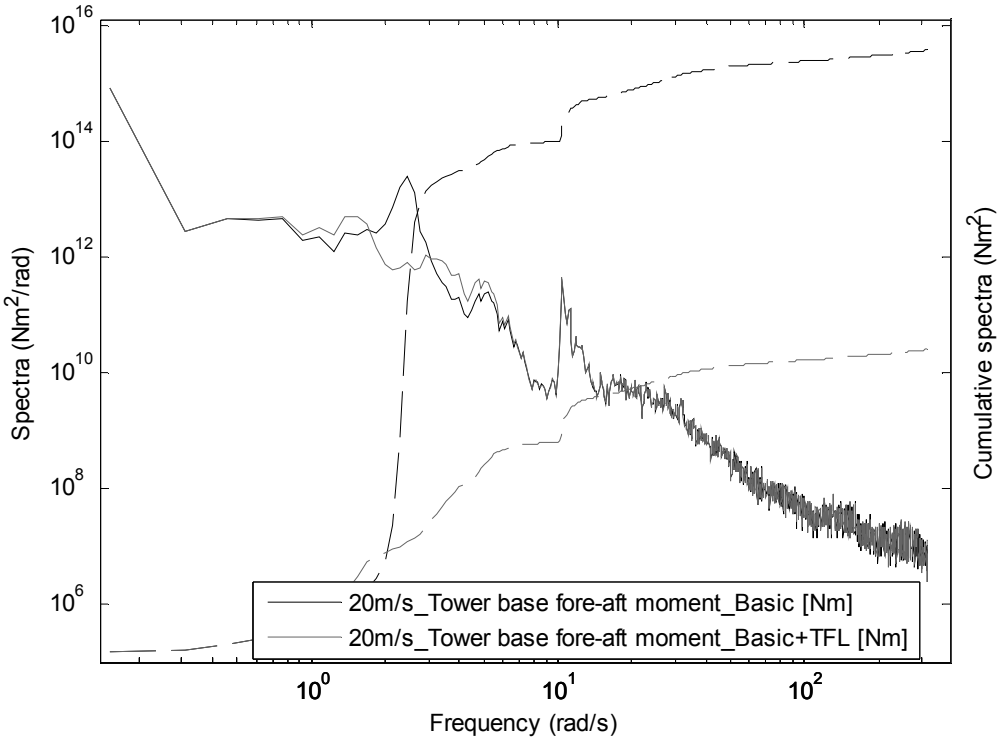

Figure B.75: Tower base fore and aft moment spectra for both controllers at 20m/s

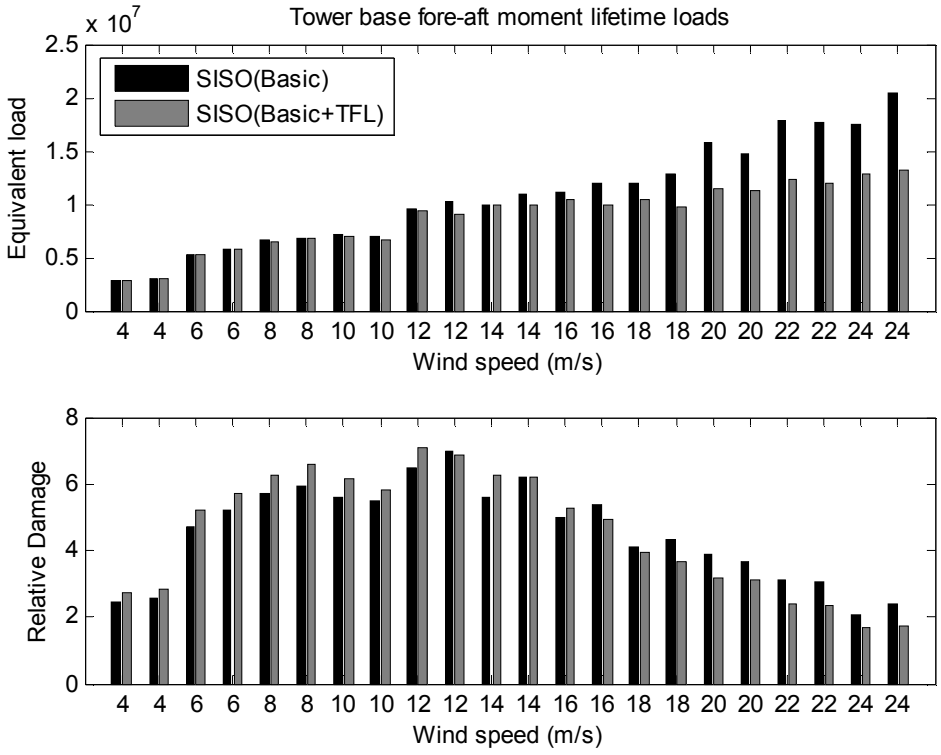

Figure B.76: Lifetime tower base fore and aft moment loads for the two controllers

Table 12: Tower base fore-aft moment lifetime loads

Tower base fore-aft moment lifetime loads		
Controller type	**Loads**	**Load reduction**
SISO(Basic)	7.2186e+06	
SISO(Basic+TFL)	6.7369e+06	6.67%

B.3 Performance of the SISO controller with ALL

(ALL: Addition of the Tower Feedback Loop, Phase Advance Mechanism, Anti-Windup Scheme)

Above rated 14m/s

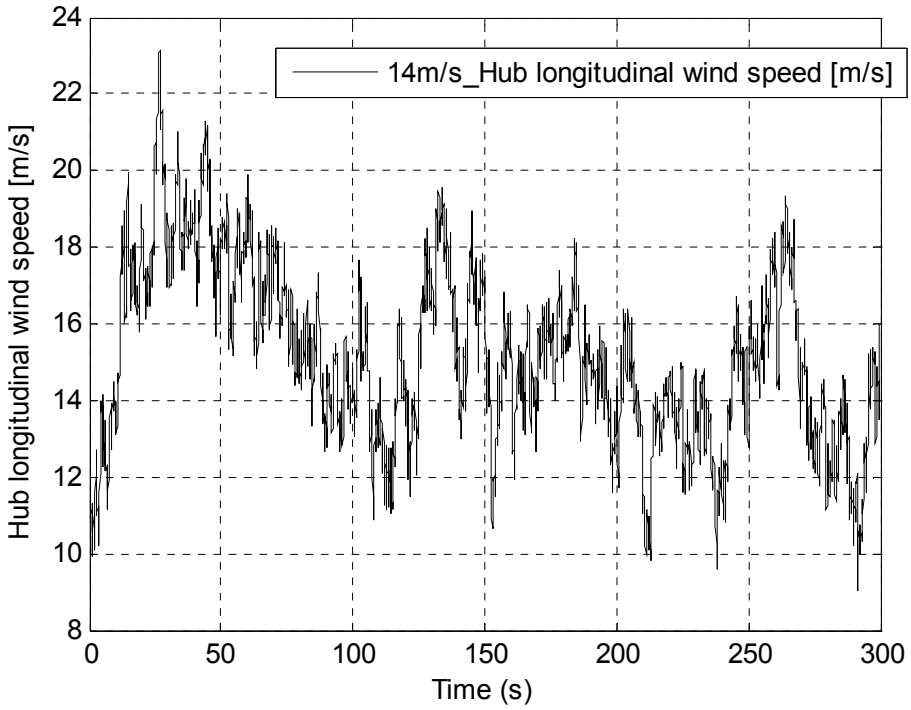

Figure B.77: Wind speed time series for 14m/s

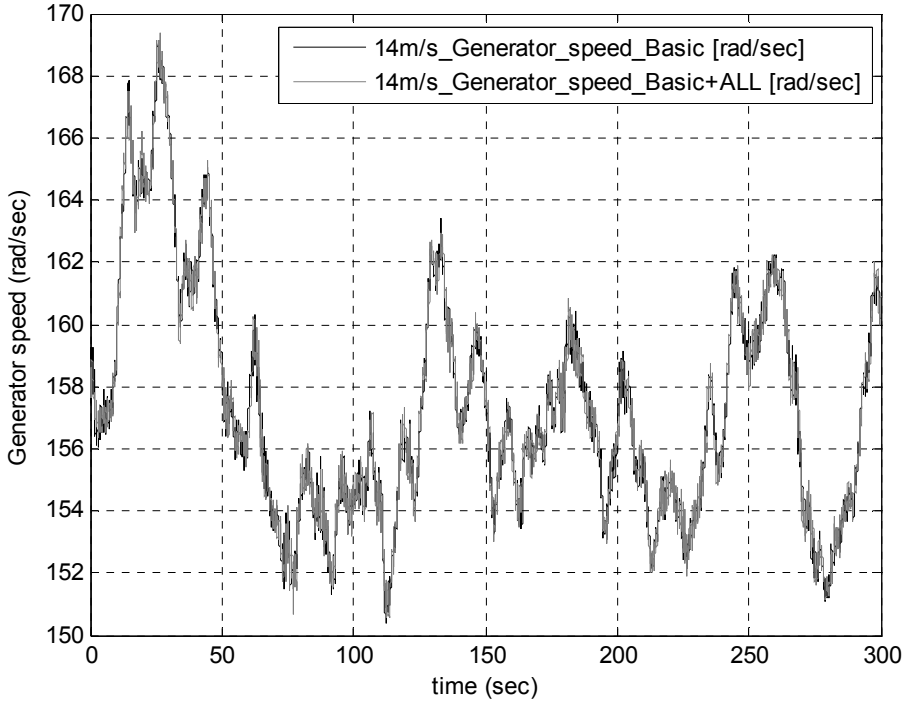

Figure B.78: Generator speed time series for both controllers at a mean wind speed of 14m/s

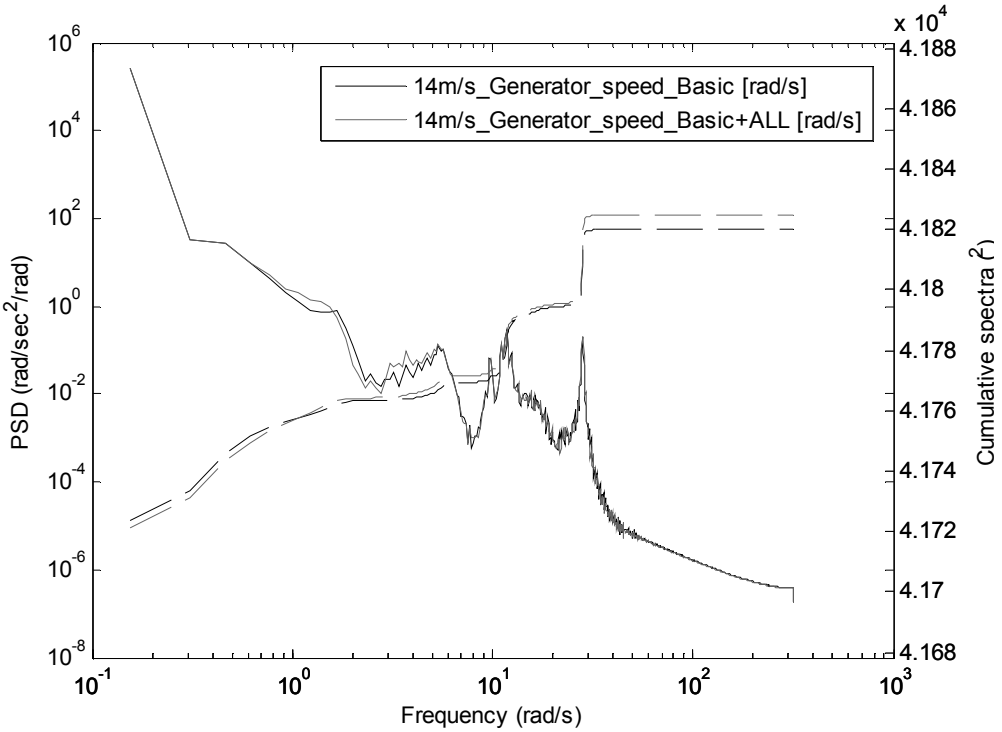

Figure B.79: Generator speed spectra for both controllers at 14m/s

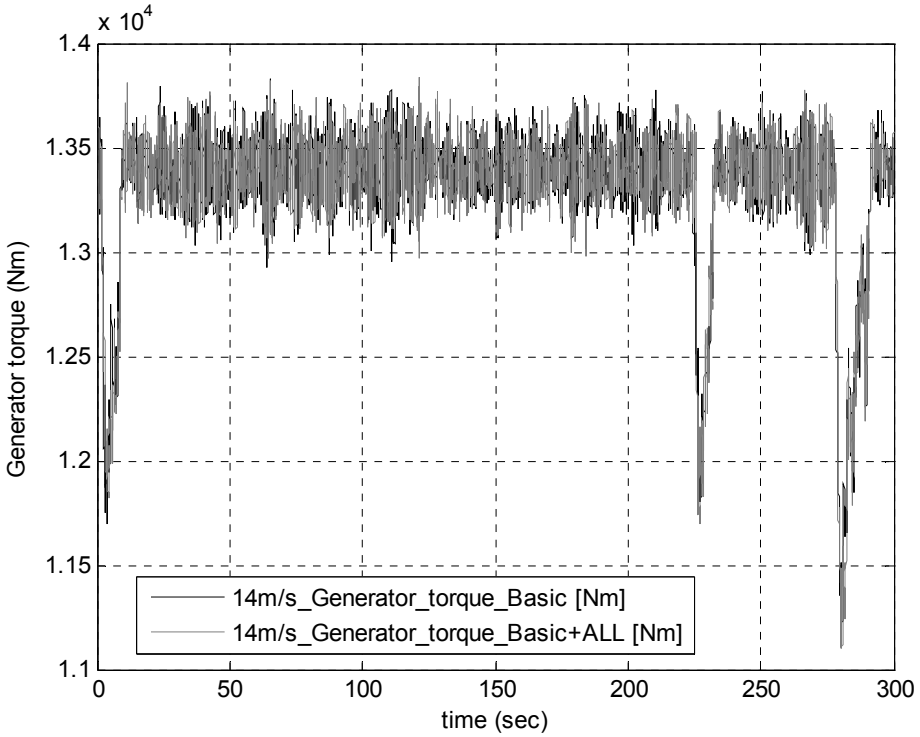

Figure B.80: Generator torque time series for both controllers at a mean wind speed of 14m/s

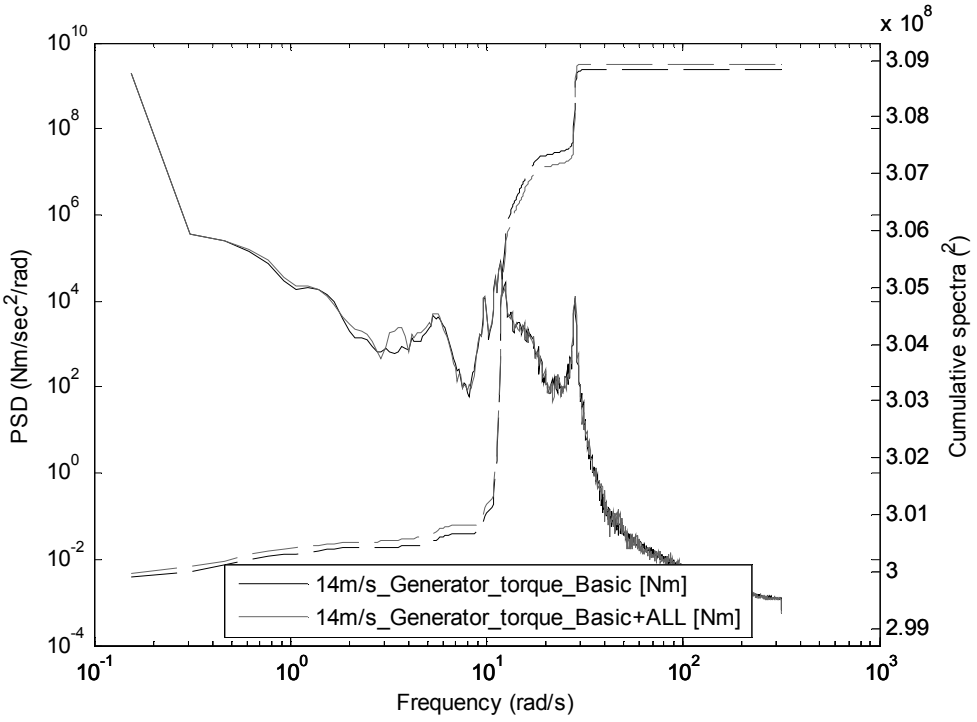

Figure B.81: Generator torque spectra for both controllers at 14m/s

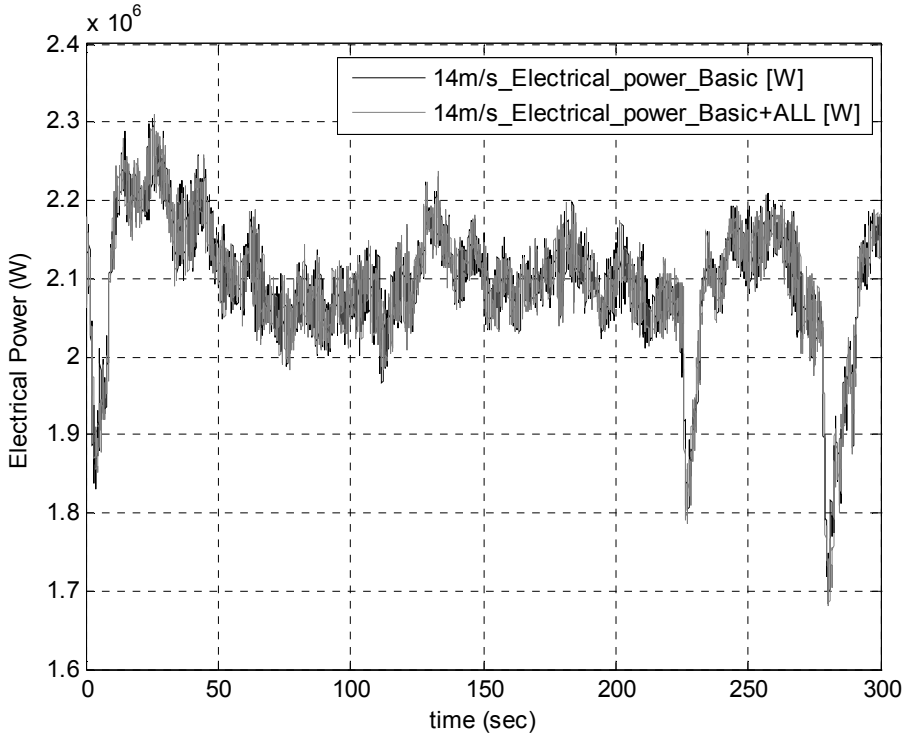

Figure B.82: Electrical power time series for both controllers at a mean wind speed of 14m/s

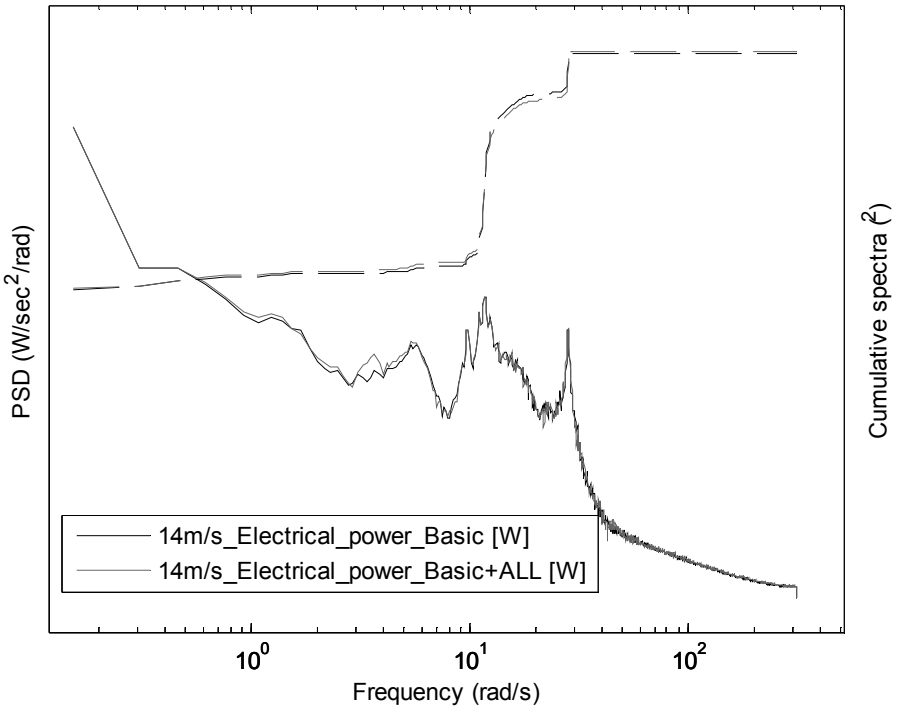

Figure B.83: Electrical power spectra for both controllers at 14m/s

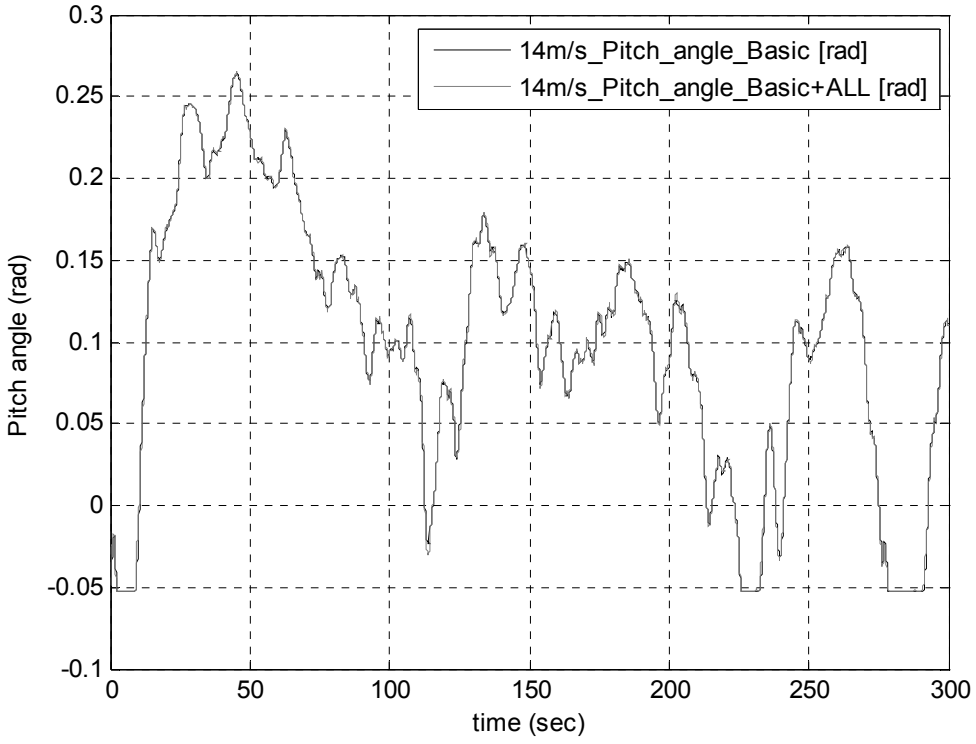

Figure B.84: Pitch angle time series for both controllers at a mean wind speed of 14m/s

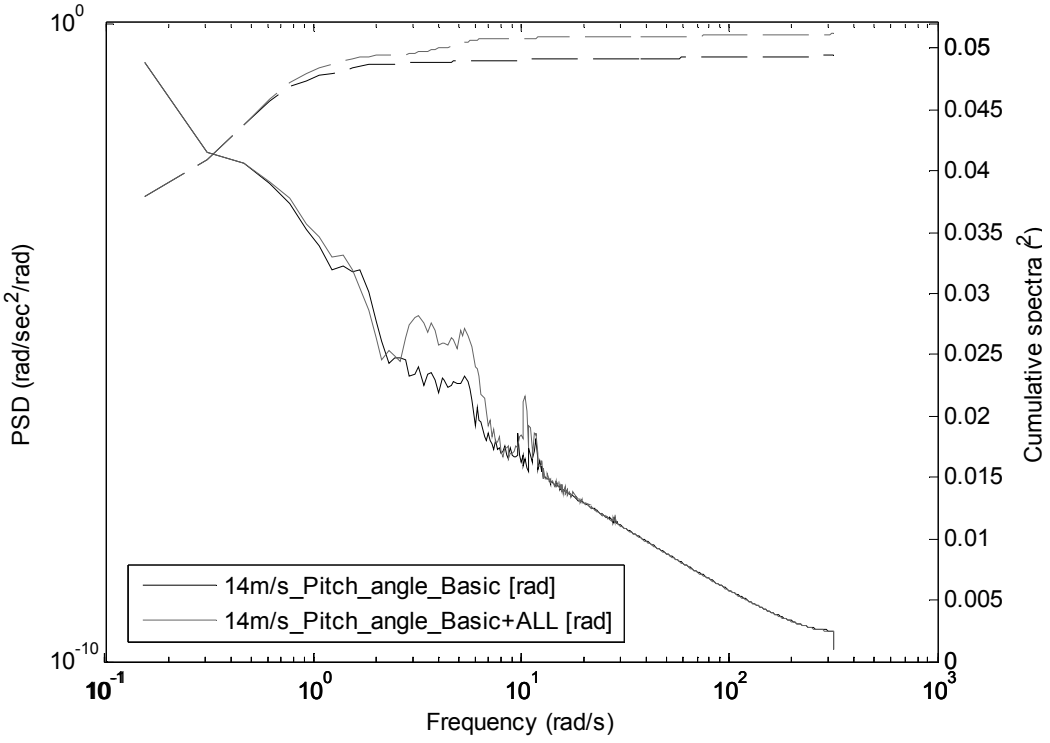

Figure B.85: Pitch angle spectra for both controllers at 14m/s

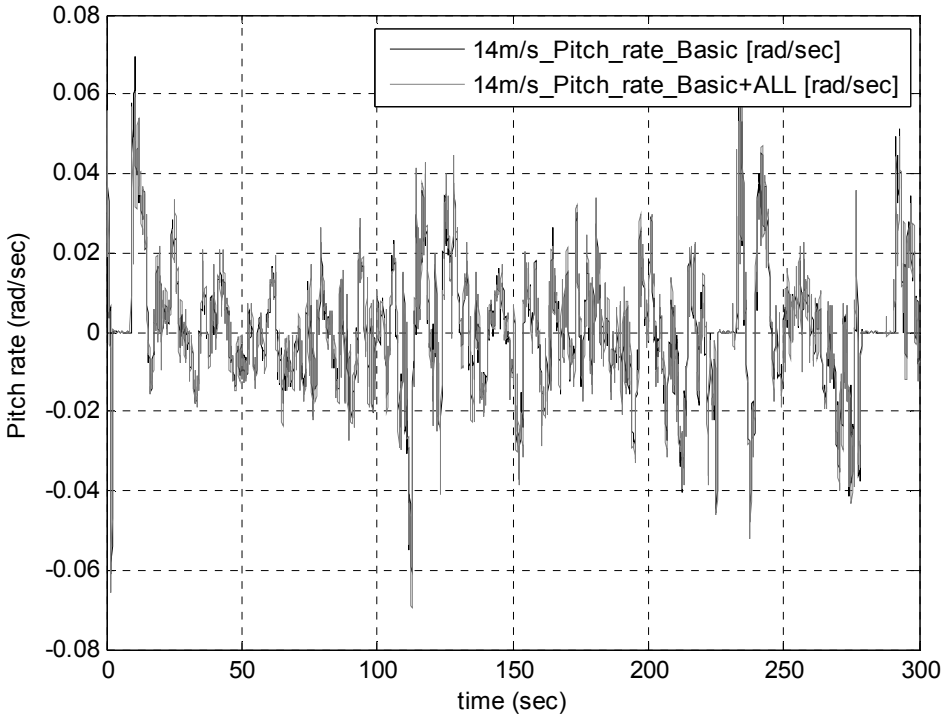

Figure B.86: Pitch rate time series for both controllers at a mean wind speed of 14m/s

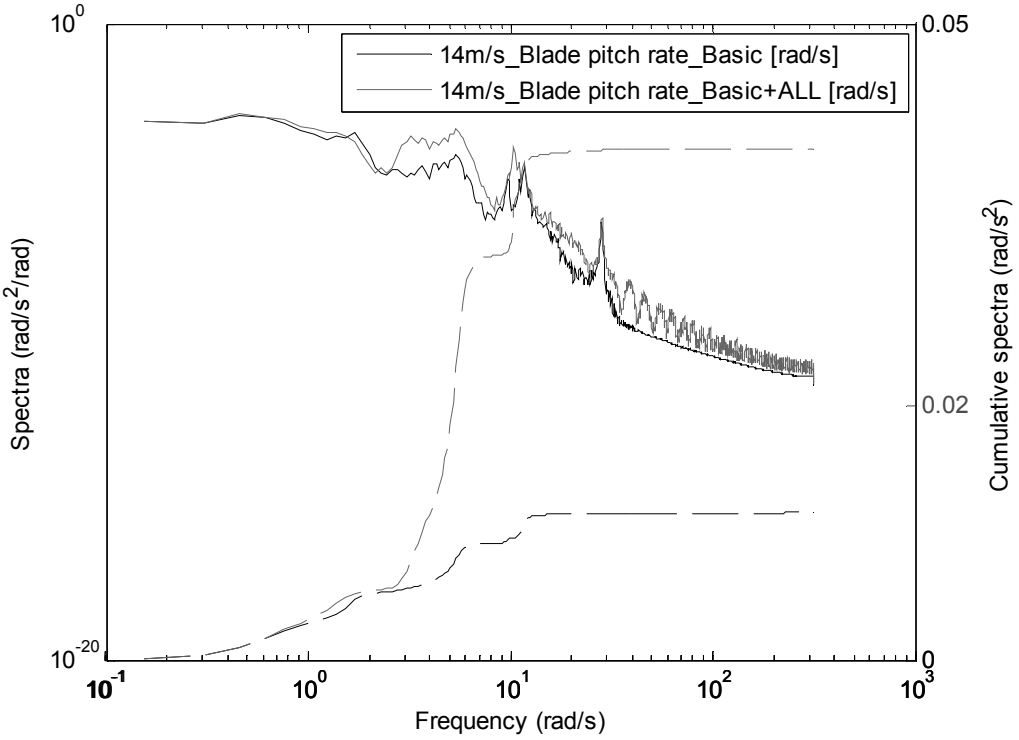

Figure B.87: Pitch rate spectra for both controllers at 14m/s

Above rated 20m/s

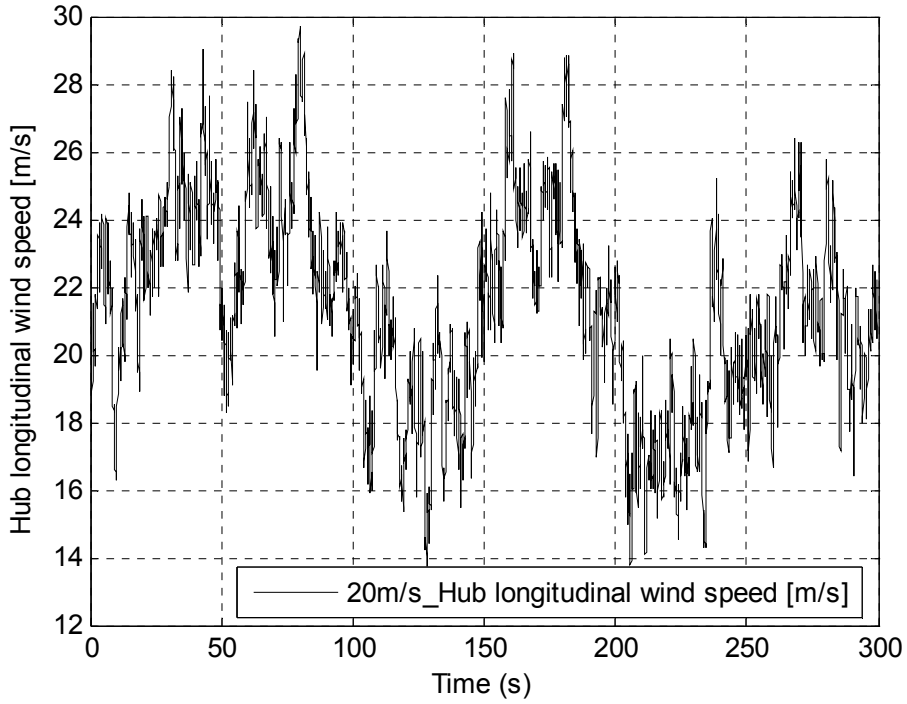

Figure B.88: Wind speed time series for 20m/s

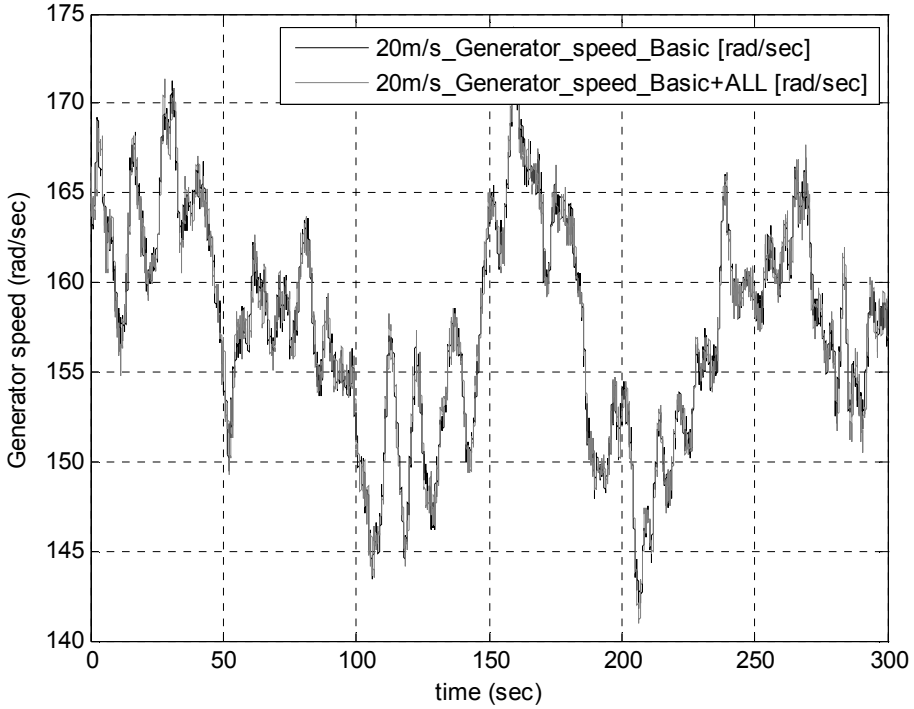

Figure B.89: Generator speed time series for both controllers at a mean wind speed of 20m/s

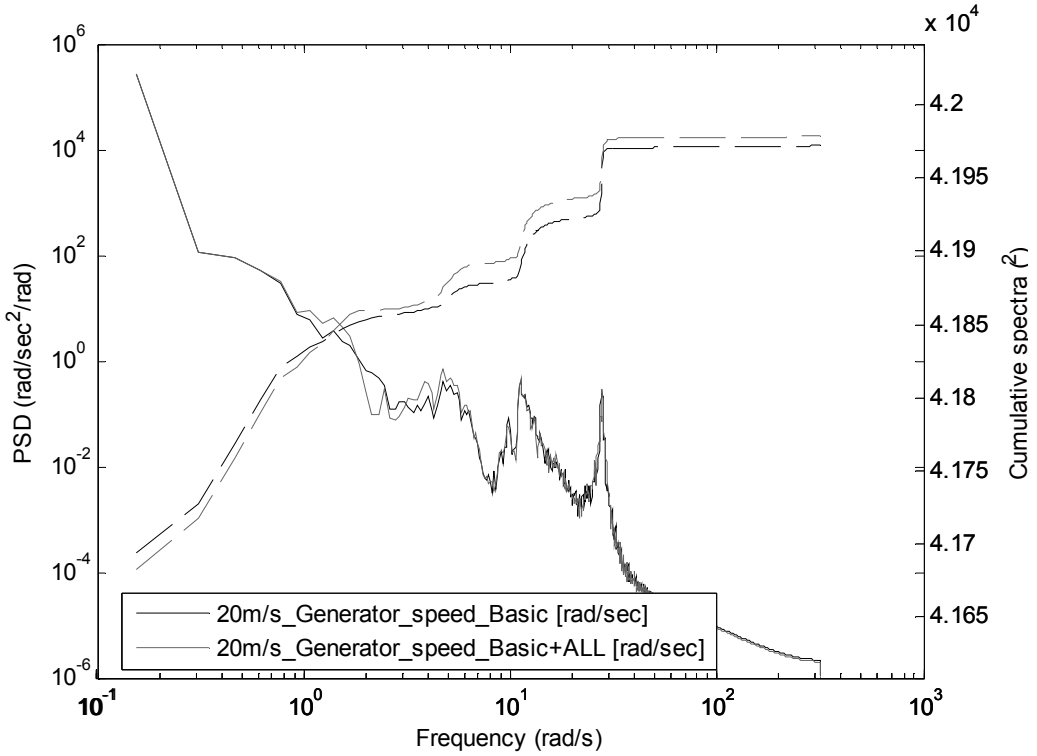

Figure B.90: Generator speed spectra for both controllers at 20m/s

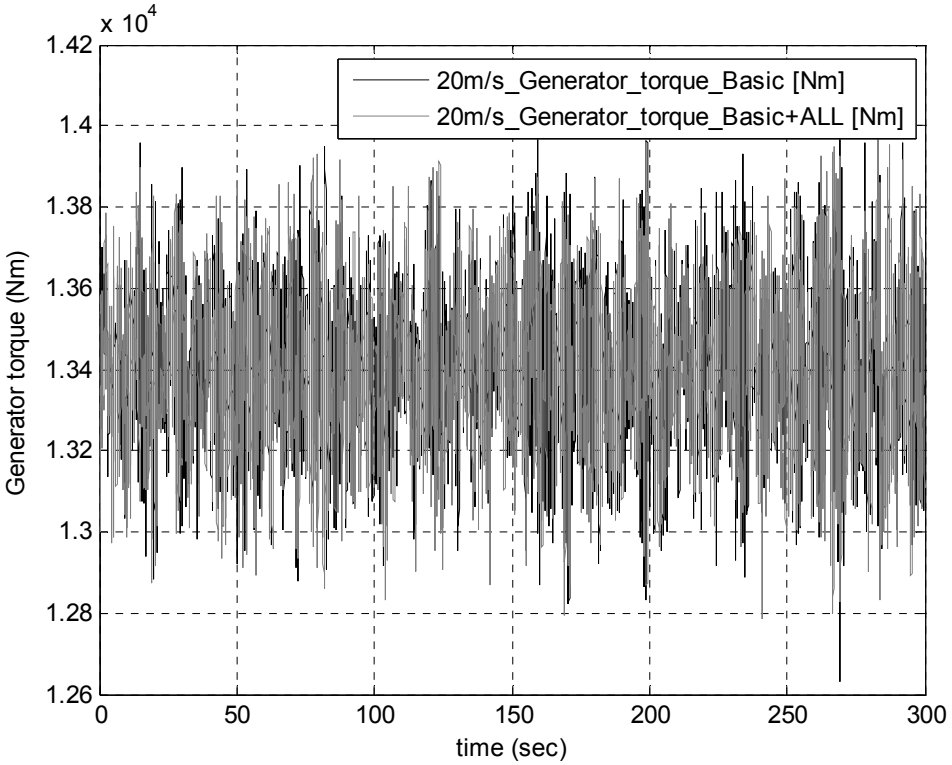

Figure B.91: Generator torque time series for both controllers at a mean wind speed of 20m/s

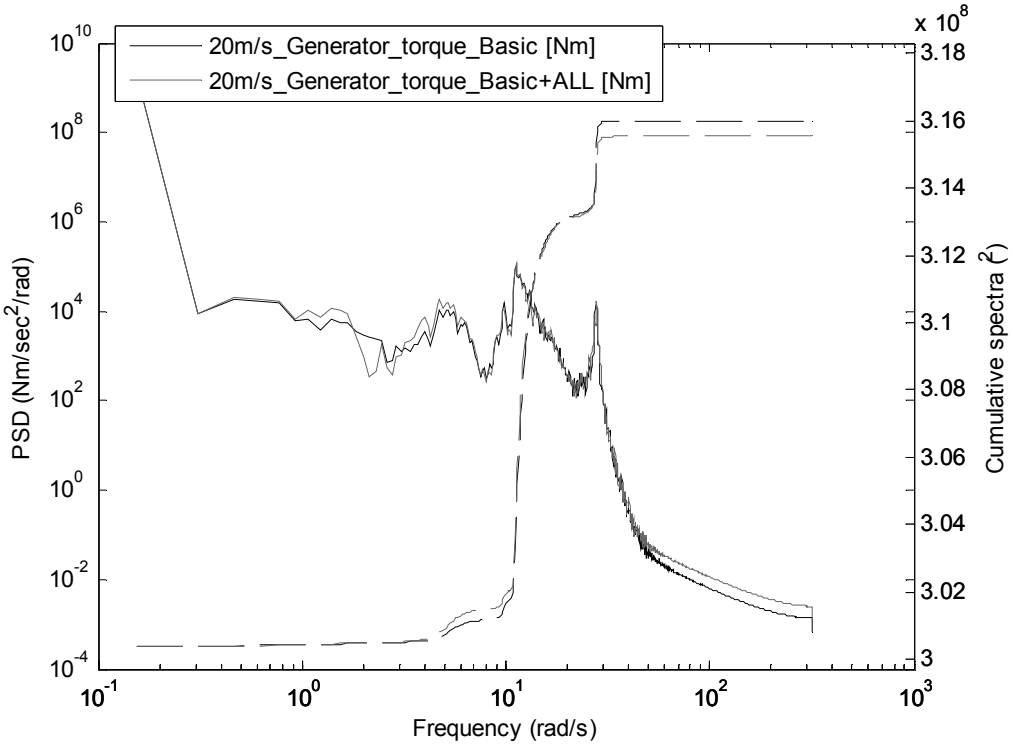

Figure B.92: Generator torque spectra for both controllers at 20m/s

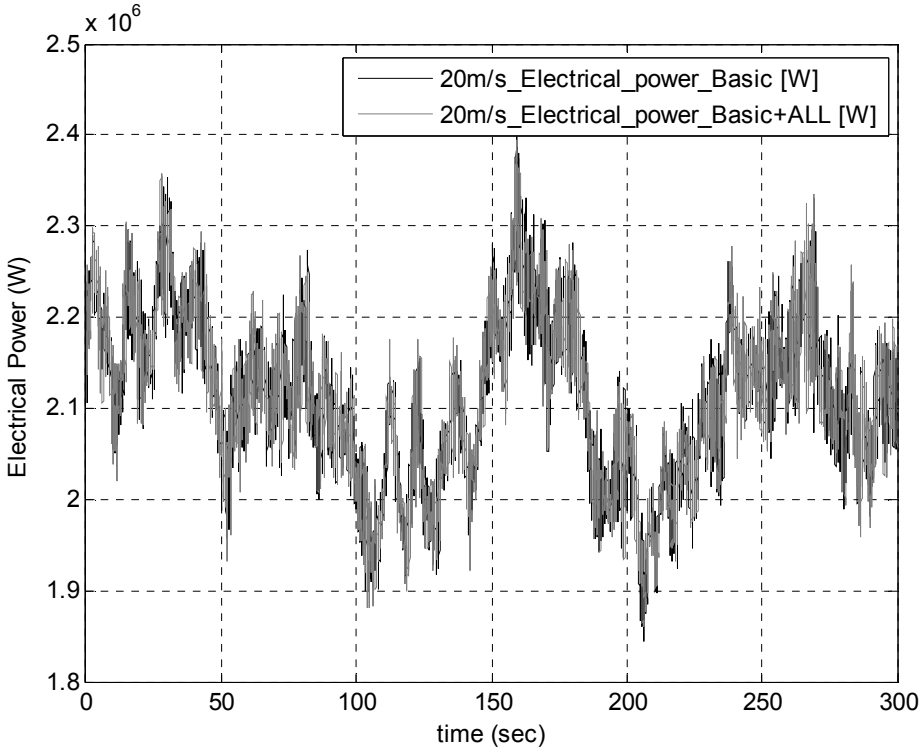

Figure B.93: Electrical power time series for both controllers at a mean wind speed of 20m/s

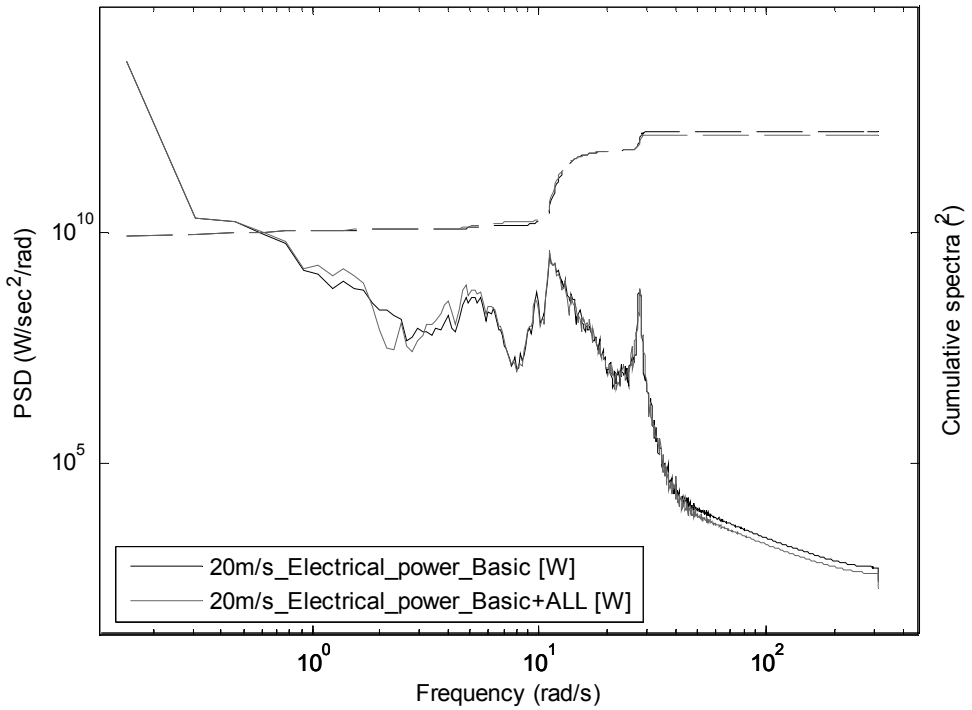

Figure B.94: Electrical power spectra for both controllers at 20m/s

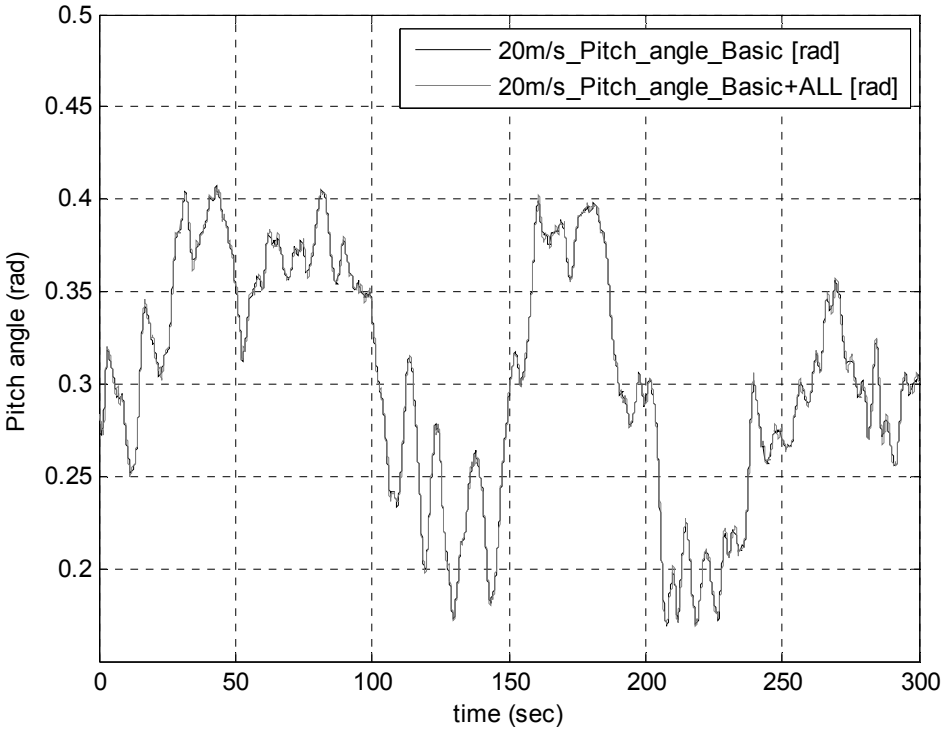

Figure B.95: Pitch angle time series for both controllers at a mean wind speed of 20m/s

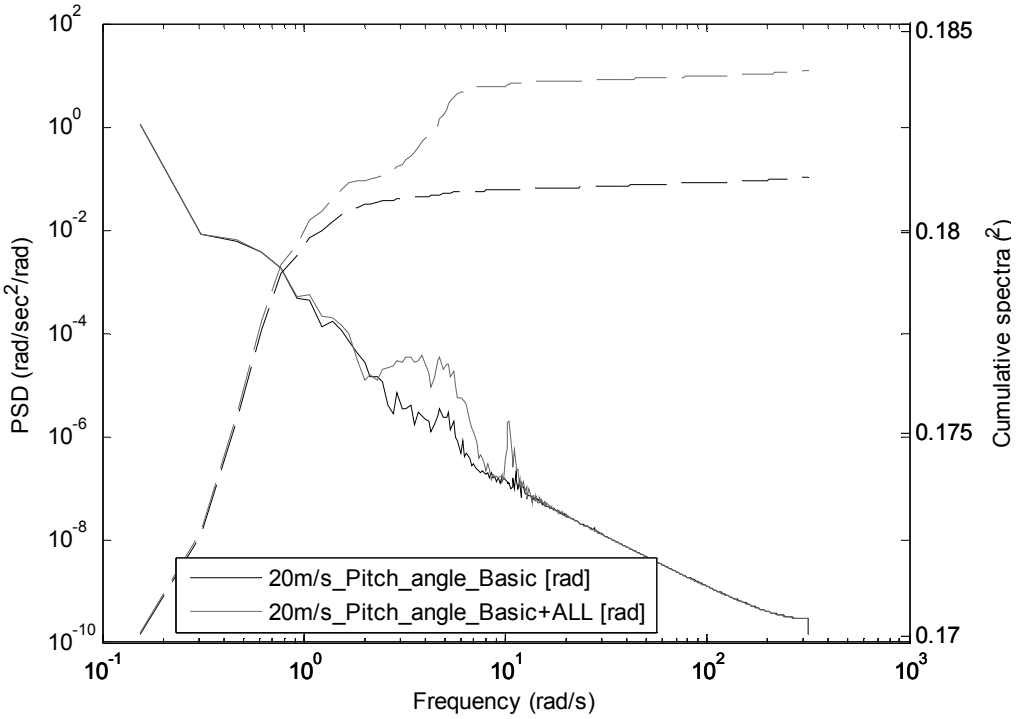

Figure B.96: Pitch angle spectra for both controllers at 20m/s

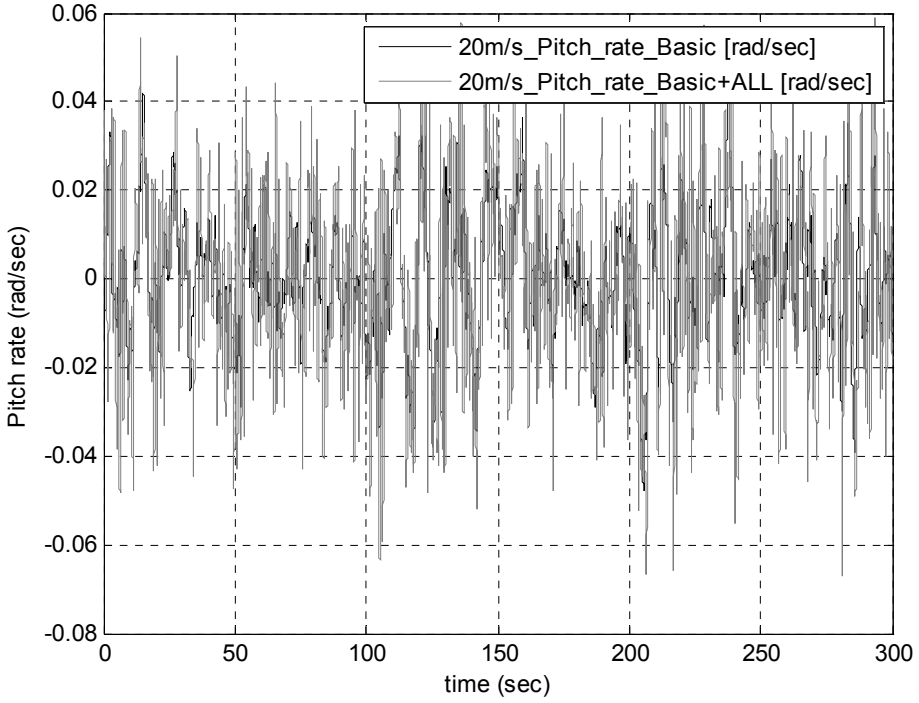

Figure B.97: Pitch rate time series for both controllers at a mean wind speed of 20m/s

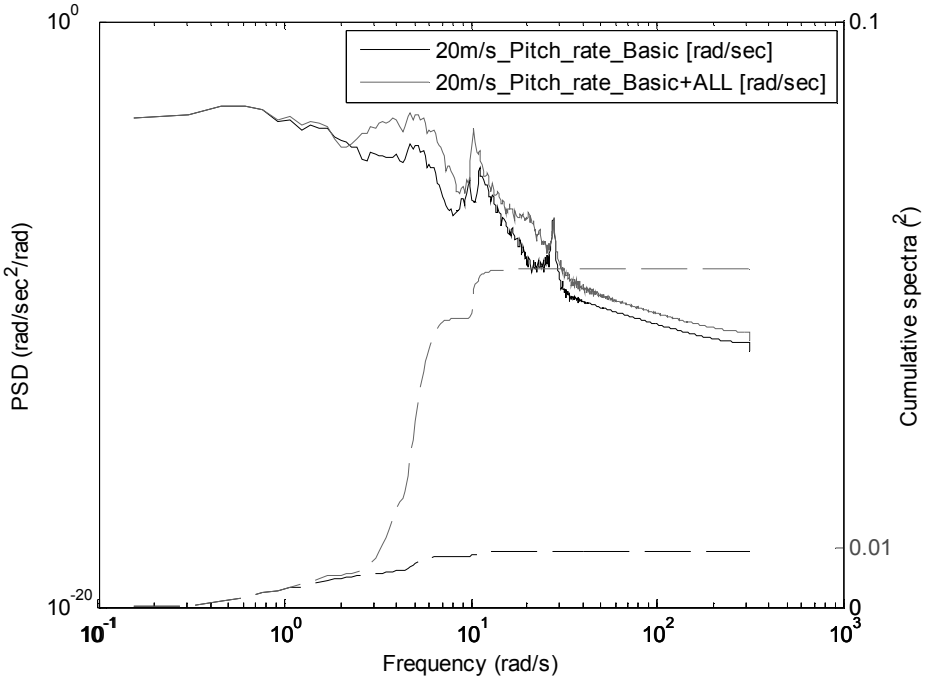

Figure B.98: Pitch rate spectra for both controllers at 20m/s

Fatigue Loads

Blade root edgewise moments

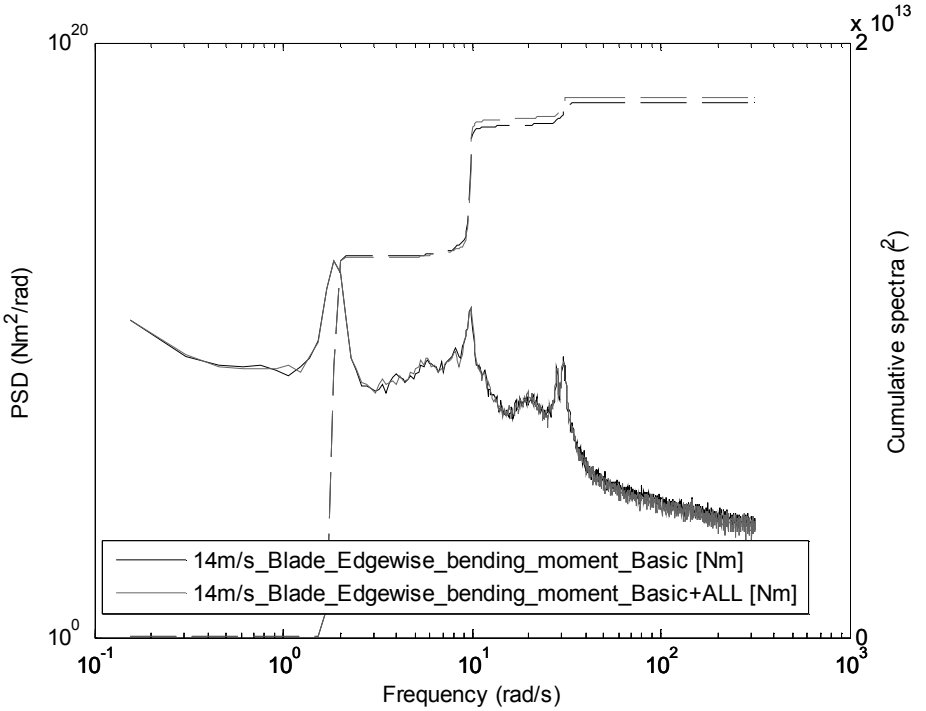

Figure B.99: Blade edgewise bending moment spectra for two controllers at 14m/s

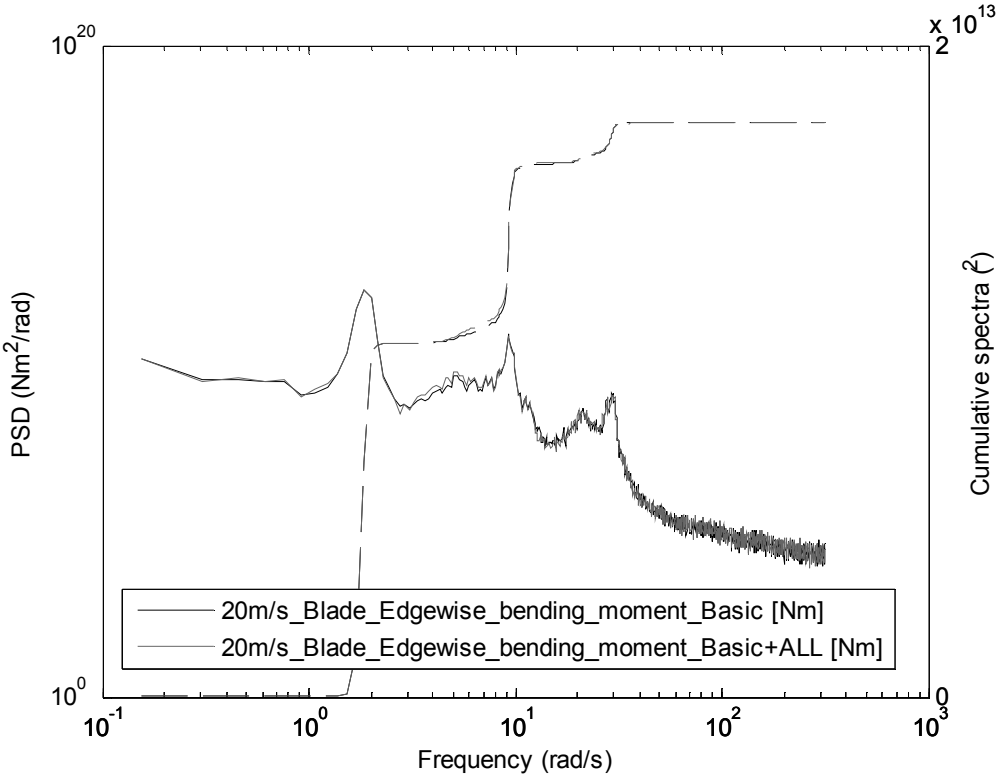

Figure B.100: Blade edgewise bending moment spectra for two controllers at 20m/s

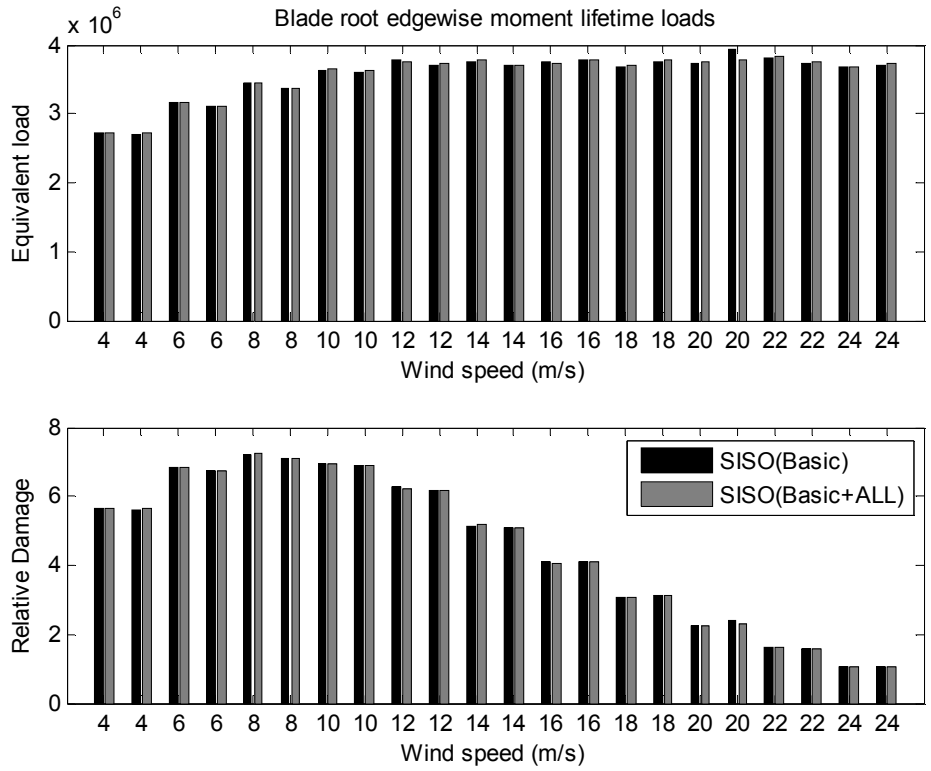

Figure B.101: Lifetime blade root edgewise bending moment loads for the two controllers

Table 13: Blade root edgewise bending moment lifetime loads

Blade root edgewise bending moment lifetime loads	
Controller type	**Loads**
SISO(Basic)	3.2113e+06
SISO(Basic+ALL)	3.2168e+06

Blade flapwise moments

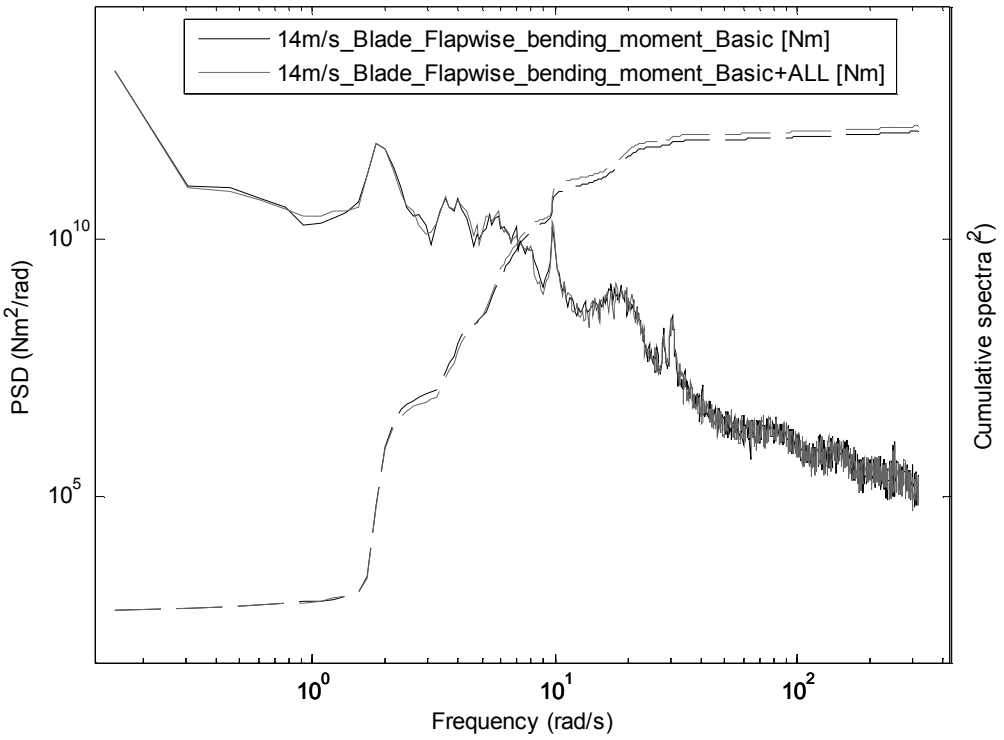

Figure B.102: Blade flapwise bending moment spectra for two controllers at 14m/s

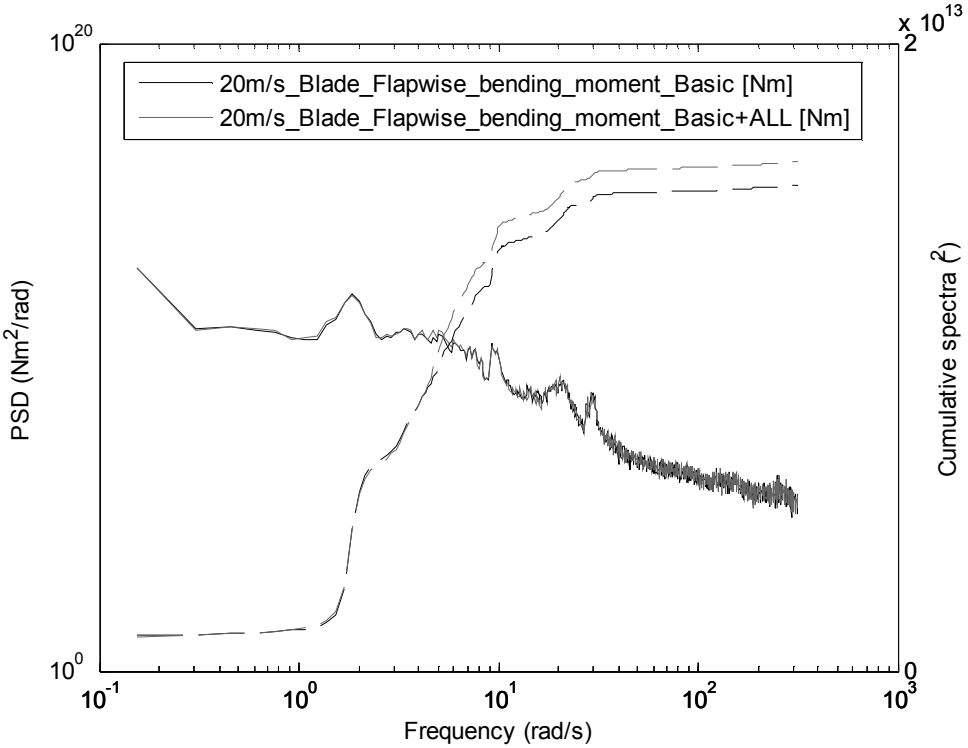

Figure B.103: Blade flapwise bending moment spectra for two controllers at 20m/s

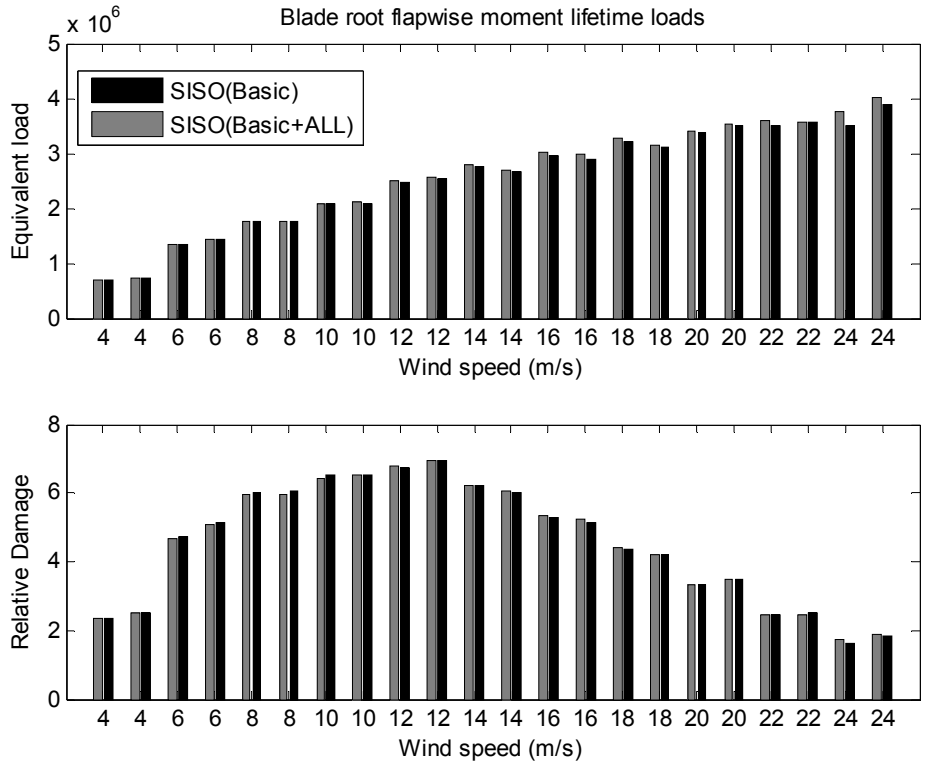

Figure B.104: Lifetime blade root flapwise bending moment loads for the two controllers

Table 14: Blade root flapwise bending moment lifetime loads

Blade root flapwise bending moment lifetime loads	
Controller type	**Loads**
SISO(Basic)	1.8698e+06
SISO(Basic+ALL)	1.8868e+06

Tower base side to side moment loads

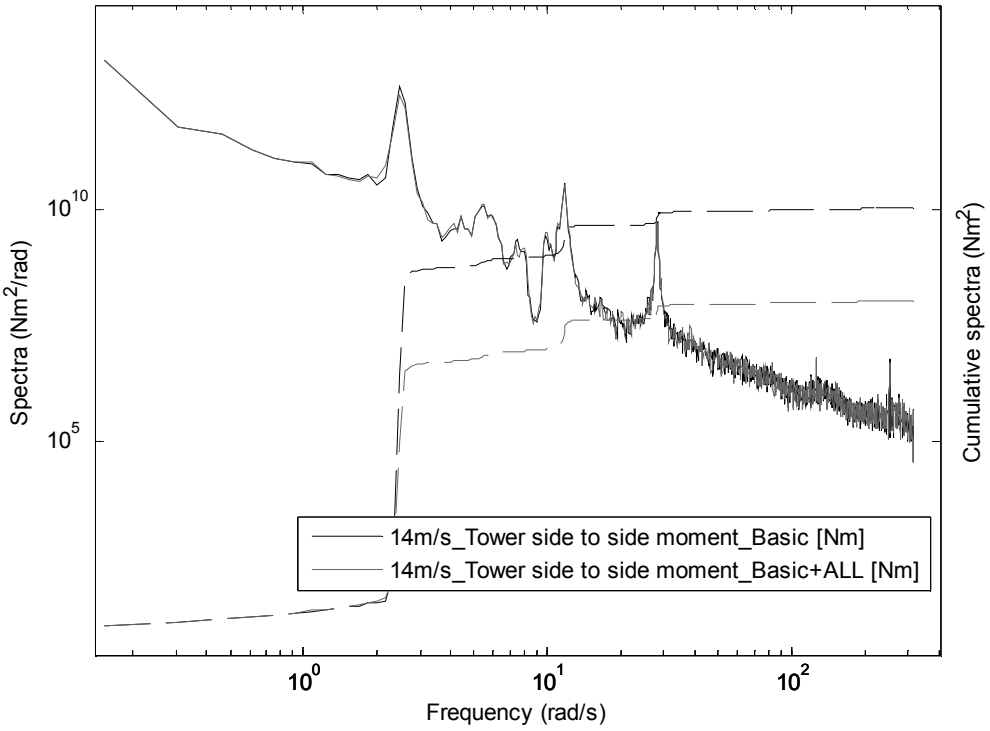

Figure B.105: Tower base side to side moment spectra for both controllers at 14m/s

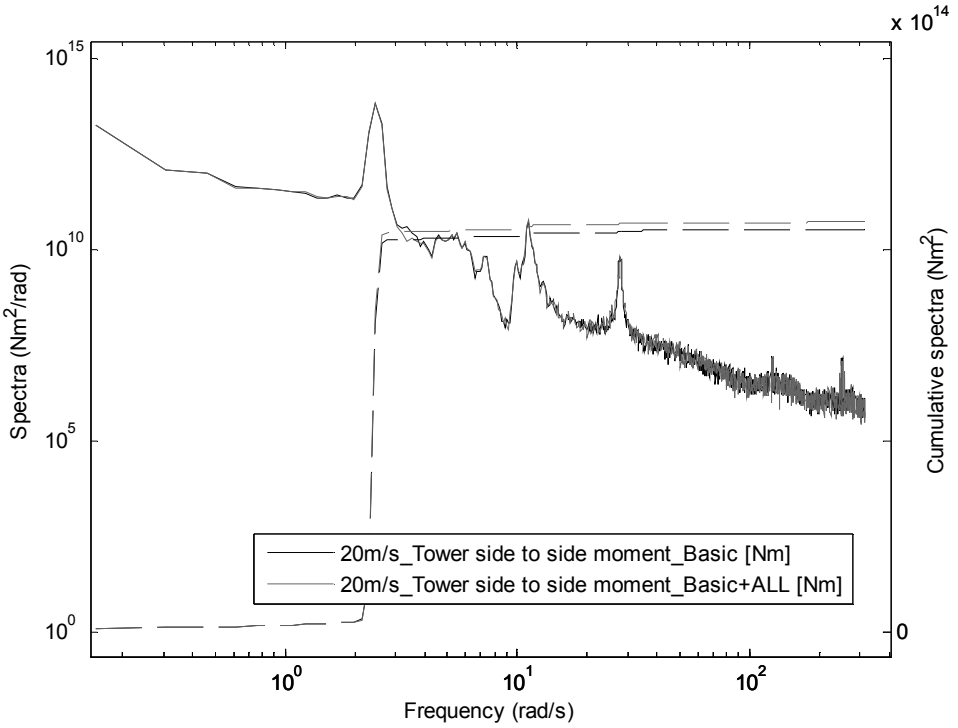

Figure B.106: Tower base side to side moment spectra for both controllers at 20m/s

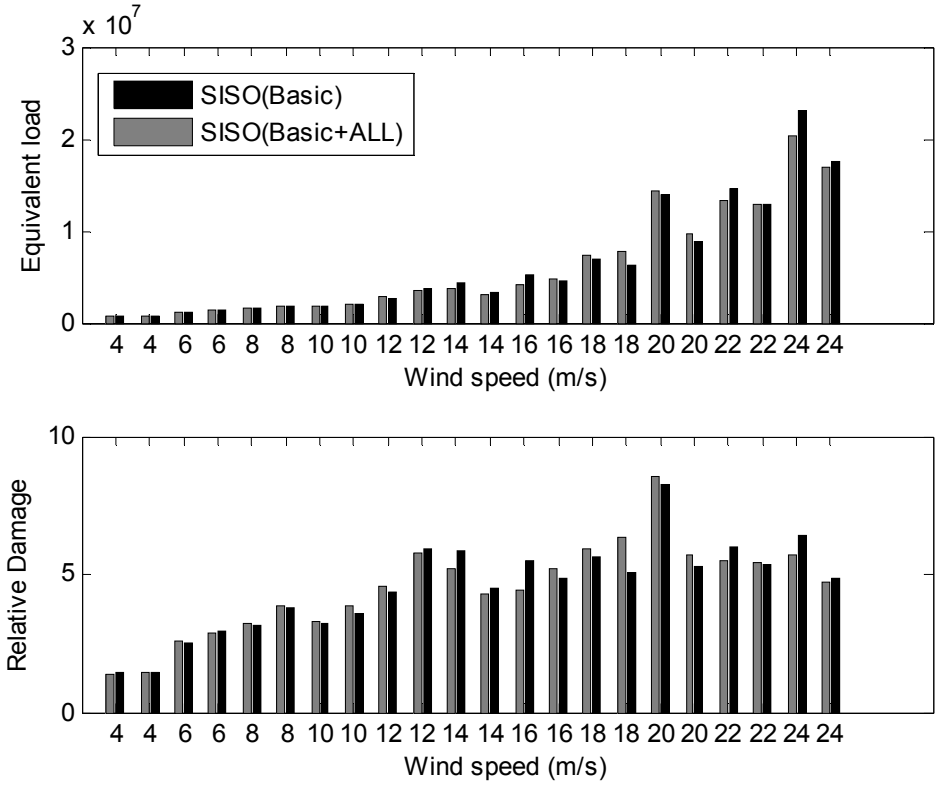

Figure B.107: Lifetime tower base side to side moment loads for the two controllers

Table 15: Tower base side-to-side moment lifetime loads

Tower base side-to-side moment lifetime loads	
Controller type	**Loads**
SISO(Basic)	3.1154e+06
SISO(Basic+ALL)	3.0913e+06

Tower fore-aft moment loads

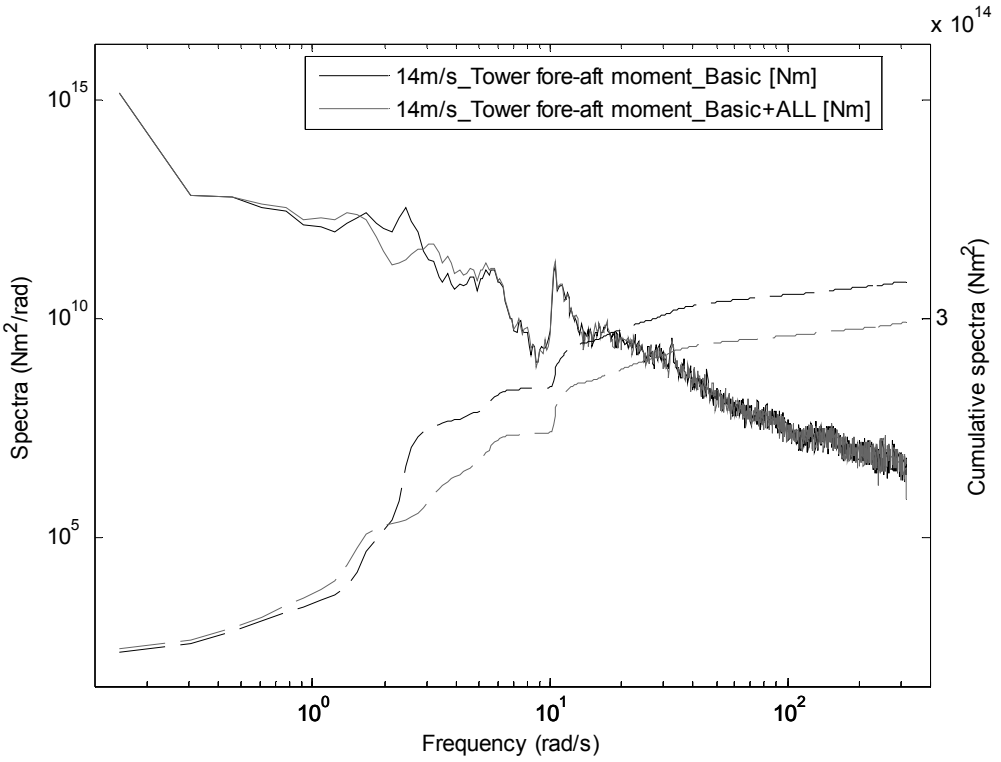

Figure B.108: Tower base fore and aft moment spectra for both controllers at 14m/s

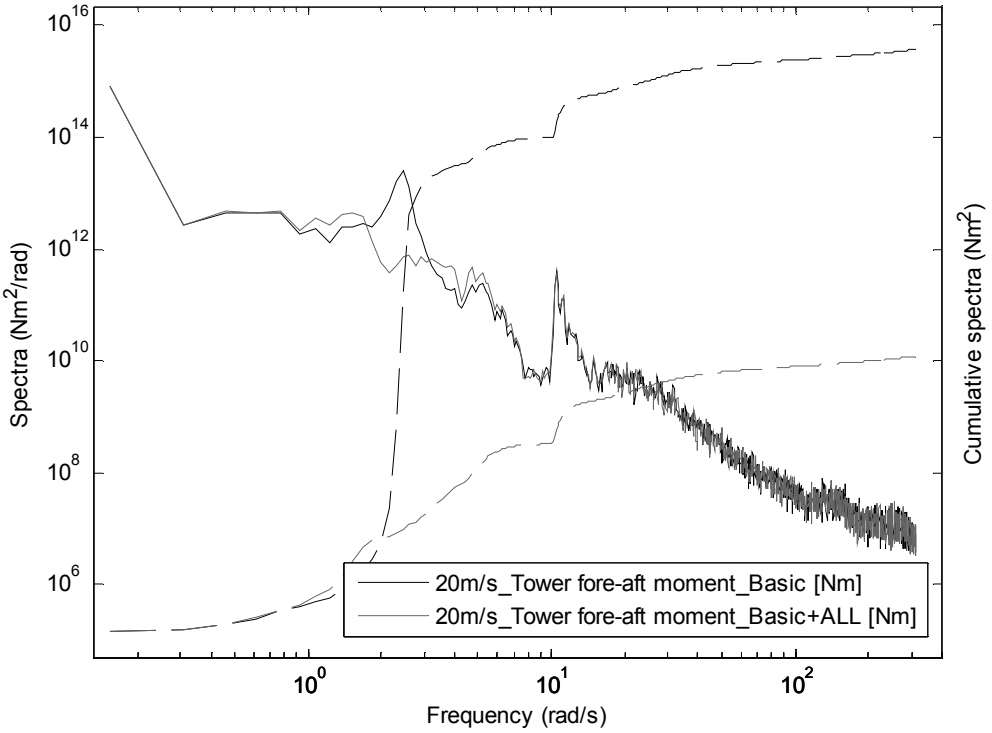

Figure B.109: Tower base fore and aft moment spectra for both controllers at 20m/s

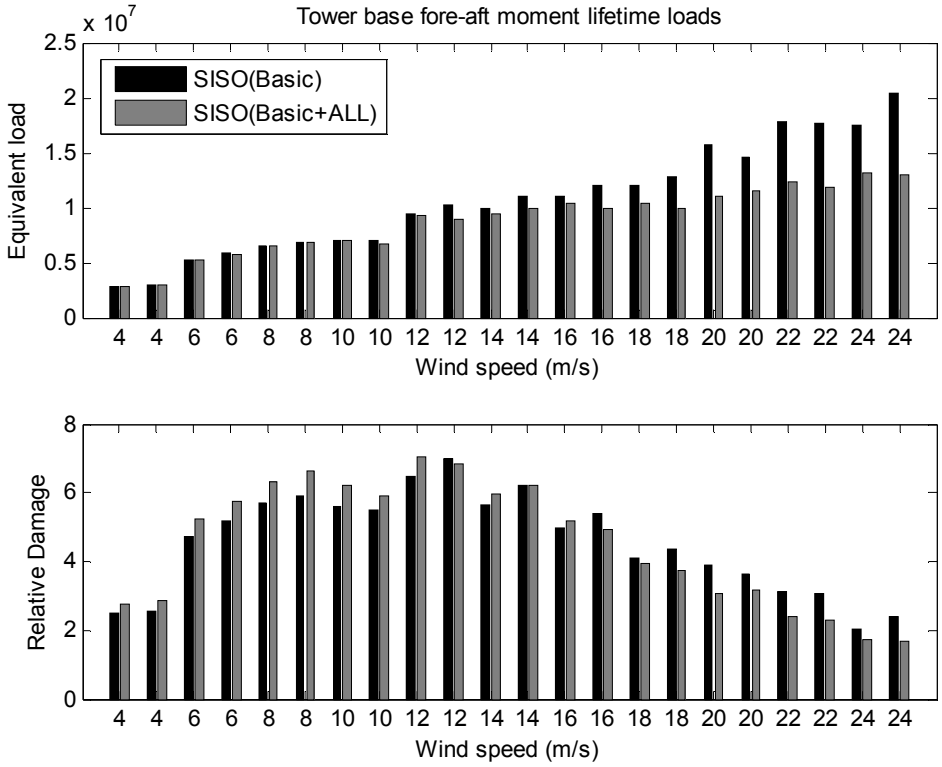

Figure B.110: Lifetime tower base fore and aft moment loads for the two controllers

Table 16: Tower base fore-aft moment lifetime loads

Tower base fore-aft moment lifetime loads		
Controller type	**Loads**	**Load reduction**
SISO(Basic)	7.2186e+06	6.97%
SISO(Basic+ALL)	6.7150e+06	

Appendix C

Fatigue Load Estimation

For the estimation of the lifetime fatigue loads in the current thesis, Rainflow counting algorithms are employed which are well established and widely used for this purpose. A Weibull distribution function in the form of eq. (35), is used for the wind speed distribution, see Figure C.1.

$$f(V) = \frac{k}{c}\left(\frac{V}{c}\right)^{k-1} e^{-\left(\frac{V}{c}\right)^{k}} \tag{35}$$

This function is used in conjunction with the fatigue estimation algorithms, to describe the distribution for each different wind speed and finally to obtain the total Equivalent loads for a twenty year lifetime of the wind turbine. A site with a mean wind speed of 7.5m/s and a Weibull Shape Factor of $k = 2$ are assumed in the distribution. At each wind speed, 10 minutes of simulation data are used.

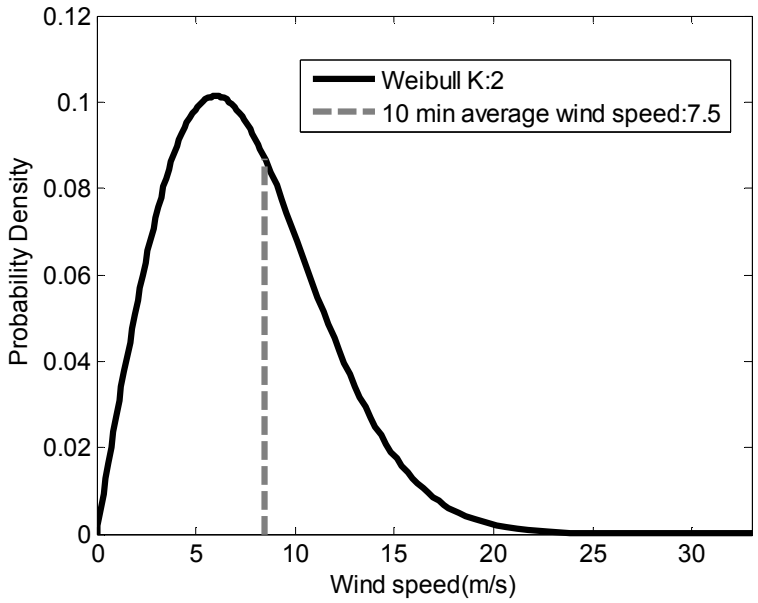

Figure C.1: Weibull distribution for the estimation of wind speed

After the number of cycles has been determined by counting "peaks and valleys" from the 10minute runs using the Rainflow counting method, the Palmgren-Miner

rule is employed for evaluating the damage corresponding to each of the load cases [35], [65]. This is estimated by using the S-N curve (magnitude of cyclic stress S, against logarithmic scale of cycles to failure N), [47], with a Wöhler exponent of M=3 (slope of the fatigue line), see Figure C.2 .

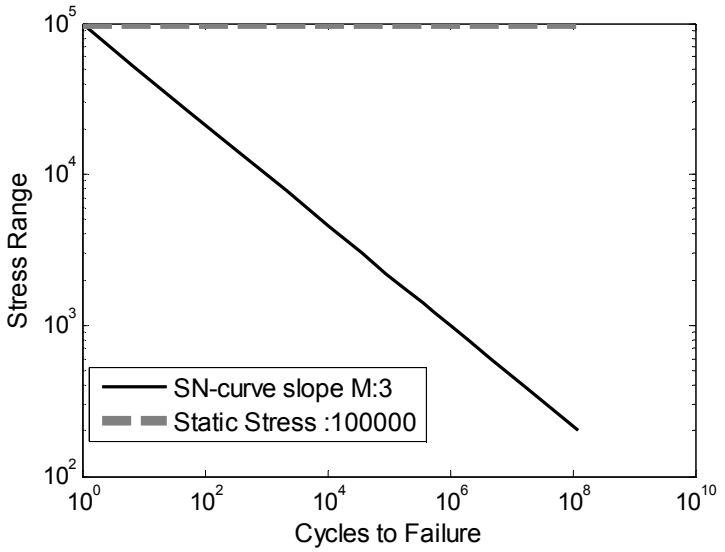

Figure C.2: Stress versus cycles to failure curve (S-N curve)

According to this rule, the cumulative damage D, is estimated according to (36).

$$D = \sum_{i=1}^{m} \frac{n_i}{N_i} \tag{36}$$

In eq. (36), n is the number of stress cycles of the stress range S, of Figure C.2, and N is the number of cycles to failure at the same stress range.

The cumulative damage over the twenty year lifespan of the wind turbine, is evaluated for all the simulation runs (i.e. each wind speed), and the Equivalent loads is a combination of the fatigue damage corresponding to every load case using the Weibull distribution. The lifetime Equivalent loads for every wind speed is shown in the Bar graphs for each different controller considered in Chapter 6. Moreover, the Bar graph depicting "Relative damage", which is defined as the Ratio of the percentage of the lifetime Equivalent loads of each wind speed, over the total Equivalent loads, is presented for each load case. Tower fore-aft (longitudinal) movement is examined here since it is the main driver of fatigue in the tower.